ÇUKUROVA UNIVERSITY
INSTITUTE OF NATURAL AND APPLIED SCIENCES

MSc THESIS

Zekiye Dicle TOPAL

A COMPARISON OF APPROACHES TO INVOLUTE HELICAL GEAR DESIGN

DEPARTMENT OF MECHANICAL ENGINEERING

ADANA-2019

ÇUKUROVA UNIVERSITY
INSTITUTE OF NATURAL AND APPLIED SCIENCES

A COMPARISON OF APPROACHES TO INVOLUTE HELICAL GEAR
DESIGN

Zekiye Dicle TOPAL

MSc THESIS

DEPARTMENT OF MECHANICAL ENGINEERING

We certify that the thesis titled above was reviewed and approved for the award of
degree of the Master of Science by the board of jury on 24/10/2019

………….…….................   ………….……..........................   ………………….....
Prof. Dr. Necdet GEREN   Prof. Dr. Melih BAYRAMOĞLU   Prof. Dr. Uğur EŞME
SUPERVISOR   MEMBER   MEMBER

This MSc Thesis is written at the Department of Mechanical Engineering of
Institute of Natural and Applied Sciences of Çukurova University.
Registration Number:

Prof. Dr. Mustafa GÖK
Director
Institute of Natural and Applied Sciences

ABSTRACT

MSc THESIS

A COMPARISON OF APPROACHES TO INVOLUTE HELICAL GEAR DESIGN

Zekiye Dicle Topal

ÇUKUROVA UNIVERSITY
INSTITUTE OF NATURAL AND APPLIED SCIENCES
DEPARTMENT OF MECHANICAL ENGINEERING

In this thesis, helical gears are designed according to different design approaches. The analytical iterations were made using MATLAB tool and the design results, module (m) and face width (F) were obtained for each design approach. Afterwards, three dimensional solid modeling was created using CATIA with the aid of design result of analytical calculations. The results obtained from the analytical method were confirmed by "Finite Element Analysis" using ANSYS. The design results of each design approach used in this study are compared with each other. Useful graphs, outputs, tables and charts are presented. In addition, the conversion factors of four different design approaches with respect to ANSI / AGMA Standard were obtained.

Key Words: Helical gear, Design approaches, Design output, Converting, Comparison

ÖZ

YÜKSEK LİSANS TEZİ

EVOLVENT HELİSEL DİŞLİ TASARIM YAKLAŞIMLARININ KIYASLANMASI

Zekiye Dicle Topal

ÇUKUROVA ÜNİVERSİTESİ
FEN BİLİMLERİ ENSTİTÜSÜ
MAKİNE MÜHENDİSLİĞİ ANABİLİM DALI

Bu tez çalışmasında helisel dişlilerin farklı tasarım yaklaşımlarına göre tasarımı ele alınmıştır. Analitik iterasyonlar MATLAB kullanılarak yapılmış ve tasarım sonuçları her bir tasarım yaklaşımı için modül (m) ve yüzey genişliği (F) elde edilmiştir. Daha sonrasında analitik hesaplamaların sonucu kullanılarak üç boyutlu katı modellemesi CATIA kullanılarak yapılmıştır. ANSYS kullanarak "Sonlu Eleman Analizi" ile analitik metottan elde edilen sonuçlar doğrulanmıştır. Bu çalışmada kullanılan her bir tasarım yaklaşımlarının sonuçları birbiriyle kıyaslanmıştır. Faydalı grafikler, çıktılar, tablolar ve çizelgeler sunuldu. Buna ek olarak, bu çalışma dört farklı tasarım yaklaşımının ANSI/AGMA Standardına göre dönüşüm faktörleri elde edildi.

Anahtar Kelimeler: Helisel Dişli, Tasarım yaklaşımları, Tasarım çıktıları, Dönüştürme, Karşılaştırma

EXTENDED ABSTRACT

Gear boxes are used for transmitting power and rotary motions consist of a set of gears, shafts and bearings that are mounted in an enclosed lubricated housing. This transmission is achieved with or without change of speed or direction. Helical gear is widely used in industry. The teeth on helical gears are cut at an angle to the face of the gear. When two teeth on a helical gear system engage, the contact starts at one end of the tooth and gradually spreads as the gears rotate, until the two teeth are in full engagement. This gradual engagement makes helical gears operate much more smoothly and quietly than spur gears.

There are two primary failure modes for gears. First one is tooth breakage from excessive bending stress and the second one is surface pitting from excessive contact stress. In both cases, main interest is the tooth load which comes from applied load or torque during the transmission of power. Bending stress occurs at the root of the tooth profile mainly. Bending stress is highest at the fillet and can cause breakage or fatigue failure of tooth in root region. Even though a gear tooth may not break due to bending stresses during its lifetime, it could develop pits on the tooth face due to high contact stresses fatiguing the surface by compression. The contact pressure is intensified near the pitch circle, where the contact is pure rolling with zero sliding velocity.

After the material selection for pinion and gear, the best combination of two design parameters that are *module (m)* and *face width (F)*. After defining the pinion and gear materials, module is estimated and calculations are carried out to determine the face width. Module and face width calculations are iterated until the face width is in a range of $3p \leq F \leq 5p$ where p is circular pitch that is dependent on the selected module. The iteration may require considerable time depending on the initially selected module, which is   dependent on expertise. Various design formulas are available in the machine elements or machine design text books for the design or finding "m" or "F". In addition to this, the international and national

standards such as ANSI-AGMA, ISO JGMA provide different formulae with different level of difficulty. However, the results of using different approaches have not been compared so far. Thus the designer does not aware of the success or loss gained using each of the approach. Therefore, there is a need to compare the results of each of the most accepted design formula or design approach for the involute helical gear design. Hence, this study aims to compare the design results (F and m) obtained using the design formula or design approaches to determine loss or gain obtained in each of the approach. The results of this study may provide usable outputs for teaching and designers practicing gear design.

The main intention is to compare the design results given by the most commonly used gear design approaches. Hence, the designer can be aware of the success or loss gained using each of the approach. The results of the study may also help to select the proper gear design approach depending on the requirements of the particular design.

An involute helical gear design has been performed at speed ratios of 1:1, 2:1, 3:1, 4:1, 5:1, 6:1, 7:1 and 8:1, in this thesis work. And these speed reductions has been carried out at different amount of power transmissions from 1 kW to 1000kW.

This thesis meets a need of selecting and using appropriate involute helical gear design approaches for all designers including the expert designers and novice learners who are practicing a helical gear design. This was made by comparing the most commonly used involute helical gear design approaches available in the literature. The selected approaches are given as follow;

1. Shigley's Mechanical Engineering Design 9th Edition (SI), Budynas R.G. and Nisbett J.K., 2011
2. Fundamental of Machine Component Design 5th Edition, Juvinall R.C. and Marshek K.M., 2011
3. ISO 6336 Standards, 2006 and ISO 9085:2002 Standards, 2002
4. ANSI/AGMA 2101-D04 Standards, 2004

This study proposes to use the easier and the most appropriate approach

provided in the common text books considering the verified results of FEA, if there is no obligation to use ISO or ANSI/AGMA Standards. Because these standards are more challenging, time consuming and include complicated equations. Conversion factors for the conversion of text books results to the verified results were developed. Now, the results obtained by text books can be converted to the standards with the aid of conversion factors developed in this study. As a result of these, gear designers do not have to deal with the computational load of the standards. This does not only allow saving time and resources, but also provides safer and reliable designs.

A systematic methodology which relies on dimensionless numbers called as GR_i and CFs, has been described and proposed to rate most common design approaches with ANSI/AGMA 2001-D04 (2004) based on bending fatigue failure for helical gears. Although the results of four design approaches differ from each other, good similarity and continuity of the charts were found out. This allowed to obtain CFs between the standards. Now, these two approaches can be converted to each other with minimum of error. Beyond the investigations already available in the literature, following conclusions can be drawn in this study.

Dimensionless conversion factors (CFs) were generated for helical gears to convert the design results, module (m) and face width (F) of ISO Standard, B&N textbook and J&M textbook into AGMA with a minor error.

Scatter and radar charts presented to make a relative comparison between design approaches. The results showed that gear design approaches have similar behaviour in all power ranges.

Two methods are now available to obtain CFs. One can be made by linear interpolation from Table 4.12 for pressure angle of 20° and Table 4.15 for pressure angle of 25°. Secondly, C_p expressions can be used for any desired speed ratio from Table 4.13 for pressure angle of 20° and Table 4.16 for pressure angle of 25°.

Universality of CFs were verified by case studies and worked reasonably well. The maximum total Gear Volume error (GV_e) was found as 9,2% for pressure

angle of 20° in Table 4.14 and 9.72% for pressure angle of 25° in Table 4.17 with the aid of CFs.

Briefly, this study may serve as a guideline for a designer who deals with the design of an involute helical gear. This study is only valid for most common used helix angle which is 30°. For other helix angles, all results would change. If a designer concerns with light weighted applications, the overall size of a gear is important as well as material usage that are objectives of optimization. On the other hand helical gear design is the subject of almost all machine design courses. And it is important to introduce clear, easy to understand and reliable design approach for learners and students. Consequently, the results of this work interests both expert and novice designers and learners.

GENİŞLETİLMİŞ ÖZET

Dişli kutuları, güç iletmek için kullanılır ve döner hareketler, kapalı bir yağlanmış mahfazaya monte edilmiş bir dişliler, miller ve yataklardan oluşur. Bu aktarma, hız veya yön değişikliği ile veya hız veya yön değişikliği olmadan elde edilir. Helis dişli endüstride yaygın olarak kullanılmaktadır. Helisel dişlilerdeki dişler dişlinin yüzeyine açılı olarak kesilir. Helisel dişli sistemindeki iki diş birbirine geçtiğinde, temas dişin bir ucundan başlar ve dişler döndükçe, iki diş tam olarak oturana kadar yavaşça yayılır. Bu kademeli ilişki helisel dişlilerin düz dişliye göre çok daha yumuşak ve sessiz çalışmasını sağlar.

Dişliler için iki ana arıza modu vardır. Birincisi, aşırı bükülme stresinden diş kırılması ve ikincisi aşırı temas stresinden yüzeyde oyuklaşmadır. Her iki durumda da ana ilgi, güç iletimi sırasında uygulanan yük veya torktan gelen diş yüküdür. Eğilme gerilmesi esas olarak diş profilinin kökünde meydana gelir. Bükülme stresi, fillet bölgesinde en yüksektir ve kök bölgesinde dişlerde kırılmaya veya yorgunluğa neden olabilir. Bir dişli dişi, kullanım ömrü boyunca bükülme gerilmeleri nedeniyle kırılmasa da, yüzeyi sıkıştırarak sıkıştıran yüksek temas gerilmeleri nedeniyle diş yüzeyinde çukurlar oluşturabilir. Temas basıncı adım çemberi etrafında yoğunlaşır.

Pinyon ve dişli için malzeme seçiminden sonra, modül (m) ve yüz genişliği (F) tasarım parametrelerinin en iyi kombinasyonudur. Pinyon ve dişli malzemelerinin tanımlanmasından sonra, modül tahmin edilir ve yüz genişliğini belirlemek için hesaplamalar yapılır. Modül ve yüz genişliği hesaplamaları, yüz genişliği 3p≤F≤5p aralığında oluncaya kadar tekrarlanır; burada p, seçilen modüle bağlı dairesel aralıktır. İterasyon, uzmanlığa bağlı olan başlangıçta seçilen modüle bağlı olarak oldukça zaman alabilir. Makine elemanları veya makine tasarımı ders kitaplarında, tasarım veya "m" veya "F" bulma için çeşitli tasarım formülleri bulunmaktadır. Buna ek olarak, ANSI-AGMA, ISO JGMA gibi uluslararası ve ulusal standartlar, farklı zorluk seviyelerinde farklı formüller sunar. Ancak, farklı

yaklaşımlar kullanmanın sonuçları şu ana kadar karşılaştırılmamıştır. Böylece tasarımcı, yaklaşımın her birini kullanarak kazanılan başarı veya kaybın farkında değildir. Bu nedenle, helisel dişli tasarımı için en çok kabul edilen tasarım formülünün veya tasarım yaklaşımının sonuçlarının karşılaştırılmasına ihtiyaç vardır. Bu nedenle, bu çalışma, her bir yaklaşımda elde edilen kayıp veya kazancı belirlemek için tasarım formülü veya tasarım yaklaşımları kullanılarak elde edilen tasarım sonuçlarını (F ve m) karşılaştırmayı amaçlamaktadır. Bu çalışmanın sonuçları, dişli tasarımı uygulayan öğretim ve tasarımcılar için kullanılabilir çıktılar sağlayabilir.

Temel amaç, en yaygın kullanılan dişli tasarım yaklaşımları tarafından verilen tasarım sonuçlarını karşılaştırmaktır. Bu nedenle, tasarımcı yaklaşımın her birini kullanarak kazanılan başarı veya kaybın farkında olabilir. Çalışmanın sonuçları ayrıca, belirli tasarımın gerekliliklerine bağlı olarak uygun dişli tasarım yaklaşımının seçilmesine de yardımcı olabilir.

Bu tez çalışmasında 1: 1, 2: 1, 3: 1, 4: 1, 5: 1, 6: 1, 7: 1 ve 8: 1 hız oranlarında helisel dişli tasarımları yapılmıştır. Ve bu hız düşüşleri 1 kW'dan 1000kW'a kadar farklı güç iletimlerinde gerçekleştirilmiştir.

Bu tez, uygun tasarımı seçme ve kullanma ihtiyacını karşılar; helisel dişli tasarımı uygulayan uzman tasarımcılar ve acemi öğrenenler dahil tüm tasarımcılar için helisel dişli tasarımı yaklaşımları içerir. Bu, literatürde bulunan en yaygın kullanılan helisel dişli tasarım yaklaşımlarını karşılaştırarak yapıldı. Seçilen yaklaşımlar aşağıdaki gibi verilmiştir;

1. Shigley's Mechanical Engineering Design 9th Edition (SI), Budynas R.G. and Nisbett J.K., 2011
2. Fundamental of Machine Component Design 5th Edition, Juvinall R.C. and Marshek K.M., 2011
3. ISO 6336 Standards, 2006 and ISO 9085:2002 Standards, 2002
4. ANSI/AGMA 2101-D04 Standards, 2004

Bu çalışma, ISO veya ANSI / AGMA Standartlarını kullanma zorunluluğu yoksa, FEA'nın doğrulanmış sonuçlarını dikkate alarak, ortak kitaplarda sağlanan en kolay ve en uygun yaklaşımı kullanmayı önermektedir. Çünkü bu standartlar daha zor, zaman alıcı ve karmaşık denklemler içeriyor. Ders kitaplarının sonuçlarının doğrulanmış sonuçlara dönüştürülmesi için dönüşüm faktörleri geliştirilmiştir. Şimdi, ders kitaplarında elde edilen sonuçlar, bu çalışmada geliştirilen dönüşüm faktörleri ile standartlara dönüştürülebilir. Bunun bir sonucu olarak, dişli tasarımcılarının standartların hesaplamalı yüküyle uğraşması gerekmez. Bu sadece zamandan ve kaynaklardan tasarruf sağlamaz, aynı zamanda daha güvenli ve güvenilir tasarımlar sunar.

GR$_i$ ve CF olarak adlandırılan boyutsuz sayılara dayanan sistematik bir metodoloji tanımlanmış ve helisel dişliler için yorulma arızasına bağlı olarak ANSI / AGMA 2001-D04 (2004) ile en yaygın tasarım yaklaşımlarını değerlendirmek için önerilmiştir. Dört tasarım yaklaşımının sonuçları birbirinden farklı olsa da, grafiklerin iyi benzerliği ve sürekliliği tespit edildi. Bu, standartlar arasında CF'lerin elde edilmesine izin verdi. Şimdi, bu iki yaklaşım minimum hata ile birbirine dönüştürülebilir. Literatürde zaten mevcut olan araştırmaların ötesinde, bu çalışmada aşağıdaki sonuçlar çıkarılabilir.

Helisel dişliler için tasarım sonuçlarını, modül (m) ve yüz genişliğini (F), ISO Standardı, B&N ders kitabı ve J&M ders kitabını, küçük bir hatayla AGMA'ya dönüştürmek için boyutsuz dönüştürme faktörleri (CF'ler) üretildi.

Tasarım yaklaşımları arasında göreceli bir karşılaştırma yapmak için dağılım ve radar grafikleri sunulmuştur. Sonuçlar, dişli tasarımı yaklaşımlarının tüm güç aralıklarında benzer davranışlara sahip olduğunu göstermiştir.

CF'leri elde etmek için iki yöntem mevcuttur. Biri 20 ° 'lik basınç açısı için Tablo 4.12'den ve 25 °' lik basınç açısı için Tablo 4.15'ten doğrusal enterpolasyon ile yapılabilir. İkinci olarak, Cp ifadeleri, 20 ° basınç açısı için Tablo 4.13'ten Tablo 4.13'ten ve 25 ° basınç açısı için Tablo 4.16'dan istenen herhangi bir hız oranı için kullanılabilir.

CF'lerin evrenselliği vaka çalışmaları ile doğrulanmış ve oldukça iyi çalışmıştır. Maksimum toplam Dişli Hacmi hatası (GVe), CF'lerin yardımıyla Tablo 4.14'te 20 ° basınç açısı için% 9,2 ve Tablo 4.17'de 25 ° basınç açısı için% 9.72 olarak bulunmuştur.

Kısaca, bu çalışma, ilgili bir helisel dişli tasarımıyla ilgilenen bir tasarımcı için bir rehber görevi görebilir. Bu çalışma sadece 30° olan en yaygın kullanılan helis açısı için geçerlidir. Diğer helis açıları için tüm sonuçlar değişecektir. Bir tasarımcı hafif ağırlıklı uygulamalarla ilgileniyorsa, genel olarak bir dişli boyutu, optimizasyonun amacı olan malzeme kullanımı kadar önemlidir. Öte yandan, helisel dişli tasarımı hemen hemen tüm makine tasarım derslerinin konusudur. Ve açık, anlaşılması kolay ve güvenilir tasarım yaklaşımını tanıtmak önemlidir.

ACKNOWLEDGEMENT

CONTENTS   PAGE

XII

XIII

LIST OF FIGURES **PAGE**

LIST OF TABLES **PAGE**

XVIII

XIX

1. INTRODUCTION

The most common way to classify gears is by category type and by the orientation of axes. Gears are classified into 3 categories; parallel axes gears, intersecting axes gears, and nonparallel and nonintersecting axes gears. Spur and helical gears are parallel axes gears. Bevel gears are intersecting axes gears. Screw or crossed helical, worm gear and hypoid gears belong to the third category. In this study, helical gear is the main focus.

1.1. Helical Gears

Helical gears, used to transmit motion between parallel shafts. The helix angle is the same on each gear, but one gear must have a right-hand helix and the other a left-hand helix. The shape of the tooth is an involute helicoid.

The angled teeth engage more gradually than do spur gear teeth, causing them to run more smoothly and quietly. With parallel helical gears, each pair of teeth first make contact at a single point at one side of the gear wheel; a moving curve of contact then grows gradually across the tooth face to a maximum, then recedes until the teeth break contact at a single point on the opposite side. In spur gears, teeth suddenly meet at a line contact across their entire width, causing stress and noise. Spur gears make a characteristic whine at high speeds. For this reason spur gears are used in low-speed applications and in situations where noise control is not a problem, and helical gears are used in high-speed applications, large power transmission, or where noise abatement is important.

Figure 1.1 provides the general nomenclature which is used in this thesis work for gear.
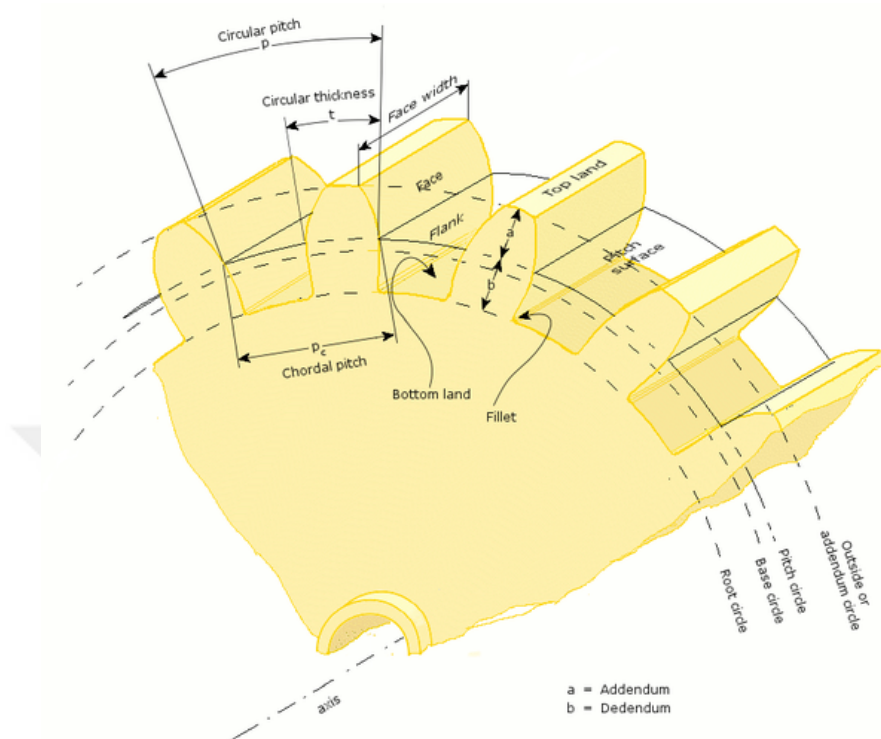
Figure1. 1. General nomenclature for gear

1.2. Significance and Goal of Study

Gear boxes are used for transmitting power and rotary motions consist of a set of gears, shafts and bearings that are mounted in an enclosed lubricated housing. This transmission is achieved with or without change of speed or direction. Helical gear is widely used in industry. The teeth on helical gears are cut at an angle to the face of the gear. When two teeth on a helical gear system engage, the contact starts at one end of the tooth and gradually spreads as the gears rotate, until the two teeth are in full engagement. This gradual engagement makes helical gears operate much more smoothly and quietly than spur gears.

There are two primary failure modes for gears. First one is tooth breakage from excessive bending stress and the second one is surface pitting from excessive contact stress. In both cases, main interest is the tooth load which comes from

applied load or torque during the transmission of power. Bending stress occurs at the root of the tooth profile mainly. Bending stress is highest at the fillet and can cause breakage or fatigue failure of tooth in root region. Even though a gear tooth may not break due to bending stresses during its lifetime, it could develop pits on the tooth face due to high contact stresses fatiguing the surface by compression. The contact pressure is intensified near the pitch circle, where the contact is pure rolling with zero sliding velocity.

After the material selection for pinion and gear, the best combination of two design parameters that are *module (m)* and *face width (F)*. After defining the pinion and gear materials, module is estimated and calculations are carried out to determine the face width. Module and face width calculations are iterated until the face width is in a range of $3p \leq F \leq 5p$ where p is circular pitch that is dependent on the selected module. The iteration may require considerable time depending on the initially selected module, which is   dependent on expertise. Various design formulas are available in the machine elements or machine design text books for the design or finding "m" or "F". In addition to this, the international and national standards such as ANSI-AGMA, ISO JGMA provide different formulae with different level of difficulty. However, the results of using different approaches have not been compared so far. Thus the designer does not aware of the success or loss gained using each of the approach. Therefore, there is a need to compare the results of each of the most accepted design formula or design approach for the involute helical gear design. Hence, this study aims to compare the design results (F and m) obtained using the design formula or design approaches to determine loss or gain obtained in each of the approach. The results of this study may provide usable outputs for teaching and designers practicing gear design.

The main intention is to compare the design results given by the most commonly used gear design approaches. Hence, the designer can be aware of the success or loss gained using each of the approach. The results of the study may also

3

help to select the proper gear design approach depending on the requirements of the particular design.

An involute helical gear design has been performed at speed ratios of 1:1, 2:1, 3:1, 4:1, 5:1, 6:1, 7:1 and 8:1, in this thesis work. And these speed reductions has been carried out at different amount of power transmissions from 1 kW to 1000kW.

2. PREVIOUS STUDIES

There have been so many studies in the literature for helical gear design and stress analysis such as bending stress at the root of tooth and surface contact stress at the gear tooth surface while a pair of gear is in transmission of power.

Because of the lower dynamic load, the noise level during operation and the demand for lighter and smaller automotive transmissions, helical gears have become the subject of attention.

2.1. Verification of FEM Analysis by Making Analytical Approach

Rao, Ch Rama Mohana et al. (1993) has analyzed the stress of helical gear teeth by finite element method. They explained the geometry of helical gears by simple mathematical equations, the load distribution for various positions of the contact line and the stress analysis of helical gears using the three-dimensional finite element method.

Vishal Singh et al. (2018) have analyzed the tooth bending stresses and contact stresses in a helical gear pair which is calculated using AGMA theory and finite element analysis(FEA).They observed that the bending stresses and contact stresses, both decreases with an increase in the helix angle if pressure angle remains constant.

Patil, Santosh S. et al. (2014) have studied the contact stresses among the helical gear pairs, under static conditions, by using a 3D finite element method. The variation of contact stresses with helix angle and also with friction coefficients has been discussed. The commercial finite element software used was ANSYS and the results were compared with analytical calculations. As a result, increasing the coefficient of friction increases the contact stresses and increasing the helix angle of gear pairs decreases the contact stresses.

Chen, Yi-Cheng et al. (2002); Rao, Ch Rama Mohana et al. (1993); Tsay, Chung-Biau (1988) have analysed helical gear set stresses with localized bearing contact by using a finite element method and compared with theoretical calculations. They all have concluded that FEM is in a good agreement with analytical approaches.

In conclusion, they have analyzed the stresses of the finite elements and compares them with the theoretical calculations. All of the researchers working on the finite element method in gear design have decided that FEM results can be compared well with analytical approaches.

2.2. The studies on the Effect of Profile Modification

Wu, Yong-jun et al. (2012) have studied both static and dynamic behaviours of gear drives. At first, a precise tooth profile modification (TPM) approach of the helical gear pair is presented. The type and amount of the TPM are accurately determined by the static contact FEA results. Then dynamic contact simulations for the helical gear pairs with and without TPM are, respectively, carried out to evaluate the effect of the presented TPM approach on vibration reduction. Results show that the presented precise TPM of helical gears is effective on vibration reduction around the working load, and the dynamic contact simulation is effective in estimating the effect of the TPM on vibration reduction in the designing stage.

Zhang, Y. et al. (1997) have studied analysis of transmission errors under load of helical gears with modified tooth surfaces. This study presents a model which accommodates the modification of tooth surfaces, gear misalignments and the deformation of tooth surfaces caused by contact load. In this model, the gear contact load is assumed to be nonlinearly distributed along the direction of the relative principal curvature between the two contacting tooth surfaces. As compared with conventional tooth contact analysis (TCA) that assumes gear surfaces as rigid bodies, the model presented in this study provides more realistic

6

simulation results on the gear transmission errors and other gear meshing characteristics when the tooth surfaces are deformed under load.

Tsay, Chung-Biau (1988) has studied influence of tooth profile modification on helical gear durability. A nonlinear finite element contact mechanics model of a helical gear pair was used to study the effect of intentional tooth profile modifications on durability of helical gear pairs. Both two-dimensional (2D) and three-dimensional (3D) modifications were considered in his study. A detailed parametric study was performed to quantify the changes in the contact and bending stresses as a function of tooth profile modification parameters as compared to an unmodified gear pair baseline. The combined influence of modification parameters and torque transmitted on the maximum stresses is described.

Briefly, the pre-search on the literature has indicated that there are only limited studies on the literature and most of these are comparing the design results of individual formula with the results obtained from FEM analyses. Hence, the design results obtained by the most accepted helical gear design formula or design approach have not been compared yet.

3. MATERIAL AND METHOD

3.1. Material

Gear and pinion materials have to be selected before starting to gear design. The combination of a steel pinion and cast iron gear represent a very well-balanced design. This is because cast iron has low cost, ease of casting, good machinability, high wear resistance, and good noise abatement. Cast iron gears typically have greater surface fatigue strength than bending fatigue strength (Ugural A.C., 2003). Table 3.1 shows the selected material types in this study. Nevertheless, design of a gear based on bending fatigue failure primarily considers only pinion material properties. This is because it is the smallest and weakest one in a meshing couple during power transfer.

Table 3.1. Material properties of pinion and gear

Material Property	Pinion Type1	Pinion Type 2	Pinion Type3	Gear
Yield strength	441 MPa	1140 MPa	1640 MPa	621 MPa
Ultimate tensile strength	586 MPa	1250 MPa	1770 MPa	827 MPa
Brinell hardness number	207 HB	370	510	400 HB
Density	7850 kg ^{x} m^3	7850 kg ^{x} m^3	7850 kg ^{x} m^3	7850 kg ^{x} m^3
Poisson's ratio	0,3	0,3	0,3	0,3
Modulus of elasticity	200	200	200	170

3.2. Method

3.2.1. Helical Gear Design

In this thesis work, design of an involute helical gear has been performed based on bending fatigue failure theories according to the four most common design approaches. These are;

1. Shigley's Mechanical Engineering Design 9th Edition (Budynas R.G. and Nisbett J.K., 2011),
2. Fundamentals of Machine Component Design 5th Edition (Juvinall R.C. and Marshek K.M., 2011),
3. American Gear Manufacturers Association (ANSI/AGMA) 2001 - D04 Standard (2004) and
4. ISO Standards 6336-Part 1-3 (2006), -Part 5 (2003), -Part 6 (2004), and ISO 9085:2002 (2002).

In addition, the reliability of the obtained results have been verified by using ANSYS Workbench 15.0 after the design calculations have been carried out for each of the design approaches used in this work. The design results, module (m) and face width (F), has been determined analytically using bending fatigue failure theories according to the four most common design approaches mentioned above. Afterwards, three dimensional helical gear has been modelled on CATIA R18 with the aid of design results. Finally 3D models of helical gears have been subjected to gear stresses on ANSYS Workbench 15.0, and then numerically obtained results have been compared with analytical calculations.

Two important design parameters, module (m) and face width (F) calculations have been carried out with the four most common design approaches mentioned above. In each of the above approaches, bending fatigue failure has depended on design variables that affect the material strength and failure stresses. But it has been found out that different kinds of design approaches uses various

design variables which have to be tackled in some different ways in each of the approach.

Module and face width are two essential parameters for sizing a gear. In this study, these two important parameters have been determined based on gear stresses called as "bending stress" which is occurred in tooth root. Module selection and face width determination have been performed iteratively with the aid of design variables required for determining failure stresses considering the operating conditions while the bending stress is limited by the material strength. When the face width is in between 3p and 5p where p is the circular pitch ($\pi.m$), iteration is ended, and the last iteration step gives the proper module of the target gear set (see Figure 3.2). A comprehensive comparison has been made between four types of design approaches by defining a dimensionless geometric rating number, GR_i, in this work. Afterwards, conversion factors, CFs, for each design approach are defined with the aid of geometric rating numbers. This allows the designer to use any design approach to perform the design, and then multiply the results by CFs instead of using more complex gear design standards. A flow chart has been introduced in Figure 3.1 and Figure 3.2 with the intention of exhibiting the step by step procedure for the helical gear design used in this thesis.

```
┌─────────────────────────────────┐
│     Obtain inputs from statements │
│        of design problem          │
└─────────────────────────────────┘
                  │
                  ▼
┌─────────────────────────────────┐
│   Selection of material for a pair of │
│   gear considering the operating   │
│             conditions             │
└─────────────────────────────────┘
                  │
                  ▼
┌───────────────────────────────────────┐
│   Selection of design approaches:       │
│                                         │
│ Shigley's Mechanical Engineering Design 9th Ed. │
│                                         │
│ Fundamentals of Machine Component Design 5th Ed. │
│                                         │
│     ISO 6336, ISO 9805:2002 Standards   │
│                                         │
│     ANSI/AGMA 2001-D04 Standards        │
└───────────────────────────────────────┘
                  │
                  ▼
┌─────────────────────────────────┐
│     Carry out the design for the  │
│         selected approach          │
└─────────────────────────────────┘
                  │
                  ▼
┌─────────────────────────────────┐
│   Development of MATLAB Tool for   │
│           each design              │
└─────────────────────────────────┘
                  │
                  ▼
┌─────────────────────────────────┐
│  Obtain design results and compare │
│        m, F, GRi CFs               │
└─────────────────────────────────┘
                  │
                  ▼
┌─────────────────────────────────┐
│      Validation of results by     │
│      Finite Element Analysis       │
└─────────────────────────────────┘
                  │
                  ▼
┌─────────────────────────────────┐
│   Comparison & Recommendations     │
└─────────────────────────────────┘
```
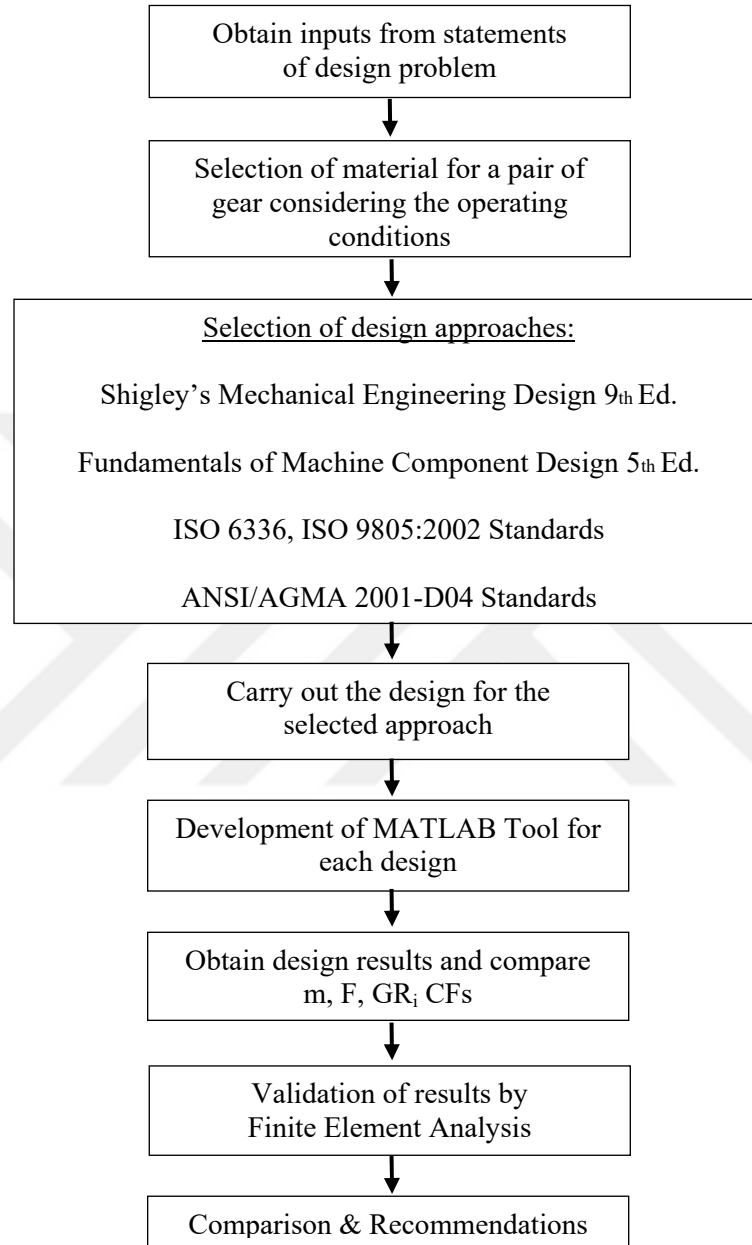
Figure 3.1. General systematic approach used for obtaining the results for the comparison of gear design approaches

```
┌──────────────────────┐        ┌──────────────────────┐
│ Estimation of a module│───────→│ Determine the number  │
│ depending upon the    │        │ of teeth on           │
│ amount of power       │        │ pinion at a certain   │
│ transmission          │        │ speed reduction       │
└──────────────────────┘        └──────────────────────┘
                                            │
                                            ↓
                                 ┌──────────────────────┐
                                 │ Find force which      │
                                 │ exerted to gear tooth │
                                 └──────────────────────┘
                                            │
                                            ↓
                                 ┌──────────────────────┐
                                 │ Determine the design  │
                                 │ variables that affect │
                                 │ the gear stresses     │
                                 └──────────────────────┘
                                            │
                                            ↓
                                 ┌──────────────────────┐
                                 │ Define a design factor│
                                 │ of safety (DFoS)      │
                                 └──────────────────────┘
                                            │
                                            ↓
                                 ┌──────────────────────┐
                                 │ Determine the strength│
                                 │ of pinion material at │
                                 │ a certain operating   │
                                 │ conditions            │
                                 └──────────────────────┘
                                            │
                                            ↓
                                 ┌──────────────────────┐
                                 │ Find the face width, F,│
                                 │ with the aid of ratio │
                                 │ of strength of pinion │
                                 │ material to DFoS      │
                                 └──────────────────────┘
                                            │
                                            ↓
                                 ┌──────────────────────┐
                                 │ Find face width, F,   │
                                 │ based on analytical   │
                                 │ methods               │
                                 └──────────────────────┘
                                            │
                                            ↓
                                        ◇ Face width, F, in the
                                          range of $3p \leq F \leq 5p$
                                   No ←──◇
                                          │ Yes
                                          ↓
                                 ┌──────────────────────┐
                                 │ Stop iteration and use│
                                 │ this module and face  │
                                 │ width                 │
                                 └──────────────────────┘
```
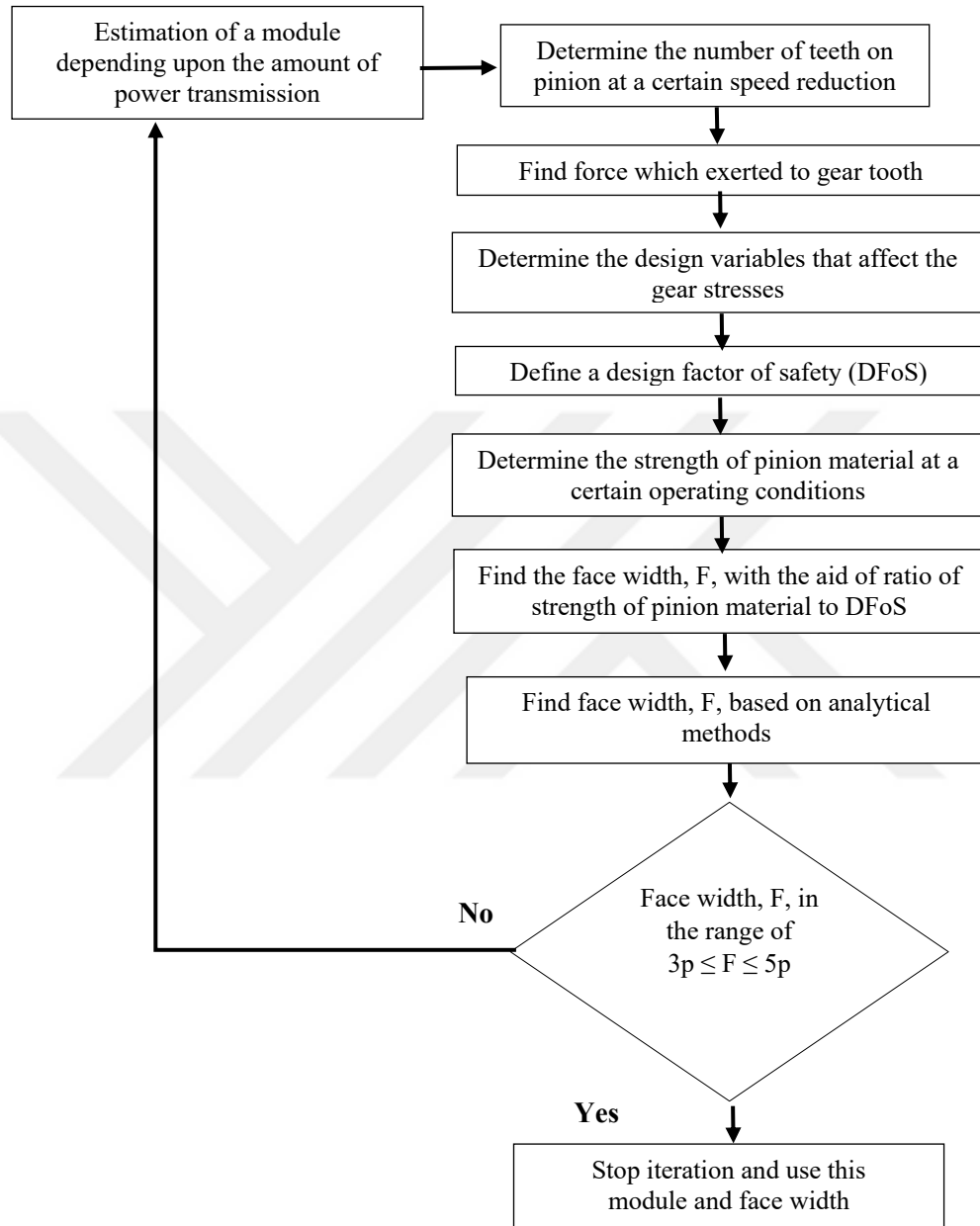
Figure 3. 2. Flow chart for the design of an involute helical gear

In each type of design approach, the operating conditions such as number of cycles, gear speed ratio, gear transmission accuracy, input speed of a power source, design factor of safety, reliability, etc. have been kept identical throughout the study. This has provided fair comparison of the results in the work.

Table 3. 2. Values for the input parameters for each design approaches

Input parameters	Value
Pressure angle Ø (°)	20° and 25°
Gear tooth geometry (standard)	Interference free involute helical, full depth teeth
Input speed of power source (rpm)	1200
Number of life cycles, N	10^8
Design factor of safety, n_d	2.1
Reliability (%)	99.9
Operating temperature, T (°C)	Moderate or low, ~120
Quality number for gears	AGMA:9 and ISO:8 B&N-J&M: shaved and ground
Material properties of gear pair	see Table 3.1
Working characteristics of driving and driven machines	Uniform
Transmitted power range	1-1000 kW
Gear speed ratio range	1:1 – 2:1 – 3:1 – 4:1 – 5:1 – 6:1 – 7:1 – 8:1

To provide the same conditions for the comparison of the results obtained from the each approaches a safety factor of 2,1 has been taken. Design of involute helical gear has been defined for a life cycles of 10^8.

Since helical gears are used as speed reducers or to transmit power and motion all calculations have been done at a gear speed ratio from 1:1 up to 8:1 which is limited speed ratio recommendation for helical gears. The results are

given by the increment of 1:1 and power transmission range is selected between 1 and 1000 kW for each of the speed ratio. All results have been plotted on a same diagram or tabulated into the same diagram for the ease of comparison. All of the calculations have been executed on MATLAB scripts. The results obtained from MATLAB was also verified for only 1:1 gear speed ratio and at 10 kW power transmissions by using numerical finite element method, ANSYS Workbench 15.0.

Gear bending stresses are going to be determined numerically for each design approach by using ANSYS software. On the other hand, analytical design results of helical gears that are modelled with the same input parameters using each design approach have also been made available. These allow us to compare them with each other. Hence, the difference is calculated by using following equation;

$$Difference = \left(\frac{Numerical - Analytical}{Analytical}\right)100 (\%) \tag{3.1}$$

In this study, only the design of pinion has been considered for the comparison of the results of the different approaches. This is because the pinion gear is the smallest and weakest member in meshing couple, and rotates more than the gear itself for the speed ratios greater than 1:1. This approach is also used commonly for the design of gears. The work aims to determine the effect of speed ratio, therefore gear speed ratios of 1:1, 2:1, 3:1, 4:1, 5:1, 6:1, 7:1 and 8:1 were considered, and for these speed ratios the minimum number of teeth on pinion has been selected to be the same and determined at the following section considering the interference-free involute profile.

3.2.2. Defining Geometric Rating Numbers (GR_i) for Design Approaches

The design data for both module and face width can be generated to obtain GR_i for the combination of many power and speed ratios. For GR_i, m times F results are combined to obtain a more like a geometrical value which may be used as a representative for the cross-sectional area at the pitch diameter (Geren N.,

Uzay Ç., Bayramoglu M., 2017). This is because half of the circular pitch ($\frac{p}{2} = \pi \frac{m}{2}$) approximately equals to tooth thickness in SI units. Hence, a dimensionless parameter, which may be called as "geometric rating number", GR_i, may be defined specifically as

$$GR_i = \frac{\frac{\pi m_i F_i}{2}}{\frac{\pi m_0 F_0}{2}} = \frac{m_i F_i}{m_0 F_0} \qquad (3.2)$$

where m_i and F_i are the module and face width obtained from each of the gear design approaches respectively, and m_0 and F_0 obtained according to the selected technical design standard. In this thesis, ANSI/AGMA 2001-D04 Gear Standards have been considered. GR_i numbers may be used to rate the design approaches for gear tooth volume or weight with respect to AGMA Standards.

3.2.3. Defining AGMA Conversion Factors (CFs) for Design Approaches

The main aim of this thesis work is to find out a correlation between commonly used design approaches (ISO, B&N, J&M) and AGMA. Therefore, conversion factors are generated to convert module (m) and face width (F) obtained from each design approaches (ISO, B&N, J&M) to AGMA standard. The mean values of conversion factors for module ($\overline{CF_{mi}}$) and face width ($\overline{CF_{Fi}}$) with their standard deviations are provided in . 3.3.

Table 3. 3. Expressions of mean and standard deviation for module and face width
(Geren N., Uzay Ç., Bayramoğlu M., 2017)

Conversion factor	Mean	Standard deviation
Module	$\overline{CF}_{mt} = \frac{1}{N}\sum_{j=1}^{N} m_i^*$	$\sigma_{CF_{mi}} = \sqrt{\frac{1}{N}\sum_{j=1}^{N}(m_{ij}^* - \overline{CF}_{mt})^2}$
Face width	$\overline{CF}_{Ft} = \frac{1}{N}\sum_{j=1}^{N} F_i^*$	$\sigma_{CF_{Fi}} = \sqrt{\frac{1}{N}\sum_{j=1}^{N}(F_{ij}^* - \overline{CF}_{Ft})^2}$

$$m_i^* = \frac{m_i}{m_{AGMA}} \quad and \quad F_i^* = \frac{F_i}{F_{AGMA}} \tag{3.3}$$

$$\overline{CF}_{mt} = \frac{m_i}{m_{c,AGMA}} \quad and \quad \overline{CF}_{Ft} = \frac{F_i}{F_{c,AGMA}} \tag{3.4}$$

where

Subscript "i" : represents each of the design approaches (ISO, B&N, J&M)

Subscript "c": represents converted value

N: number of points at selected transmitted power

m_{ij}^*: the value of m_i^* at a certain transmitted power

F_{ij}^*: the value of F_i^* at a certain transmitted power

Dimensionless number of $\overline{CF}_{mt}$ and $\overline{CF}_{Ft}$ obtained using expressions given in Table 3.3 may be used to convert the design results of the target approach to AGMA if we have m_i and F_i values for a gear designed using any of ISO, B&N, or J&M design approaches. This allows any gear designer to find converted values "$m_{c, AGMA}$" and "$F_{c, AGMA}$" using simple expressions. Total error considering converted m times F ($(mxF)_{AGMA}$) values of AGMA is obtained using a gear volume error (GV_e) expression;

$$GV_e = \left[\frac{(m\,F)_{c,AGMA} - (m\,F)_{AGMA}}{(m\,F)_{AGMA}}\right]100 \tag{3.5}$$

A flow chart has been introduced to obtain GR_i and CFs in Figure 3.3 with the intention of exhibiting the step by step procedure used in this thesis.

HELICAL GEAR DESIGN

Carry out the design process iteratively considering the all input parameters and design variables

DATA COLLECTION

Repeat to obtain design results (module (m) and face width (F)) for all combinations of gear speed reduction ratios (from 1:1 to 8:1 with increment of 1:1) and power transmissions (from 1 to 1000kW)

Obtain GR_i NUMBERS

Generate GR_{AGMA} numbers to show the similarities between the standards and to draw a useful charts for comparison

Obtain CONVERSION FACTORS

Derive correlation equations for obtaining CFs to convert the design results (m and b) from AGMA to ISO, Shigley and Juvinal R.C

Figure 3.3. General systematic approach to obtain GR_i and CFs

3.2.4. Determination of Interference-Free Pinion Gear Teeth Number

If the mating gear has more teeth than the pinion, then the smallest number of teeth, Np, on the pinion without interference is given by Budynas R.G. and Nisbett J.K. (2011),

$$N_P = \frac{2k\cos\psi}{(1+2m)\sin^2\phi_t}\left(m + \sqrt{m^2 + (1+2m)\sin^2\phi_t}\right) \qquad (3.6)$$

where

N_P :   Number of teeth for pinion

m :   Speed ratio of gear train

ϕ_n: Normal pressure angle

ϕ_t: Transverse pressure angle

ψ :   Helix angle

k: For a full depth teeth, k=1

where $m = m_G = N_G/N_P$

$$\cos\psi = \frac{\tan\phi_n}{\tan\phi_t} \qquad (3.7)$$

$\phi_n = 20^\circ$, $\psi = 30^\circ$, $\phi_t = 22.80^\circ$

The shape of the tooth in the normal plane is nearly the same as the shape of a spur gear tooth. The equivalent number of teeth (also called virtual number of teeth) is defined in below equation. It is necessary to determine Lewis form factor, Y. Determination of geometry factor, J, is also based on the virtual number of teeth.

$$N' = \frac{N}{\cos^3\psi} \qquad (3.8)$$

N' :   Virtual number of teeth

Table 3.4 provides calculated minimum number of teeth for helical pinion with corresponding virtual number of teeth for various speed ratios.

Table 3.4. Minimum number of teeth on pinion for various speed ratios

Speed ratio	Minimum number of teeth on pinion			
	$\phi_n = 20^o$		$\phi_n = 25^o$	
	N_P	N^1	N_P	N^1
1:1	$N_P = 9$	$N^1 = 14$	$N_P = 6$	$N^1 = 10$
2:1	$N_P = 10$	$N^1 = 16$	$N_P = 7$	$N^1 = 11$
3:1	$N_P = 11$	$N^1 = 17$	$N_P = 7$	$N^1 = 11$
4:1	$N_P = 11$	$N^1 = 17$	$N_P = 8$	$N^1 = 13$
5:1	$N_P = 11$	$N^1 = 17$	$N_P = 8$	$N^1 = 13$
6:1	$N_P = 11$	$N^1 = 17$	$N_P = 8$	$N^1 = 13$
7:1	$N_P = 11$	$N^1 = 17$	$N_P = 8$	$N^1 = 13$
8:1	$N_P = 11$	$N^1 = 17$	$N_P = 8$	$N^1 = 13$

3.2.5. Helical Gear Design Based on Bending Fatigue Failure

3.2.5.1. Design Approach Using ISO Standards 6336 - Part 3

These ISO Standards (ISO 6336-1, 2006; ISO 6336-3, 2006; ISO6336-5, 2003; ISO 6336-6, 2004; ISO 9085-2002, 2002) give three methods to calculate these factors included in the parts. These methods are mentioned as A, B or C in decreasing order of accuracy.

- Method -A often includes full size testing as would be appropriate in the aerospace industry.
- Method-B uses detailed calculations to correlate field data to similar designs and is the method typically used in the industrial gear market.
- Method-C is a simplified method used for narrow applications.

Tooth root stress σ_F is the maximum tensile stress at the surface in the root. Tooth root stress is calculated as

$$\sigma_F = \sigma_{F0} K_A K_V K_{F\beta} K_{F\alpha} \leq \sigma_{FP} \qquad (3.9)$$

with

$$\sigma_{F0} = \frac{F_t}{b \, m_n} Y_F Y_S Y_\beta Y_B Y_{DT} \qquad (3.10)$$

where

σ_{F0} : Nominal tooth root stress, which is the maximum local principal stress produced at the tooth root

σ_{FP} : Permissible bending stress

K_A : Application factor

K_V : Dynamic factor

$K_{F\beta}$: Face load factor for tooth root stress

$K_{F\alpha}$: Transverse load factor for tooth root stress

F_t : Nominal tangential load

b : Face width

m_n : Normal module

Y_F : Form factor

Y_S : Stress correction factor

Y_β : Helix angle factor

Y_B : Rim thickness factor

Y_{DT} : Deep tooth factor

The application factor, K_A, adjusts the nominal load F_t in order to compensate for incremental gear loads from external sources. The value of K_A is

determined from Table 3.5 which is obtained from ISO Standard 6336 - Part 6 (2004).

Table 3. 5. Application factor, K_A

Working characteristics of the driving machine	Working characteristics of the driven machine			
	Uniform	Light shocks	Moderate shocks	Heavy shocks
Uniform	1,00	1,25	1,50	1,75
Light shocks	1,10	1,35	1,60	1,85
Moderate shocks	1,25	1,50	1,75	2,00
Heavy shocks	1,50	1,75	2,00	2,25 or higher

The internal dynamic factor, K_V, relates the total tooth load, including internal dynamic effects of a multi resonance system, to the transmitted tangential tooth load. The value of K_V is determined by Equation (3.9) with the aid of Table 3.6.

$$K_V = 1 + \left[\frac{K_1}{K_A \frac{F_t}{b}} + K_2 \right] \frac{V N_1}{100} K_3 \sqrt{\frac{m^2}{1 + m^2}}$$
(3.11)

Table 3. 6. Values of factors K_1 and K_2 for calculation of K_V (ISO 6336 Part 1, 2006)

	K_1, Accuracy grades as specified in ISO 1328-1										K_2, All accuracy grades
	3	4	5	6	7	8	9	10	11	12	
Spur gears	2,1	3,9	7,5	14,9	26,8	39,1	52,8	76,6	102,6	146,3	0,0193
Helical gears	1,9	3,5	6,7	13,3	23,9	34,8	47,0	68,2	91,4	130,3	0,0087

To find K_3;

$$if \quad \frac{VN_p}{100}\sqrt{\frac{m^2}{1+m^2}} \leq 0{,}2 \rightarrow K_3 = 2 \tag{3.12}$$

$$if \quad \frac{VN_p}{100}\sqrt{\frac{m^2}{1+m^2}} \geq 0{,}2 \rightarrow K_3 = -0{,}357\frac{VN_p}{100}\sqrt{\frac{m^2}{1+m^2}} + 2{,}071 \tag{3.13}$$

The face load factors, $K_{F\beta}$ and $K_{H\beta}$, takes into account the effects of the non-uniform distribution of load over the gear face width on the surface stress ($K_{H\beta}$) and on the tooth root stress ($K_{F\beta}$).

ISO Standard 9085:2002 suggests for gear pairs without helix correction and crowning, the minimum value for $K_{H\beta}$ is 1,25 for lowest speed stages (also for single reduction gear drives) and 1,45 for all other stages. For the calculation of $K_{F\beta}$;

$$K_{F\beta} = (K_{H\beta})^{N_F} \tag{3.14}$$

$K_{F\beta}$:   Face load factor (root stress)

$K_{H\beta}$:   Face load factor (contact stress)

N_F: exponent

$$if \quad {}^b/_h \geq 3 \quad N_F = \frac{\left({}^b/_h\right)^2}{1+{}^b/_h+\left({}^b/_h\right)^2} = \frac{1}{1+{}^h/_b+\left({}^h/_b\right)^2} \tag{3.15}$$

$$if \quad {}^b/_h \leq 3 \quad N_F = 0{,}6923 \tag{3.16}$$

h: tooth height from tip to root

$$h = addendum + dedendum \tag{3.17}$$

23

$$addendum = 1 * module \tag{3.18}$$
$$dedendum = 1{,}25 * module \tag{3.19}$$

The transverse load factors, $K_{F\alpha}$ for surface stress and $K_{H\alpha}$ for tooth root stress, account for the effect of the non-uniform distribution of transverse load between several pairs of simultaneously contacting gear teeth as follows. The values for $K_{F\alpha}$ and $K_{H\alpha}$ are determined from Figure 3.4.

Table 3. 7. Transverse load factors for tooth bending stress and surface stress (Babalık F.C., 2010)

$K_A \frac{F_t}{b}$			>100 N/mm							≤100 N/mm
Quality of gear→			6	7	8	9	10	11	12	<6
Hardened	Spur	$K_{H\alpha}$								$1/Z_\varepsilon^2 \geq 1{,}2$
		$K_{F\alpha}$	1,0		1,1	1,2				$1/Y_\varepsilon \geq 1{,}2$
	Helical	$K_{H\alpha}$								$\varepsilon_\alpha/\cos^2\beta_b \geq 4$
		$K_{F\alpha}$	1,0	1,1	1,2	1,4				
Unhardened	Spur	$K_{H\alpha}$								$1/Z_\varepsilon^2 \geq 1{,}2$
		$K_{F\alpha}$	1,0				1,1	1,2		$1/Y_\varepsilon \geq 1{,}2$
	Helical	$K_{H\alpha}$								$\varepsilon_\alpha/\cos^2\beta_b \geq$
		$K_{F\alpha}$	1,0		1,1	1,2	1,4			

Form factor, Y_F, which takes into account the influence on nominal tooth root stress of the tooth form with load applied at the outer point of single pair tooth contact. The value of Y_F is determined from Figure 3.4.

z ; z_e							Profil Kaydırma Faktörü x													
	-0.6	-0.5	-0.4	-0.3	-0.2	-0.1	0	+0.1	+0.2	+0.3	+0.4	+0.5	+0.6	+0.7	+0.8	+0.9	+1.0	+1.1	+1.2	+1.3	+1.4
7																					
8												2.84									
9											2.98	2.69	2.47	2.22							
10											2.84	2.50	2.40	2.18	2.05						
11										2.99	2.73	2.52	2.34	2.16	2.04						
12									3.15	2.67	2.65	2.46	2.30	2.14	2.03	1.96					
13									2.93	2.79	2.58	2.41	2.27	2.12	2.03	1.95					
14							3.36	3.10	2.86	2.66	2.48	2.34	2.22	2.11	2.03	1.95	1.89				
15							3.25	3.01	2.79	2.60	2.44	2.31	2.20	2.10	2.02	1.95	1.89				
16					3.45	3.16	2.95	2.74	2.56	2.42	2.29	2.18	2.09	2.02	1.95	1.89	1.85				
17					3.35	3.09	2.88	2.69	2.53	2.39	2.27	2.17	2.08	2.01	1.95	1.90	1.86				
18				3.53	3.26	3.02	2.82	2.65	2.50	2.37	2.26	2.16	2.08	2.01	1.95	1.90	1.85				
19			3.72	3.44	3.20	2.96	2.78	2.61	2.47	2.35	2.24	2.15	2.07	2.01	1.95	1.90	1.87	1.83			
20			3.62	3.35	3.12	2.91	2.74	2.58	2.45	2.33	2.23	2.14	2.07	2.01	1.90	1.90	1.87	1.84			
21			3.53	3.28	3.07	2.87	2.70	2.55	2.43	2.32	2.22	2.14	2.06	2.01	1.95	1.91	1.87	1.84			
22			3.45	3.20	3.01	2.83	2.67	2.52	2.41	2.30	2.21	2.13	2.06	2.01	1.95	1.91	1.88	1.85	1.82		
23		3.54	3.38	3.15	2.96	2.80	2.64	2.50	2.39	2.29	2.20	2.12	2.06	2.00	1.95	1.91	1.88	1.85	1.83		
24		3.55	3.30	3.10	2.92	2.75	2.61	2.48	2.37	2.27	2.19	2.12	2.06	2.00	1.95	1.91	1.88	1.85	1.83	1.82	
25	3.73	3.45	3.25	3.05	2.88	2.72	2.58	2.46	2.36	2.27	2.19	2.12	2.05	2.00	1.95	1.91	1.86	1.86	1.84	1.83	
30	3.51	3.35	3.16	3.01	2.85	2.72	2.60	2.48	2.38	2.30	2.22	2.16	2.10	2.04	2.00	1.96	1.93	1.93	1.86	1.84	1.83
40	3.15	3.00	2.86	2.75	2.63	2.54	2.45	2.37	2.30	2.24	2.18	2.13	2.08	2.04	2.01	1.97	1.95	1.93	1.88	1.85	1.85
50	2.90	2.78	2.68	2.59	2.50	2.43	2.36	2.31	2.25	2.20	2.15	2.11	2.07	2.03	2.02	1.98	1.97	1.94	1.93	1.92	1.89
60	2.75	2.65	2.57	2.50	2.42	2.37	2.32	2.25	2.22	2.17	2.13	2.10	2.08	2.04	2.02	1.99	1.96	1.94	1.94	1.94	1.91
100	2.46	2.40	2.35	2.32	2.26	2.24	2.21	2.17	2.15	2.13	2.10	2.08	2.06	2.04	2.02	2.01	2.00	1.99	1.98	1.98	1.93
200	2.27	2.24	2.21	2.19	2.17	2.15	2.14	2.12	2.10	2.10	2.08	2.06	2.06	2.04	2.03	2.01	2.00	1.99	1.98	2.00	1.97
400	2.17	2.15	2.14	2.13	2.12	2.11	2.10	2.09	2.08	2.06	2.08	2.07	2.06	2.06	2.05	2.04	2.04	2.01	1.98	2.00	2.00
∞	2.07	2.07	2.07	2.07	2.07	2.07	2.07	2.07	2.07	2.07	2.07	2.07	2.07	2.07	2.07	2.07	2.07	2.07	2.07	2.07	2.07

Figure 3. 4. Tooth form factor (Babalık F.C., 2010)

The stress correction factor, Y_S, is used to convert the nominal tooth root stress to local tooth root stress and, by means of this factor, the stress amplifying effect of section change at the fillet radius at the tooth root is taken into consideration (ISO 6336-Part 3, 2006).

Form factor, Y_F, the stress correction factor, Y_S, are determined considering the number of teeth and profile shifting factor (x). The value of Y_S is determined from Figure 3.5.
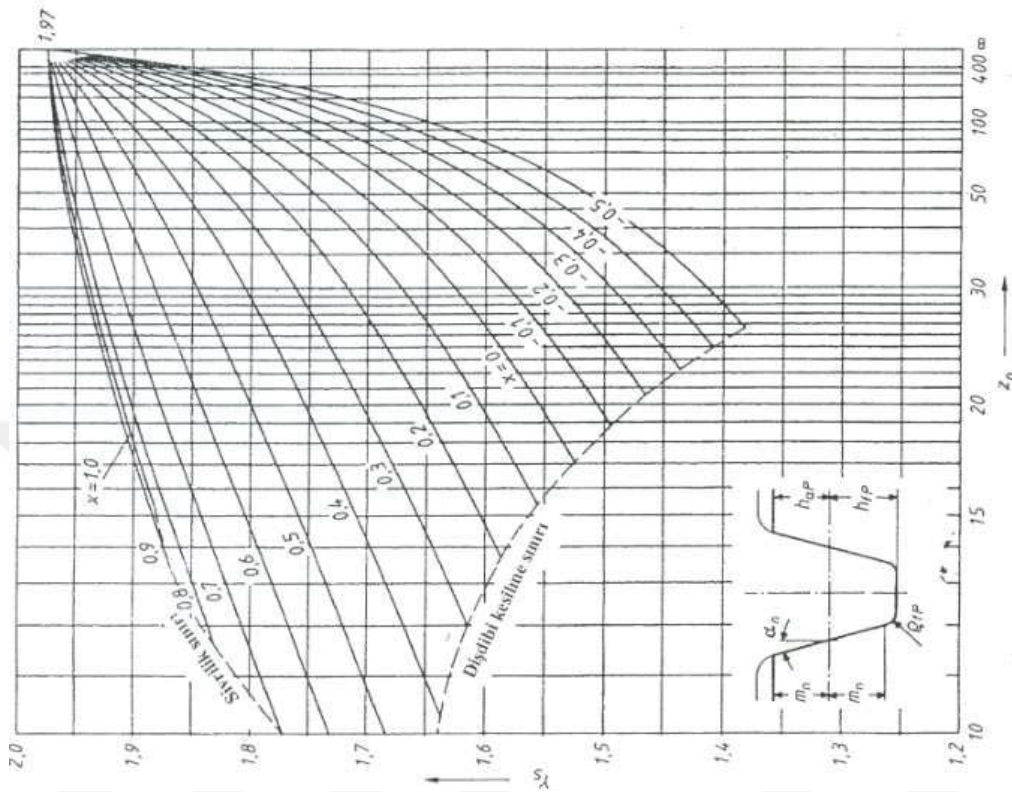
Figure 3. 5. Stress correction factor (Babalık F.C., 2010)

The factor Y_β can be calculated using Equation (3.18), which is consistent with the curves illustrated in Figure 3.6.
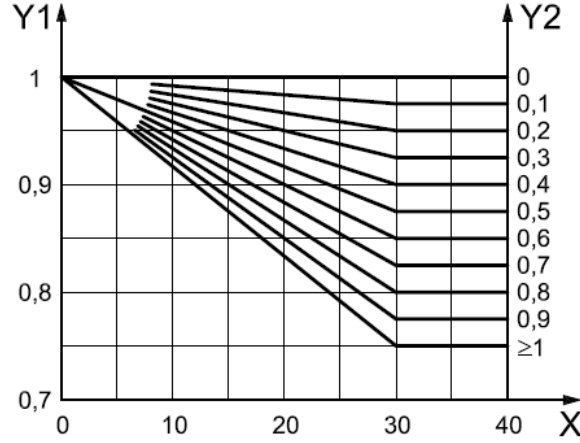
Figure 3.6. Value of helix factor, Y_β (ISO 6336 Part 3, 2006)

X   reference helix angle, β, degrees

Y1   helix factor, Y_β

Y2   overlap ratio, ε_β

$$Y_\beta = 1 - \varepsilon_\beta \frac{\beta}{120^\nu} \tag{3.20}$$

where β is the reference helix angle, in degrees. The value 1,0 is substituted for ε_β when $\varepsilon_\beta > 1,0$, and 30° is substituted for β when $\beta > 30°$. ($Y_\beta = 0,75$ when $\varepsilon_\beta = 1$)

   Where the rim thickness is not sufficient to provide full support for the tooth root, the location of bending fatigue failure may be through the gear rim, rather than at the root fillet. Y_B can be calculated using following equations and Figure 3.7.

$$if \quad \frac{S_R}{h_t} \geq 1,2 \quad then \ Y_B = 1,0 \tag{3.21}$$

$$\text{if} \quad \frac{S_R}{h_t} > 0{,}5 \quad \text{and} \quad \frac{S_R}{h_t} < 1{,}2 \qquad \text{then } Y_B = 1{,}6\ln\left(2{,}242\,\frac{h_t}{S_R}\right) \qquad (3.22)$$
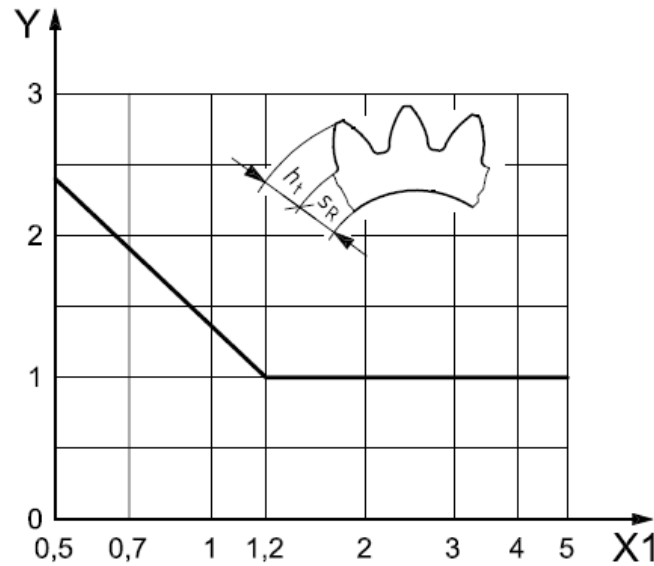
Figure 3. 7. Value of rim thickness factor (ISO 6336 Part 3, 2006), Y_B

X1   backup ratio $\frac{S_R}{h_t}$

Y   rim thickness factor Y_B

For gears of high precision (accuracy grade ≤ 4) with contact ratios in the range of $2 \leq \varepsilon_{\alpha n} < 2{,}5$ and with applied actual profile modification to obtain a trapezoidal load distribution along the path of contact, the nominal tooth root stress σ_{F0} is adjusted by the deep tooth factor, Y_{DT} which may be read from Figure 3.8.

28
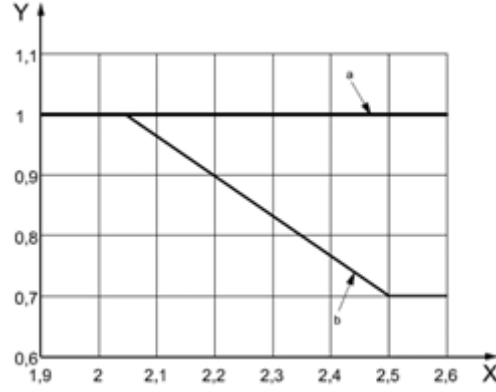
Figure 3. 8. Deep tooth factor, Y_{DT} (ISO 6336 Part 3, 2006)

X   virtual contact ratio, $\varepsilon_{\alpha n}$

Y   deep tooth factor, Y_{DT}

a   Accuracy grade > 4.

b   Accuracy grade ≤ 4.

Permissible tooth root bending stress, σ_{FP}, is calculated as;

$$\sigma_{FP} = \frac{\sigma_{Flim} Y_{ST} Y_{NT}}{S_{Fmin}} Y_{\delta relT} Y_{RrelT} Y_X$$ (3.23)

where;

σ_{Flim}:   Nominal stress number (bending) from reference test gears

Y_{ST}:   Stress correction factor

Y_{NT}:   Life factor for tooth root stress

S_{Fmin}:   Minimum required safety factor for tooth root stress

$Y_{\delta relT}$: Relative notch sensitivity factor

Y_{RrelT}: Relative surface factor

Y_X: Size factor relevant to tooth root strength

29

The nominal stress number (bending), σ_{Flim}, was determined by testing reference test gears. It is the bending stress limit value relevant to the influences of the material, the heat treatment and the surface roughness of the test gear root fillets. ISO 6336-Part 5 (2003), see Table 3.7. provides information on commonly used gear materials, methods of heat treatment and the influence of gear quality on values for nominal stress numbers which is used for nominal stress.

$$\sigma_{Flim} = Ax + B \qquad\qquad (3.24)$$

where
x is the surface hardness HBW or HV;
A, B are constants (see Table 3.8).

Table 3. 8. Factors that affect nominal stress number (ISO 6336 Part 5, 2003)

No.	Material	Stress	Type	Abbre-viation	Fig.	Quality	A	B	Hard-ness	Min. hardness	Max. hardness
1	Normalized low carbon steels/cast steels [a]	contact	wrought normalized low carbon steels	St	1 a)	ML/MQ	1,000	190	HBW	110	210
2						ME	1,520	250		110	210
3			cast steels	St (cast)	1 b)	ML/MQ	0,986	131	HBW	140	210
4						ME	1,143	237		140	210
5		bending	wrought normalized low carbon steels	St	2 a)	ML/MQ	0,455	69	HBW	110	210
6						ME	0,386	147		110	210
7			cast steels	St (cast)	2 b)	ML/MQ	0,313	62	HBW	140	210
8						ME	0,254	137		140	210
9	Cast iron materials	contact	black malleable cast iron	GTS (perl.)	3 a)	ML/MQ	1,371	143	HBW	135	250
10						ME	1,333	267		175	250
11			nodular cast iron	GGG	3 b)	ML/MQ	1,434	211	HBW	175	300
12						ME	1,500	250		200	300
13			grey cast iron	GG	3 c)	ML/MQ	1,033	132	HBW	150	240
14						ME	1,465	122		175	275
15		bending	black malleable cast iron	GTS (perl.)	4 a)	ML/MQ	0,345	77	HBW	135	250
16						ME	0,403	128		175	250
17			nodular cast iron	GGG	4 b)	ML/MQ	0,350	119	HBW	175	300
18						ME	0,380	134		200	300
19			grey cast iron	GG	4 c)	ML/MQ	0,256	8	HBW	150	240
20						ME	0,200	53		175	275
21	Through hardened wrought steels [b]	contact	carbon steels	V	5	ML	0,963	283	HV	135	210
22						MQ	0,925	360		135	210
23						ME	0,838	432		135	210
24			alloy steels	V	5	ML	1,313	188	HV	200	360
25						MQ	1,313	373		200	360
26						ME	2,213	260		200	390
27		bending	carbon steels	V	6	ML	0,250	108	HV	115	215
28						MQ	0,240	163		115	215
29						ME	0,283	202		115	215
30			alloy steels	V	6	ML	0,423	104	HV	200	360
31						MQ	0,425	187		200	360
32						ME	0,358	231		200	390

Table 3.8.(continued)

No.	Material	Stress	Type	Abbre-viation	Fig.	Quality	A	B	Hard-ness	Min. hardness	Max. hardness
33	Through hardened cast steels	contact	carbon steels	V	7	ML/MQ	0,831	300	HV	130	215
34				(cast)		ME	0,951	345		130	215
35			alloy steels	V	7	ML/MQ	1,276	298	HV	200	360
36				(cast)		ME	1,350	356		200	360
37		bending	carbon steels	V	8	ML/MQ	0,224	117	HV	130	215
38				(cast)		ME	0,286	167		130	215
39			alloy steels	V	8	ML/MQ	0,364	161	HV	200	360
40				(cast)		ME	0,356	186		200	360
41	Case hardened wrought steels [c]	contact		Eh	9	ML	0,000	1 300	HV	600	800
42						MQ	0,000	1 500		660	800
43						ME	0,000	1 650		660	800
44		bending	core hardness:	Eh	10	ML	0,000	312	HV	600	800
45			⩾ 25 HRC, lower			MQ	0,000	425		660	800
46			⩾ 25 HRC, upper				0,000	461		660	800
47			⩾ 30 HRC				0,000	500		660	800
48						ME	0,000	525		660	800
49	Flame or induction hardened wrought and cast steels	contact		IF	11	ML	0,740	602	HV	485	615
50						MQ	0,541	882		500	615
51						ME	0,505	1 013		500	615
52		bending		IF	12	ML	0,305	76	HV	485	615
53						MQ	0,138	290		500	570
54							0,000	369		570	615
55						ME	0,271	237		500	615
56	Nitrided wrought steels/nitriding steels [d] /through hardening steels [b] nitrided	contact	nitriding steels (a)	NT (nitr.)	13 a)	ML	0,000	1 125	HV	650	900
57						MQ	0,000	1 250		650	900
58						ME	0,000	1 450		650	900
59			through hardening steels (b)	NV (nitr.)	13 b)	ML	0,000	788	HV	450	650
60						MQ	0,000	998		450	650
61						ME	0,000	1 217		450	650
62		bending	nitriding steels (a)	NT (nitr.)	14 a)	ML	0,000	270	HV	650	900
63						MQ	0,000	420		650	900
64						ME	0,000	468		650	900
65			through hardening steels (b)	NV (nitr.)	14 b)	ML	0,000	258	HV	450	650
66						MQ	0,000	363		450	650
67						ME	0,000	432		450	650
68	wrought steels nitro-carburized [e]	contact	through hardening steels	NV (nitro-car.)	15	ML	0,000	650	HV	300	650
69						MQ/ME	1,167	425		300	450
70							0,000	950		450	650
71		bending	through hardening steels	NV (nitro-car.)	16	ML	0,000	224	HV	300	650
72						MQ/ME	0,653	94		300	450
73							0,000	388		450	650

[a]   In accordance with ISO 4948-2.
[b]   In accordance with ISO 683-1.
[c]   In accordance with ISO 683-11.
[d]   In accordance with ISO 683-10.
[e]   In accordance with ISO 683-1, ISO 683-10 or ISO 683-11.

32

For the calculation of stress correction factor, Y_{ST}, the ISO Standard recommends that the tooth root stress limit values for materials, according to ISO 6336 - Part 5 (2003), were derived from results of tests of standard reference test gears for which either $Y_{ST} = 2,0$ or for which test results were recalculated to this value.

The life factor, Y_{NT}, accounts for the higher tooth root stress, which may be tolerable for a limited life (number of load cycles), as compared with the allowable stress at 3×10^6 cycles. Y_{NT} may be read from Figure 3.9.
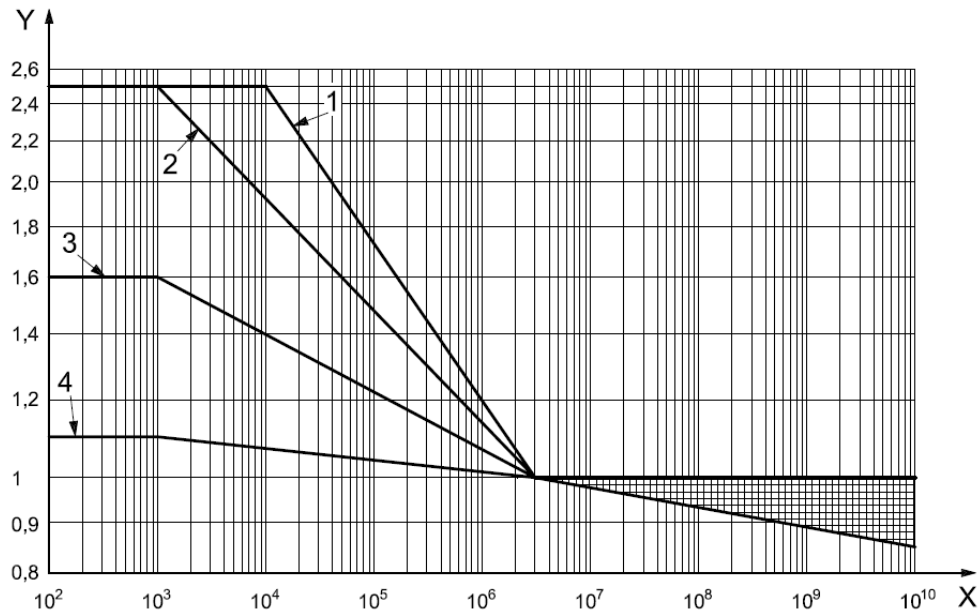
Figure 3.9. Life factor for number of load cycles (ISO 6336 Part 3, 2006)

X   number of load cycles, NL

Y   life factor, YNT

1	GTS (perl.), St, V, GGG (perl. bai.)	2	Eh, IF (root)
3	NT, NV (nitr.), GGG (ferr.), GG	4	NV (nitrocar.)

Relative notch sensitivity factor, $Y_{\delta relT}$, which is the quotient of the notch sensitivity factor of the gear of interest divided by the standard test gear factor and which enables the influence of the notch sensitivity of the material to be taken into account. The reference value $Y_{\delta relT} = 1{,}0$ for the standard reference test gear coincides with the stress correction factor $Y_S = 2{,}0$. $Y_{\delta relT}$ may be read from Figure 3.10.
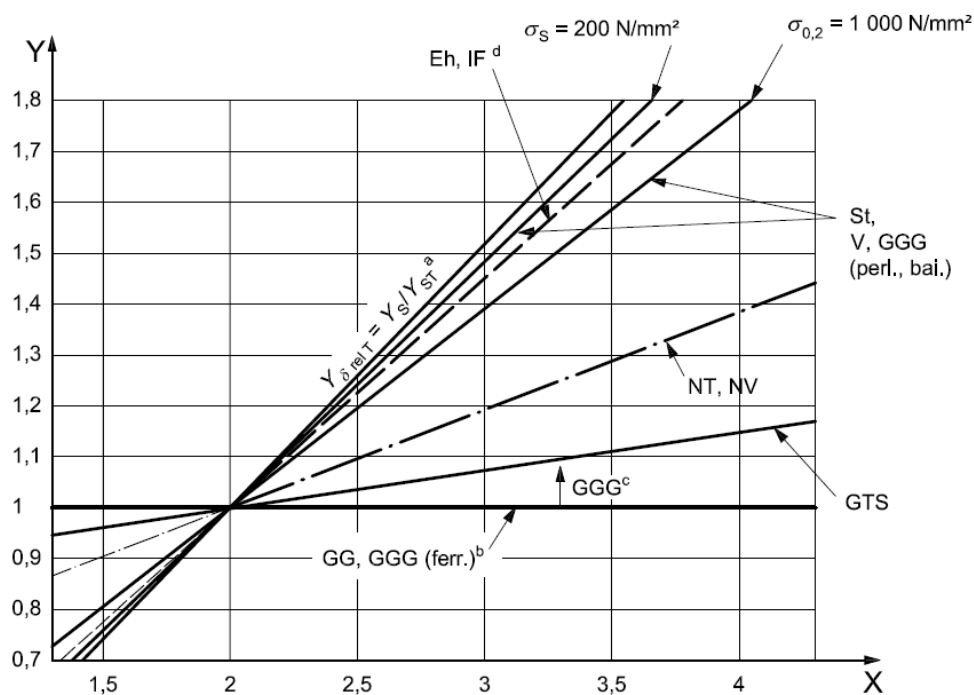
Figure 3. 10. Relative notch sensitivity factor (ISO 6336 Part 3, 2006)

X   stress correction factor, Y_S

Y   relative notch sensitivity factor, $Y_{\delta relT}$, for static stress

a   Fully insensitive to notches.

b   Fully sensitive to notches.

c   With increasingly pearlitic structure.

d   (root).

For Eh and IF(root) with stress up to crack initiation:

$$Y_{\delta relT} = 0{,}44 Y_S + 0{,}12 \tag{3.25}$$

Equation is consistent with the curve in Figure 3.10.

The surface factor, Y_{RrelT}, accounts for the influence on tooth root stress of the surface condition in the tooth roots.

For V, GGG (perl., bai.), Eh and IF (root) :

$$Y_{RrelT} = 1{,}674 - 0{,}529(R_z + 1)^{0,1} \quad 1\,\mu m < R_z < 40\,\mu m \tag{3.26}$$

The size factor, Y_X, is used to take into consideration on the influence of size on the probable distribution of weak points in the structure of the material, the stress gradients, which, in accordance with strength of materials theory, decrease with increasing dimensions, the quality of the material as determined by the extent and effectiveness of forging, the presence of defects, etc. Y_X may be determined from Table 3.9.

Table 3.9. Size factor (root), Y_X (ISO 6336 Part3, 2006)

Material [a]		Normal module, m_n	Size factor, Y_X
St, V, GGG (perl., bai.), GTS (perl.),		$m_n \leqslant 5$ $5 < m_n < 30$ $30 \leqslant m_n$	$Y_X = 1{,}0$ $Y_X = 1{,}03 - 0{,}006\,m_n$ $Y_X = 0{,}85$
Eh, IF (root), NT, NV	For 3×10^6 cycles	$m_n \leqslant 5$ $5 < m_n < 25$ $25 \leqslant m_n$	$Y_X = 1{,}0$ $Y_X = 1{,}05 - 0{,}01\,m_n$ $Y_X = 0{,}8$
GG, GGG (ferr.)		$m_n \leqslant 5$ $5 < m_n < 25$ $25 \leqslant m_n$	$Y_X = 1{,}0$ $Y_X = 1{,}075 - 0{,}015\,m_n$ $Y_X = 0{,}7$
All materials for static stress		—	$Y_X = 1{,}0$
[a] See ISO 6336-1:2006, Table 2 for an explanation of the abbreviations used.			

3.2.5.2. Design Approach Using ANSI/AGMA 2001 - D04 Standards

ANSI/AGMA 2001 - D04 (2004) Standards provide a simpler gear design approach than ISO 6336. The fundamental formula for bending stress number in a gear tooth is given by ANSI/AGMA 2001 - D04 (2004):

$$\sigma_F = F_t K_o K_v K_s \frac{1}{b \, m_t} \frac{K_m K_B}{Y_J} \qquad (3.27)$$

where

σ_F: Bending stress number, N/mm^2

F_t: Transmitted tangential load, N

K_o: Overload factor

K_v: Dynamic factor

K_s: Size factor

b: Net face width of narrowest member, mm

m_t: Transverse metric module, m_n, for spur gears

K_B: Rim thickness factor

Y_J: Geometry factor for bending strength

K_m: Load distribution factor

The overload factor, K_o, is intended to make allowance for all externally applied loads in excess of the nominal tangential load F_t in a particular application (ANSI/AGMA 2001 - D04, 2004).

The value of K_o can be read from Table 3.10.

Table 3. 10. Overload correction factor, K_o(Shigley J.E., 1985)

Source of Power	Driven Machinery		
	Uniform	Moderate Shock	Heavy Shock
Uniform	1,00	1,25	1,75
Light shock	1,25	1,50	2,00
Medium shock	1,50	1,75	2,25

Dynamic factor, K_v, accounts for internally generated gear tooth loads which are induced by non-conjugate meshing action of the gear teeth (ANSI/AGMA 2001 - D04, 2004).

$$K_v = \left(\frac{A + \sqrt{200V_t}}{A}\right)^B \tag{3.28}$$

$$A = 50 + 56(1 - B) \quad for \ 5 \le Q_v \le 11 \tag{3.29}$$

$$B = 0.25(12 - Q_v)^{0.667} \tag{3.30}$$

where

Q_v is the transmission accuracy level number.
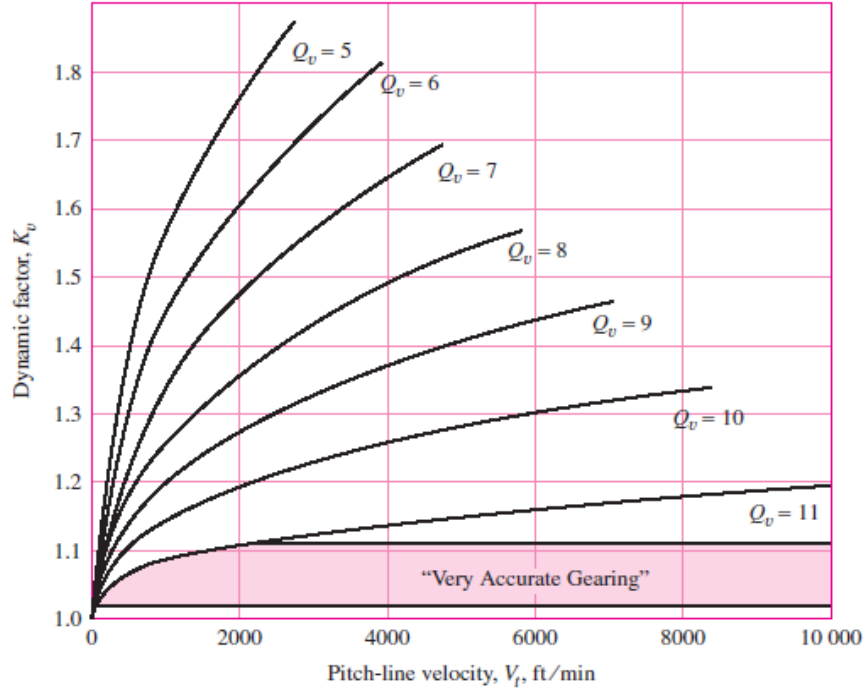
Figure 3.11. Dynamic factor K_v as a function of pitch-line speed for graphical estimates of K_v. (ANSI/AGMA 2001-D04, Annex A)

The size factor, K_s, reflects non-uniformity of material properties. It depends primarily on tooth size, diameter of parts, ratio of tooth size to diameter of part, face width, area of stress pattern, and ratio of case depth to tooth size, hardenability and heat treatment of materials (ANSI/AGMA 2001 - D04, 2004).

The load distribution factor K_m, is defined as the peak load intensity divided by the average, or uniformly distributed, load intensity; i.e., the ratio of peak to mean loading (ANSI/AGMA 2001 - D04, 2004).

$$K_m = C_{mf} = 1 + C_{mc}(C_{pf}C_{pm} + C_{ma}C_e) \tag{3.31}$$

where

$$C_{mc} = \begin{cases} 1 & for\ uncrowned\ teeth \\ 0,8 & for\ crowned\ teeth \end{cases} \tag{3.32}$$

38

$$C_{pf} = \begin{cases} \dfrac{F}{10\,d} - 0.025 & F \le 25 \text{ mm} \\[2mm] \dfrac{F}{10\,d} - 0.0375 + 4.92(10^{-4})F & 25 < F \le 425 \text{ mm} \\[2mm] \dfrac{F}{10\,d} - 0.1109 + 8.15(10^{-4})F - 3.53(10^{-7})F^2 & 425 < F \le 1000 \text{ mm} \end{cases} \qquad (3.33)$$

$$C_{pm} = \begin{cases} 1 & for\ straddle - mounted\ pinion\ with\ {}^{S_1}/_S < 0.175 \\ 1.1 & for\ straddle - mounted\ pinion\ with\ {}^{S_1}/_S \ge 0.175 \end{cases} \qquad (3.34)$$

The definition of S and S_1 used in evaluating C_{pm} is illustrated in Figure 3.12.
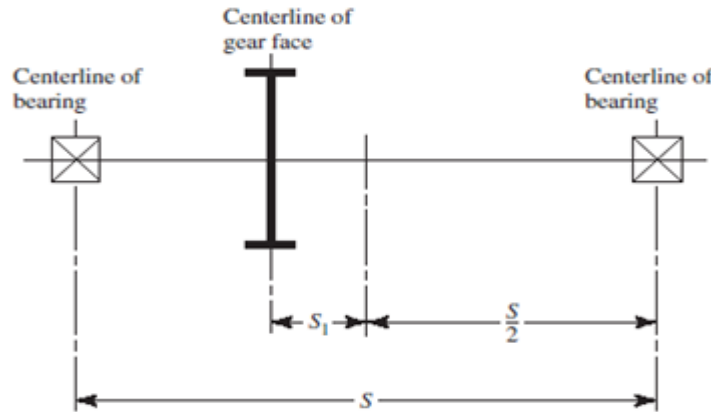
Figure 3.12. Definition of distances S and S_1 used in evaluating C_{pm}. (ANSI/AGMA 2001-D04, 2004.)

where

S_1:   Offset of the pinion; i.e., the distance from the bearing span centerline to the pinion mid face

S: Bearing span; i.e., the distance between the bearing center lines

K_m :   Load distribution factor

C_{mf} :   Face load-distribution factor

C_{pf} :   Pinion proportion factor

C_{mc} :   Load correction factor

C_{pm} :   Pinion proportion modifier

C_e :   Mesh alignment correction factor

C_{ma} :   Mesh alignment factor

$$C_{mc} = 1 \; for \; uncrowned \; teeth \qquad (3.35)$$

$$C_{pm} = 1 \qquad (3.36)$$

$$C_e - 1 \qquad (3.37)$$

$$C_{ma} = A + BF + CF^2 \qquad (3.38)$$

For precision, enclosed units (see Table 3.11),

$$A = 0,0675 \,; B = 0,0128 \,; C = -0,926(10^{-4}) \qquad (3.39)$$

Table 3. 11. Empirical Constants A, B, and C. Face width F in Inches[*]
(ANSI/AGMA 2001-D04, 2004).

Condition	A	B	C
Open gearing	$2,47x10^{-1}$	$0,167x10^{-4}$	$-0,765x10^{-4}$
Commercial enclosed gear units	$1,27x10^{-1}$	$0,158x10^{-4}$	$-0,930x10^{-4}$
Precision enclosed gear units	$0,675x10^{-1}$	$0,128x10^{-4}$	$-0,926x10^{-4}$
Extra precision enclosed gear units	$0,0360x10^{-1}$	$0,102x10^{-4}$	$-0,822x10^{-4}$

[*]See ANSI/AGMA 2001-D04, pp. 20-22, for SI formulation.

The mesh alignment correction factor, C_e, is used to modify the mesh alignment factor when the manufacturing or assembly techniques improve the effective mesh alignment.

$$C_e = \begin{cases} 0{,}8 & \text{for gearing adjusted at assembly, or compatibility} \\ & \text{is improved by lapping, or both} \\ 1 & \text{for all other conditions} \end{cases}$$

The rim thickness factor, K_B, adjusts the calculated bending stress number for thin rimmed gears (ANSI/AGMA 2001 - D04, 2004). K_B may be read from Figure 3.13 as a function of the backup ratio, m_B,

$$m_B = \frac{t_R}{h_t} \tag{3.40}$$

where

t_R: gear rim thickness below the tooth root, mm

h_t: gear tooth whole depth, mm
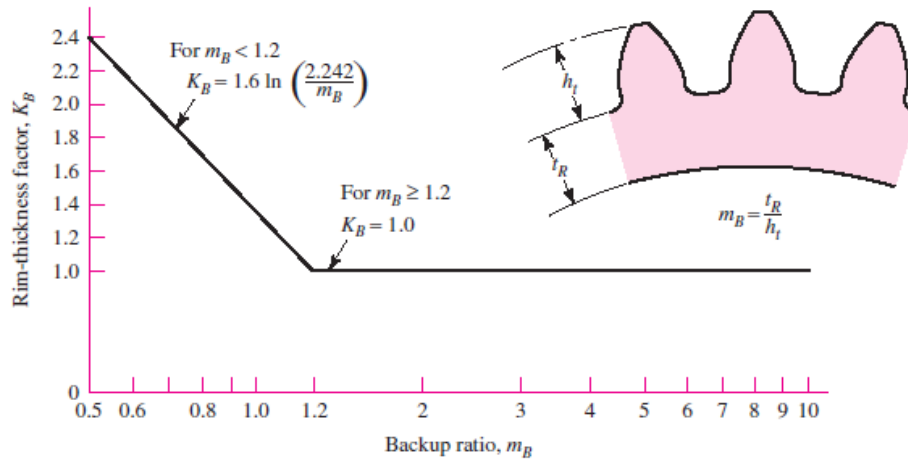
Figure 3. 13. Rim thickness factor K_B. (ANSI/AGMA 2001-D04.)

41

The bending strength geometry factor, Y_J, takes into account the effects of shape of the tooth, worst load position, stress concentration and load sharing between oblique lines of contact in helical gears (ANSI/AGMA 2001 D04, 2004). Y_J may be read from Figure 3.14.
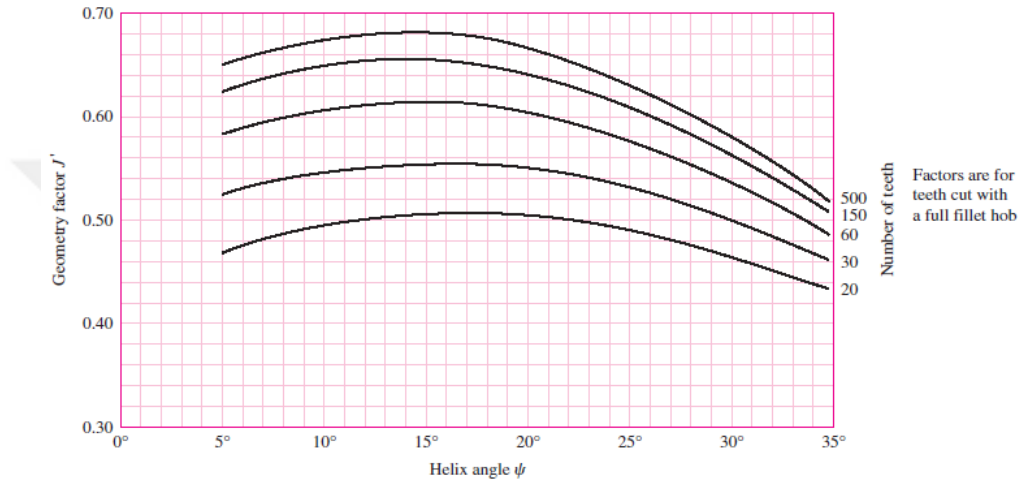
Figure 3.14. Helical gear geometry factors J' (Y_J). *Source:* The graph is from AGMA 218.01, which is consistent with tabular data from the current AGMA 908-B89 (1989). The graph is convenient for design purposes.

The relation of calculated bending stress number to allowable bending stress number is;

$$\sigma_F \leq \frac{\sigma_{FP} Y_N}{S_F Y_\theta Y_Z}$$ (3.41)

where

σ_{FP}:   Allowable bending stress number, N/mm^2

Y_N: Stress cycle factor for bending strength

S_F: Safety factor for bending strength

Y_θ: Temperature factor

Y_Z: Reliability factor

42

The allowable stress numbers, σ_{FP}, for gear materials vary with items such as material composition, cleanliness, residual stress, microstructure, quality, heat treatment, and processing practices (ANSI/AGMA 2001-D04, 2004).
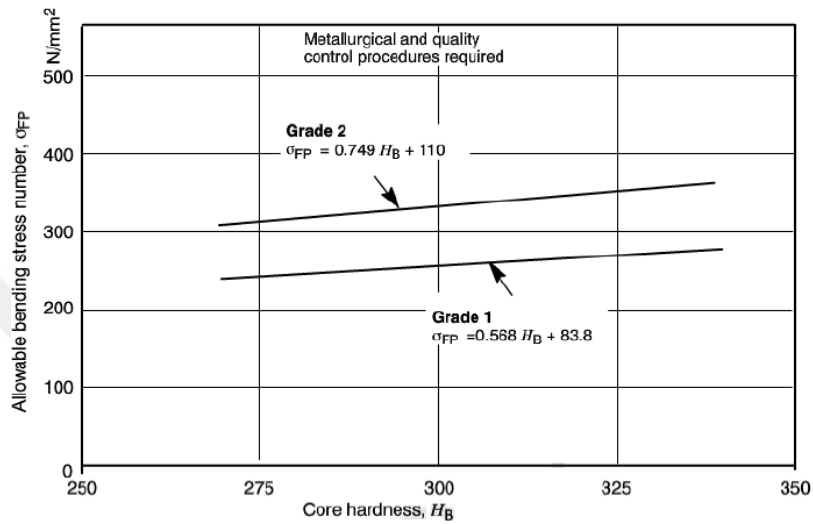
Figure 3. 15. Allowable bending stress numbers for nitrided through hardened steel gears (i.e., AISI 4140, AISI 4340), σ_{FP}, (ANSI/AGMA 2001 – D04, 2004).

The stress cycle factors, Y_N, adjust the allowable stress numbers for the required number of cycles of operation (ANSI/AGMA 2001 - D04, 2004). The stress cycle factors, Y_N, may be read from Figure 3.16.
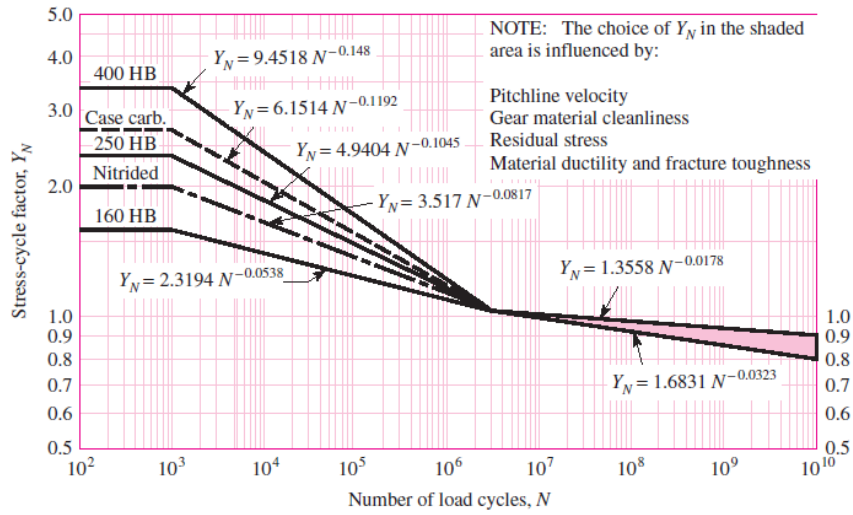
Figure 3.16. Bending strength stress-cycle factor, Y_N (ANSI/AGMA 2001-D04, 2004).

For moderate and low temperature operations, the temperature factor, Y_θ, is generally taken as unity when gears operate with temperatures of oil or gear blank not exceeding 120°C (ANSI/AGMA 2001 - D04, 2004).

The reliability factors, Y_Z, account for the effect of the normal statistical distribution of failures found in materials testing and may be read from Figure 3.17.

Reliability	K_R (Y_Z)
0.9999	1.50
0.999	1.25
0.99	1.00
0.90	0.85
0.50	0.70

Figure 3.17. Reliability Factors Y_Z (ANSI/AGMA 2001-D04.)

3.2.5.3. Design Approach Using Shigley's Mechanical Engineering Design 9th Edition

The procedure is mainly similar to the previous one but some differences exist for the factors. Failure by bending will occur when the significant tooth stress equals or exceeds either the yield strength or the bending endurance strength. Allowable bending stress has been equalized to fully corrected endurance strength of gear tooth by considering the selected design factor of safety.

$$\sigma_{all} = \frac{K_v W^t}{F\,m\,Y}$$
(3.42)

and

$$S_e = n_d \sigma_{all}$$
(3.43)

where

σ_{all}:   Allowable bending stress

W^t: Tangential component of load, in N

K_v: Dynamic factor

F: Face width, in mm

m: Module, in mm

Y: Lewis form factor

S_e: Fully corrected endurance strength

n_d: Design factor of safety

When a pair of gears is driven at moderate or high speed and noise is generated, it is certain that dynamic effects are present. For gears with shaved or ground profile;

$$K_v = \sqrt{\frac{5{,}56 + \sqrt{V}}{5{,}56}}$$
(3.44)

Lewis form factor, Y, is determined from the Table 3.12.

45

Table 3. 12. Values of the Lewis Form Factor Y (Budynas R.G. and Nisbett J.K., 2011)

Number of Teeth	Y	Number of Teeth	Y
12	0.245	28	0.353
13	0.261	30	0.359
14	0.277	34	0.371
15	0.290	38	0.384
16	0.296	43	0.397
17	0.303	50	0.409
18	0.309	60	0.422
19	0.314	75	0.435
20	0.322	100	0.447
21	0.328	150	0.460
22	0.331	300	0.472
24	0.337	400	0.480
26	0.346	Rack	0.485

Fully corrected endurance strength is calculated as;

$$S_e = k_a k_b k_c k_d k_e k_f S_e'$$ (3.45)

where

k_a: Surface condition modification factor,

k_b: Size modification factor

k_c: Load modification factor

k_d: Temperature modification factor

k_e: Reliability factor

k_f: Miscellaneous effects modification factor

S_e':   Rotary-beam test specimen endurance limit

Surface factor, k_a;

$$k_a = a S_{ut}^b$$ (3.46)

where a and b are determined from Table 3.13.

Table 3. 13. Parameters for marin surface modification factor (Budynas R.G. and Nisbett J.K., 2011)

Surface Finish	Factor a		Exponent b
	S_{ut}, kpsi	S_{ut}, MPa	
Ground	1.34	1.58	−0.085
Machined or cold-drawn	2.70	4.51	−0.265
Hot-rolled	14.4	57.7	−0.718
As-forged	39.9	272.	−0.995

Size factor, k_b;

$$k_b = 0,904(b\ m\sqrt{\overline{Y}})^{0.086} \tag{3.47}$$

where b is the face width, m is the module and Y is the Lewis form factor.

Loading factor, $k_c - 1$ for bending.

$$k_c = \begin{Bmatrix} 1 & bending \\ 0,85 & axial \\ 0,59 & torsion \end{Bmatrix} \tag{3.48}$$

Temperature factor, k_d may be determined from following Equation (3.47) or Table 3.14 according to operation temperature.

$$k_d = \frac{S_T}{S_{RT}} \tag{3.49}$$

S_T: Tensile strength at operating temperature

S_{RT}:   Tensile strength at room temperature

Table 3. 14. Effect of operating temperature on the Tensile Strength of steel Budynas R.G. and Nisbett J.K., 2011)

Temperature, °C	S_T/S_{RT}	Temperature, °F	S_T/S_{RT}
20	1.000	70	1.000
50	1.010	100	1.008
100	1.020	200	1.020
150	1.025	300	1.024
200	1.020	400	1.018
250	1.000	500	0.995
300	0.975	600	0.963
350	0.943	700	0.927
400	0.900	800	0.872
450	0.843	900	0.797
500	0.768	1000	0.698
550	0.672	1100	0.567
600	0.549		

Reliability factors, k_e may be determined using Table 3.15.

Table 3. 15. Reliability factors k_e corresponding to 8 percent standard deviation of the Endurance Limit (Budynas R.G. and Nisbett J.K., 2011)

Reliability, %	Transformation Variate z_a	Reliability Factor k_e
50	0	1.000
90	1.288	0.897
95	1.645	0.868
99	2.326	0.814
99.9	3.091	0.753
99.99	3.719	0.702
99.999	4.265	0.659
99.9999	4.753	0.620

Miscellaneous effects factor, k_f, for stress concentration is estimated as 1,66.

Rotary-beam test specimen endurance limit is determined as follow;

$$S'_{ut} = 0{,}5S_{ut} \quad for \quad S_{ut} < 1400 \, MPa \tag{3.50}$$

48

The textbook recommends that the Equation (3.40) is important because it forms the basis for the AGMA approach to the bending strength of gear teeth.

3.2.5.4. Design Approach Using Fundamentals of Machine Component Design 5th Edition

The design approach given by Juvinall R.C. and Marshek K.M. (2011) slightly differs to the previous ones for bending fatigue failure. This approach recommends that in the absence of more specific information, the factors affecting gear tooth bending stress can be taken into account by embellishing the Lewis equation to the following form;

$$\sigma - \frac{F_t}{m\, b\, J} K_v K_o (0.93 K_m)$$
(3.51)

where

σ: Bending fatigue stress,

m: Module,

b: Face width,

J: Helical gear geometry factor, determined from Figure 3.18. This factor includes the Lewis form factor Y and also a stress concentration factor.

K_v: Velocity or dynamic factor that indicating the severity of impact as successive pairs of teeth engage. This is a function of pitch line velocity and manufacturing accuracy. Gears with shaved or ground profile, it is calculated from Figure 3.19.

K_o: Overload factor that reflecting the degree of non-uniformity of driving and load torques. In the absence of better information, the values in Table 3.16 have long been used as a basis for rough estimates.

K_m: Mounting factor that reflecting the accuracy of mating gear alignment. Table 3.17 is used as a basis for rough estimates.
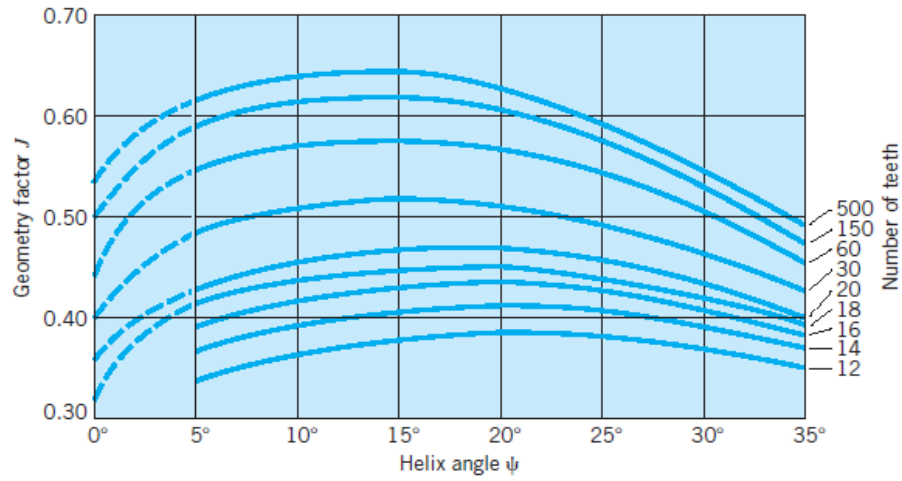
Figure 3. 18. Geometry factor J (Juvinall R.C., Marshek K.M., 2011)
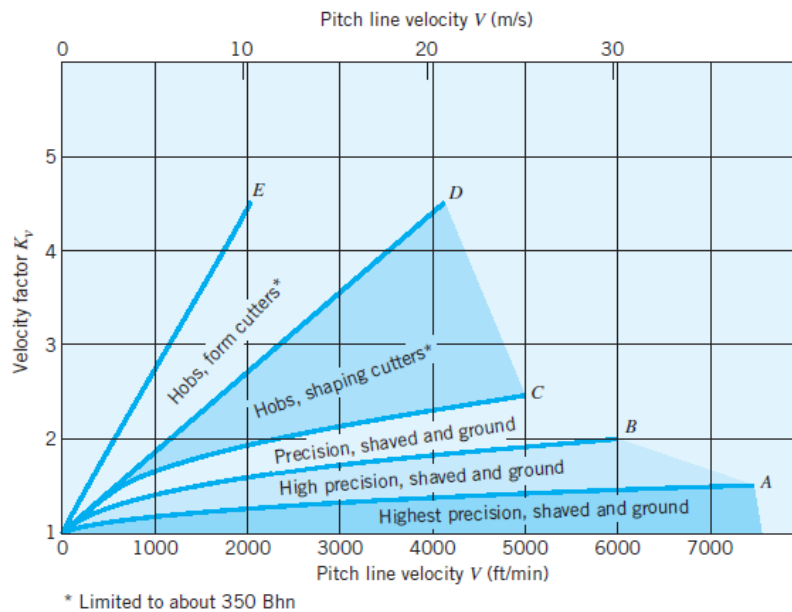
Figure 3. 19. Velocity factor K_v (Juvinall R.C., Marshek K.M., 2011)

$$K_v = \frac{78 + \sqrt{V}}{78} \qquad V \text{ is in feet per minute.} \qquad (3.52)$$

50

Table 3. 16. Overload Correction Factor K_o (Juvinall R.C., Marshek K.M., 2011)

Source of Power	Driven Machinery		
	Uniform	Moderate Shock	Heavy Shock
Uniform	1.00	1.25	1.75
Light shock	1.25	1.50	2.00
Medium shock	1.50	1.75	2.25

Introduction of the constant 0.93 with the mounting factor reflects the slightly lower sensitivity of helical gears to mounting conditions.

Table 3. 17. Mounting Correction Factor K_m (Juvinall R.C., Marshek K.M., 2011)

Characteristics of Support	Face Width (in.)			
	0 to 2	6	9	16 up
Accurate mountings, small bearing clearances, minimum deflection, precision gears	1.3	1.4	1.5	1.8
Less rigid mountings, less accurate gears, contact across the full face	1.6	1.7	1.8	2.2
Accuracy and mounting such that less than full-face contact exists	Over 2.2			

The effective fatigue stress from Equation (3.49) must be compared with the corresponding fatigue strength. For infinite life, the appropriate endurance limit is estimated from the following equation;

$$S_n = S_n' C_L C_G C_S k_r k_t k_{ms} \tag{3.53}$$

where

S_n':   Standard R. R. Moore endurance limit.

For steel $S_n' = (0,5)S_{ut}$ and

for other ductile materials $S_n' = (0,7)S_{ut}$

C_L: Load factor = 1,0 for bending loads

C_G: Gradient factor = 1,0 for P>5 (m<0,2), and 0,85 for P≤5 (m≥0,2)

51

C_S: Surface factor, Figure 3.20. Be sure that this pertains to the surface in the fillet, where a fatigue crack would likely start. (In the absence of specific information, assume this to be equivalent to a machined surface).

k_r: Reliability factor from Table 3.18.

k_t: Temperature factor. For steel gears use $k_t = 1,0$ if the temperature (usually estimated on the basis of lubricant temperature) is less than 160°F.

k_{ms}:   Mean stress factor. Use 1,0 for idler gears (subjected to two way bending) and 1,4 for input and output gears (one way bending).
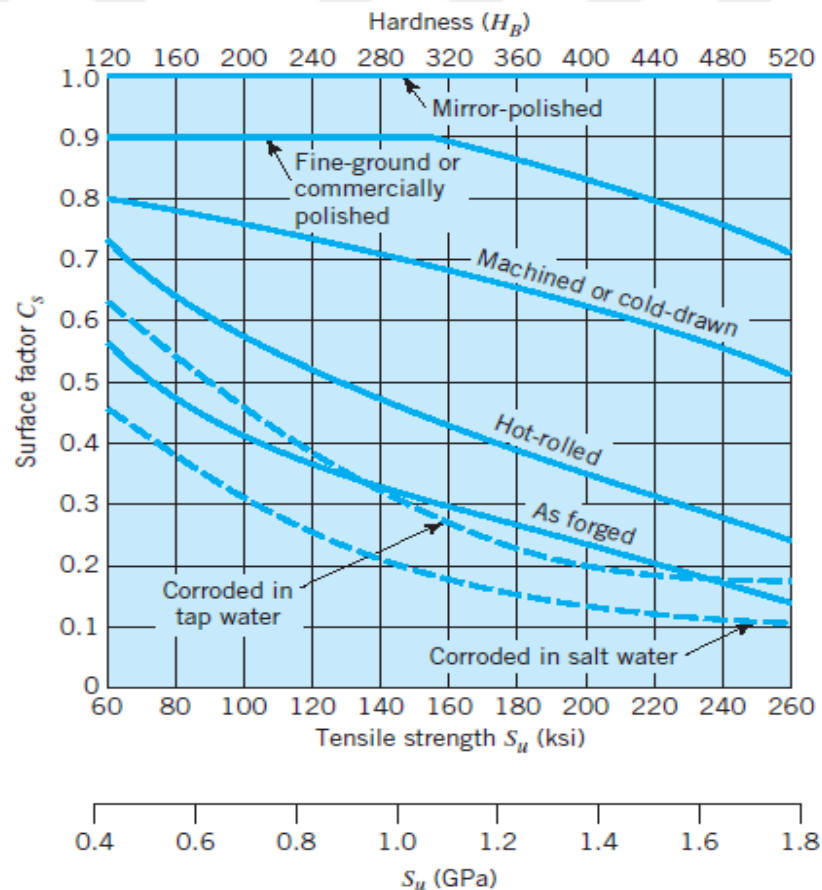
Figure 3. 20. Surface factor, C_S (Juvinall R.C., Marshek K.M., 2011)

52

Table 3. 18. Reliability factor, k_r (Juvinall R.C., Marshek K.M., 2011)

Reliability (%)	50	90	99	99,9	99,99	99,999
Factor k_r	1,000	0,897	0,814	0,753	0,702	0,659

Module selection and face width calculations were carried out based on bending fatigue failure. Table 3.19 provides fatigue bending stress, fatigue strength and face width equations for each design approach used in thesis work. Symbolic notations are kept same as in the original design approaches. The face width abbreviation "F" was used for the conversion factors throughout this text.

Table 3.19. Equations for bending stress for each design approach

Design Approaches	Fatigue bending stress	Fatigue strength	Face width
ISO	$\sigma_F = \sigma_{F0}K_A K_V K_{F\beta}K_{F\alpha} \leq \sigma_{FP}$ $$\sigma_{F0} = \frac{F_t}{b\, m_n}Y_F Y_S Y_\beta Y_B Y_{DT}$$	$$\sigma_{FP} = \frac{\sigma_{Flim}Y_{ST}Y_{NT}}{S_{Fmin}}Y_{\delta relT}Y_{RrelT}Y_X$$	$$b = \frac{S_{Fmin}F_t Y_F Y_S Y_\beta Y_B Y_{DT}K_A K_V K_{F\beta}K_{F\alpha}}{\sigma_{Flim}Y_{ST}Y_{NT}Y_{\delta relT}Y_{RrelT}Y_X m_n}$$
ANSI/ AGMA	$$\sigma_F = F_t K_o K_v K_s \frac{1}{b\, m_t}\frac{K_m K_B}{Y_J}$$	$$\sigma_F \leq \frac{\sigma_{FP}Y_N}{S_F Y_\theta Y_Z}$$	$$b = \frac{S_F Y_\theta Y_Z F_t K_o K_v K_s K_m K_B}{\sigma_{FP}Y_N Y_J m_t}$$
B&N	$$\sigma_{all} = \frac{K_v W^t}{F\, m\, Y}$$	$$S_e = k_a k_b k_c k_d k_e k_f S'_e$$	$$F = \frac{K_v W^t n_d}{m\, Y k_a k_b k_c k_d k_e k_f S'_e}$$
J&M	$$\sigma = \frac{F_t}{m\, b\, J}K_v K_o (0.93 K_m)$$	$$S_n = S'_n C_L C_G C_S k_r k_t k_{ms}$$	$$b = \frac{F_t n_d K_v K_o (0.93 K_m)}{m\, J S'_n C_L C_G C_S k_r k_t k_{ms}}$$

4. RESULTS AND DISCUSSIONS

In this thesis work, design of pinion, which is the smallest and subjected to higher number of repeated cyclic loading in a meshing gear couple for the speed ratios from 1:1 to 8:1 were performed to obtain the design outputs and make a comparison of results obtained from each design approach. Module "m" and face width "F" is obtained for 4 design approaches with different power transmissions and speed ratios. 102 different power transmission values are used for 1 speed ratio for each design approach. Each design approaches have 8 different speed ratios which give 816 design results for just one. 3264 design results for 4 different design approach is calculated for only type 1 material. Since 3 different type of material for 20° and 25° are used, 19584 design results are calculated, in total.

All input parameters are shown in Table 4.1. Input parameters are kept identical for each design approach to have a fair design comparison in the end.

Table 4. 1. Input parameters for each design approach

Input Parameters	Value
Type of gear profile	Involute
Operating temperature	Moderate or low (~120°C)
Working characteristics	Uniform
Pressure angle, Ø	20° and 25°
Reliability, %	99.9
Number of life cycles, N	10^{8}
Input speed, rpm	1200
Factor of safety	2.1
Quality number	Grade 8
Transmitted power range, kW	1-1000kW (@102 points)
Speed ratio range, m_G	1:1, 2:1, 3:1, 4:1, 5:1, 6:1, 7:1, 8:1
Material properties	see Table 3.1
Design criteria	Based on bending fatigue

4.1. Comparison of Module Selection and Face Width Results of the Design Approaches

4.1.1. Comparison of Results Based on Bending Fatigue Failure Considering Power Transmission

Comparison of results are shown in following figures and tables based on bending fatigue failure for pressure angle of 20° and material type 1. General trends of module and face width with the increment of transmitted power are shown in following figures for each design approach (see from Figure 4.1 to 4.6). Additionally, ratio of modules with respect to ANSI/AGMA 2001-D04 (2004) ($m_{Design\ Approaches}$ / m_{AGMA}) are shown in the tables for each design approach (see Table 4.2 to 4.4).

Comparison of results based on bending fatigue failure for pressure angle of 20° are given in;

- Appendix B.1 for material type 2,
- Appendix C.1 for material type 3.

Comparison of results based on bending fatigue failure for pressure angle of 25° are given in;

- Appendix D.1 for material type 1,
- Appendix E.1 for material type 2,
- Appendix F.1 for material type 3.
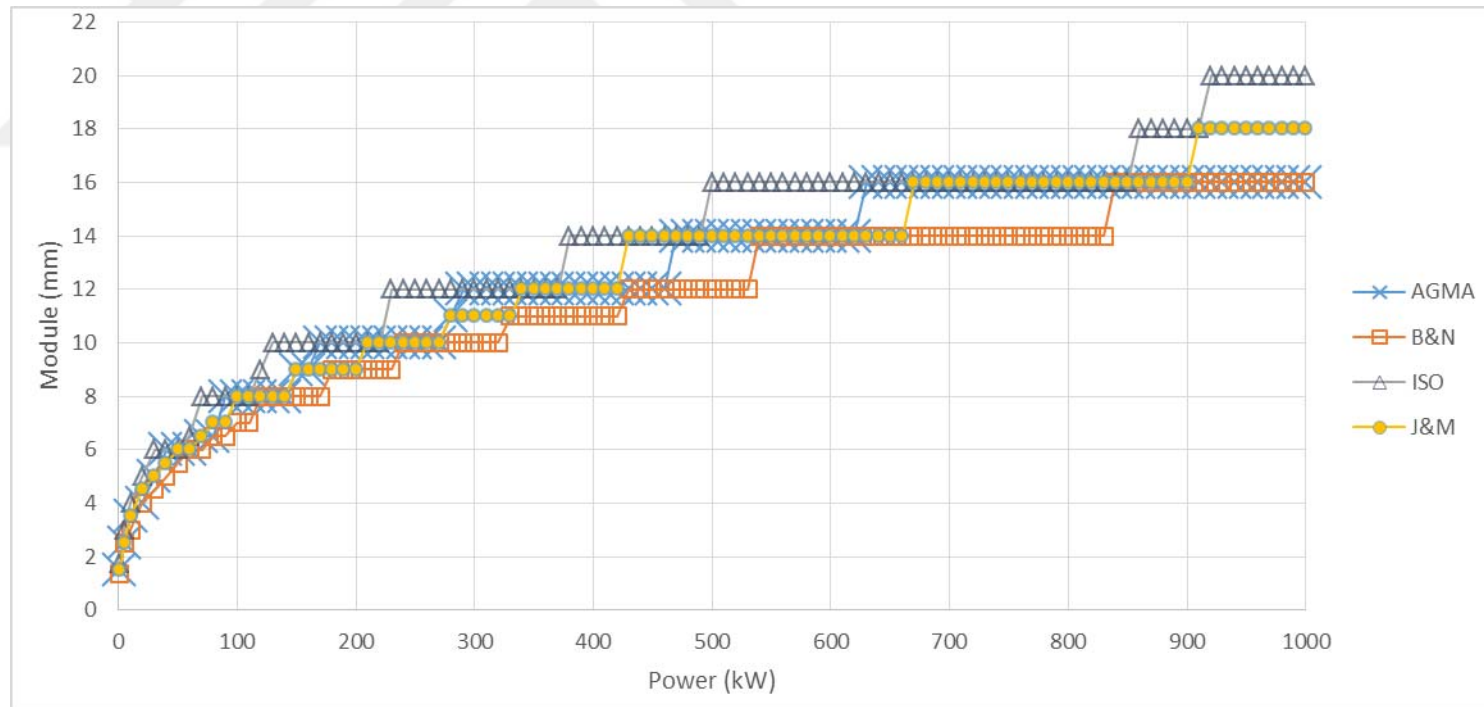
Figure 4.1. Module variation considering bending fatigue failure under increasing power at 1:1 speed ratio (Ø=20°, Type 1)
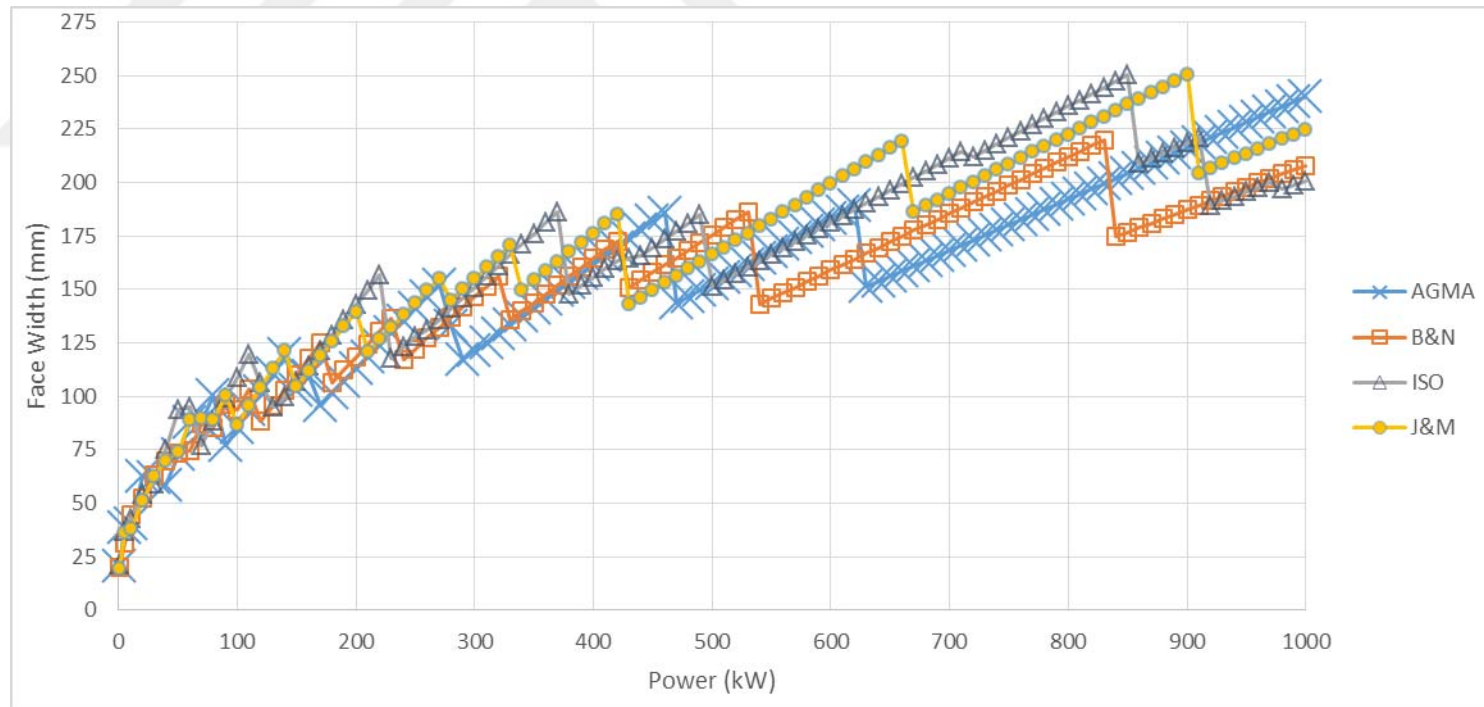
Figure 4.2. Face width variation considering bending fatigue failure under increasing power at 1:1 speed ratio (Ø=20°, Type 1)

Table 4. 2. Ratio of modules (m$_{Design Approaches}$ / m$_{AGMA}$) based on bending fatigue failure at 1:1 speed ratio with each transmitted power (Ø=20°, Type 1)

Transmitted Power [kW]	$\dfrac{m_{AGMA}}{m_{AGMA}}$	$\dfrac{m_{SHIGLEY}}{m_{AGMA}}$	$\dfrac{m_{ISO}}{m_{AGMA}}$	$\dfrac{m_{JSME}}{m_{AGMA}}$
1	1.00	1.000	0.917	1.167
5	1.00	1.000	1.000	1.200
10	1.00	0.857	1.143	1.000
100	1.00	0.875	1.000	1.000
200	1.00	0.900	1.000	0.900
300	1.00	0.833	1.000	0.917
400	1.00	0.917	1.167	1.000
500	1.00	0.857	1.143	1.000
600	1.00	1.000	1.143	1.000
700	1.00	0.875	1.000	1.000
800	1.00	0.875	1.000	1.000
900	1.00	1.000	1.125	1.000
1000	1.00	1.000	1.250	1.125
Average (1-1000kW)	1.000	0.928	1.096	1.006
Standard Deviation [σ]	0.000	0.063	0.095	0.066
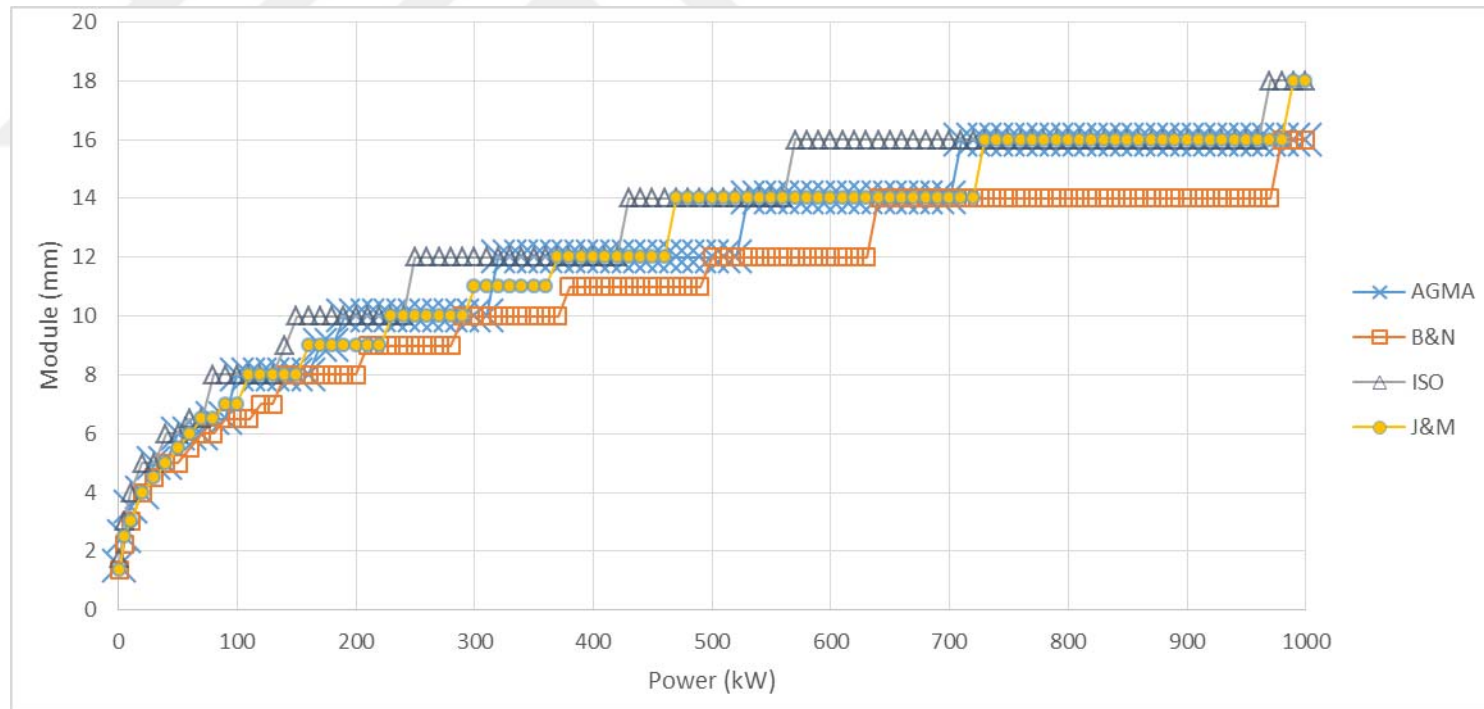
Figure 4. 3. Module variation considering bending fatigue failure under increasing power at 2:1 speed ratio (Ø=20°, Type 1)
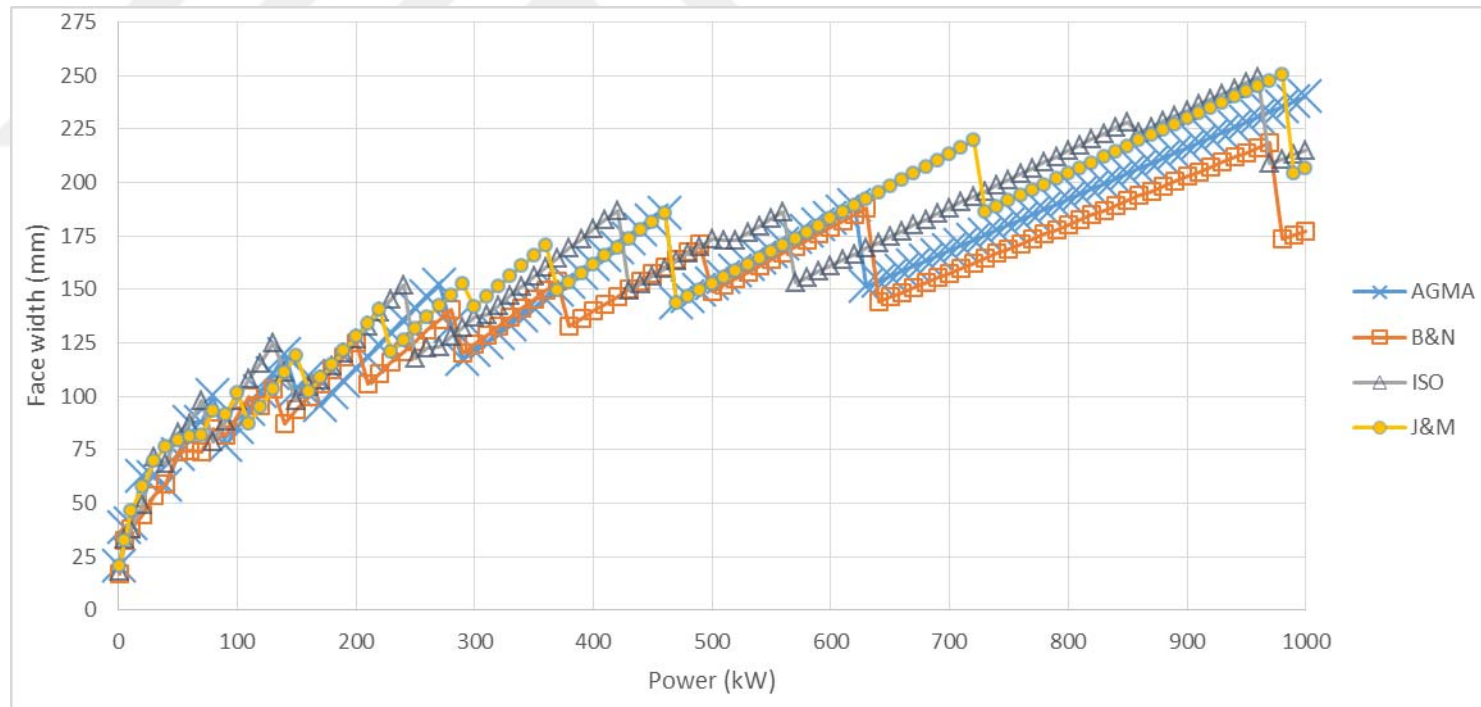
Figure 4.4. Face width variation considering bending fatigue failure under increasing power at 2:1 speed ratio (Ø=20°, Type 1)

Table 4. 3. Ratio of modules ($m_{Design\ Approaches}$ / m_{AGMA}) based on bending fatigue failure at 2:1 speed ratio with each transmitted power ($\varnothing$=20°, Type 1)

Transmitted Power [kW]	$\dfrac{m_{AGMA}}{m_{AGMA}}$	$\dfrac{m_{YARGLEY}}{m_{AGMA}}$	$\dfrac{m_{ISO}}{m_{AGMA}}$	$\dfrac{m_{T\&M}}{m_{AGMA}}$
1	1.00	1.000	0.917	1.167
5	1.00	1.000	0.900	1.200
10	1.00	1.000	0.857	1.143
100	1.00	0.813	1.000	0.875
200	1.00	0.813	1.000	1.000
300	1.00	0.875	1.000	1.000
400	1.00	0.875	1.000	1.000
500	1.00	1.000	1.125	1.000
600	1.00	1.000	1.250	1.000
700	1.00	1.000	1.250	1.125
800	1.00	0.889	1.111	1.000
900	1.00	0.889	1.111	1.000
1000	1.00	0.800	1.000	0.900
Average (1-1000kW)	1.000	0.904	1.078	1.001
Standard Deviation [σ]	0.000	0.058	0.086	0.064
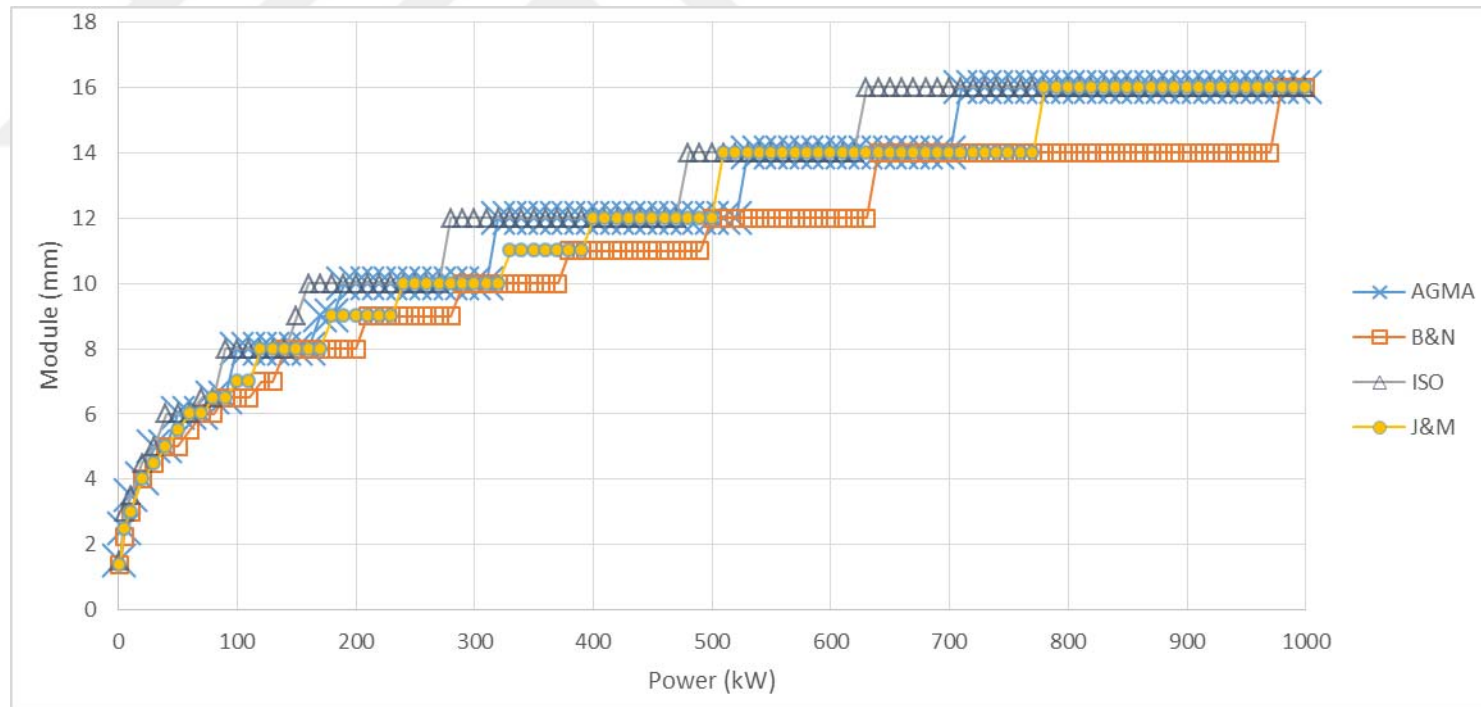
Figure 4. 5. Module variation considering bending fatigue failure under increasing power at 3:1 speed ratio (Ø=20°, Type 1)
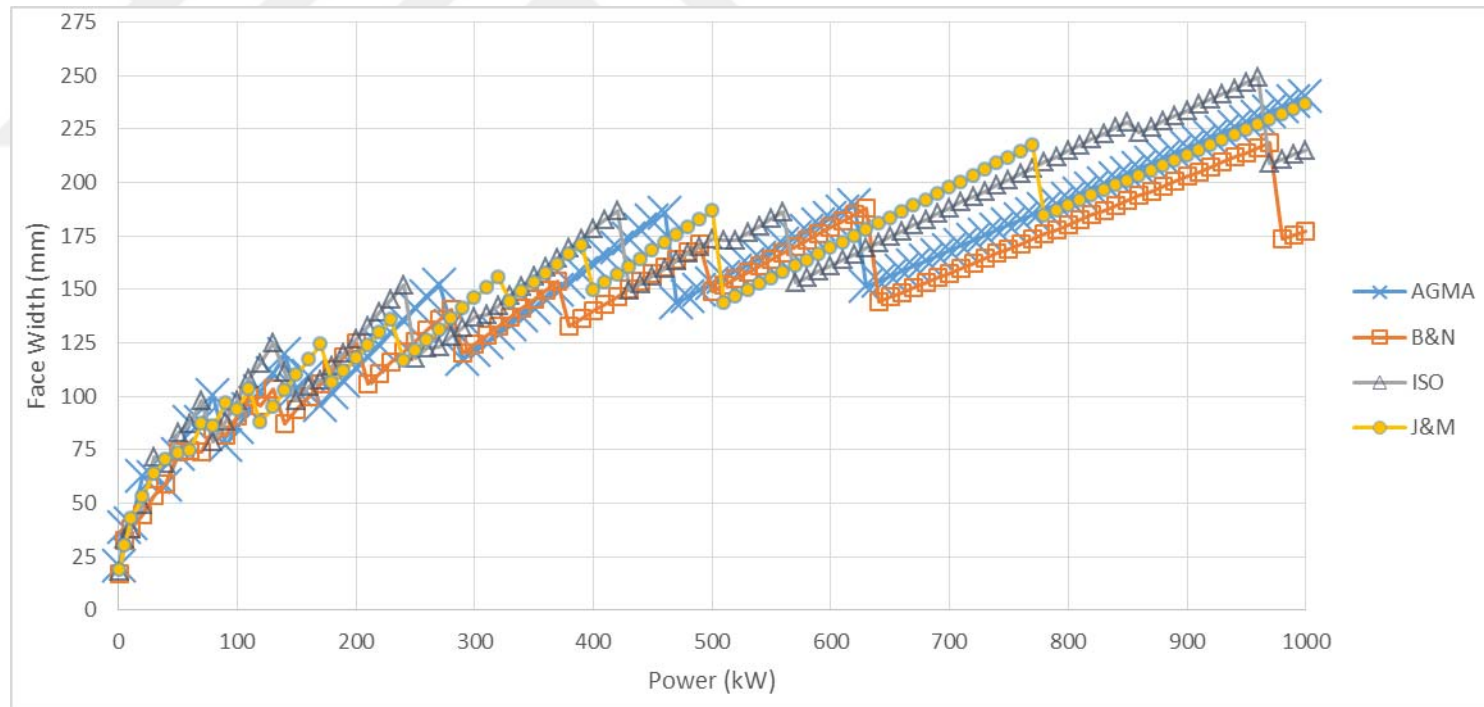
Figure 4.6. Face width variation considering bending fatigue failure under increasing power at 3:1 speed ratio (Ø=20°, Type 1)

Table 4. 4. Ratio of modules ($m_{\text{Design Approaches}}$ / m_{AGMA}) based on bending fatigue failure at 3:1 speed ratio with each transmitted power ($\varnothing=20^\circ$, Type 1)

Transmitted Power [kW]	$\dfrac{m_{AGMA}}{m_{AGMA}}$	$\dfrac{m_{SHIGLEY}}{m_{AGMA}}$	$\dfrac{m_{ISO}}{m_{AGMA}}$	$\dfrac{m_{J\&M}}{m_{AGMA}}$
1	1.00	0.833	1.000	0.917
5	1.00	0.900	1.200	1.000
10	1.00	0.917	1.167	1.000
100	1.00	1.000	1.231	1.077
200	1.00	0.889	1.111	1.000
300	1.00	0.900	1.200	1.000
400	1.00	0.833	1.000	1.000
500	1.00	0.917	1.167	1.000
600	1.00	0.857	1.000	1.000
700	1.00	0.857	1.143	1.000
800	1.00	0.875	1.000	1.000
900	1.00	0.875	1.000	1.000
1000	1.00	0.875	1.000	1.000
Average (1-1000kW)	1.000	0.896	1.076	1.005
Standard Deviation [σ]	0.000	0.055	0.087	0.058

In "Module vs Power" figures (Figure 4.1, Figure 4.3, Figure 4.5), ISO 6336 Standards (2006) show the highest module values out of 4 design approaches. Budynas R.G. and Nisbett J.K. (2011) gives the smallest module values. In addition, ratio of modules with respect to AGMA in 3:1, 4:1, 5:1 6:1, 7:1 and 8:1 speed ratios are same for each transmitted power. Since results are same for 3:1 to 8:1 speed ratio, related graphs are given in Appendix A.1.

In the "Face width vs Power" figures (Figure 4.2, Figure 4.4, Figure 4.6) with considering all design approaches, the face width exhibits a certain decrease in each module increment. Afterwards, face width continues to increase as the power increase.

4.1.2. Comparison of the Results Based on Bending Fatigue Failure Considering Speed Ratio for the Selected Power Transmissions

Comparison of results are shown in following figures based on bending fatigue failure for pressure angle of 20° and material type 1. Figures from 4.7 to 4.11 show that, module values are same at 3:1, 4:1, 5:1, 6:1, 7:1 and 8:1 speed ratios for each design approach for the selected power transmissions when the helical gear are designed based on bending fatigue failure. When below figures analyzed it is observed that;

- Budynas R.G. and Nisbett J.K. (2011) give the smallest module values at 1:1 speed ratio compared to 3:1, 4:1, 5:1, 6:1, 7:1 and 8:1 at 10 kW transmitted power while ISO 6336 Standards (2006) give the largest module value for all speed ratios.

- All design approaches give larger module values at 1:1 speed ratio compared to 3:1, 4:1, 5:1, 6:1, 7:1 and 8:1 at 1, 10, 100, 500 and 1000 kW transmitted power.
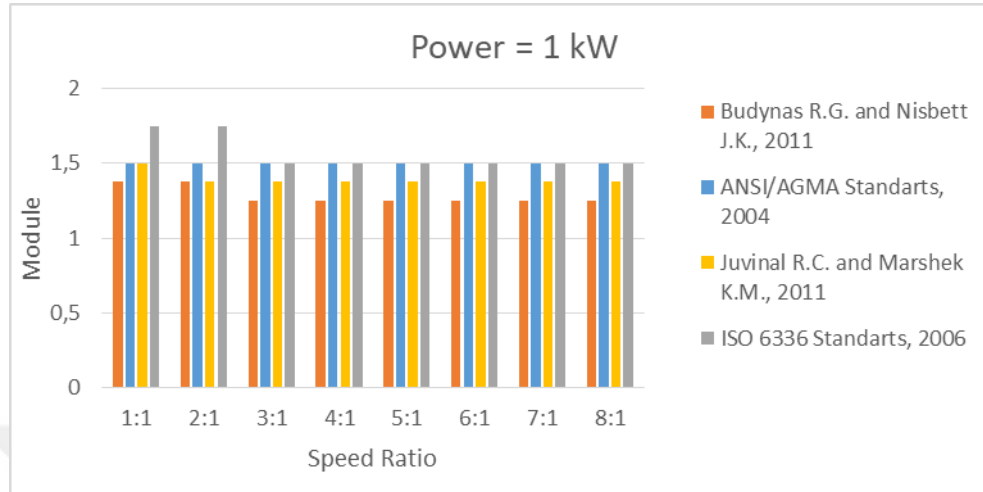
Figure 4. 7. The effect of speed ratio on module selection based on bending fatigue failure at 1 kW power transmission (Ø=20°, Type 1)
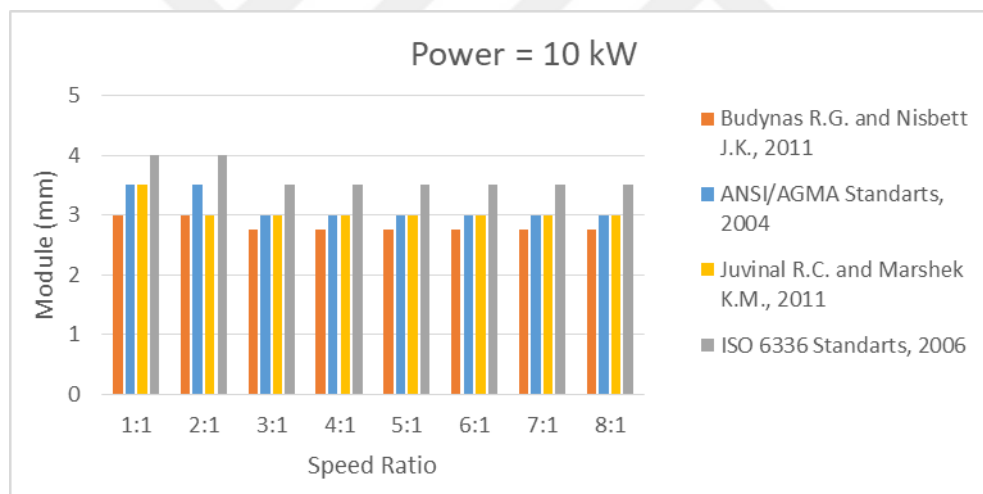
Figure 4. 8. The effect of speed ratio on module selection based on bending fatigue failure at 10 kW power transmission (Ø=20°, Type 1)
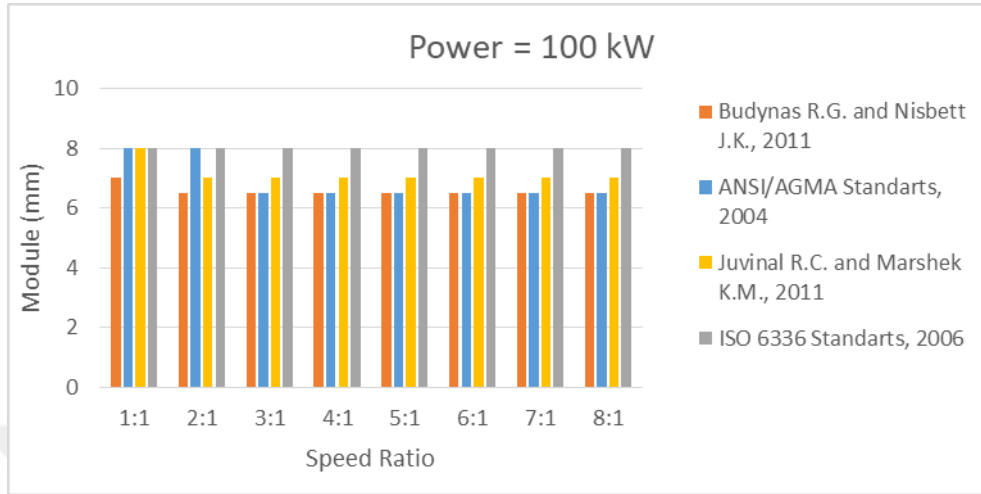
Figure 4. 9. The effect of speed ratio on module selection based on bending fatigue failure at 100 kW power transmission (Ø=20°, Type 1)
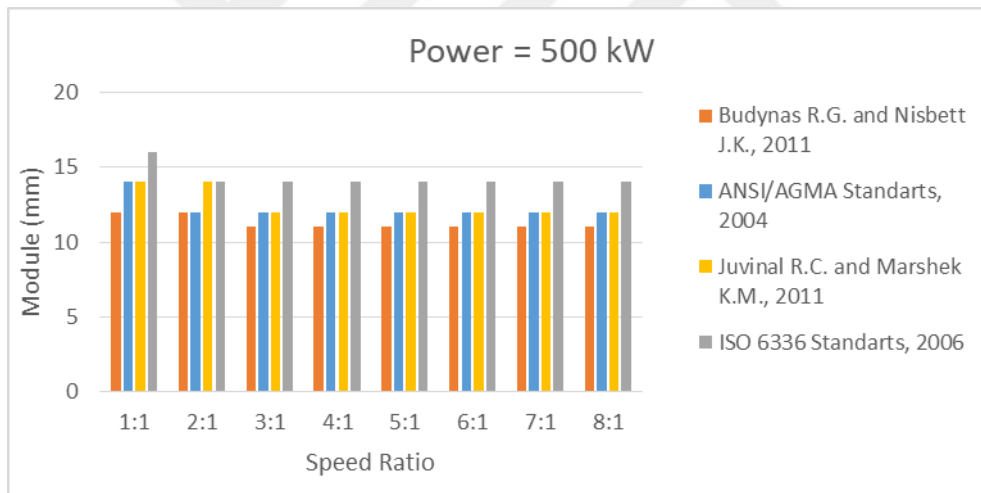
Figure 4. 10. The effect of speed ratio on module selection based on bending fatigue failure at 500 kW power transmission (Ø=20°, Type 1)
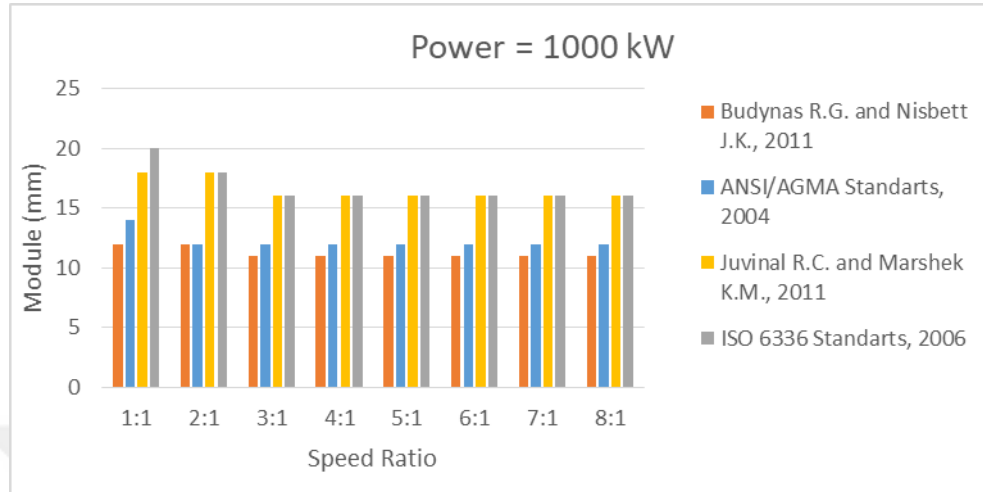
Figure 4. 11. The effect of speed ratio on module selection based on bending
fatigue failure at 1000 kW power transmission (Ø=20°, Type 1)

When the above diagrams are scrutinized, the general trend is that module
values nearly remain the same for almost all power transmission ranges as the
speed ratio increases.

Comparison of the results based on bending fatigue failure considering
speed ratio for the selected power transmissions for pressure angle of 20° are given
in;

- Appendix B.2 for material type 2,
- Appendix C.2 for material type 3.

Comparison of the results based on bending fatigue failure considering
speed ratio for the selected power transmissions for pressure angle of 25° are given
in;

- Appendix D.2 for material type 1,
- Appendix E.2 for material type 2,
- Appendix F.2 for material type 3.

4.2. Comparison of Gear Stress by Using Finite Element Method (FEM)

It is necessary to compare and validate analytical results with numerical results. First, analytical design results and bending stresses are obtained for the most critical speed ratio of 1:1 with 10 kW power transmission for each design approach. Afterwards, 3D helical gear is created with the analytical design results by using CATIA V5. The 3D design is converted to file format of "Standard for the Exchange of Product (.stp)" and it is imported to ANSYS to determine numerical bending stress result. Following major steps are involved in preprocessing stage in ANSYS Workbench 15.0.

- Material properties are defined to 'Engineering Data' in Workbench 15.0 according to Table 3.1, material type 1.
- Force vectors (tangential, radial and axial, see Figure 4.12) are applied on pitch line of pinion teeth as shown in Figure 4.13.
- Fixed support is defined to shaft contact surface of pinion (see Figure 4.14).
- Frictionless support is defined to lateral surface of pinion (see Figure 4.14).
- Element sizing to whole body of pinion and face sizing to tooth root which is under bending stress are applied.
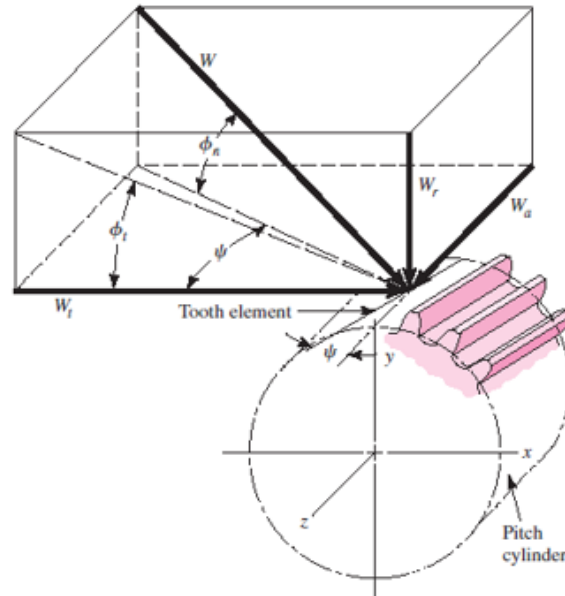
Figure 4. 12. Tooth forces acting on a right-hand helical gear
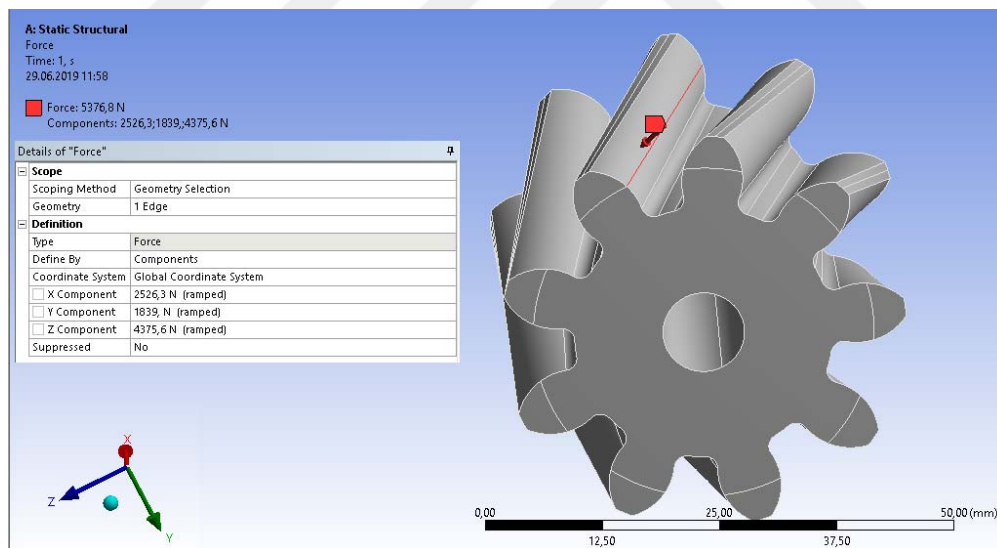
Figure 4. 13. Applied force on gear tooth pitch line in ANSYS Workbench 15.0
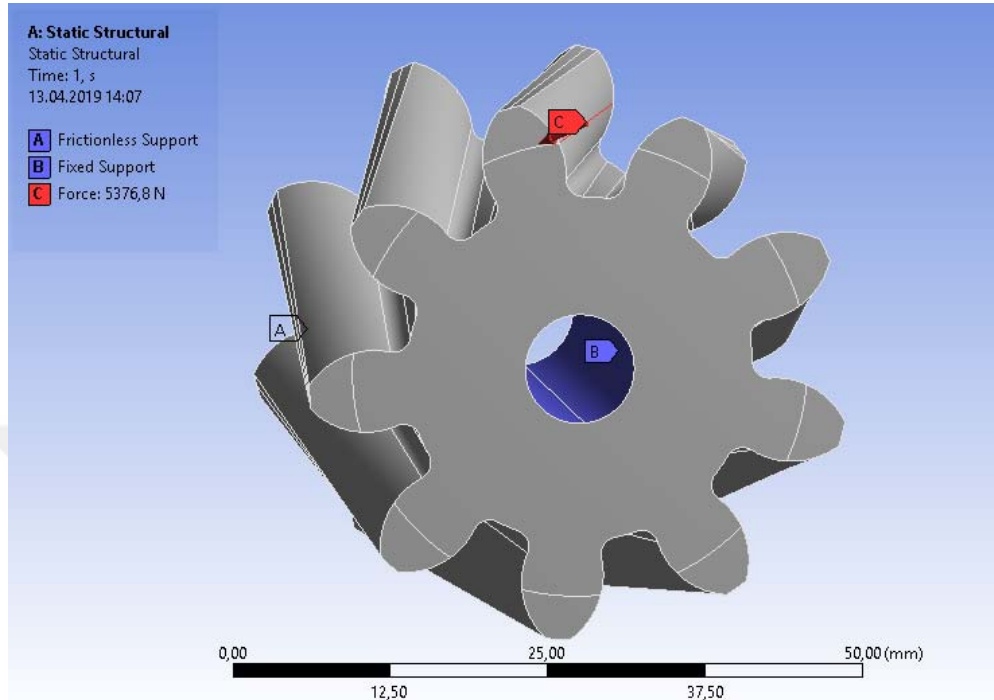
Figure 4. 14. Preprocessing steps in ANSYS Workbench 15.0

The model has been solved with different element sizing whilst keeping face size constant to find feasible element size number. Maximum Von Mises Stresses have been recorded with the different element sizing (see Table 4.10). As it can be seen in mesh sensitivity graph in Figure 4.24, stress values change slightly with the change of element sizing. In conclusion, 1 mm element sizing is selected as an optimum for meshing of whole body.

Table 4. 5. Table of Von Mises stress results according to different element sizing

Number of Nodes	Element Number	Element Sizing (mm)	Face Sizing (mm)	Von Mises Stress
15062	9106	15	0.4	97.45
17870	10575	10	0.4	97.69
20541	12241	6	0.4	99.78
25024	14736	4	0.4	102.3
26245	15426	3.5	0.4	101.94
25305	15112	3	0.4	99.607
29732	17731	2.5	0.4	99.638
35669	21269	2	0.4	100
70076	41263	1	0.4	101.77
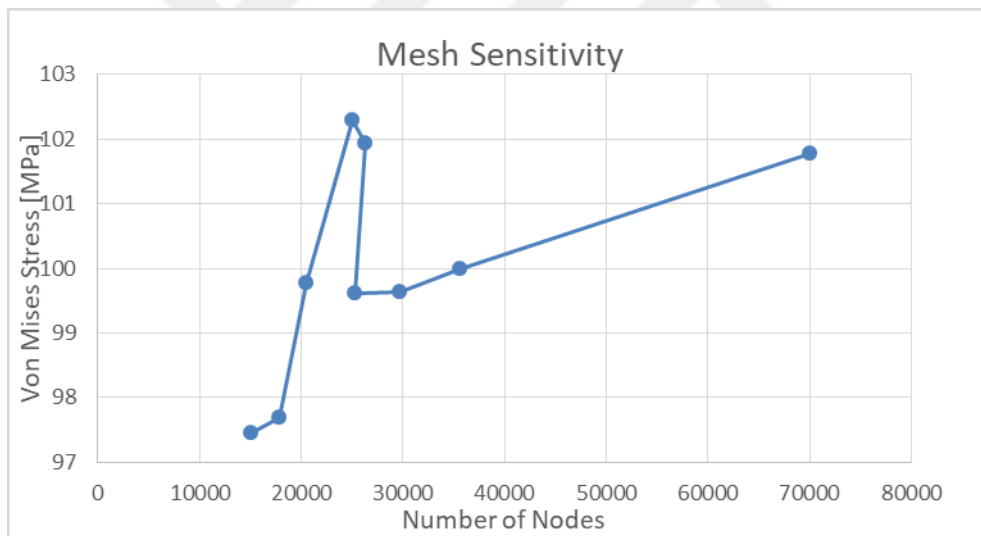
Figure 4. 15. Graph of Von Mises stress results according to different element sizing

Model has been solved with different face sizing with keeping element sizing as 1 mm to find feasible face size number. Maximum Von Mises Stresses have been recorded with the different face sizing in (see Table 4.5). As it can be

seen in face sizing sensitivity graph in Figure 4.25, stress value does not change after 35669 node number which is approximately equal to 0.4 mm face sizing. In conclusion, 0,4 mm face sizing is selected for meshing of tooth root bending region.

Table 4. 6. Table of Von Mises stress results according to different face sizing

Number of Nodes	Element Number	Element Sizing (mm)	Face Sizing (mm)	Von Mises Stress
59181	34459	1	4	66.53
59312	34547	1	3	69.89
59675	34796	1	2	77.92
60532	35301	1	1	88.57
65762	38591	1	0.5	104.62
35669	21269	1	0.4	101.77
76401	45089	1	0.3	101.16
96589	57410	1	0.2	101.7
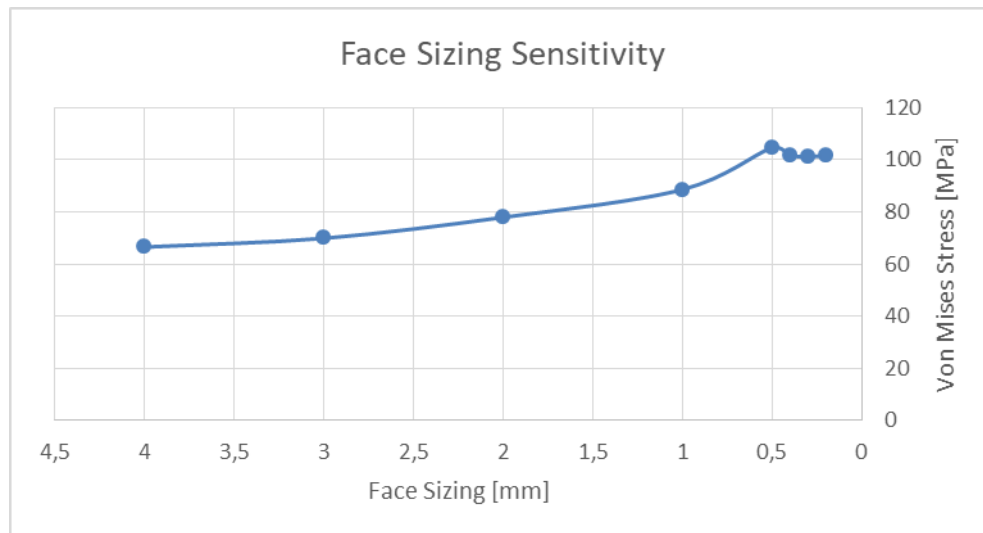
Figure 4. 16. Graph of Von Mises stress results according to different face sizing

3D body of pinion is meshed according to selected element and face sizing numbers (see Figure 4.17).
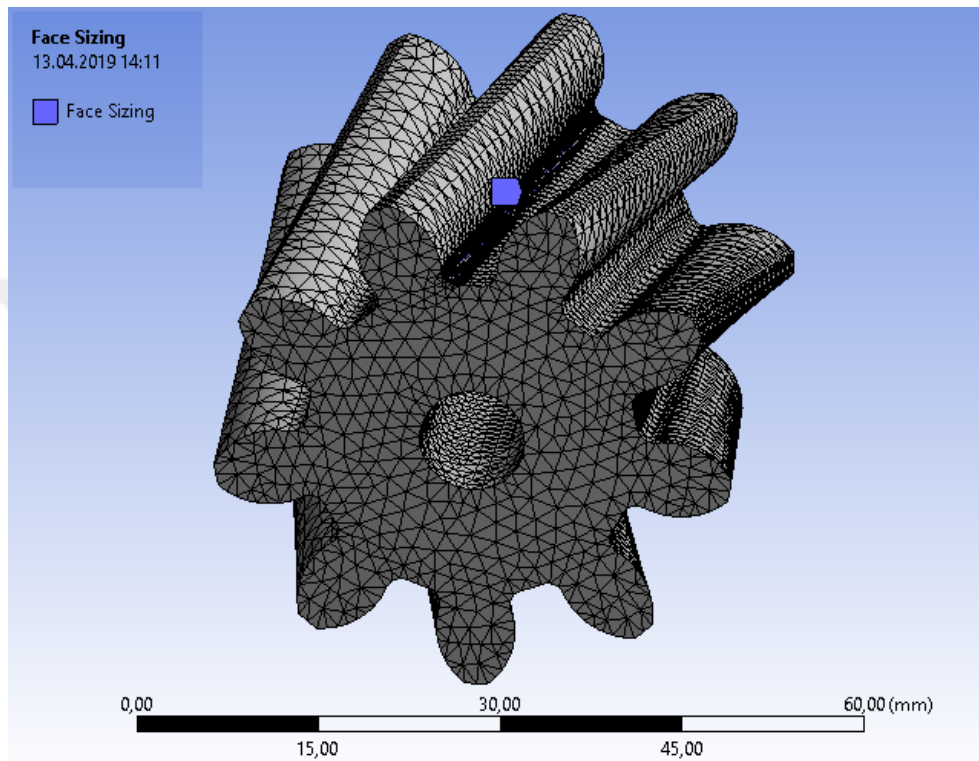
Figure 4. 17. Meshing of body in preprocessing steps in ANSYS Workbench 15.0

In Figure 4.18, the result of bending stress distribution is exhibited along the gear tooth root according to Finite Element Analysis (FEA) is shown. In Figure 4.19, total deformation behavior of the gear is shown during post analysis on ANSYS Workbench 15.0.

75
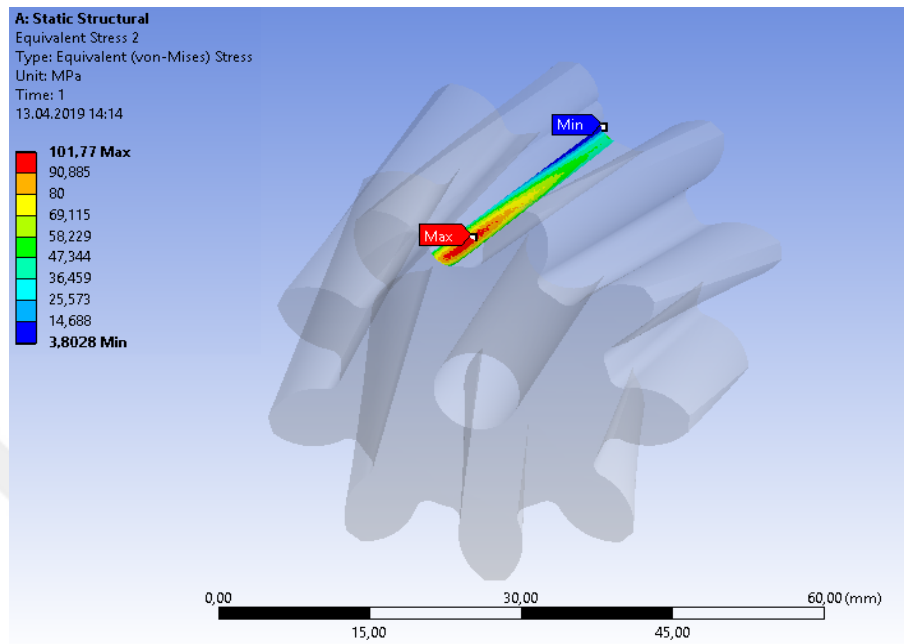
Figure 4. 18. Numerical Von Mises stress results in ANSYS Workbench 15.0
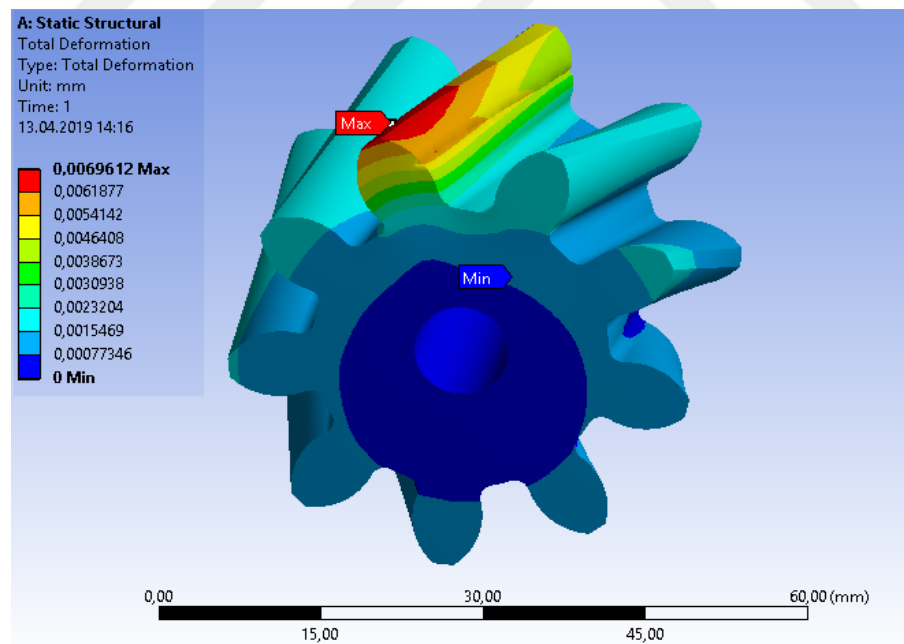
Figure 4. 19. Total deformation in post processing steps in ANSYS Workbench 15.0

Gear bending stresses have been determined numerically for each design approach by using ANSYS software. On the other hand, the design results of helical gears that are modelled with the same input parameters using each design approach have also been made available. Now numerical and analytical results can compared with each other. Hence, numerical results are compared with the analytical calculations using Equation (3.1) given in Chapter 3. The results are provided in Table 4.7.

It is observed that the numerical results are lower than analytical results except ANSI/AGMA 2001-D04 Standards. Even though lowest difference percentage between analytical and numerical calculations belongs to Juvinal R.C. and Marshek K.M., ANSI/AGMA 2001-D04 Standards has been taken a base solution for making comparisons between design approaches. The reason for this is, ANSI/AGMA 2001-D04 Standards are well-known approach than Juvinall R.C. and Marshek K.M. and it is commonly used in worldwide.

Table 4. 7. Comparison of bending stresses obtained from the four analytical approaches and numerical (FEA) method ($\emptyset=20^{\circ}$, Type 1)

Results for Bending Stress				
Design Approaches	ANSI/AGMA 2001-D04 Standards	Budynas R.G. and Nisbett J.K.	ISO 6336 Standards	Juvinall R.C. and Marshek K.M.
Module (mm)	3.5	3	4	3.5
Pitch diameter (mm)	36.37	31.17	41.56	36.37
Face Width (mm)	40.45	44.77	42.52	37.96
Number of Pinion	9	9	9	9
Tangential Force (kN)	4.375	5.104	3.828	4.375
Analytical (MPa)	95.92	153.50	80.47	112.52
Numerical (MPa)	101.77	128.27	74.52	108.1
Difference (%)	+6.09	-16.43	-7.38	-3.92

4.3. Obtaining Geometric Rating Number (GR$_i$) for Design Approaches

This thesis work investigates a translation technique from simple design text book approaches (B&N, J&M) to AGMA or ISO Standard. In addition to this if there is any possibility of constant relationship in terms of design results obtained from design approaches, the technique can be employed to any design approach including technical standards such as from ISO to AGMA or vice versa .

Geometric rating numbers, (GR$_i$) have been calculated by using Equation (3.1) to determine the effect of module and face width together. Both "Scatter" and "Radar" charts have been prepared using GR$_i$ numbers obtained for each speed ratio. Relative comparison can be seen in Figure from 4.20 to 4.22 for each design approach. Radar charts are given in Appendix A.2 for all speed ratios.
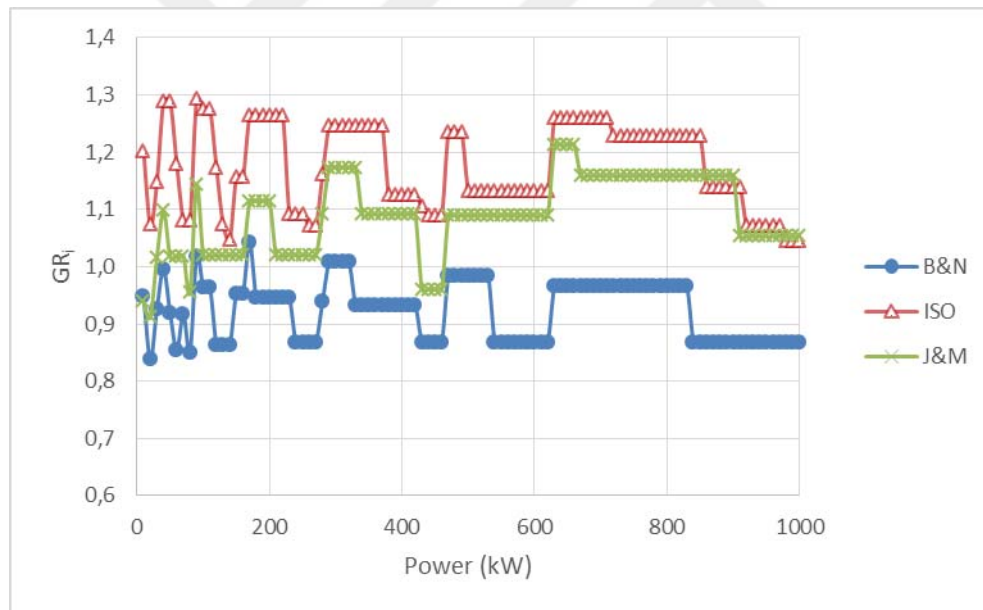
Figure 4. 20. Comparison of GR$_i$ results obtained from the design approaches at 1:1 speed ratio (Ø=20°, Type 1)

In Figure 4. 20, it is observed that ISO Standards (2006) gives highest GR$_i$ number while the approach given by B&N (2011) gives minimum result.

79
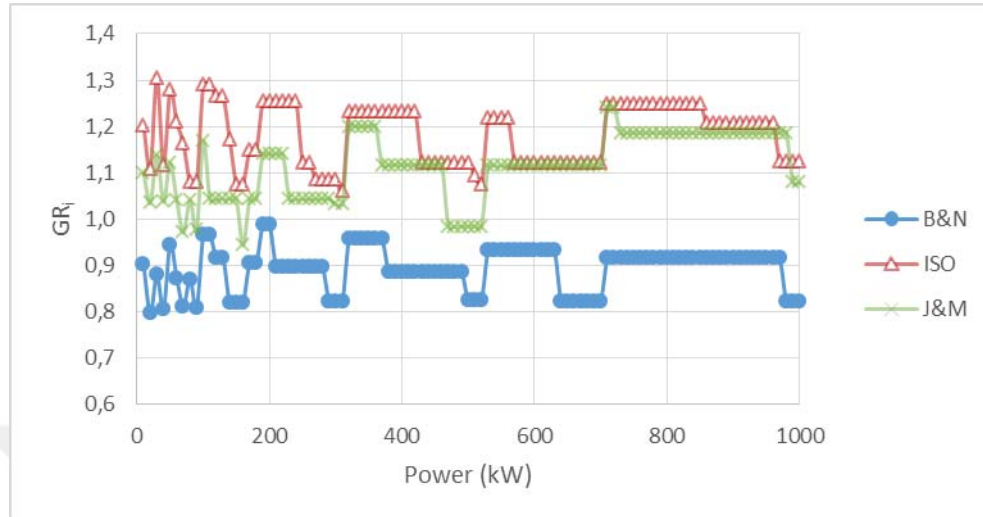
Figure 4. 21. Comparison of GR_i results obtained from the design approaches at 2:1 speed ratio ($\emptyset=20^o$, Type 1)
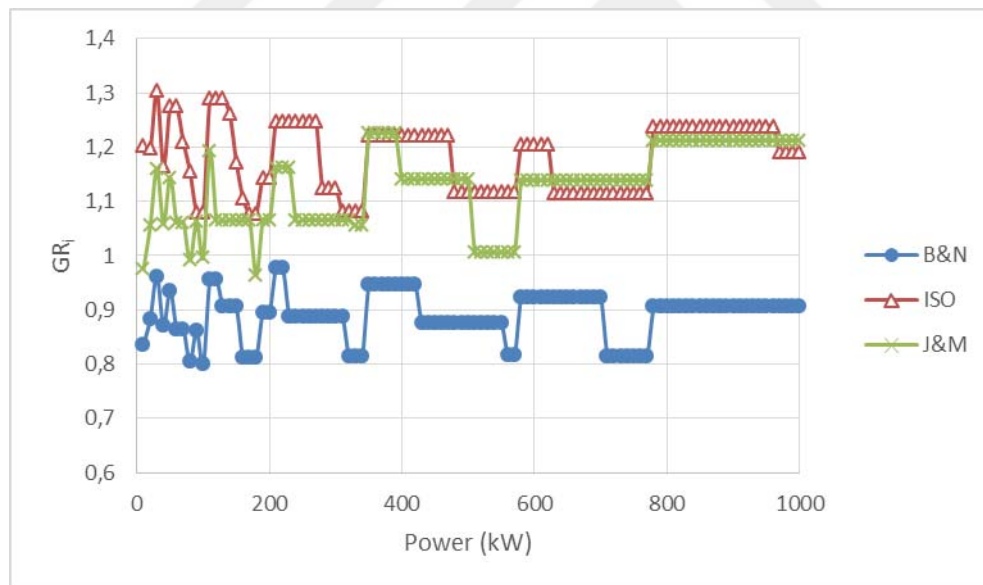
Figure 4. 22. Comparison of GR_i results obtained from the design approaches at 3:1 speed ratio ($\emptyset=20^o$, Type 1)

The same trend has still been maintained in Figures 4.21 and 4.22. In these figures, the minimum results have given by Budynas and Nisbett (2011), and maximum results have given by ISO Standards (2006).

It is seen that, geometric ratio numbers show similar pattern for each design approaches for the 3:1, 4:1, 5:1, 6:1, 7:1 and 8:1 (see Appendix F.2.) speed ratios when above graphs are investigated. ISO Standard gives the largest gear tooth volume as B&N gives the smallest for the selected speed ratios for the selected power transmission ranges.

The figures obtained by GR_i numbers derived from each of the standards have shown that very similar trends for all power transmission ranges are available between design approaches. These results show the possibility of obtaining CFs with a close approximation.

Additional figures for geometric rating number (GR_i) of design approaches for pressure angle of 20° are given in;

- Appendix B.3 for material type 2,
- Appendix C.3 for material type 3.

Additional figures for geometric rating number (GR_i) of design approaches for pressure angle of 25° are given in;
- Appendix D.3 for material type 1,
- Appendix E.3 for material type 2,
- Appendix F.3 for material type 3.

Figures show that results are very similar due to relative comparison provided by GR_i. As a result of this, ranking can be achieved for the different approaches.

Mean GR_i numbers for various design approaches for each speed ratio with 20° pressure angle are shown in Table 4.8 and with 25° pressure angle are shown in Table 4.9.

Table 4. 8. Mean GR_i numbers for the various design approaches for each speed ratio with 20° pressure angle

$\varnothing=20^o$	Material Type 1			Material Type 2			Material Type 3		
Speed ratio	B&N	ISO	J&M	B&N	ISO	J&M	B&N	ISO	J&M
1	0.922	1.175	1.088	0.750	1.165	0.818	0.748	1.165	0.830
2	0.893	1.182	1.112	0.715	1.148	0.825	0.753	1.147	0.799
3	0.890	1.185	1.126	0.709	1.144	0.837	0.763	1.135	0.790
4	0.890	1.188	1.126	0.709	1.147	0.837	0.763	1.137	0.790
5	0.890	1.189	1.126	0.709	1.148	0.837	0.763	1.138	0.790
6	0.890	1.190	1.126	0.709	1.149	0.837	0.763	1.138	0.790
7	0.890	1.190	1.126	0.709	1.149	0.837	0.763	1.139	0.790
8	0.890	1.190	1.126	0.709	1.149	0.837	0.763	1.139	0.790
Average	0.895	1.186	1.119	0.715	1.150	0.833	0.760	1.142	0.796
Std.	0.011	0.005	0.014	0.014	0.006	0.007	0.006	0.010	0.014

Table 4. 9. Mean GR_i numbers for the various design approaches for each speed ratio with 25° pressure angle

Ø=25°	Material Type 1			Material Type 2			Material Type 3		
Speed ratio	B&N	ISO	J&M	B&N	ISO	J&M	B&N	ISO	J&M
1	1.228	1.369	1.092	0.982	1.348	0.811	1.094	1.342	0.749
2	1.194	1.390	1.101	0.967	1.377	0.826	1.069	1.363	0.759
3	1.194	1.395	1.101	0.967	1.379	0.826	1.069	1.365	0.759
4	1.111	1.395	1.123	0.886	1.363	0.836	0.992	1.368	0.765
5	1.111	1.395	1.123	0.886	1.364	0.836	0.992	1.369	0.765
6	1.111	1.395	1.123	0.886	1.365	0.836	0.992	1.369	0.765
7	1.111	1.395	1.123	0.886	1.365	0.836	0.992	1.369	0.765
8	1.111	1.395	1.123	0.886	1.365	0.836	0.992	1.370	0.765
Average	1.146	1.391	1.113	0.918	1.366	0.830	1.024	1.364	0.762
Std.	0.050	0.009	0.013	0.045	0.010	0.009	0.045	0.009	0.006

83

The mean GR_i numbers are obtained for each design approach by taking average of values of GR_i at each speed ratio. The approaches are then ranked by GR_i numbers and given in Table 4.10. Results indicate that general trend for GR_i with 20° pressure angle are same. If it is sorted from highest to lowest, it will be as follow,

- Material Type 1: ISO>J&M>B&N;
- Material Type 2: ISO>J&M>B&N;
- Material Type 3: ISO>J&M>B&N.

Same study have been done for 25° pressure angle. Results indicate that general trend for GR_i with 25° pressure angle are same, as well. If it is sorted from highest to lowest, it will be as follow,

- Material Type 1: ISO >B&N>J&M;
- Material Type 2: ISO >B&N>J&M;
- Material Type 3: ISO> B&N >J&M.

In conclusion, ISO gives the highest GR_i regardless of pressure angle when considering 3 types of material.

Table 4. 10. Mean GR_i numbers for the various design approaches

Geometric rating numbers for the approaches with three types of material	GR_i					
	$\emptyset=20^o$			$\emptyset=25^o$		
	Type 1	Type 2	Type 3	Type 1	Type 2	Type 3
B&N	0.895	0.715	0.760	1.146	0.918	1.024
ISO	1.186	1.150	1.142	1.391	1.366	1.364
J&M	1.119	0.833	0.796	1.113	0.830	0.762
ANSI/AGMA	1.000	1.000	1.000	1.000	1.000	1.000

The jumps in GR_i numbers are related with module and face width changes for a given power transmission range. An example is given to explain GR_i jumps which is observed in above graphs. Calculated module and face width values are tabulated in Table 4.11 for J&M and AGMA. Geometric ratio number for J&M ($GR_{i,J\&M/AGMA}$) is given in the last column of Table 4.11. It is observed that, GR_i jumps when one of the module value changes because of the power increase.

Table 4. 11. Example for the GR_i jumps explanation

Power	AGMA		J&M		GR_i
	Module	Face Width	Module	Face Width	J&M/AGMA
430	12	173.608	14	142.907	0.960
440	12	177.645	14	146.231	0.960
450	12	181.683	14	149.554	0.960
460	12	185.720	14	152.878	0.960
470	14	143.428	14	156.201	1.089
480	14	146.480	14	159.525	1.089
490	14	149.531	14	162.848	1.089
500	14	152.583	14	166.172	1.089
510	14	155.635	14	169.495	1.089
520	14	158.686	14	172.818	1.089
530	14	161.738	14	176.142	1.089
540	14	164.790	14	179.465	1.089
550	14	167.841	14	182.789	1.089
560	14	170.893	14	186.112	1.089
570	14	173.945	14	189.436	1.089
580	14	176.996	14	192.759	1.089
590	14	180.048	14	196.082	1.089
600	14	183.100	14	199.406	1.089
610	14	186.151	14	202.729	1.089
620	14	189.203	14	206.053	1.089
630	16	151.162	14	209.376	1.212
640	16	153.562	14	212.700	1.212
650	16	155.961	14	216.023	1.212

4.4. Obtaining AGMA Conversion Factors (CFs) for Module and Face Width

Conversion factors for module (CF_{mt}) and face width (CF_{Ft}) can calculated by using the equations given in Table 3.3 together with their standard deviation, for module ($\sigma_{CF_{mt}}$) and for face width ($\sigma_{CF_{Ft}}$), respectively. The results are found and tabulated in Table 4.12 for pressure angle of $20°$ and material type 1.

Standard deviations for module ($\sigma_{CF_{mt}}$) and for face widths ($\sigma_{CF_{Ft}}$) given in Table 4.12 show that the module and face width results obtained from the design approaches (ISO, B&N, J&M) can be converted to AGMA with reasonable error at the selected speed ratios from 1:1 to 8:1. In addition to constant conversion factors at certain speed ratios, correlation equations were derived in order to obtain a conversion factor at any speed ratio. A fourth order correlation polynomial (C_p) expressions were obtained and given in Table 4.13.

A case study has been carried out to prove and validate the universality of conversion factors by using C_p expressions as seen in Table 4.14. The design results (module and face width) is selected randomly from 6 points that is obtained from design approaches. Since the both module (m) and face width (F) values affect the design, converted m_i times F_i values are considered to validate the success of expressions of $\overline{CF_{mt}}$ and $\overline{CF_{Ft}}$. Then total error considering converted m times F (($mxF)_{AGMA}$) values of AGMA is obtained using a gear volume error (GV_e) equation and the results are given in the last column of Table 4.14. The maximum total GV_e is below 9.2%.

Table 4. 12. Conversion factors for module and face width (Ø=20°, Type 1)

Design approaches		From B&N to AGMA				From ISO to AGMA				From J&M to AGMA			
m_G	N_p	$\overline{CF_{bt}}$	$\sigma_{\overline{CF_{bt}}}$	$\overline{CF_F}$	$\sigma_{\overline{CF_F}}$	$\overline{CF_{bt}}$	$\sigma_{\overline{CF_{bt}}}$	$\overline{CF_F}$	$\sigma_{\overline{CF_F}}$	$\overline{CF_{bt}}$	$\sigma_{\overline{CF_{bt}}}$	$\overline{CF_F}$	$\sigma_{\overline{CF_F}}$
1:1	9	0.928	0.063	1.004	0.125	1.094	0.095	1.088	0.159	1.006	0.067	1.092	0.125
2:1	10	0.904	0.059	0.996	0.113	1.076	0.086	1.110	0.144	1.002	0.064	1.119	0.124
3:1	11	0.897	0.055	1.000	0.106	1.074	0.087	1.113	0.142	1.006	0.058	1.127	0.118
4:1	11	0.897	0.055	1.000	0.106	1.074	0.087	1.116	0.142	1.006	0.058	1.127	0.118
5:1	11	0.897	0.055	1.000	0.106	1.074	0.087	1.116	0.142	1.006	0.058	1.127	0.118
6:1	11	0.897	0.055	1.000	0.106	1.076	0.087	1.115	0.143	1.006	0.058	1.127	0.118
7:1	11	0.897	0.055	1.000	0.106	1.076	0.087	1.116	0.143	1.006	0.058	1.127	0.118
8:1	11	0.897	0.055	1.000	0.106	1.076	0.087	1.116	0.143	1.006	0.058	1.127	0.118

Table 4. 13. Conversion factors for module and face width obtained from regression at any speed ratio in the range of 1 kW to 1000 kW (Ø=20°, Type 1)

	Design approach (from)	C_p Expressions for Module (m_i) (to AGMA) regressions for $\overline{CF_{mt}}$	R^2
1kW - 1000kW	B&N to AGMA (B-A)	$\overline{CF_{m,B-A}} = 0.0001m_G^4 - 0.0024m_G^3 + 0.0193m_G^2 - 0.0655m_G + 0.976$	0.99
	ISO to AGMA (I-A)	$\overline{CF_{m,I-A}} = 0.0001m_G^4 - 0.0025m_G^3 + 0.0187m_G^2 - 0.057m_G + 1.1347$	0.98
	J&M to AGMA (J-A)	$\overline{CF_{m,J-A}} = 0.00005m_G^4 - 0.0009m_G^3 + 0.0058m_G^2 - 0.0138m_G + 1.0144$	0.61
		C_p Expressions for Face Width (F) (to AGMA) regressions for $\overline{CF_{Ft}}$	
1kW - 1000kW	B&N to AGMA (B-A)	$\overline{CF_{F,B-A}} = 0.00007m_G^4 - 0.0015m_G^3 + 0.01m_G^2 - 0.268m_G + 1.0222$	0.77
	ISO to AGMA (I-A)	$\overline{CF_{F,I-A}} = -0.0001m_G^4 + 0.0023m_G^3 - 0.0176m_G^2 + 0.0582m_G + 1.0454$	0.98
	J&M to AGMA (J-A)	$\overline{CF_{F,J-A}} = -0.0001m_G^4 + 0.003m_G^3 - 0.0232m_G^2 + 0.0776m_G + 1.0347$	0.99

Table 4. 14. Validating and proving conversion factors with the percentage errors in the range of 1 kW to 1000 kW (Ø=20°, Type 1)

Case: Design approach, m(speed ratio), Power (kW)	m_i	F_i	m_{AGMA}	F_{AGMA}	(mxF) AGMA	$\overline{CF_{mi}}$	$m_{c, AGMA}$	m_i Error (%)	$\overline{CF_{Fi}}$	$F_{c, AGMA}$	F_i Error (%)	$(mxF)_{c, AGMA}$	GV_e (%)
										m_i and F_i converted to $m_{c, AGMA}$ and $F_{c, AGMA}$			
J&M (4.5:1) 225	9	132.65	10	102.65	1026.51	1.01	8.93	-10.74	1.15	115.70	+12.71	1032.78	0.61
J&M (2.6:1) 680	14	207.27	14	185.90	2602.67	1.00	13.94	-0.42	1.13	183.79	-1.14	2562.24	-1.55
B&N (3.3:1) 125	6.5	101.19	8	86.00	688.03	0.90	7.26	-9.28	1.00	101.49	+18.01	736.57	7.06
B&N (6.7:1) 400	10	148.66	12	130.88	1570.50	0.88	11.32	-5.65	0.98	151.47	+15.74	1714.99	9.20
ISO (7.3:1) 775	16	188.06	16	151.08	2417.31	1.03	15.59	-2.59	1.14	164.52	+8.89	2564.14	6.07
ISO (1.8:1) 330	12	146.61	12	119.28	1431.31	1.08	11.12	-7.34	1.11	132.62	+11.18	1474.67	3.03

Conversion factors for module ($\overline{CF}_{mi}$) and face width ($\overline{CF}_{Fi}$) are found and tabulated in Table 4.15 for pressure angle of $25°$ and material type 1.

Standard deviations for module ($\sigma_{\overline{CF}_{mi}}$) and for face widths ($\sigma_{\overline{CF}_{Fi}}$) given in Table 4.15   show that the module and face width results obtained from the design approaches (ISO, B&N, J&M) can be converted to AGMA with reasonable error at the selected speed ratios from 1:1 to 8:1. In addition to constant conversion factors at certain speed ratios, correlation equations were derived in order to obtain a conversion factor at any speed ratio. A fourth order correlation polynomial (C_p) expressions were obtained and given in Table 4.16.

 The second case study has been carried out to prove and validate the universality of conversion factors by using C_p expressions for pressure angle of $25°$ as seen in Table 4.17. The design results (module and face width) selection is same as first case study (see Table 4.14) for each design approaches. Since the both module (m) and face width (F) values affect the design, converted m_i times F_i values are considered to validate the success of expressions of $\overline{CF}_{mi}$ and $\overline{CF}_{Fi}$. Then total error considering converted m times F (($m \times F$)$_{AGMA}$) values of AGMA is obtained using a gear volume error (GV_e) equation and the results are given in the last column of Table 4.17. The maximum total GV_e is below 9.72%.

Table 4. 15. Conversion factors for module and face width (Ø=25°, Type 1)

Design approaches		From B&N to AGMA				From ISO to AGMA				From J&M to AGMA			
m_G	N_p	$\overline{CF_m}$	$\sigma_{\overline{CF_m}}$	$\overline{CF_F}$	$\sigma_{\overline{CF_F}}$	$\overline{CF_m}$	$\sigma_{\overline{CF_m}}$	$\overline{CF_F}$	$\sigma_{\overline{CF_F}}$	$\overline{CF_m}$	$\sigma_{\overline{CF_m}}$	$\overline{CF_F}$	$\sigma_{\overline{CF_F}}$
1:1	6	1.059	0.066	1.167	0.129	1.167	0.089	1.185	0.164	0.996	0.066	1.104	0.126
2:1	7	1.061	0.070	1.134	0.135	1.194	0.081	1.174	0.147	1.014	0.070	1.094	0.124
3:1	7	1.061	0.070	1.134	0.135	1.195	0.082	1.177	0.149	1.014	0.070	1.094	0.124
4:1	8	1.007	0.054	1.109	0.106	1.190	0.083	1.183	0.154	1.011	0.062	1.117	0.124
5:1	8	1.007	0.054	1.109	0.106	1.190	0.083	1.185	0.154	1.011	0.062	1.117	0.124
6:1	8	1.007	0.054	1.109	0.106	1.191	0.083	1.183	0.154	1.011	0.062	1.117	0.124
7:1	8	1.007	0.054	1.109	0.106	1.194	0.079	1.178	0.144	1.011	0.062	1.117	0.124
8:1	8	1.007	0.054	1.109	0.106	1.194	0.079	1.178	0.144	1.011	0.062	1.117	0.124

Table 4. 16. Conversion factors for module and face width obtained from regression at any speed ratio in the range of 1 kW to 1000 kW ($\emptyset=25^{\circ}$, Type 1)

	Design approach (from)	C_p Expressions for Module (m_i) (to AGMA) regressions for $\overline{CF_{mt}}$	R^2
1kW - 1000kW	B&N to AGMA (B-A)	$\overline{CF_{m,B-A}}$ =-0.0005 m_G^4 + 0.0092m^3 - 0.0594m^2 + 0.131m + 0.9776	0.91
	ISO to AGMA (I-A)	$\overline{CF_{m,I-i}}$ =-0.0002 m_G^4 + 0.0049m^3 - 0.0345m^2 + 0.0982m + 1.0993	0.99
	J&M to AGMA (J-A)	$\overline{CF_{m,J-A}}$ =-0.0001 m_G^4 + 0.0029m^3 - 0.0206m^2 + 0.0597m + 0.9547	0.97
	C_p Expressions for Face Width (F) (to AGMA) regressions for $\overline{CF_{Ft}}$		
1kW - 1000kW	B&N to AGMA (B-A)	$\overline{CF_{F,B-A}}$ =0.000002m_G^4 - 0.0003m_G^3 + 0.0059m_G^2 - 0.0407m_G+1.201	0.94
	ISO to AGMA (I-A)	$\overline{CF_{F,I-A}}$ = 0.0002m_G^4 - 0.0036m_G^3 + 0.0239m_G^2 - 0.06 m_G +1.2246	0.99
	J&M to AGMA (J-A)	$\overline{CF_{F,J-A}}$ =0.0003m_G^4 - 0.0052m_G^3 + 0.0346m_G^2 - 0.0836m_G + 1.1581	0.90

92

Table 4. 17. Validating and proving conversion factors with the percentage errors in the range of 1 kW to 1000 kW (Ø=25º, Type 1)

Case: Design approach, m(speed ratio), Power (kW)	m_i	F_i	m_{AGMA}	F_{AGMA}	(mxF) AGMA	m_i and F_i converted to $m_{c,AGMA}$ and $F_{c,AGMA}$							
						$\overline{CF}_{mi}$	$m_{c,AGMA}$	m_i Error (%)	$\overline{CF}_{Fi}$	$F_{c,AGMA}$	F_i Error (%)	(mxF)$_{c,AGMA}$	GV_e (%)
J&M (4.5:1) 225	10	123.31	10	116.41	1164.11	1.03	9.71	-2.86	1.13	108.96	-6.40	1058.42	-9.08
J&M (2.6:1) 680	16	200.67	16	170.75	2732.05	1.02	15.73	-1.68	1.10	182.94	+7.14	2877.88	5.34
B&N (3.3:1) 125	9	112.57	8	112.26	898.04	1.03	8.70	+8.76	1.12	100.48	-10.49	874.26	-2.65
B&N (6.7:1) 400	12	165.88	12	148.06	1776.70	0.95	12.65	+5.45	1.11	149.85	+1.21	1896.27	6.73
ISO (7.3:1) 775	18	220.69	16	170.22	2723.60	1.32	13.68	-14.51	1.23	179.75	+5.60	2458.89	-9.72
ISO (1.8:1) 330	14	167.15	12	139.88	1678.61	1.19	11.76	-2.02	1.18	142.24	+1.69	1672.37	-0.37

The percentage differences of conversion factors concerning different pressure angles are tabulated in following Table 4.18 for module and Table 4.19 for face width to find out the correlation in between. As a result, the highest difference observed with B&N design approach while the lowest difference is with J&M design approach. This is valid for both module and face width.

Table 4. 18. Conversion factor differences considering pressure angle of $20^{°}$ and $25^{°}$ for module

Speed ratio	From B&N to AGMA			From ISO to AGMA			From J&M to AGMA		
	$\overline{CF_m}$, $\emptyset=20^{o}$	$\overline{CF_m}$, $\emptyset=25^{o}$	Difference (%)	$\overline{CF_m}$, $\emptyset=20^{o}$	$\overline{CF_m}$, $\emptyset=25^{o}$	Difference (%)	$\overline{CF_m}$, $\emptyset=20^{o}$	$\overline{CF_m}$, $\emptyset=25^{o}$	Difference (%)
1:1	1.059	0.928	14.15	1.167	1.094	6.69	0.996	1.006	0.99
2:1	1.061	0.904	17.36	1.194	1.076	10.96	1.014	1.002	1.15
3:1	1.061	0.897	18.28	1.195	1.074	11.29	1.014	1.006	0.75
4:1	1.007	0.897	12.25	1.190	1.074	10.78	1.011	1.006	0.46
5:1	1.007	0.897	12.25	1.190	1.074	10.78	1.011	1.006	0.46
6:1	1.007	0.897	12.25	1.191	1.076	10.69	1.011	1.006	0.46
7:1	1.007	0.897	12.25	1.194	1.076	10.96	1.011	1.006	0.46
8:1	1.007	0.897	12.25	1.194	1.076	10.96	1.011	1.006	0.46

Table 4. 19. Conversion factor differences considering pressure angle of $20°$ and $25°$ for face width

Speed ratio	From B&N to AGMA			From ISO to AGMA			From J&M to AGMA		
	$\overline{CF_F}$, $\varnothing=20°$	$\overline{CF_F}$, $\varnothing=25°$	Difference (%)	$\overline{CF_F}$, $\varnothing=20°$	$\overline{CF_F}$, $\varnothing=25°$	Difference (%)	$\overline{CF_F}$, $\varnothing=20°$	$\overline{CF_F}$, $\varnothing=25°$	Difference (%)
1:1	1.167	1.004	16.28	1.185	1.088	8.93	1.104	1.092	1.08
2:1	1.134	0.996	13.89	1.174	1.110	5.77	1.094	1.119	2.23
3:1	1.134	1.000	13.44	1.177	1.113	5.78	1.094	1.127	2.92
4:1	1.109	1.000	10.89	1.183	1.116	6.03	1.117	1.127	0.86
5:1	1.109	1.000	10.89	1.185	1.116	6.14	1.117	1.127	0.86
6:1	1.109	1.000	10.89	1.183	1.115	6.13	1.117	1.127	0.86
7:1	1.109	1.000	10.89	1.178	1.116	5.54	1.117	1.127	0.86
8:1	1.109	1.000	10.89	1.178	1.116	5.54	1.117	1.127	0.86

5. CONCLUSION

This thesis meets a need of selecting and using appropriate involute helical gear design approaches for all designers including the expert designers and novice learners who are practicing a helical gear design. This was made by comparing the most commonly used involute helical gear design approaches available in the literature. The selected approaches are given as follow;

5. Shigley's Mechanical Engineering Design 9th Edition (SI), Budynas R.G. and Nisbett J.K., 2011

6. Fundamental of Machine Component Design 5th Edition, Juvinall R.C. and Marshek K.M., 2011

7. ISO 6336 Standards, 2006 and ISO 9085:2002 Standards, 2002

8. ANSI/AGMA 2101-D04 Standards, 2004

This study proposes to use the easier and the most appropriate approach provided in the common text books considering the verified results of FEA, if there is no obligation to use ISO or ANSI/AGMA Standards. Because these standards are more challenging, time consuming and include complicated equations. Conversion factors for the conversion of text books results to the verified results were developed. Now, the results obtained by text books can be converted to the standards with the aid of conversion factors developed in this study. As a result of these, gear designers do not have to deal with the computational load of the standards. This does not only allow saving time and resources, but also provides safer and reliable designs.

A systematic methodology which relies on dimensionless numbers called as GR_i and CFs, has been described and proposed to rate most common design approaches with ANSI/AGMA 2001-D04 (2004) based on bending fatigue failure for helical gears. Although the results of four design approaches differ from each

97

other, good similarity and continuity of the charts were found out. This allowed to obtain CFs between the standards. Now, these two approaches can be converted to each other with minimum of error. Beyond the investigations already available in the literature, following conclusions can be drawn in this study;

1. Differences of GR_i numbers provide a relative comparison between each approach. For example, mean values of
   - GR_{AGMA} minus $GR_{J\&M}$ (1.00-1.12=-0.12)
   - GR_{AGMA} minus GR_{ISO} (1.00-1.19=-0.19)
   - GR_{AGMA} minus $GR_{B\&N}$ (1.00-0.89=0.11)

   provides relative gear tooth volume differences for pressure angle of 20° and material type 1. Under this comparison, m times F values of the simple approach J&M are approximately 12% outside of the verified AGMA as the ISO Standard is outside by 19%.

2. Likewise for pressure angle of 25° and material type 1, mean values of
   - GR_{AGMA} minus $GR_{J\&M}$ (1.00-1.11=-0.11)
   - GR_{AGMA} minus GR_{ISO} (1.00-1.39=-1.39)
   - GR_{AGMA} minus $GR_{B\&N}$ (1.00-1.15=-0.15)

   provides relative gear tooth volume differences. Under this comparison, m times F values of the simple approach J&M are approximately 11% outside of the verified AGMA as the ISO Standard is outside by 39%.

3. Dimensionless conversion factors (CFs) were generated for helical gears to convert the design results, module (m) and face width (F) of ISO Standard, B&N textbook and J&M textbook into AGMA with a minor error.

4. Scatter and radar charts presented to make a relative comparison between design approaches. The results showed that gear design approaches have similar behaviour in all power ranges.

5. Two methods are now available to obtain CFs. One can be made by linear interpolation from Table 4.12 for pressure angle of 20° and Table 4.15 for

98

pressure angle of 25°. Secondly, C_p expressions can be used for any desired speed ratio from Table 4.13 for pressure angle of 20° and Table 4.16 for pressure angle of 25°.

6. Universality of CFs were verified by case studies and worked reasonably well. The maximum total Gear Volume error (GV_e) was found as 9,2% for pressure angle of 20° in Table 4.14 and 9.72% for pressure angle of 25° in Table 4.17 with the aid of CFs.

Briefly, this study may serve as a guideline for a designer who deals with the design of an involute helical gear. This study is only valid for most common used helix angle which is 30°. For other helix angles, all results would change. If a designer concerns with light weighted applications, the overall size of a gear is important as well as material usage that are objectives of optimization. On the other hand helical gear design is the subject of almost all machine design courses. And it is important to introduce clear, easy to understand and reliable design approach for learners and students. Consequently, the results of this work interests both expert and novice designers and learners.

As future work, conversion factors between spur and helical gear could investigated. Spur gear design is relatively easy when it is compared with helical gear design. If this is studied as future work, it would be even easier to design helical gears. Secondly, a future study can be done for different speed ratios which is bigger than 8:1. Lastly, this study can be extended with different helix angles and pressure angles.

REFERENCES

ANSI/AGMA 2001-D04 Standards, 2004. Fundamental rating factors and calculation methods for involute spur and helical gear teeth. 59 pages, Virginia, USA.

AGMA 908-B89, 1989. Geometry factors for determining the pitting resistance and bending strength of spur, helical and herringbone gear teeth. 73 pages, Virginia, USA.

Babalık F.C., 2010. Makine Elemanları ve Konstrüksiyon Örnekleri. Dora BasımYayınevi, 4. Baskı, 860 sayfa.

Budynas R.G. and Nisbett J.K., 2011. Shigley's Mechanical Engineering Design. Ninth Edition, McGraw-Hill, 1120 pages.

Chen, Y., Tsay, C., 2002. Stress analysis of a helical gear set with localized bearing contact. Finite Elements in Analysis and Design, 38.8: 707-723.

Geren N., Uzay Ç., Bayramoglu M., 2017. "Introducing gear ratings and AGMA conversion factors for the steel spur gear design under bending fatigue", Materials Testing-Materials and Components Technology and application, vol.59, pp.1043-1053.

Geren N., Uzay Ç., Method for rating and converting text book spur gear design results to ISO gear standards. The 17th International Conference on Machine Design and Production, July 12 - July 15, Bursa, Turkey

ISO Standards 6336 – Part 1, 2006. Calculation of load capacity of spur and helical gears – Basic principles, introduction and general influence factors. 109 pages, Switzerland.

ISO Standards 6336 – Part 3, 2006. Calculation of load capacity of spur and helical gears – Calculation of tooth bending strength. 42 pages, London, UK.

ISO Standards 6336 – Part 5, 2003. Calculation of load capacity of spur and helical gears – Strength and quality of materials. 43 pages, Switzerland.

ISO Standards 6336 – Part 6, 2004. Calculation of load capacity of spur and helical gears – Calculation of service life under variable load. 23 pages, Switzerland.

ISO 9085:2002, 2002. Calculation of load capacity of spur and helical gears – Application for industrial gears. 57 pages, Switzerland.

Juvinall R.C., Marshek K.M., 2011. Fundamentals of Machine Component Design. Wiley 5th Edition, 928 pages.

Patil, S. et al., 2014. Contact stress analysis of helical gear pairs, including frictional coefficients. International Journal of Mechanical Sciences, 85: 205-211.

Rao, C., Muthuveeraooan, G., 1993. Finite element modelling and stress analysis of helical gear teeth. Computers & structures, 49.6: 1095- 1106.

Shigley J.E., 1985. Mechanical Engineering Design: First Metric Edition. Mcgraw-Hill, 698 pages.

Tsay, C., 1988. Helical gears with involute shaped teeth: geometry, computer simulation, tooth contact analysis, and stress analysis. Journal of mechanisms, transmissions, and automation in design, 110.4: 482-491.

Ugural A.C., 2003. Mechanical Design an Integrated Approach 1st Edition. McGraw Hill, 864 pages.

Uzay C., 2014. A comparison of approaches to involute spur gear design. 195 pages, Adana, Turkey.

Vishal S. et al.,2018. Finite element analysis of contact and bending stresses in helical gear pair. Ijder, volume 6, issue 2, p. 185-191.

Wu, Y., Wang, J.,; Han, Q., 2012. Static/dynamic contact FEA and experimental study for tooth profile modification of helical gears. Journal of Mechanical Science and Technology, 26.5: 1409-1417.

Zhang, Y., Fang, Z., 1997. Analysis of transmission errors under load of helical gears with modified tooth surfaces. Journal of Mechanical Design, 119.1: 120-126.

BIOGRAPHY

Zekiye Dicle Topal was born in 10.03.1993 and raised in Adana, TURKEY. She graduated from Piri Reis Anatolian High School in 2010. She enrolled Mechanical Engineering Department in Çukurova University after graduating from high school. She graduated from University with her Bachelor of Science in 2015. She began her Master of Science education at Mechanical Engineering Department of Çukurova University in the same year of 2015, September. She started to work for Robert Bosch Gmbh as a development engineer in research and development department in 2016 in Bursa, TURKEY.

APPENDIX

A.1. Comparison of Module Selection and Face Width Results of the Design Approaches for Ø=20°, Material type 1
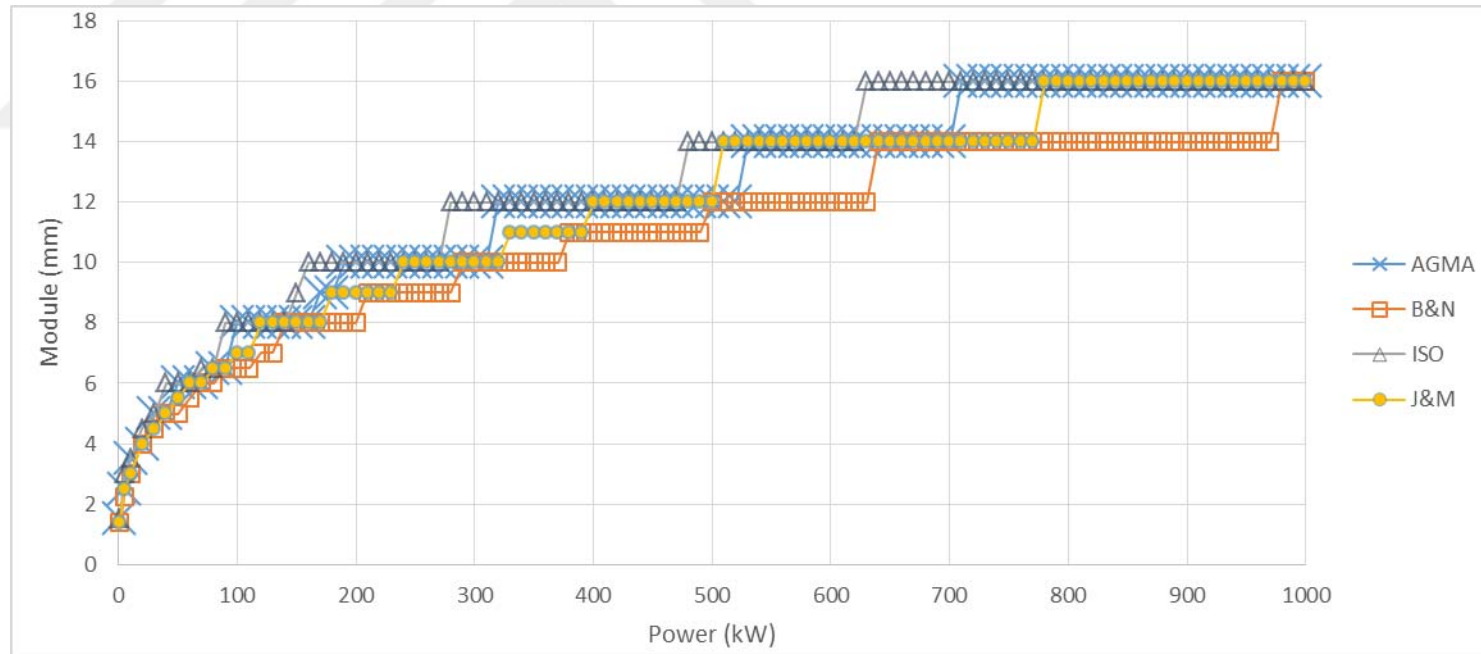
Figure A. 1. Module variation considering bending fatigue failure under increasing power at 4:1 speed ratio (Ø=20°, Type 1)
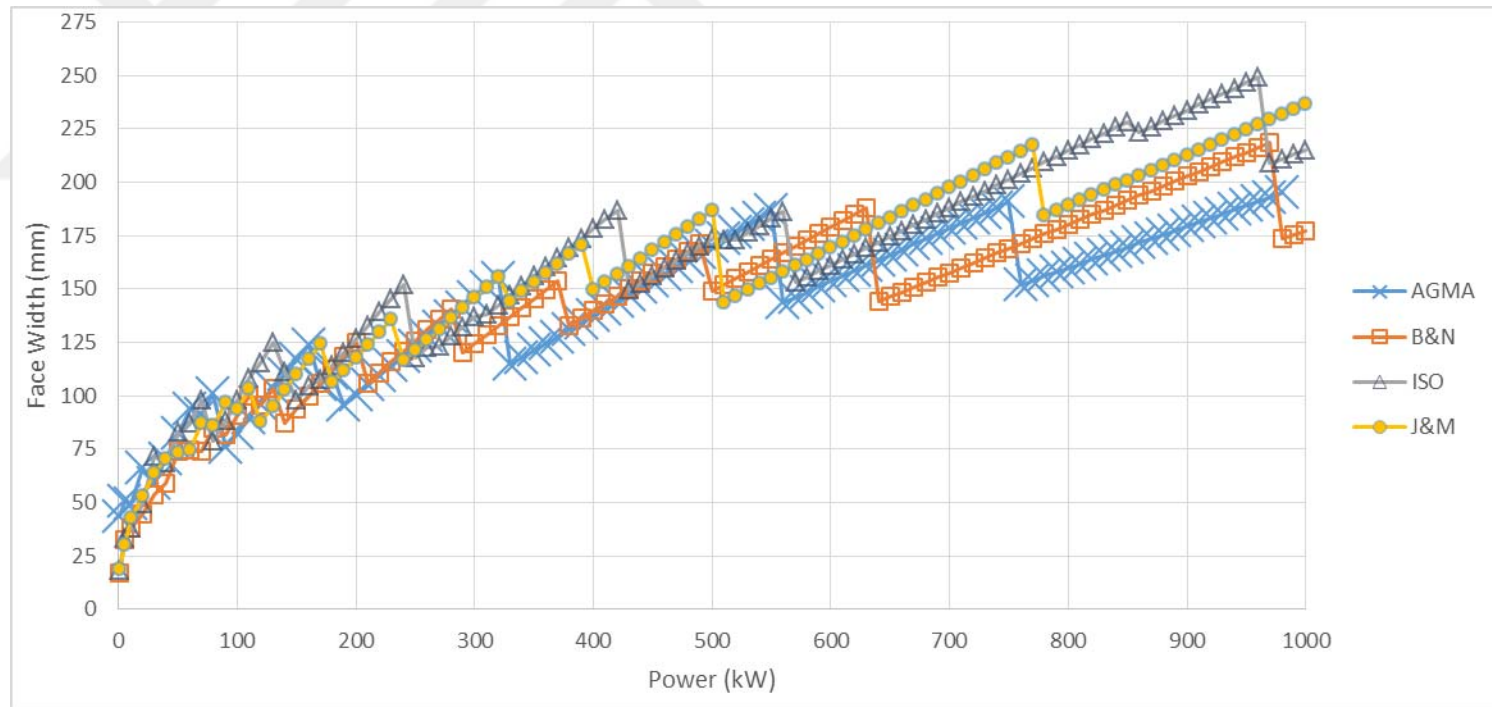
Figure A. 2. Face width variation considering bending fatigue failure under increasing power at 4:1 speed ratio (Ø=20°, Type1)
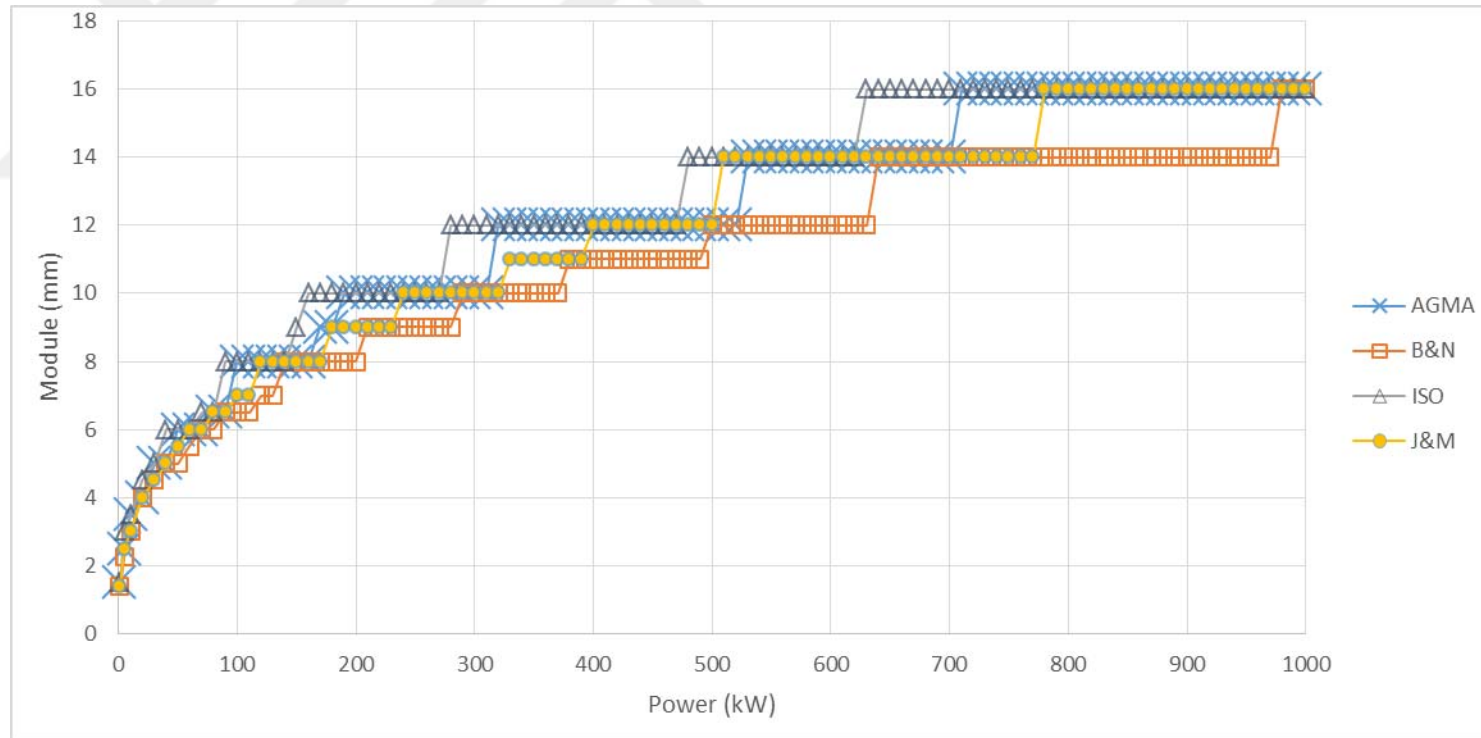
Figure A. 3. Module variation considering bending fatigue failure under increasing power at 5:1 speed ratio (Ø=20°, Type 1)
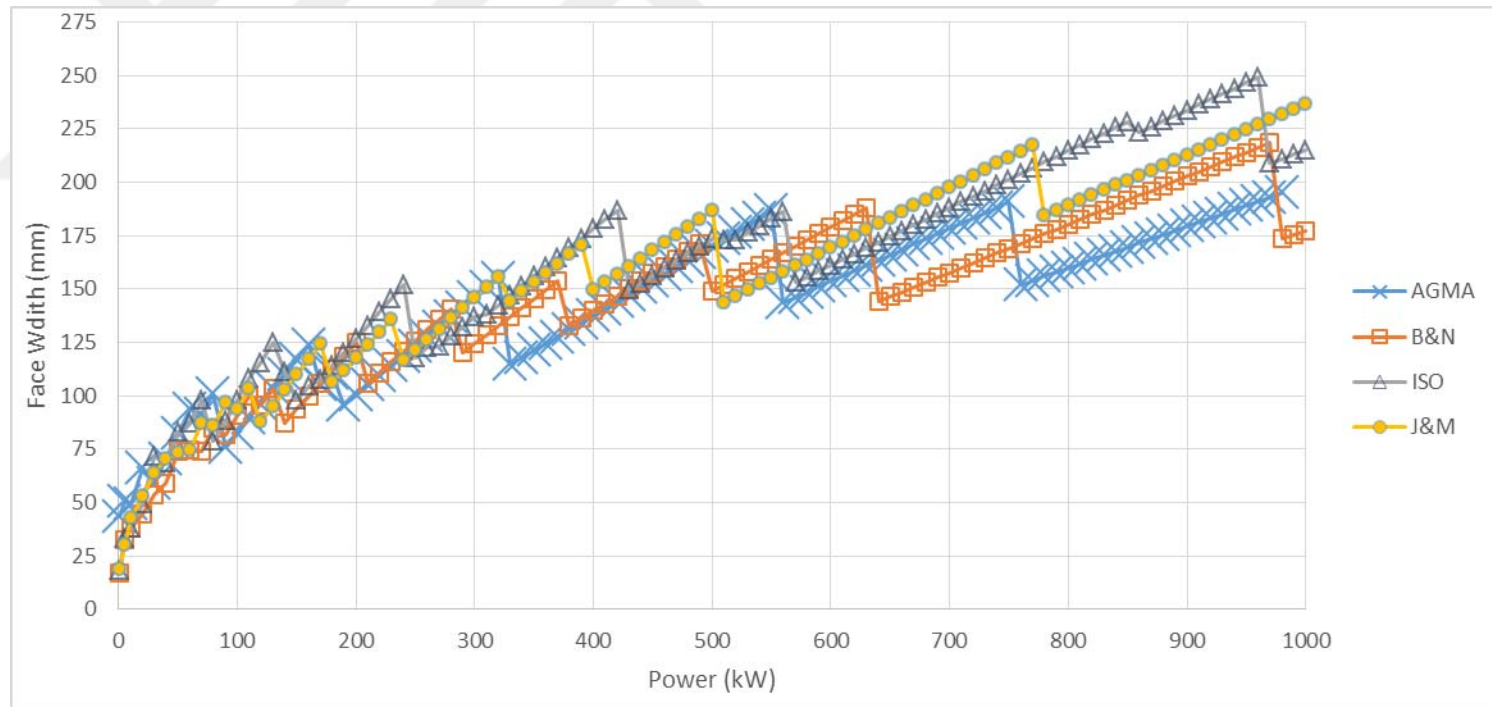
Figure A.4.Face width variation considering bending fatigue failure under increasing power at 5:1 speed ratio (Ø=20°, Type 1)
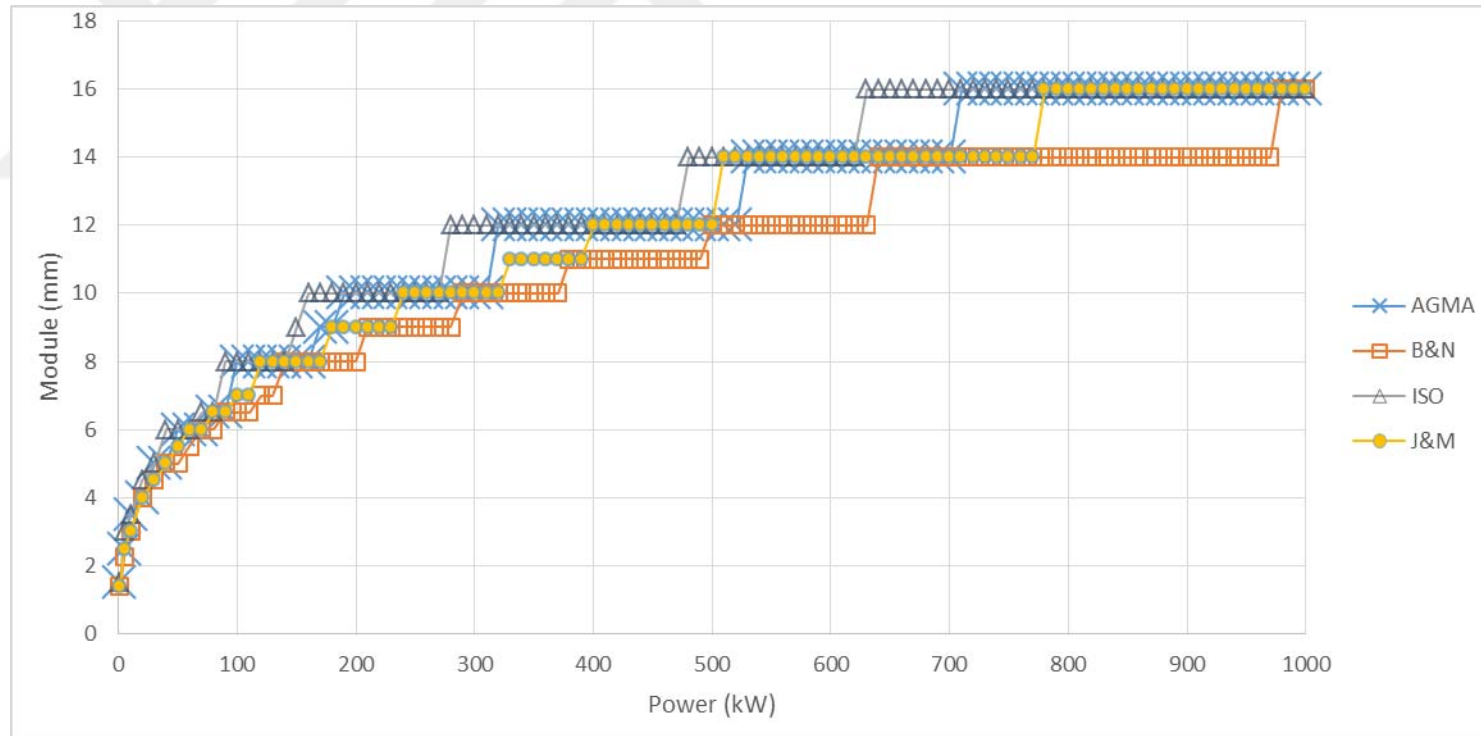
Figure A.5. Module variation considering bending fatigue failure under increasing power at 6:1 speed ratio (Ø=20°, Type 1)
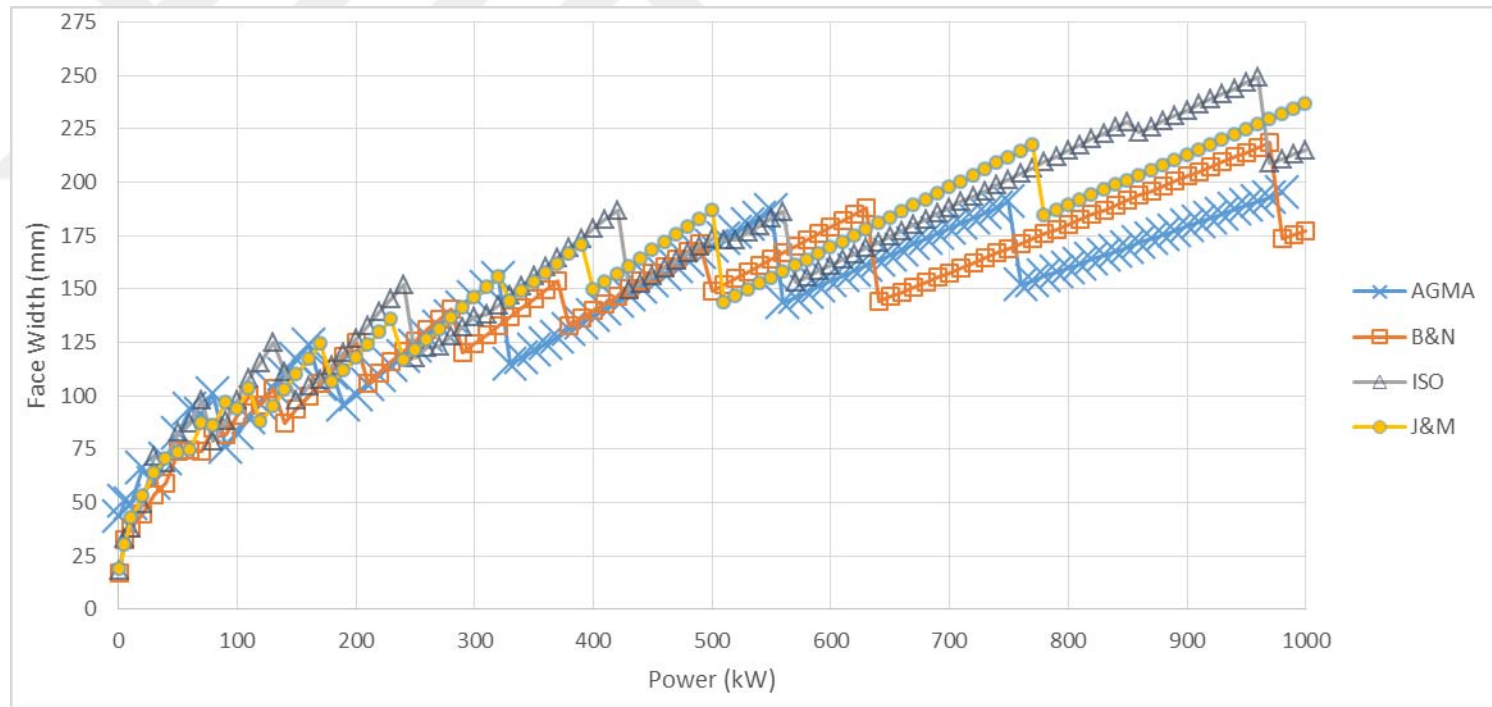
Figure A.6.Face width variation considering bending fatigue failure under increasing power at 6:1 speed ratio (Ø=20°, Type 1)
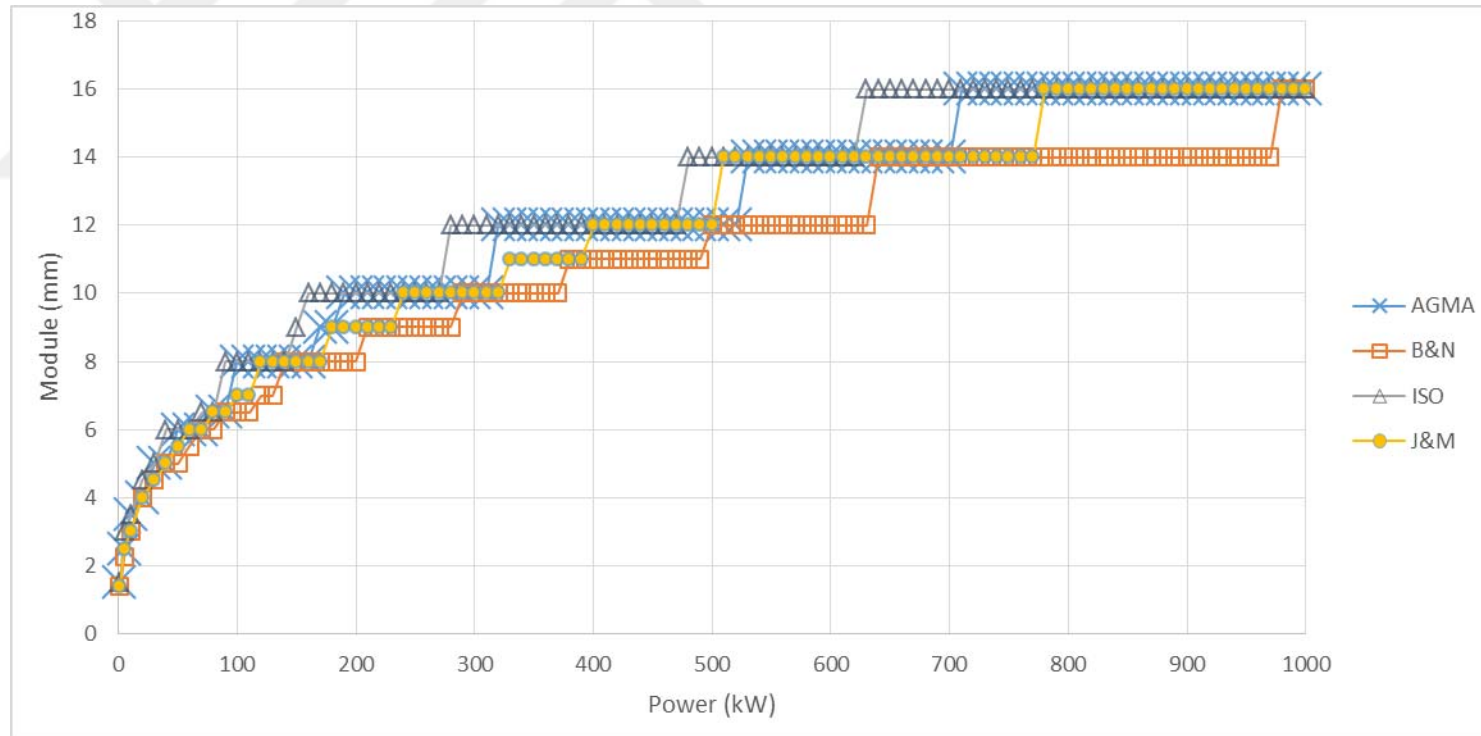
Figure A.7. Module variation considering bending fatigue failure under increasing power at 7:1 speed ratio (Ø=20°, Type 1)
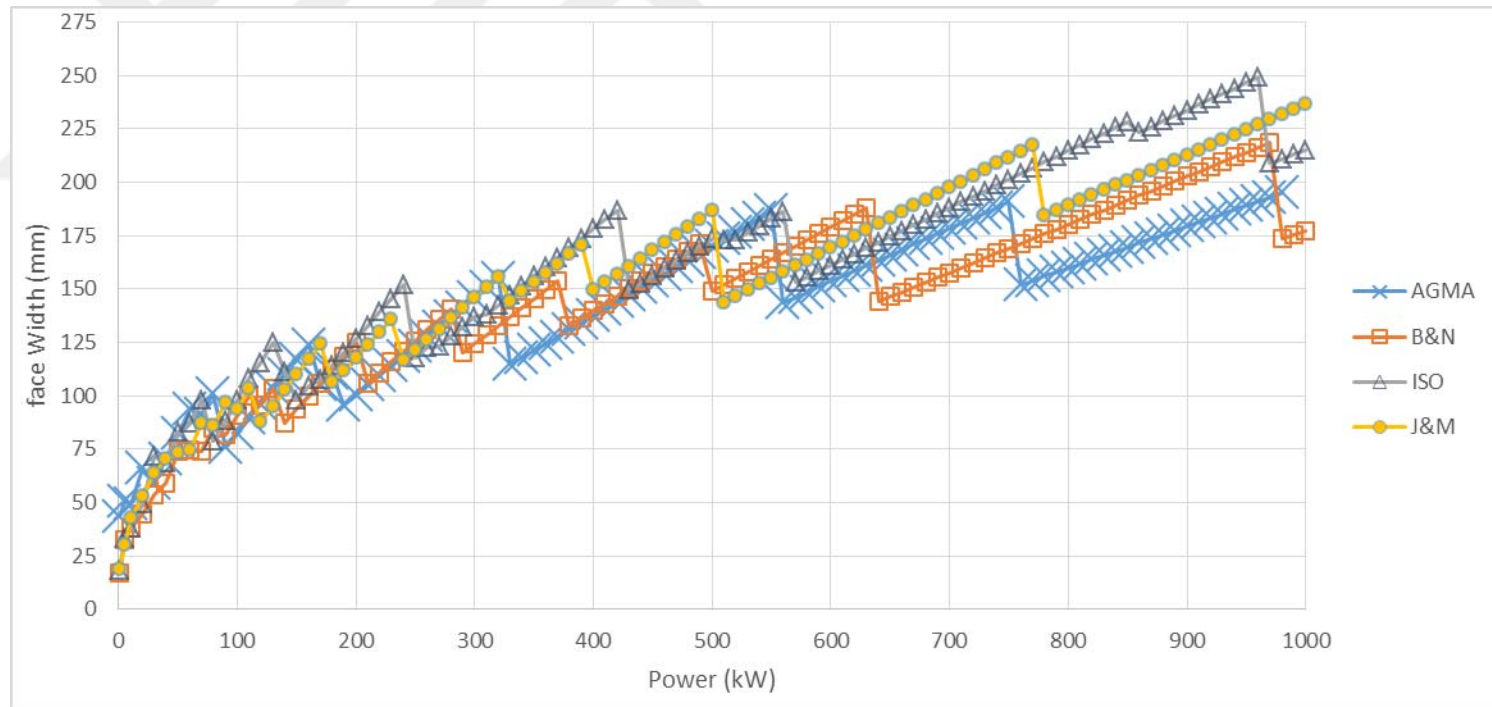
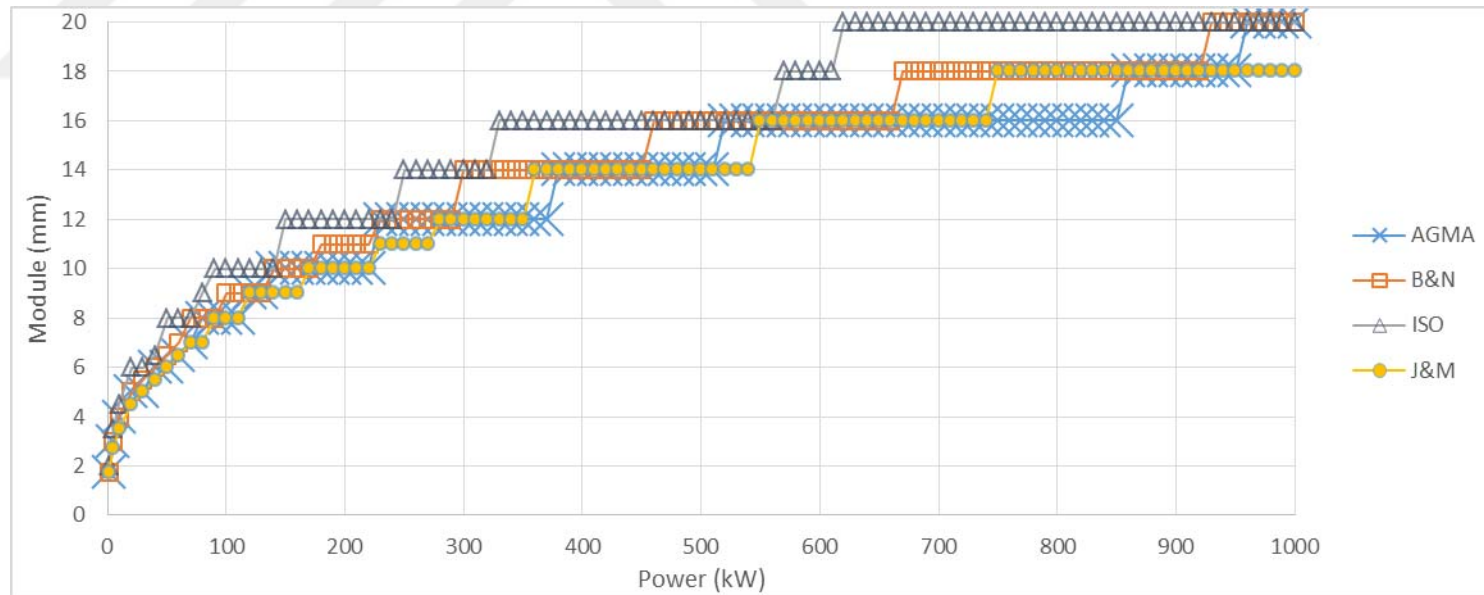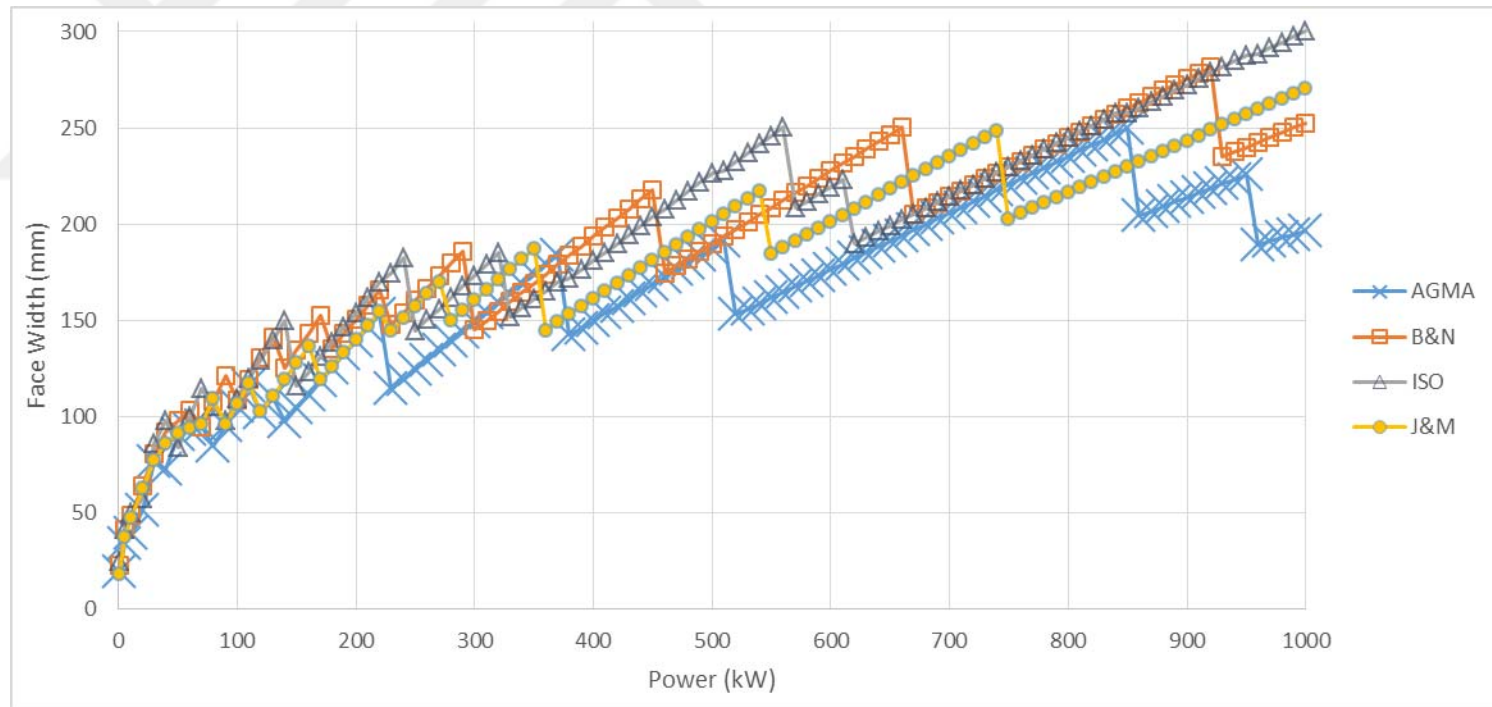Figure A.8.Face width variation considering bending fatigue failure under increasing power at 7:1 speed ratio (Ø=20°, Type 1)
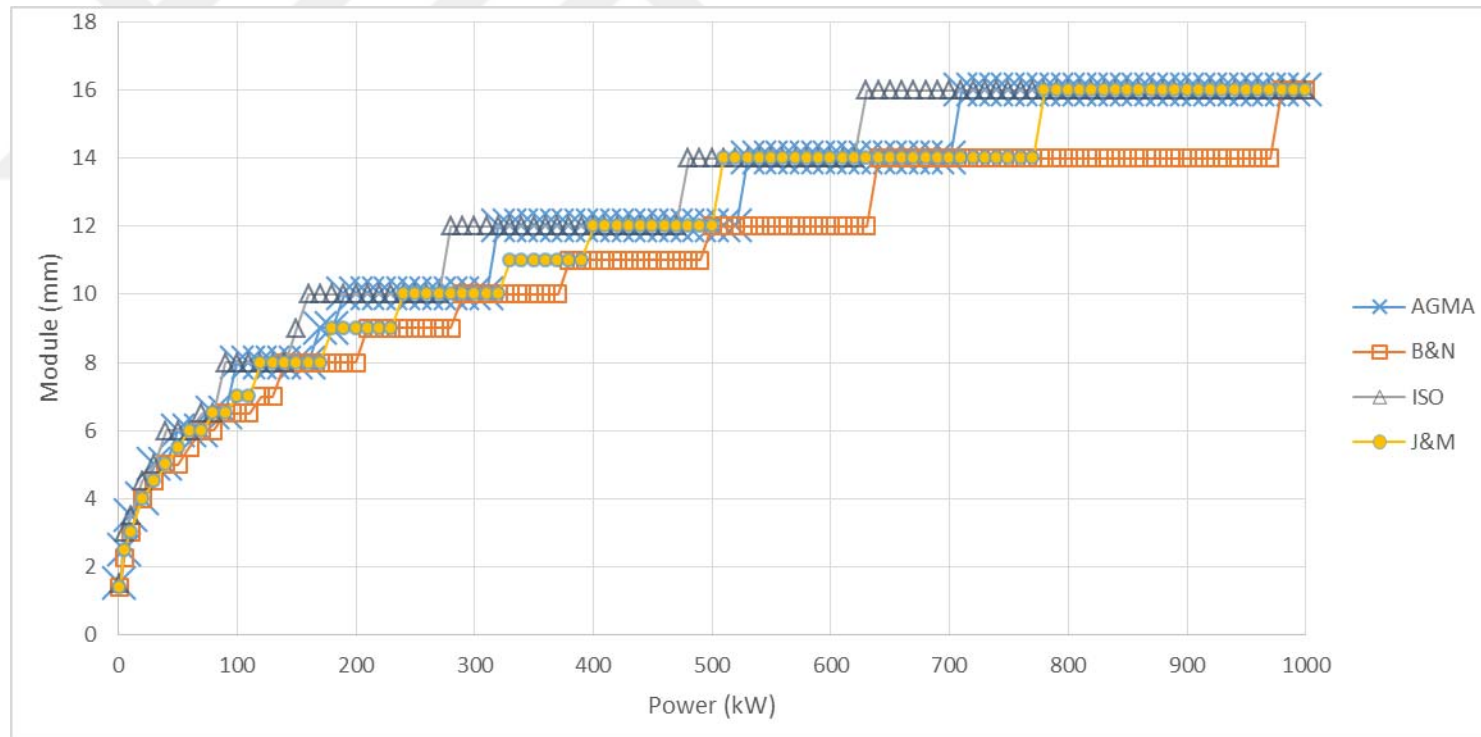
Figure A.9.Module variation considering bending fatigue failure under increasing power at 8:1 speed ratio (Ø=20°, Type 1)

Figure A.10. Face width variation considering bending fatigue failure under increasing power at 8:1 speed ratio (Ø=20°, Type1)

A.2. Obtaining Geometric Rating Number (GR$_i$) for Design Approaches for Ø=20°, Material type 1
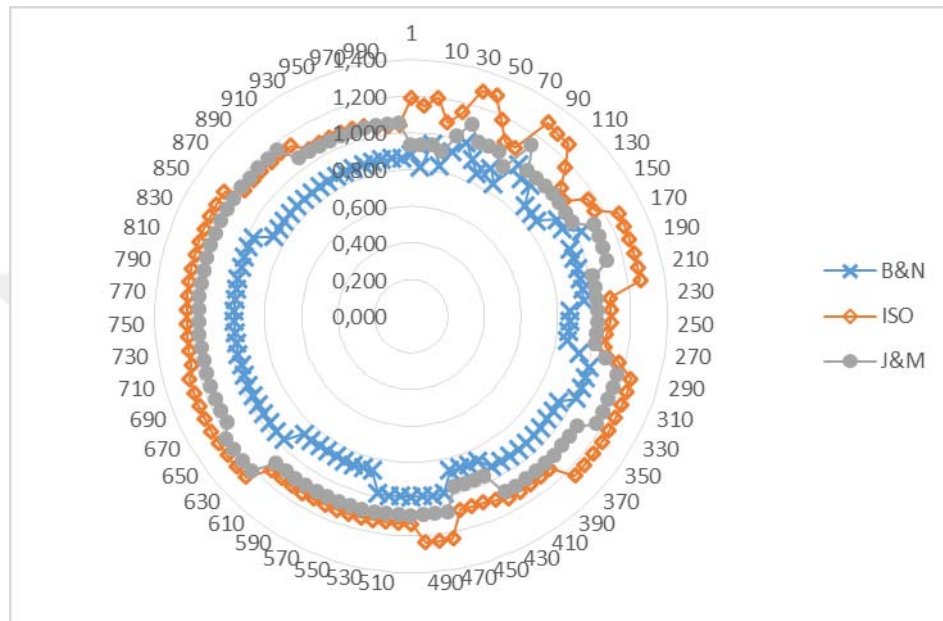
Figure A.11. GR$_i$ (m$_i$F$_i$/m$_0$F$_0$) results comparison for each design approach for 1:1 speed ratio (Ø=20°, Type 1)
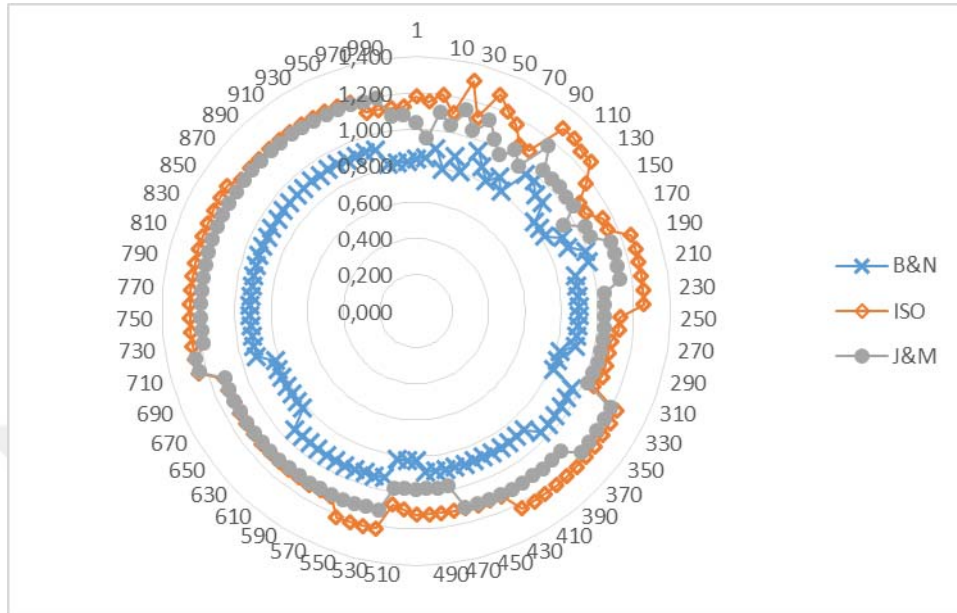
Figure A.12. GR$_i$ (m$_i$F$_i$/m$_0$F$_0$) results comparison for each design approach for 2:1 speed ratio (Ø=20°, Type 1)
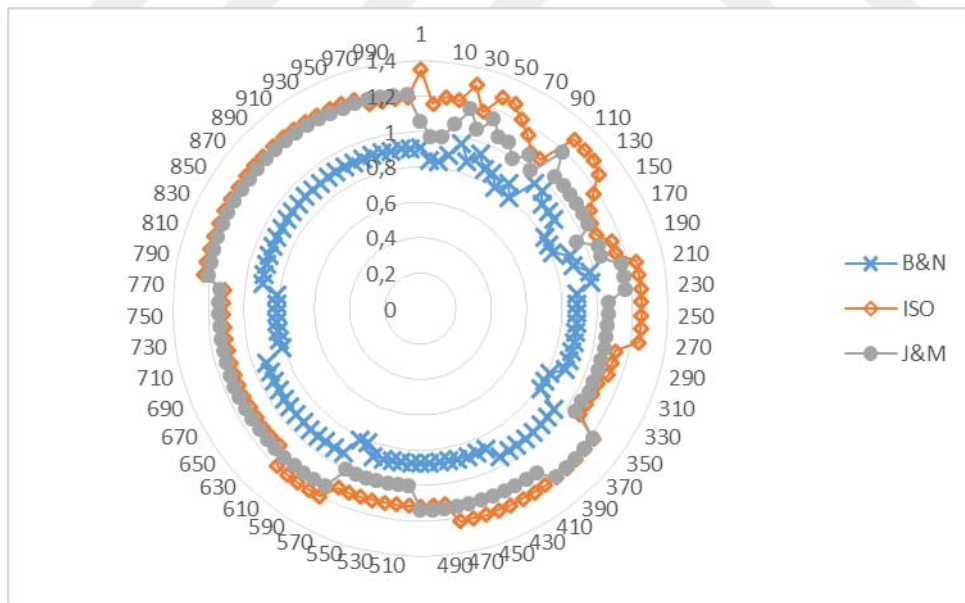
Figure A.13. GR$_i$ (m$_i$F$_i$/m$_0$F$_0$) results comparison for each design approach for 3:1 speed ratio (Ø=20°, Type 1)
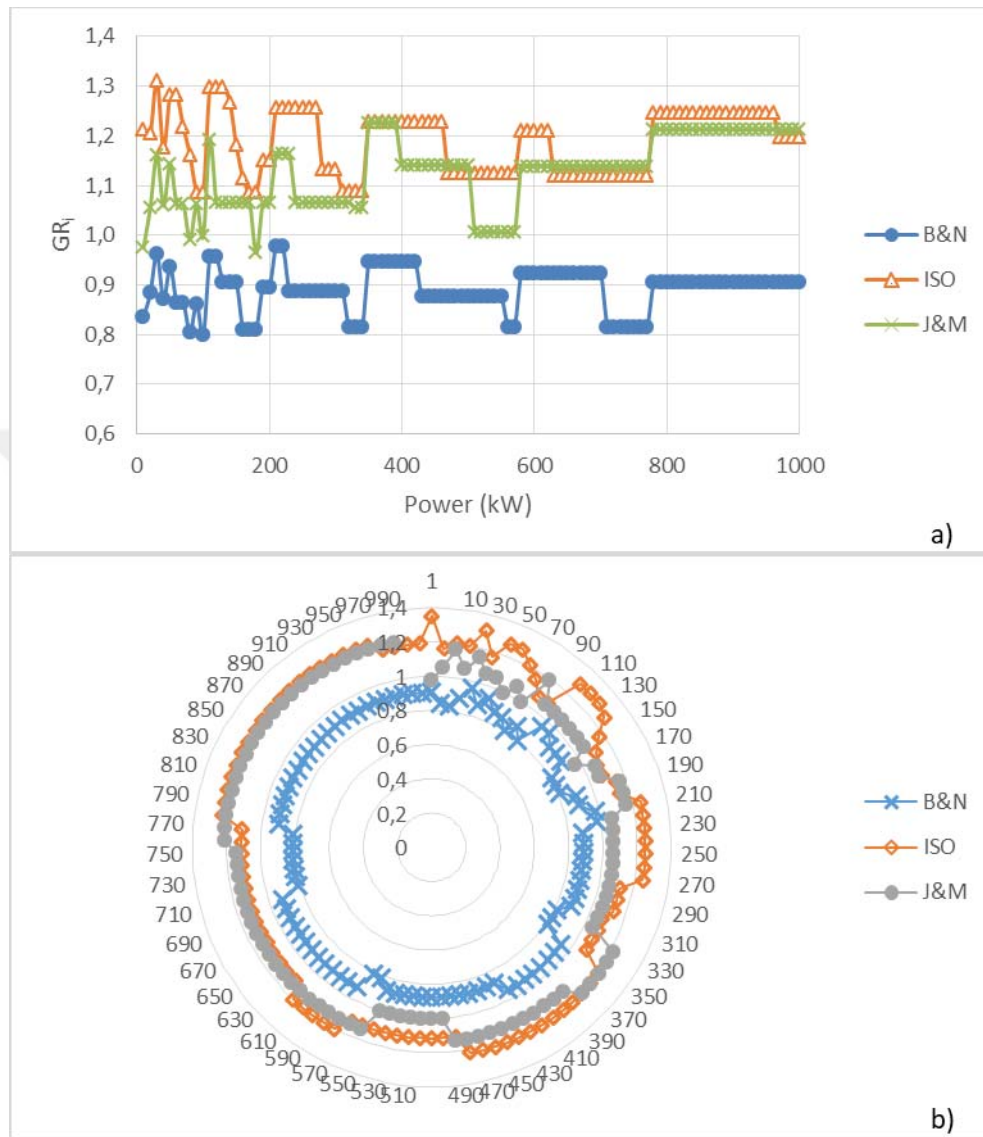
Figure A.14. Comparison of GR$_i$ results obtained from the design approaches at 4:1 speed ratio (Ø=20°, Type 1), a) scatter chart, b) radar chart
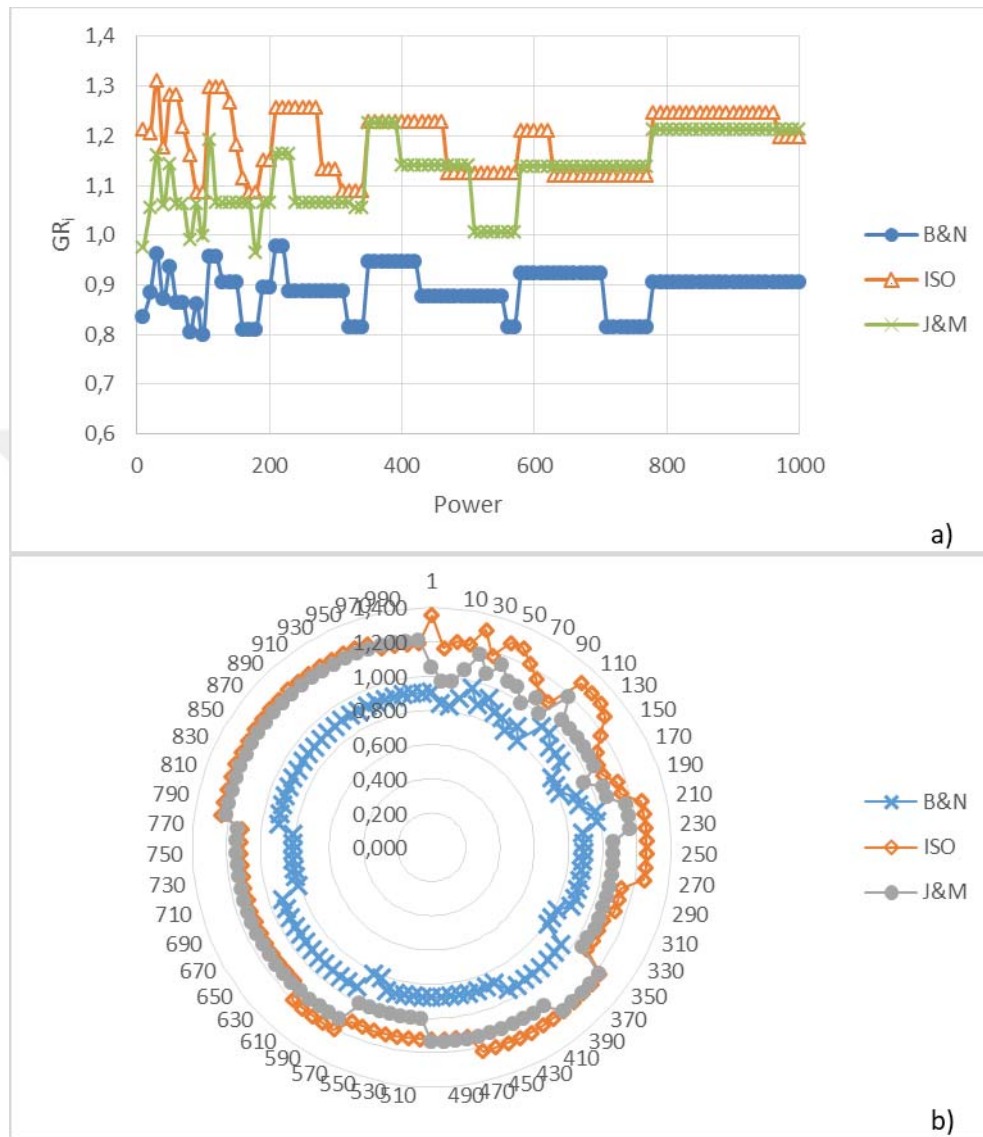
Figure A.15. Comparison of GR_i results obtained from the design approaches at 5:1 speed ratio ($\emptyset=20^o$, Type 1), a) scatter chart, b) radar chart
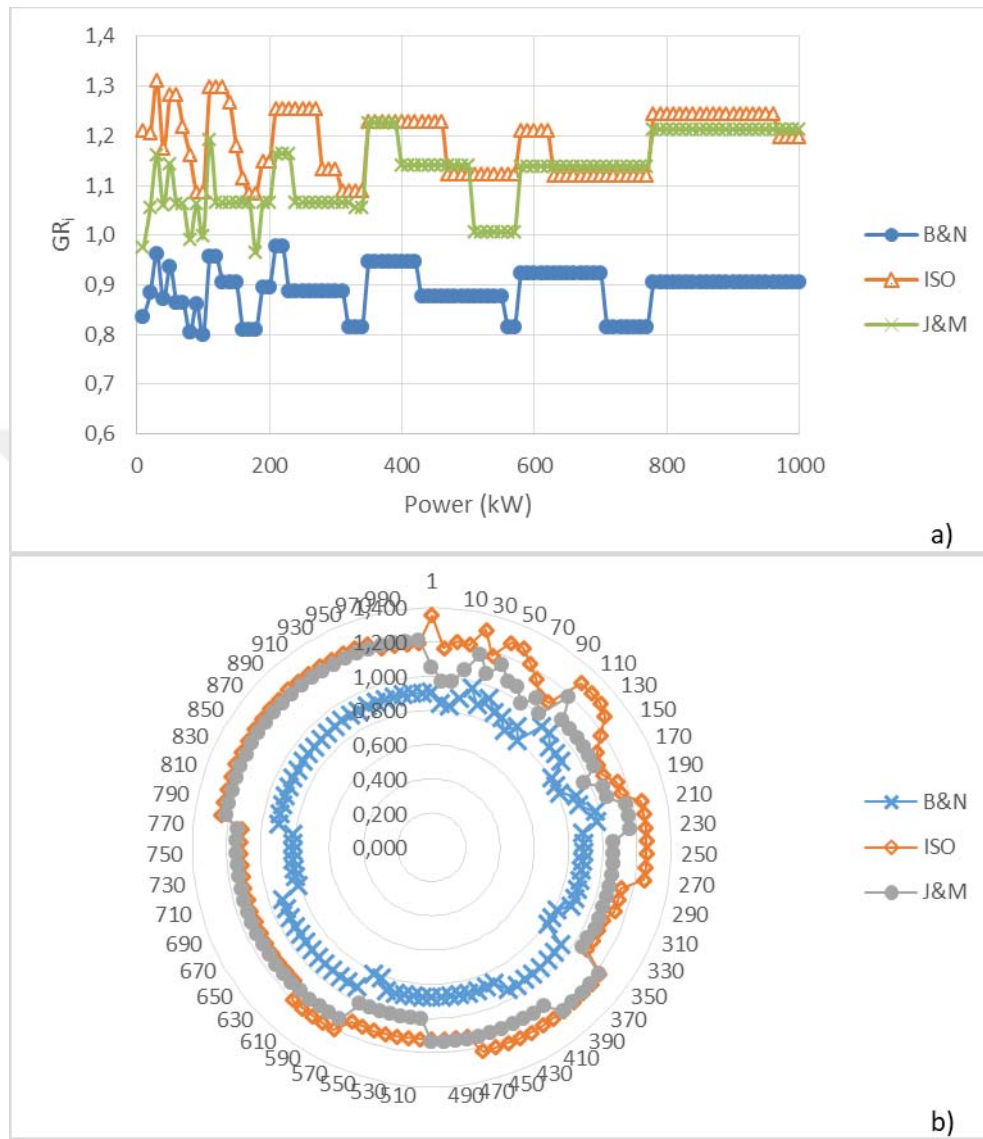
Figure A.16. Comparison of GR_i results obtained from the design approaches at 6:1 speed ratio (Ø=20°, Type 1), a) scatter chart, b) radar chart

120
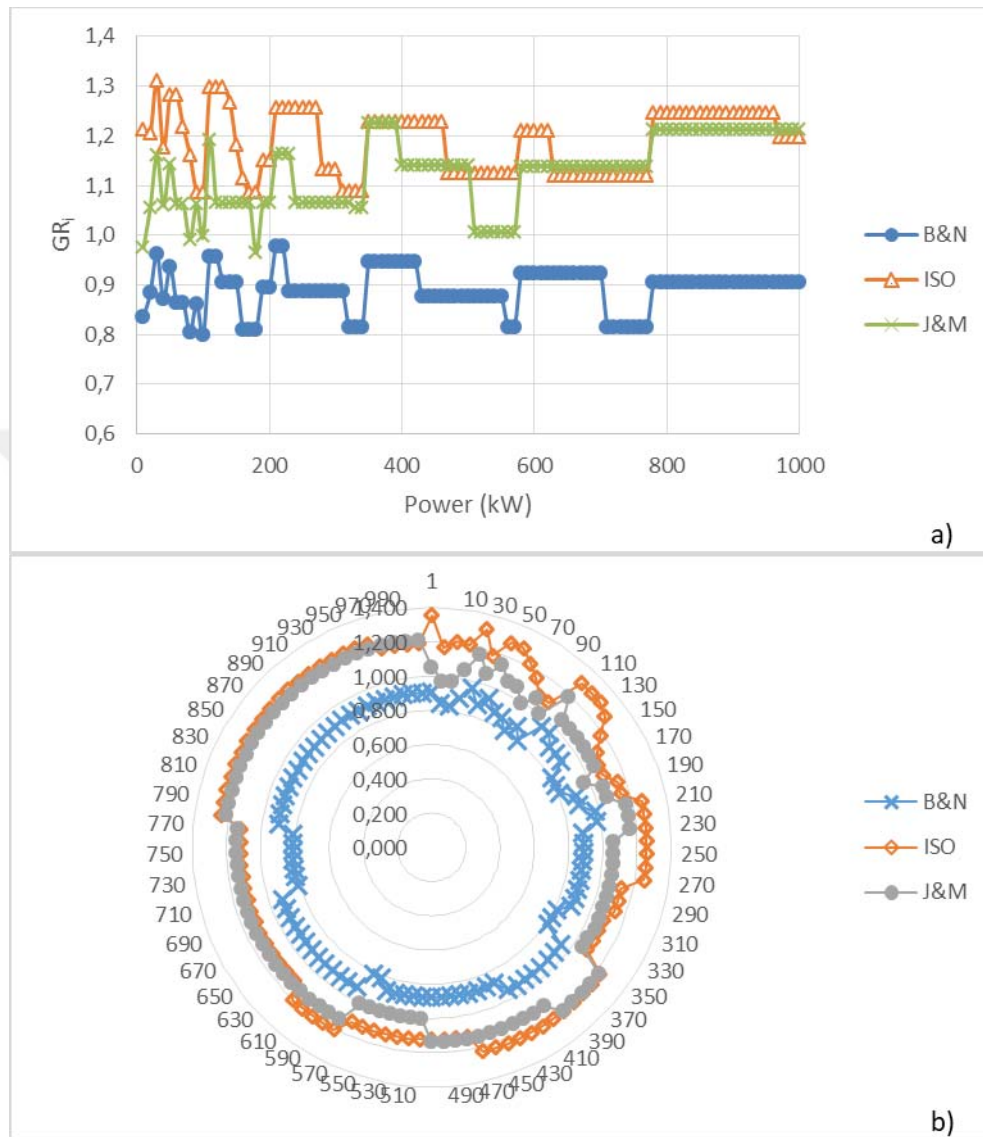
Figure A.17. Comparison of GR_i results obtained from the design approaches at 7:1 speed ratio ($\emptyset=20^o$, Type 1), a) scatter chart, b) radar chart

121
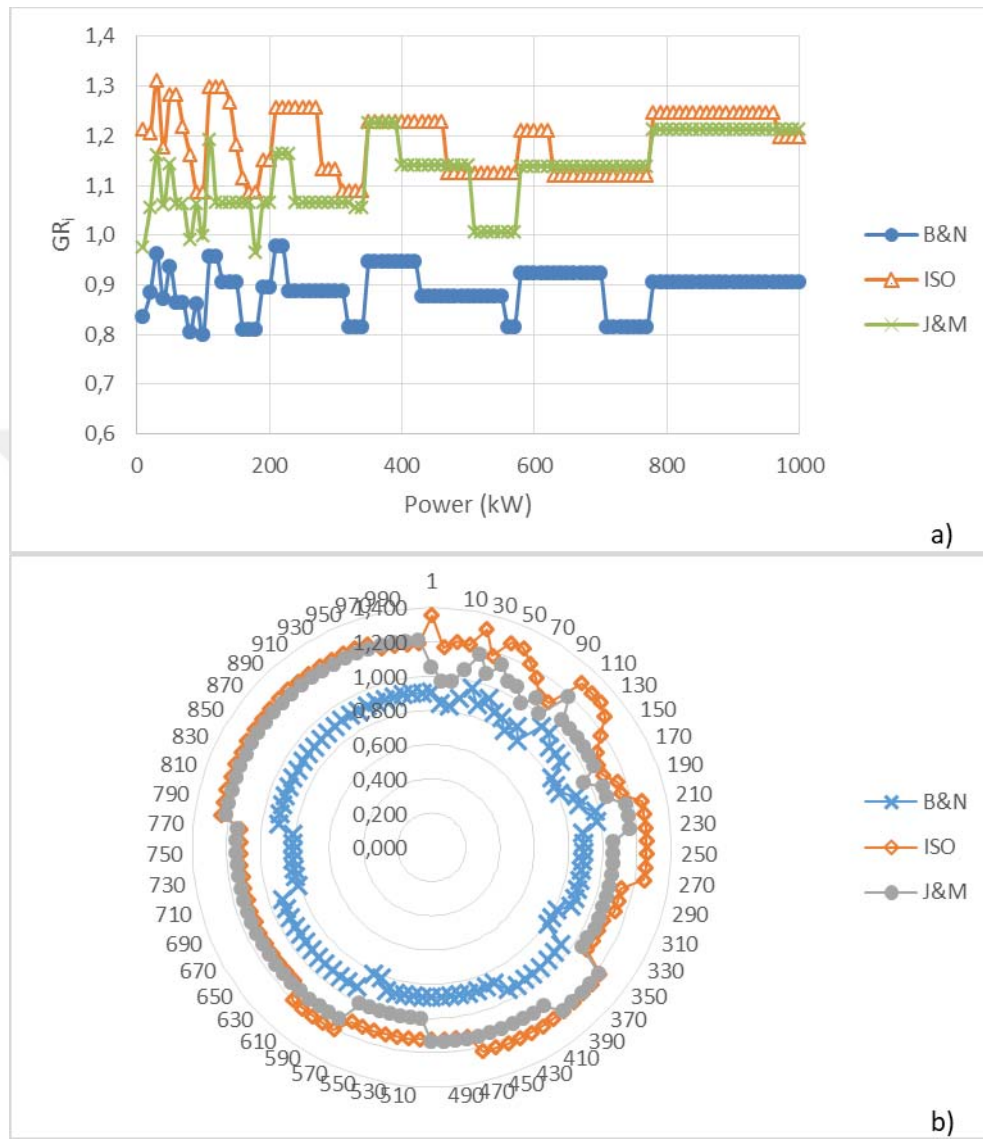
Figure A.18. Comparison of GR_i results obtained from the design approaches at 8:1 speed ratio (Ø=20°, Type 1), a) scatter chart, b) radar chart

APPENDIX B

B.1. Comparison of Module Selection and Face Width Results of the Design Approaches for Ø=20°, Material type 2
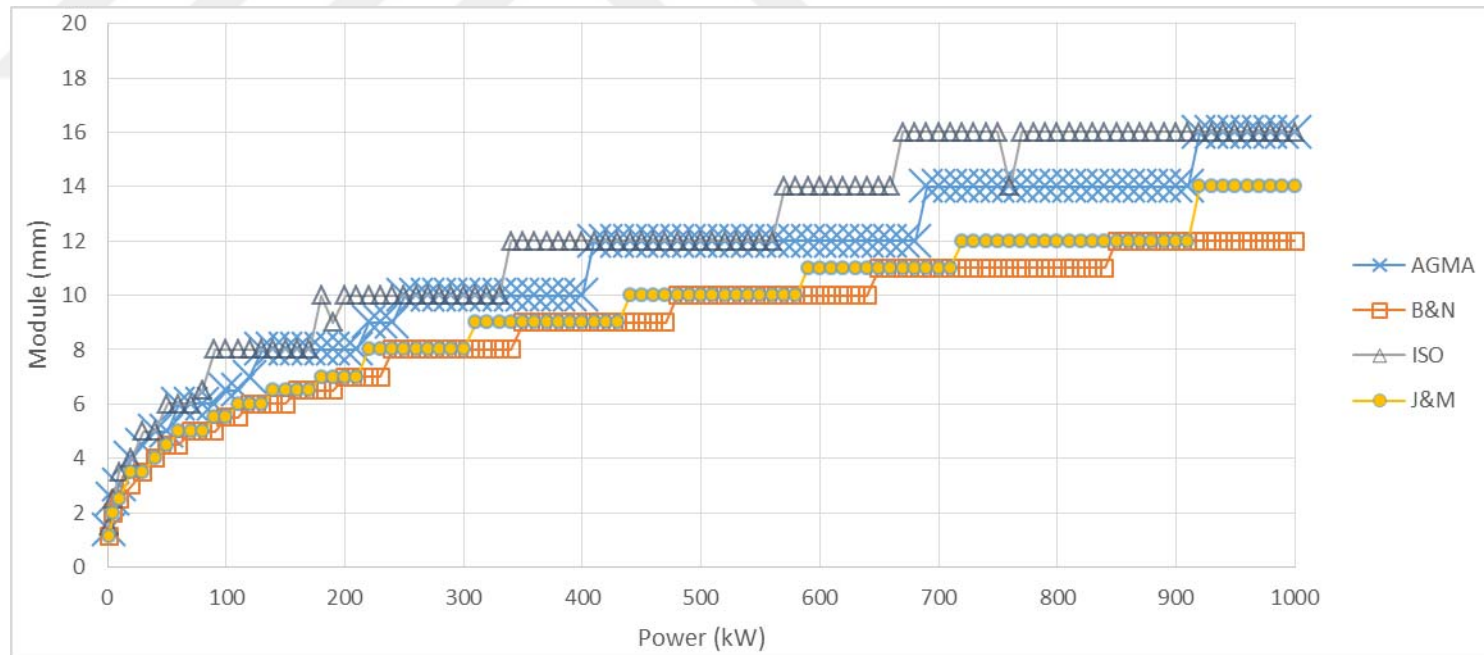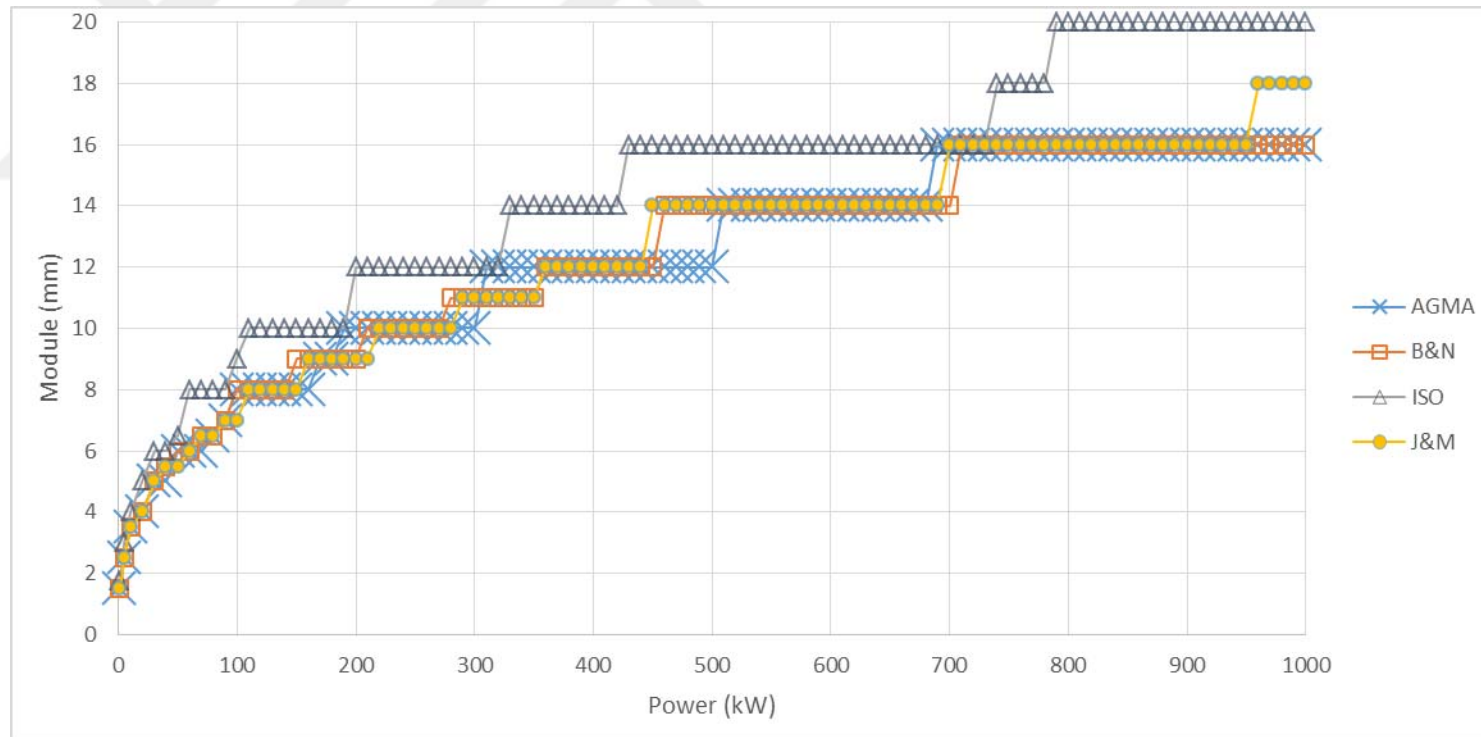

Figure B. 1. Module variation considering bending fatigue failure under increasing power at 1:1 speed ratio (Ø=20°, Type 2)
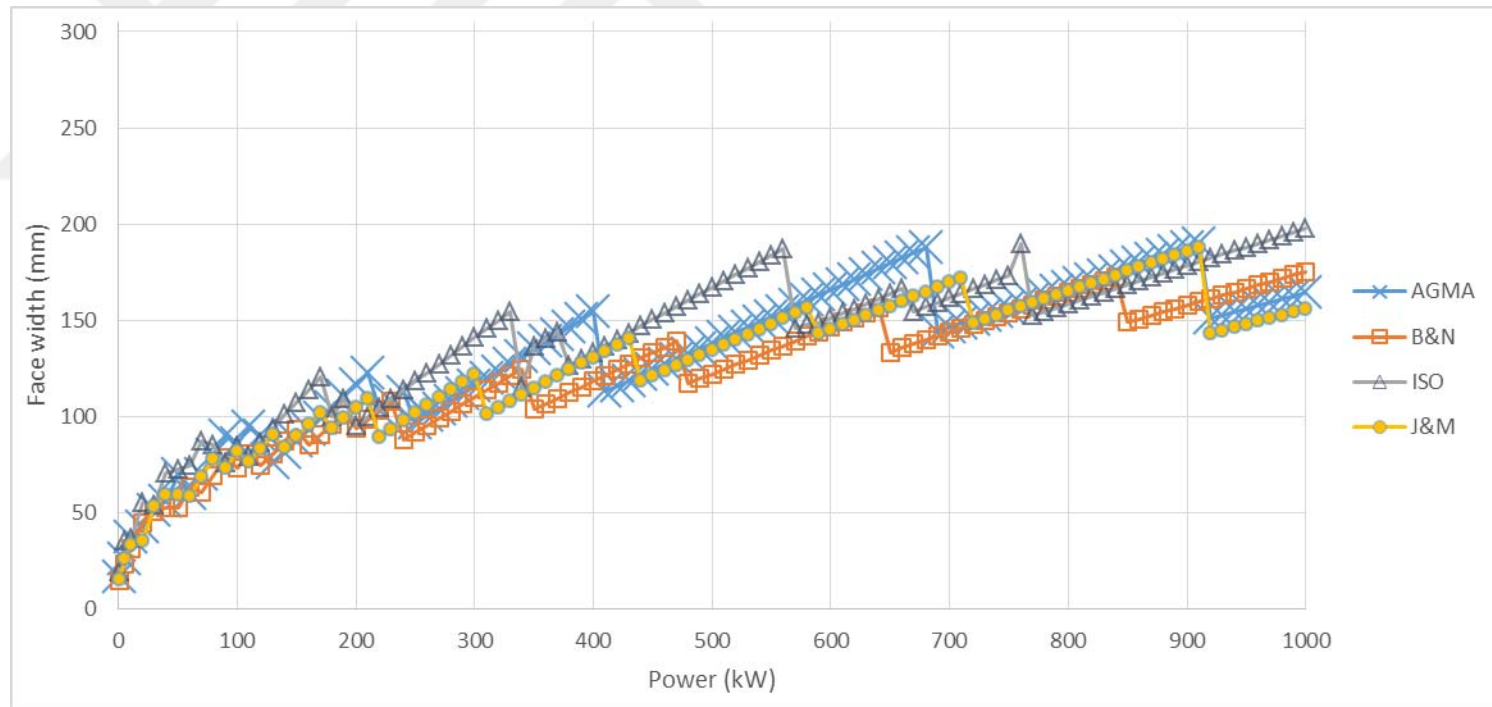
Figure B.2.Face width variation considering bending fatigue failure under increasing power at 1:1speed ratio (Ø=20°, Type 2)
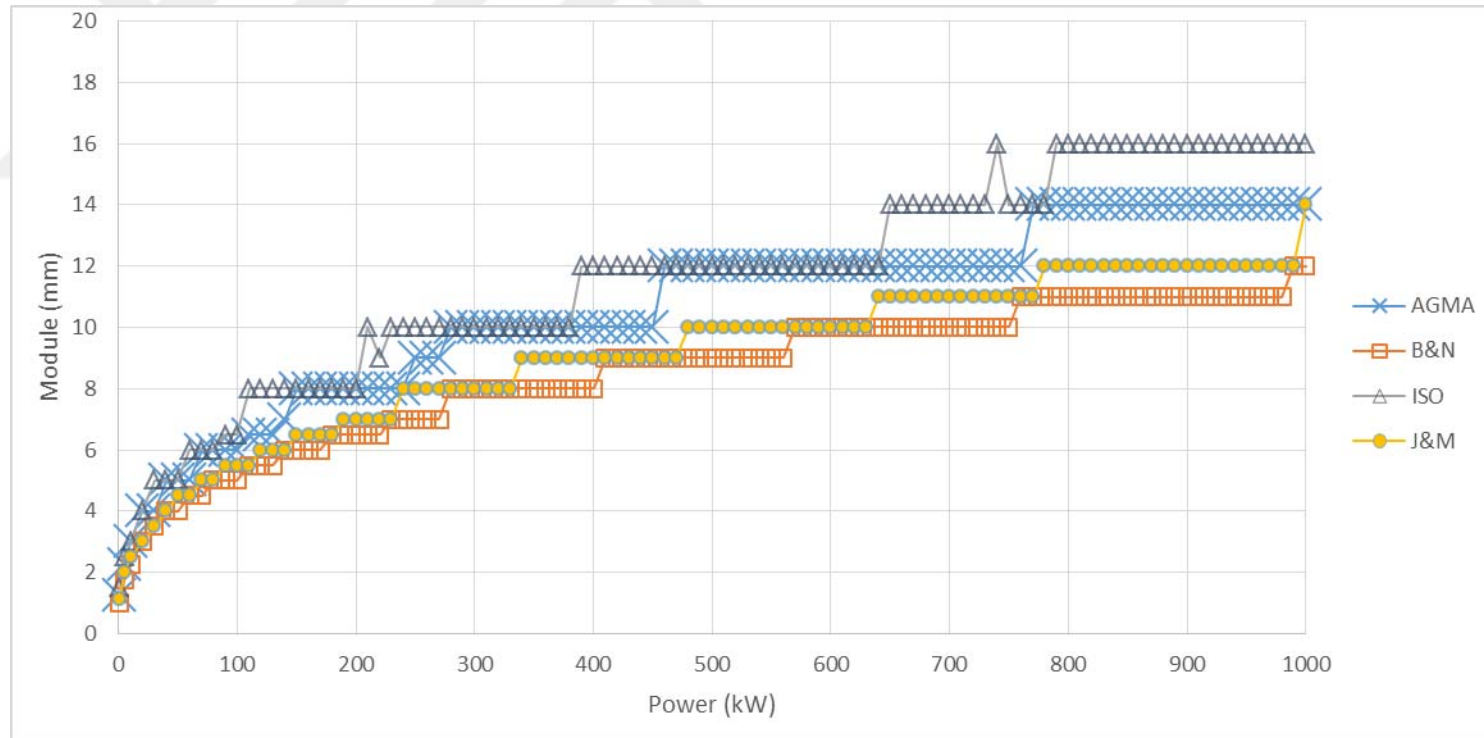
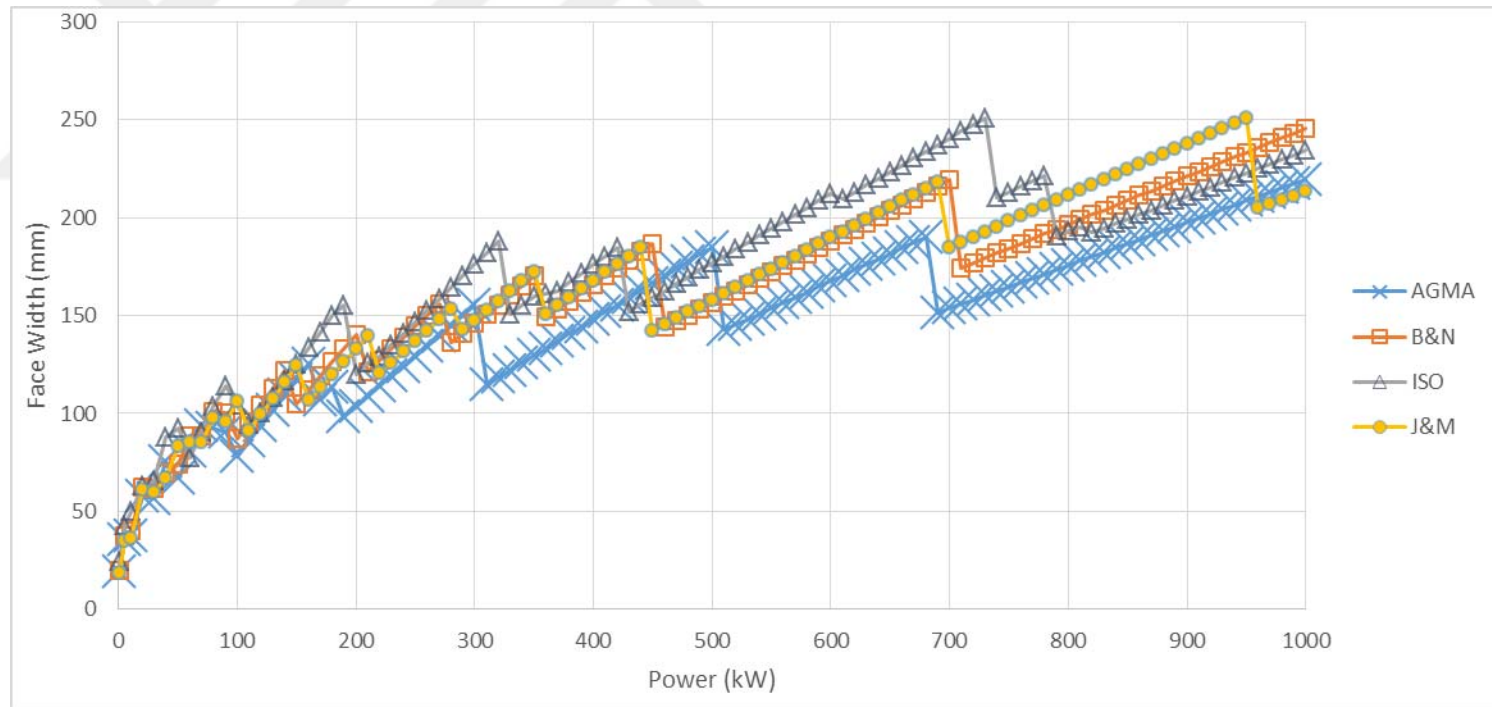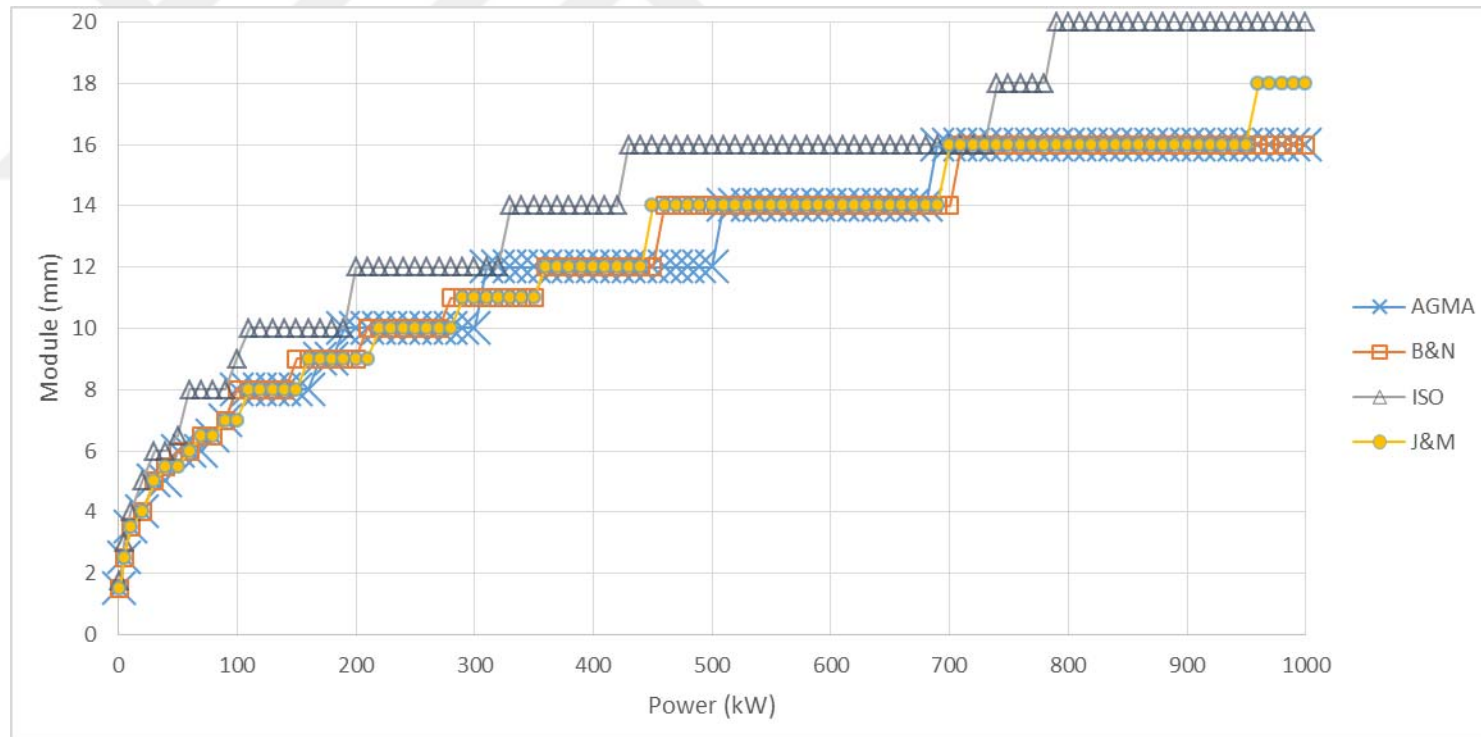Figure B. 3. Module variation considering bending fatigue failure under increasing power at 2:1 speed ratio (Ø=20°, Type 2)
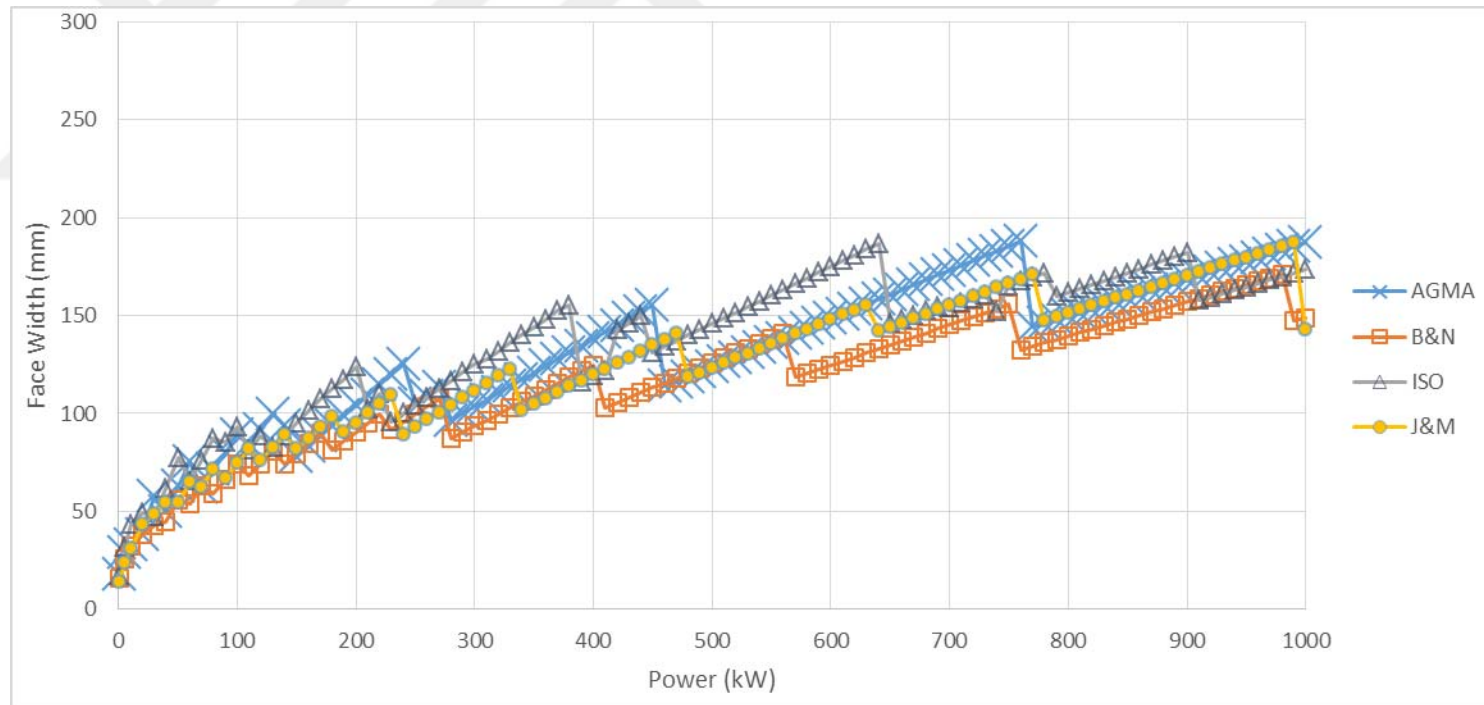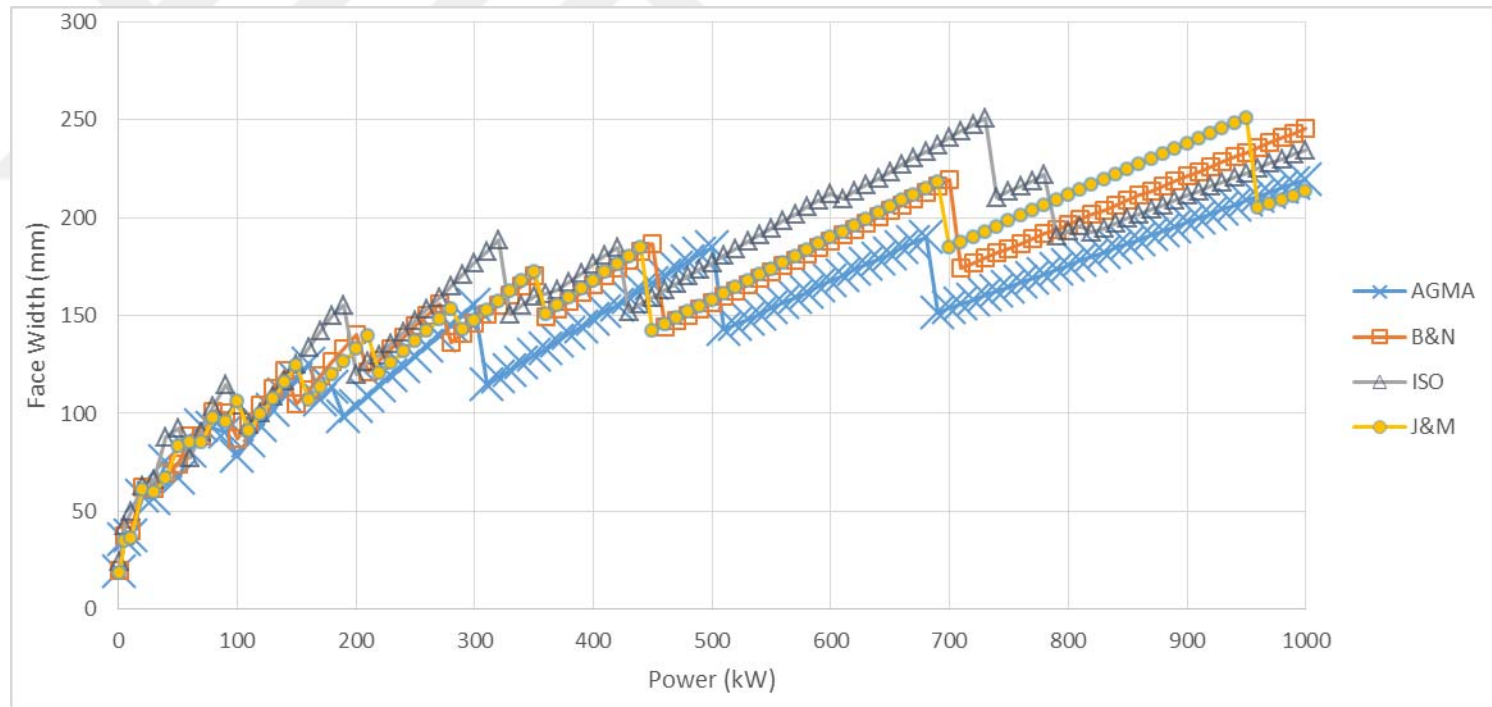
Figure B.4.Face width variation considering bending fatigue failure under increasing power at 2:1 speed ratio (Ø=20°, Type 2)
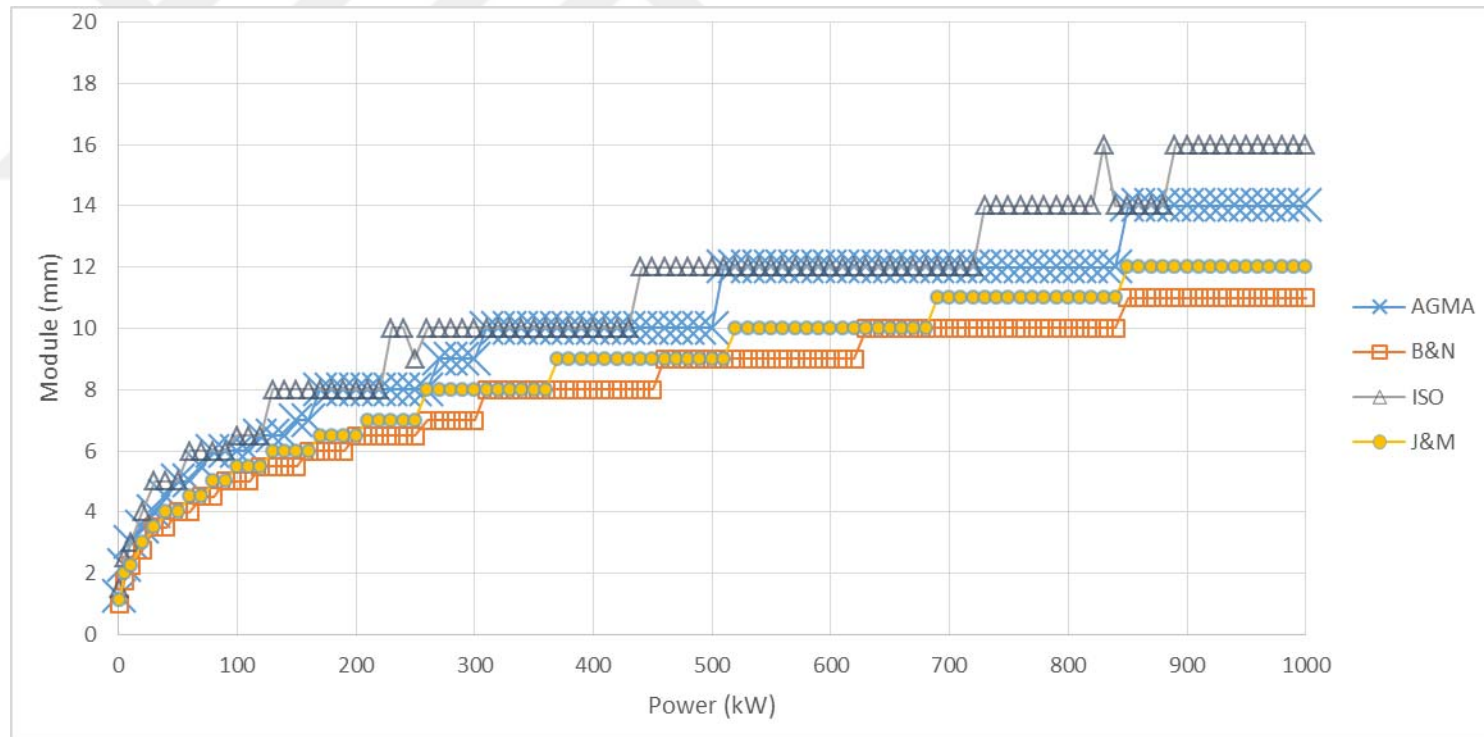
Figure B. 5. Module variation considering bending fatigue failure under increasing power at 3:1 speed ratio (Ø=20°, Type 2)
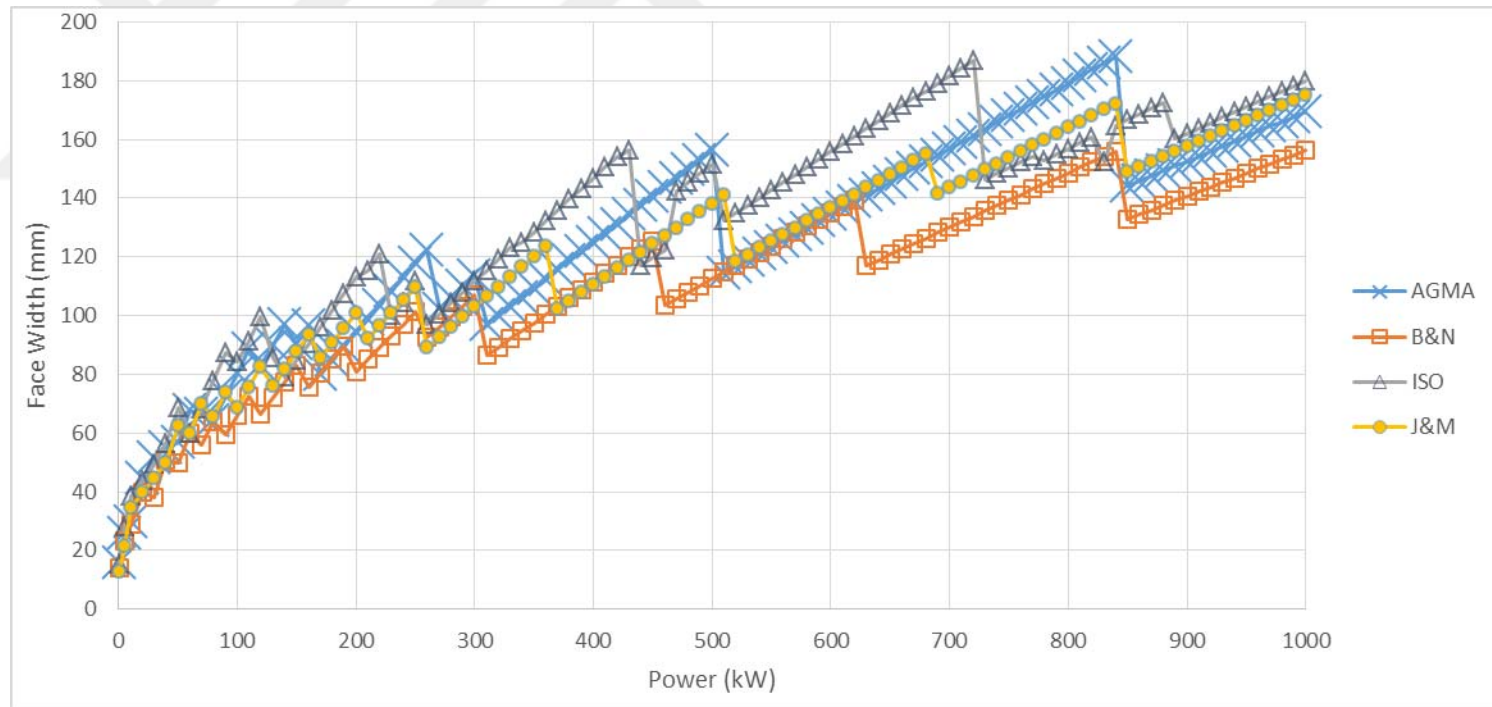
Figure B.6.Face width variation considering bending fatigue failure under increasing power at 3:1speed ratio (Ø=20º, Type 2)
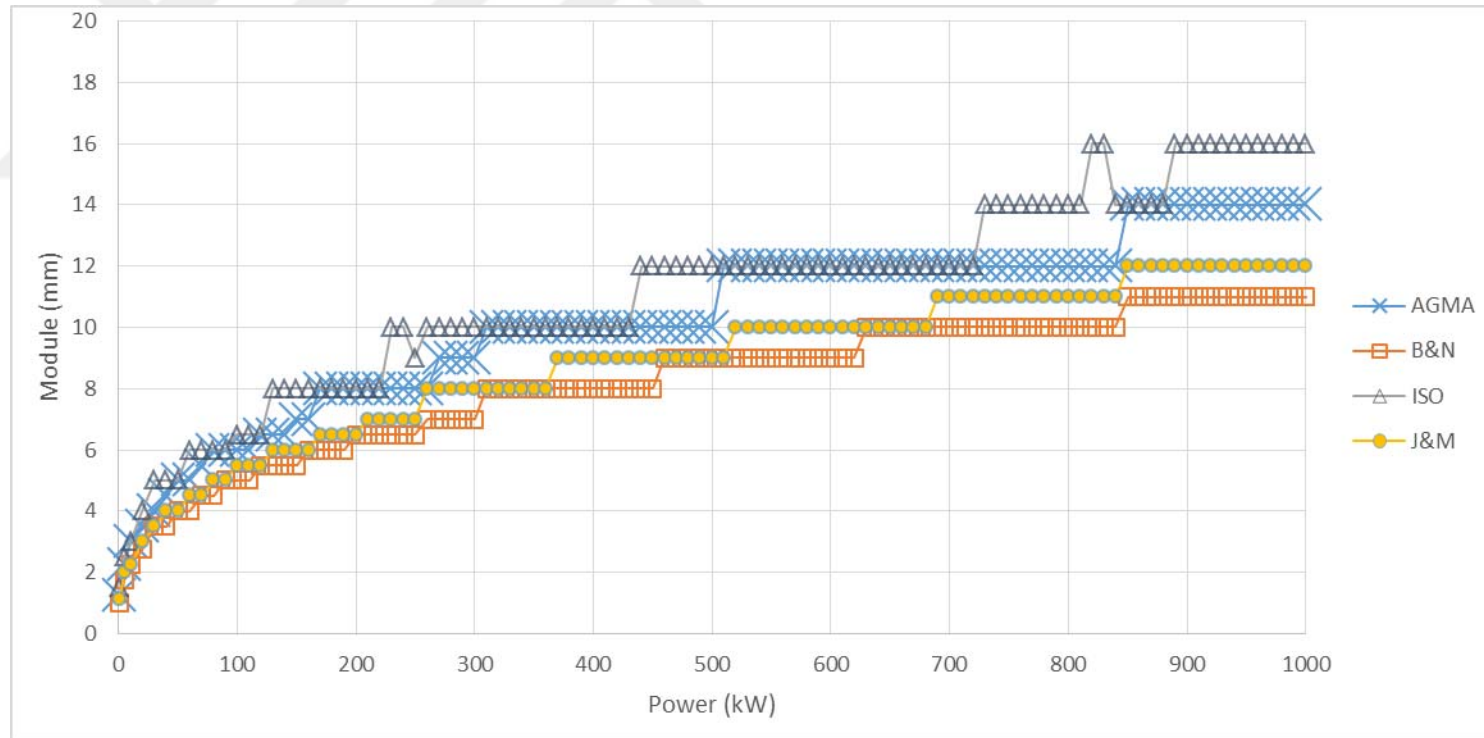
Figure B. 7. Module variation considering bending fatigue failure under increasing power at 4:1 speed ratio (Ø=20$^{\text{o}}$, Type 2)
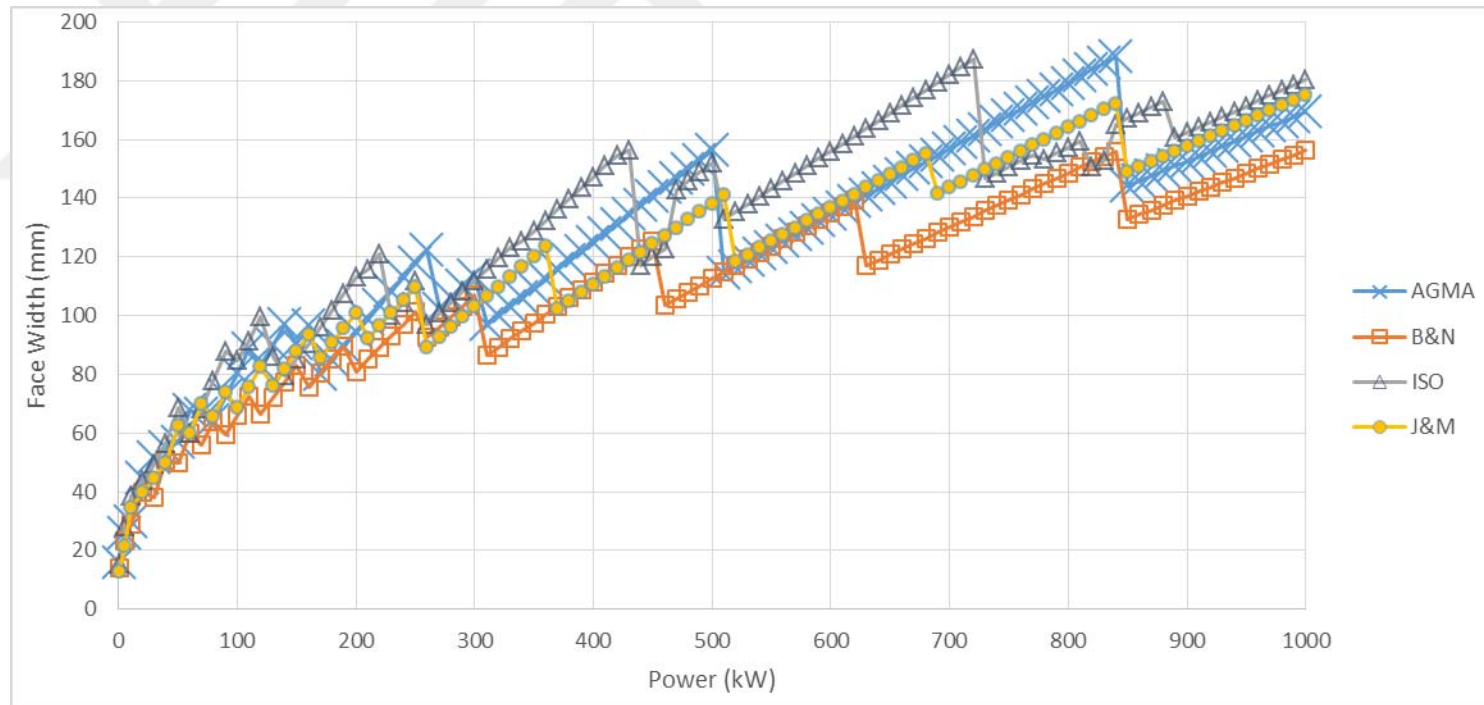
Figure B.8.Face width variation considering bending fatigue failure under increasing power at 4:1 speed ratio (Ø=20°, Type 2)
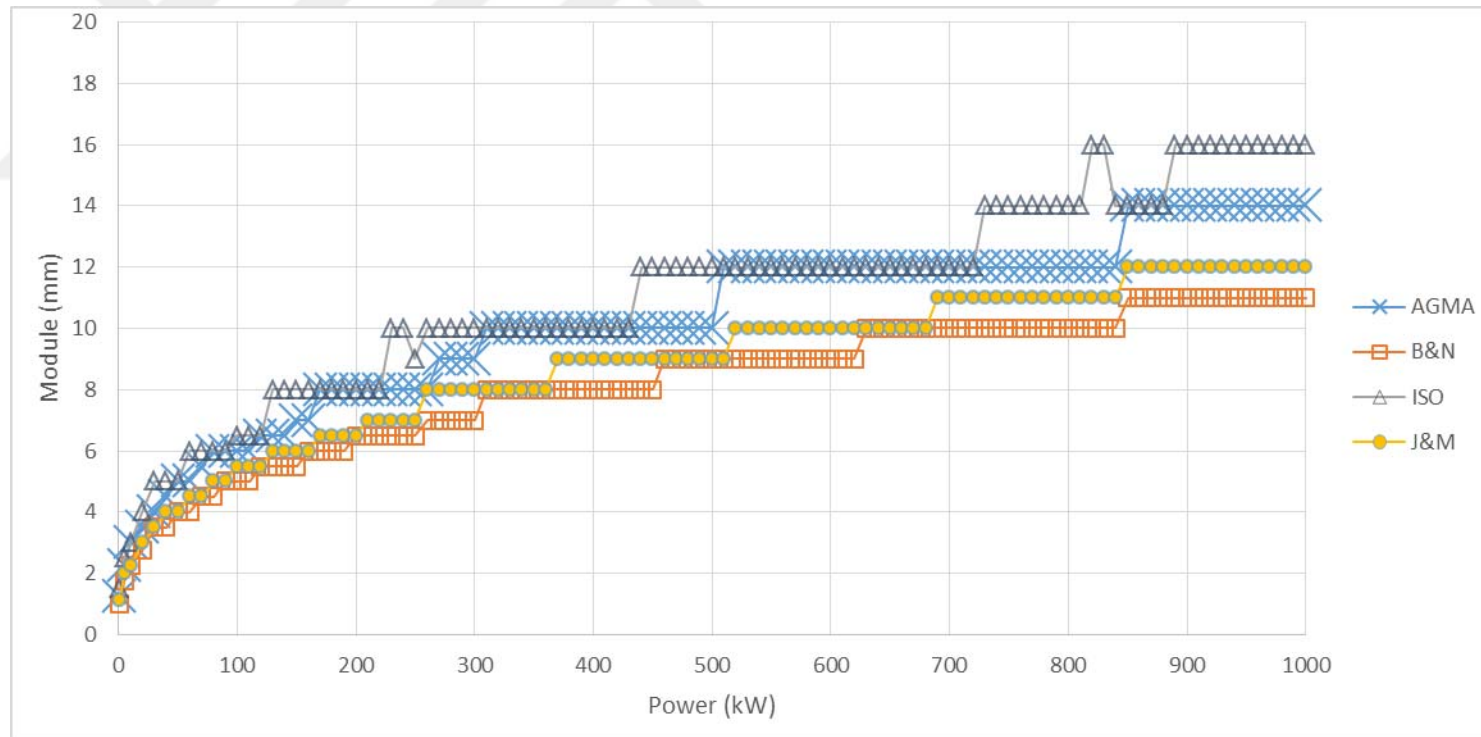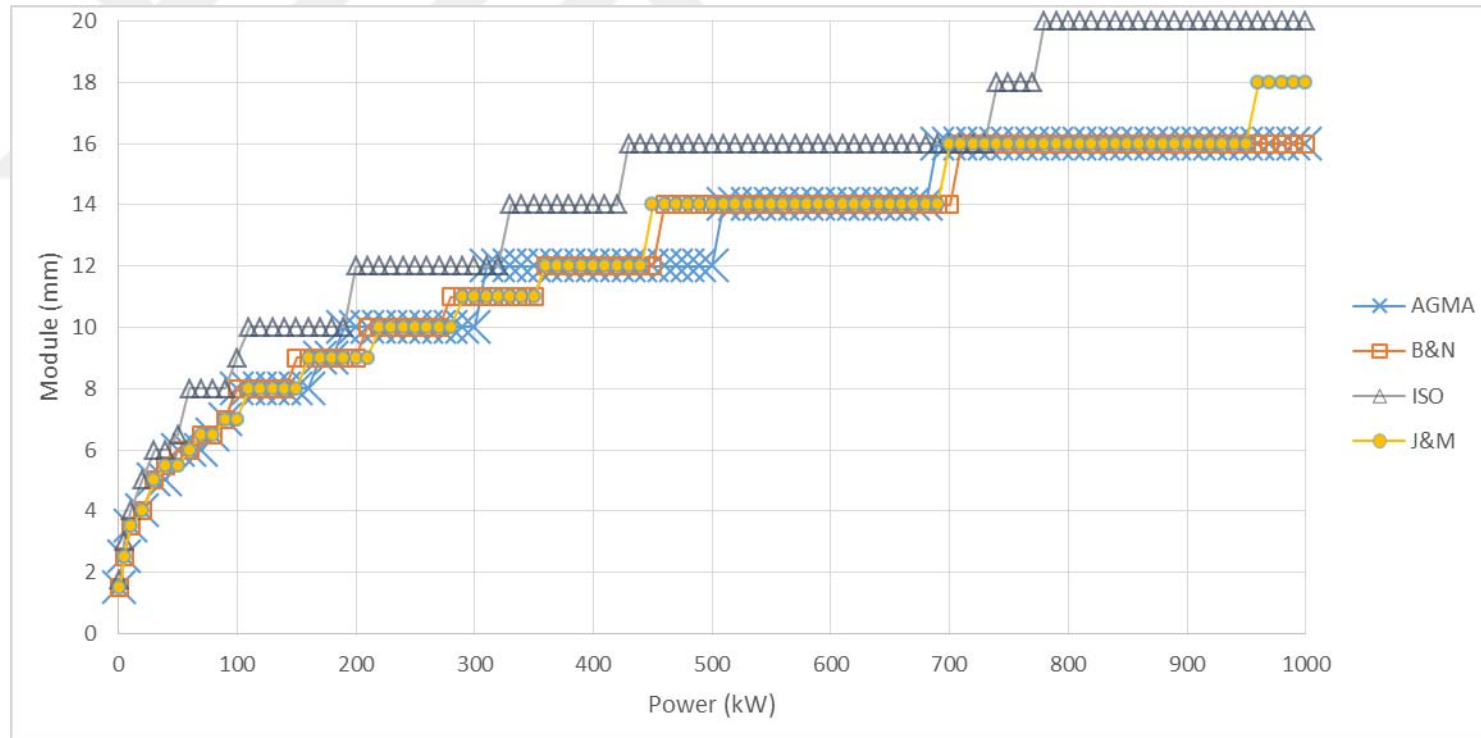
Figure B. 9. Module variation considering bending fatigue failure under increasing power at 5:1 speed ratio (Ø=20$^{\text{o}}$, Type 2)
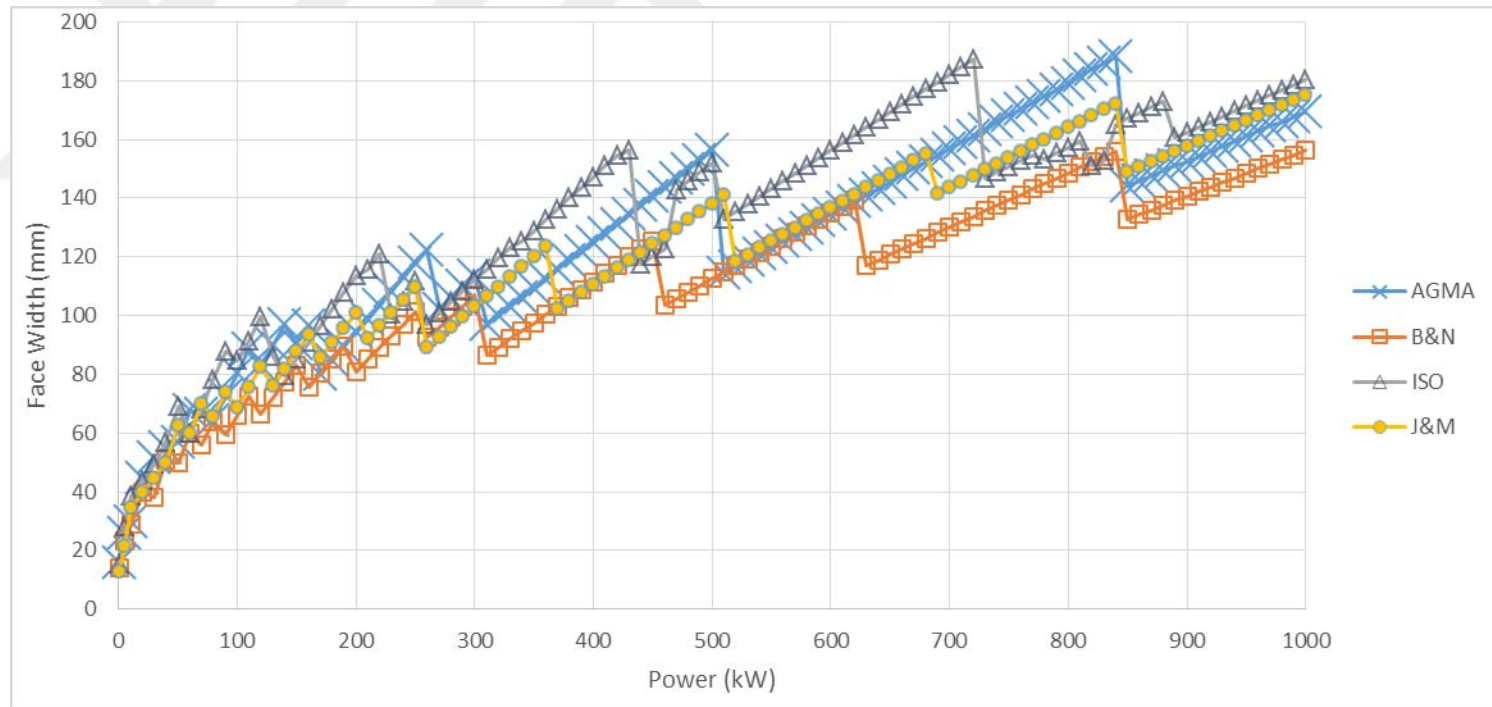
Figure B. 10. Face width variation considering bending fatigue failure under increasing power at 5:1 speed ratio (Ø=20°, Type2)
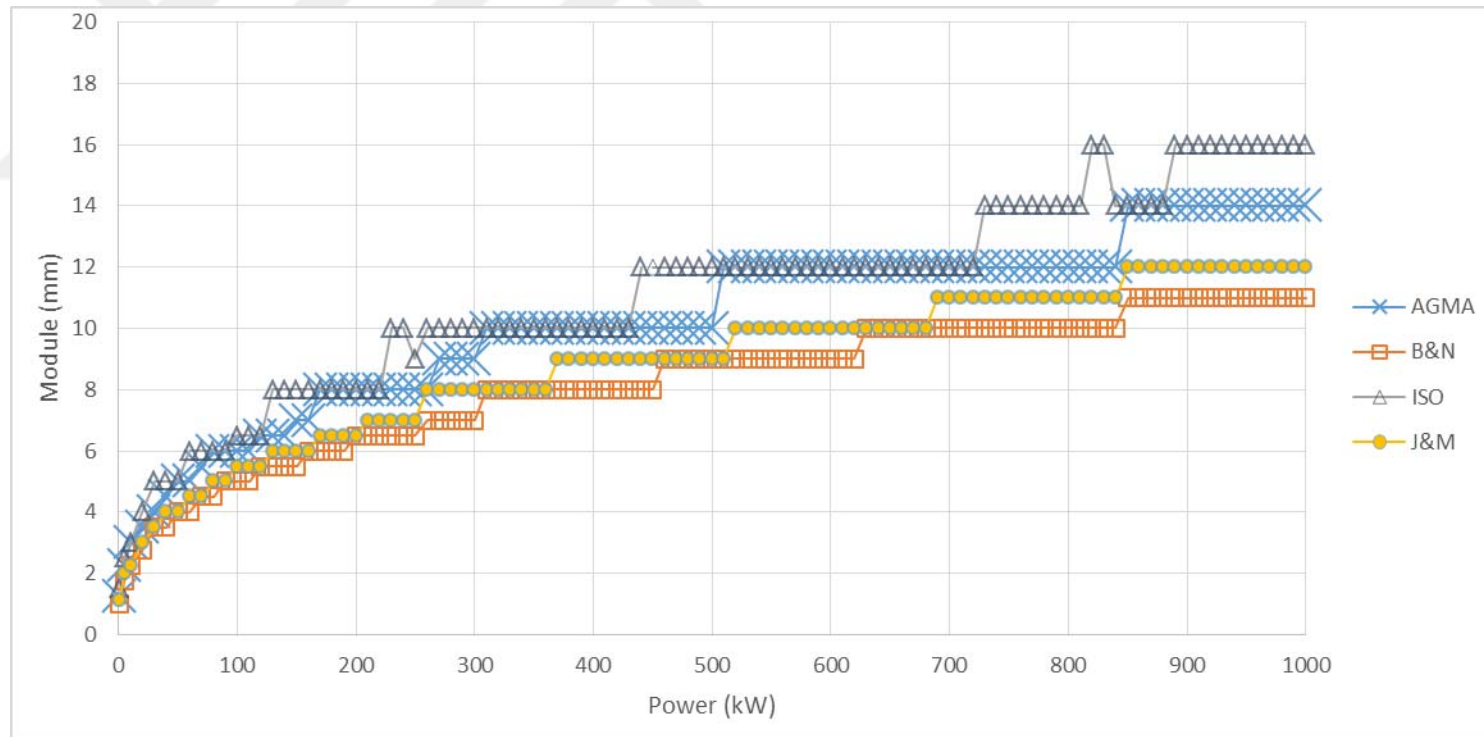
Figure B. 11. Module variation considering bending fatigue failure under increasing power at 6:1 speed ratio (Ø=20°, Type 2)

133
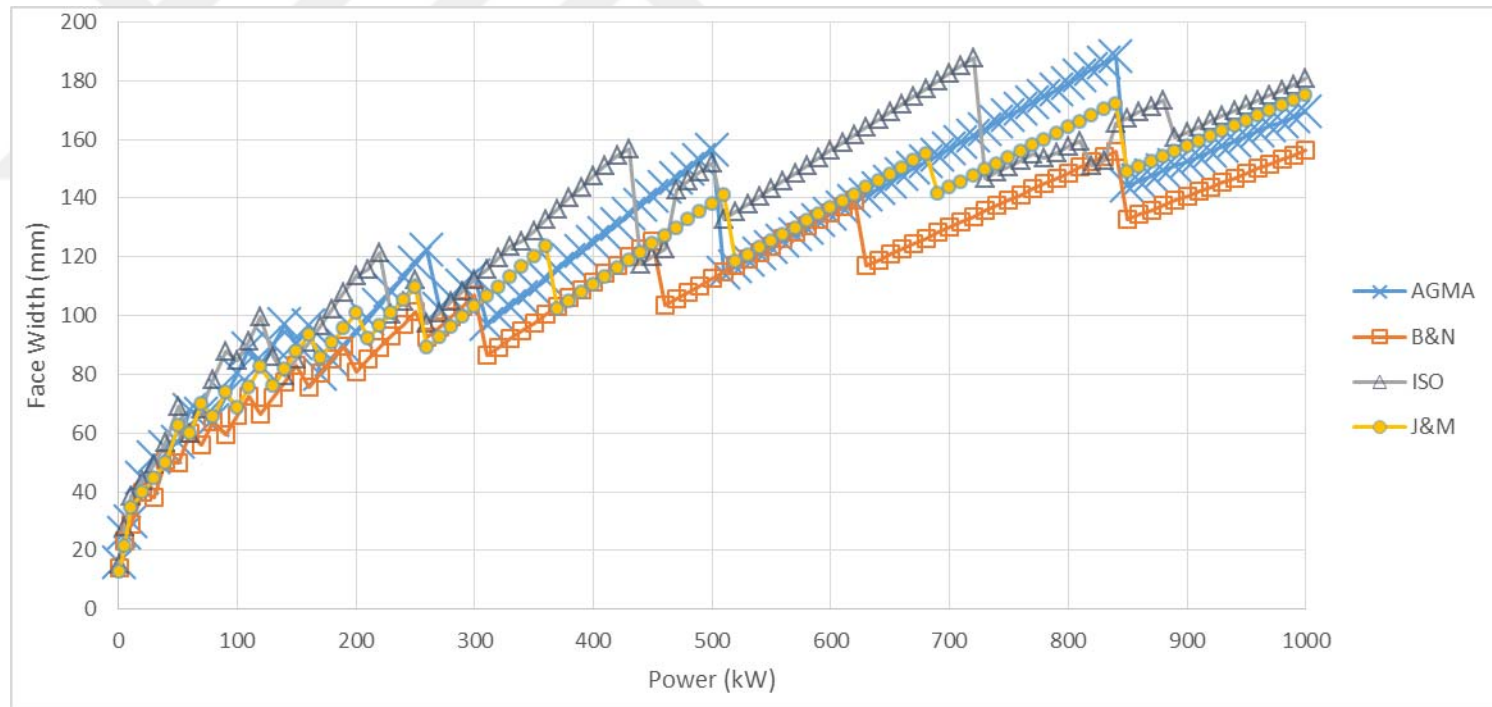
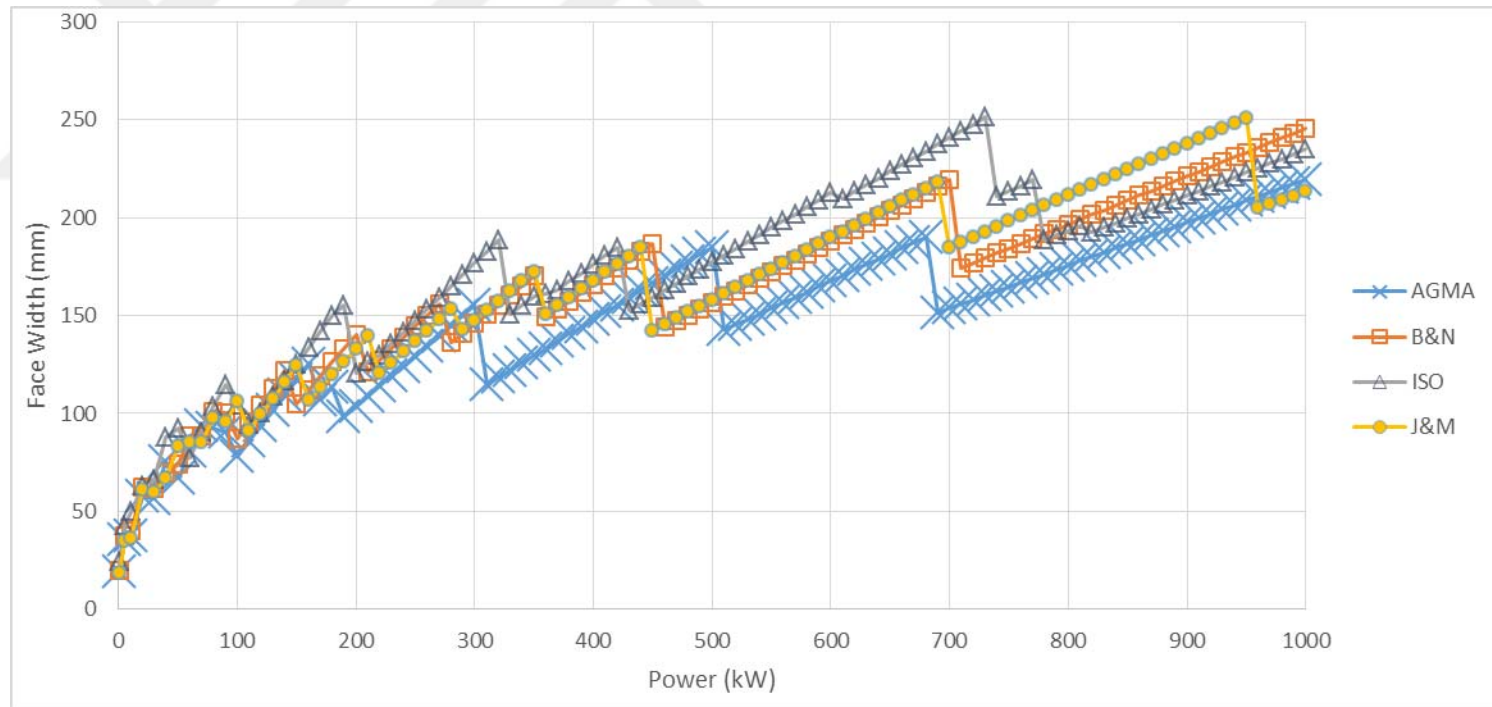Figure B. 12. Face width variation considering bending fatigue failure under increasing power at 6:1 speed ratio (Ø=20°, Type2)
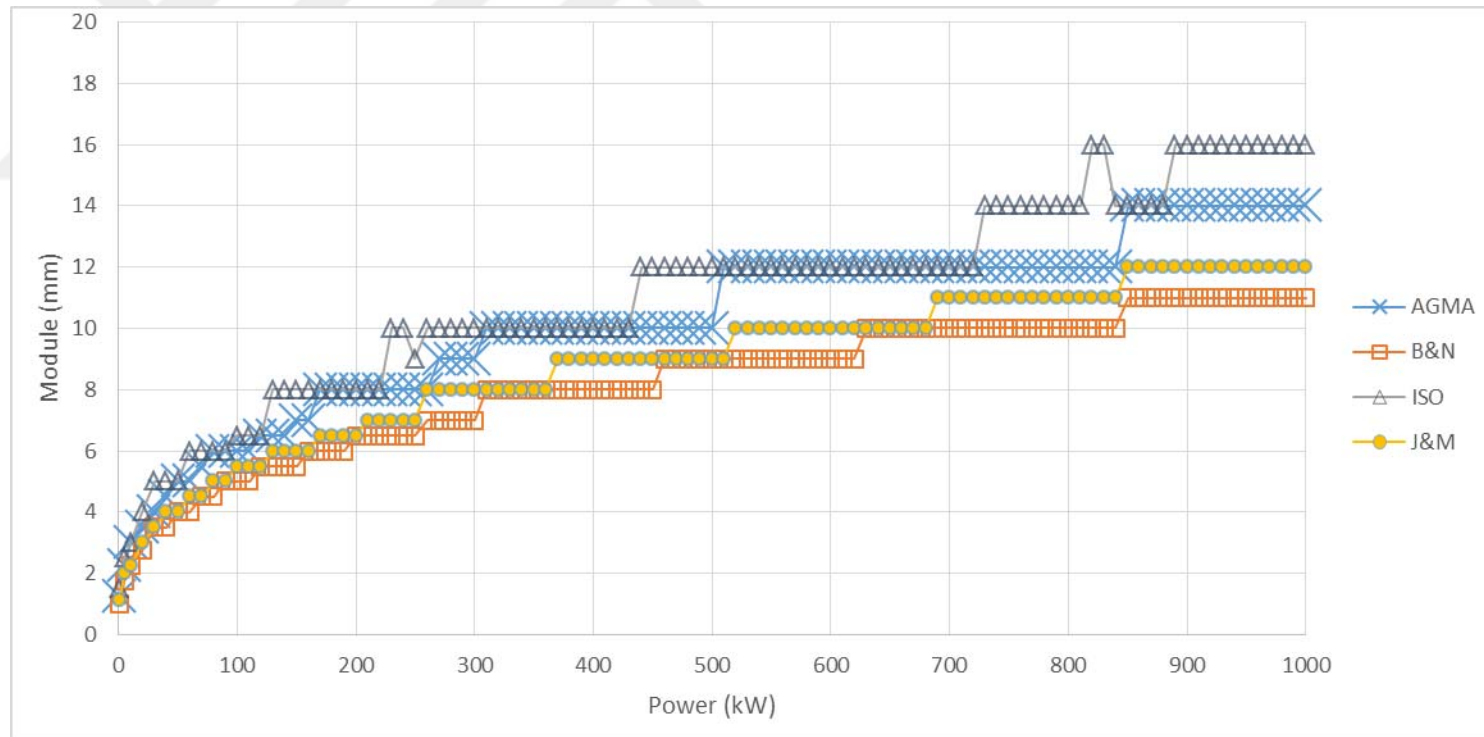
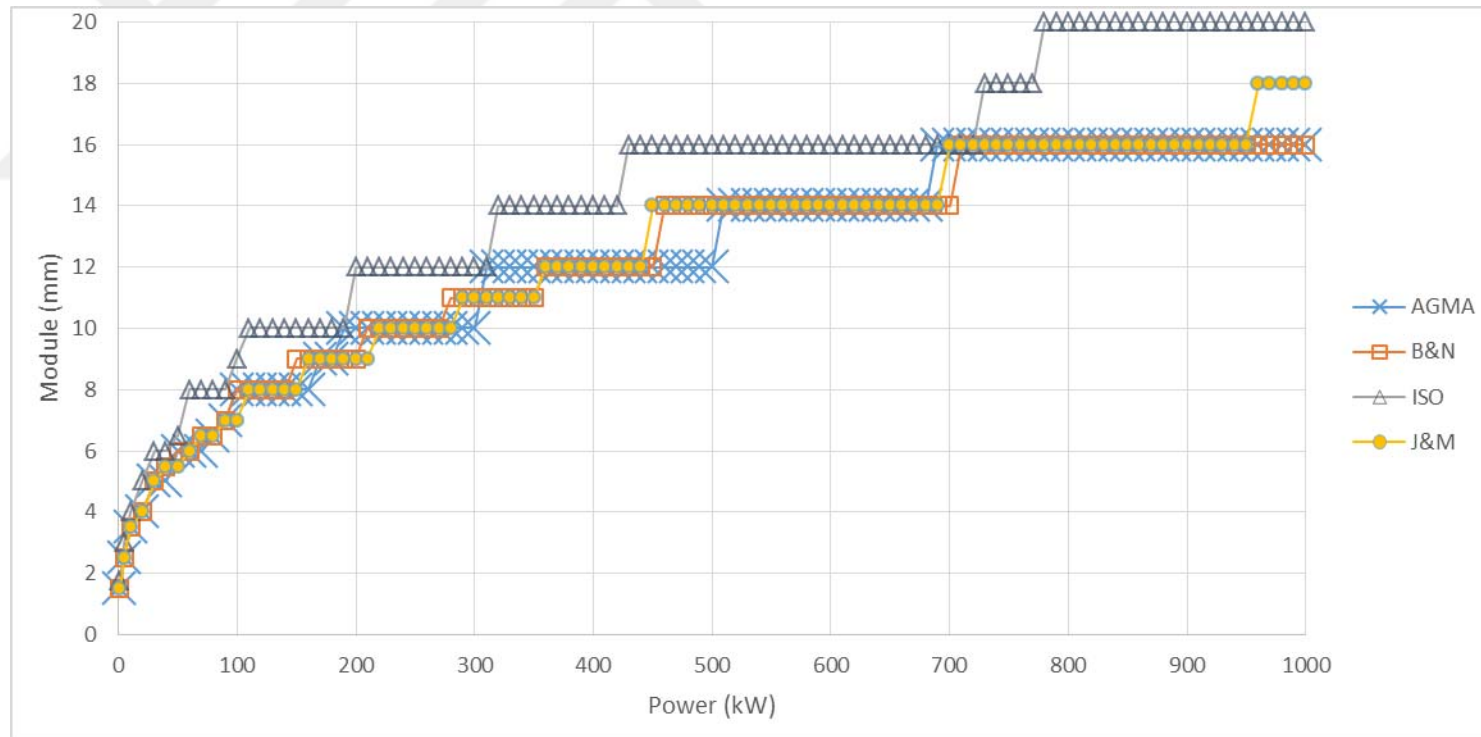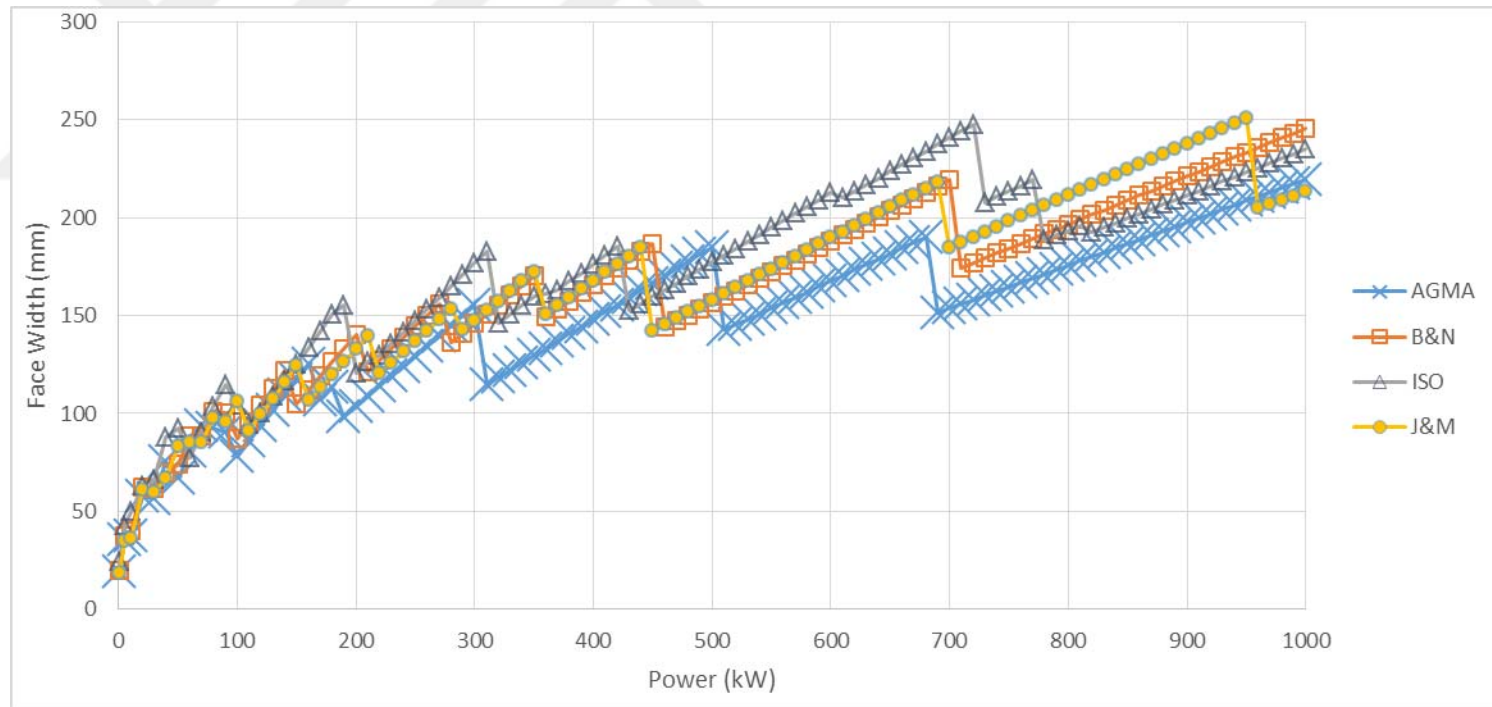Figure B. 13. Module variation considering bending fatigue failure under increasing power at 7:1 speed ratio (Ø=20°, Type 2)
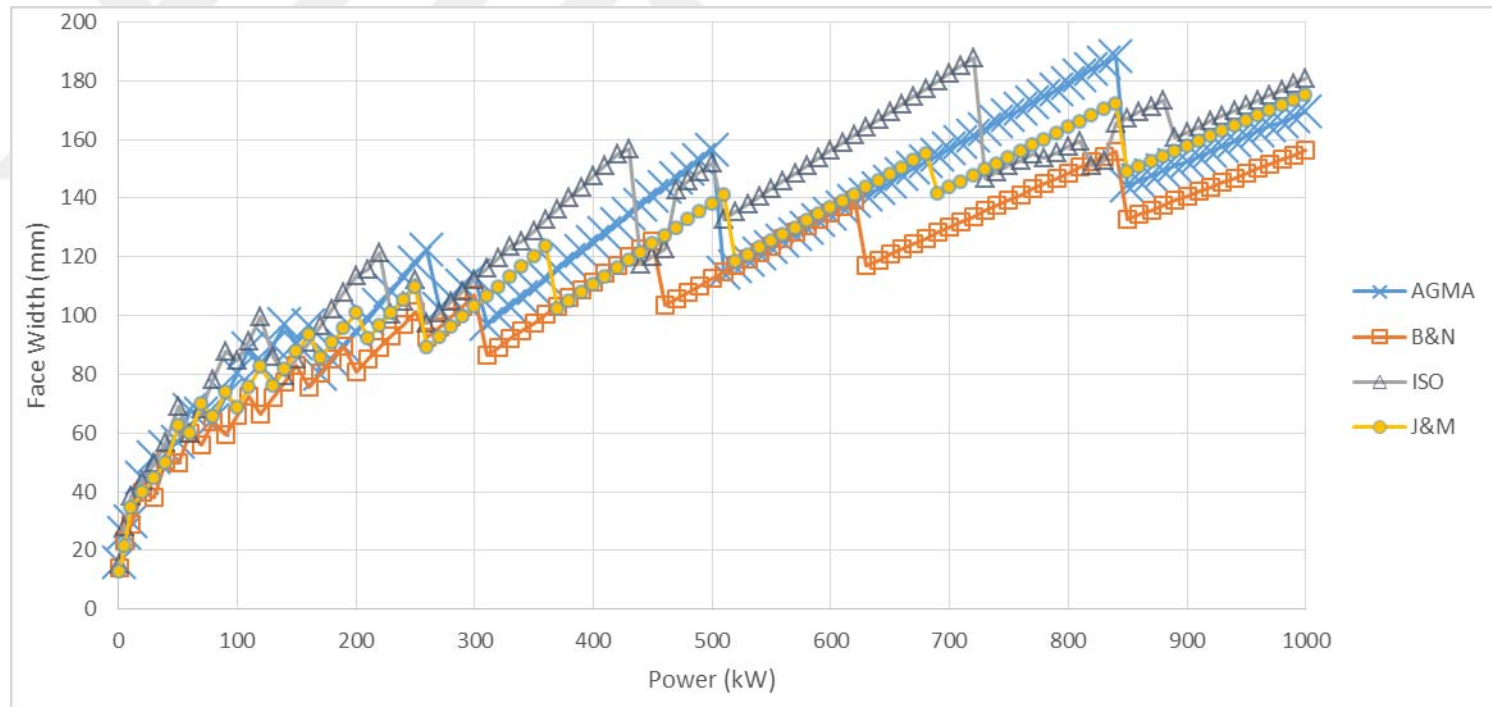
Figure B. 14. Face width variation considering bending fatigue failure under increasing power at 7:1 speed ratio (Ø=20°, Type2)
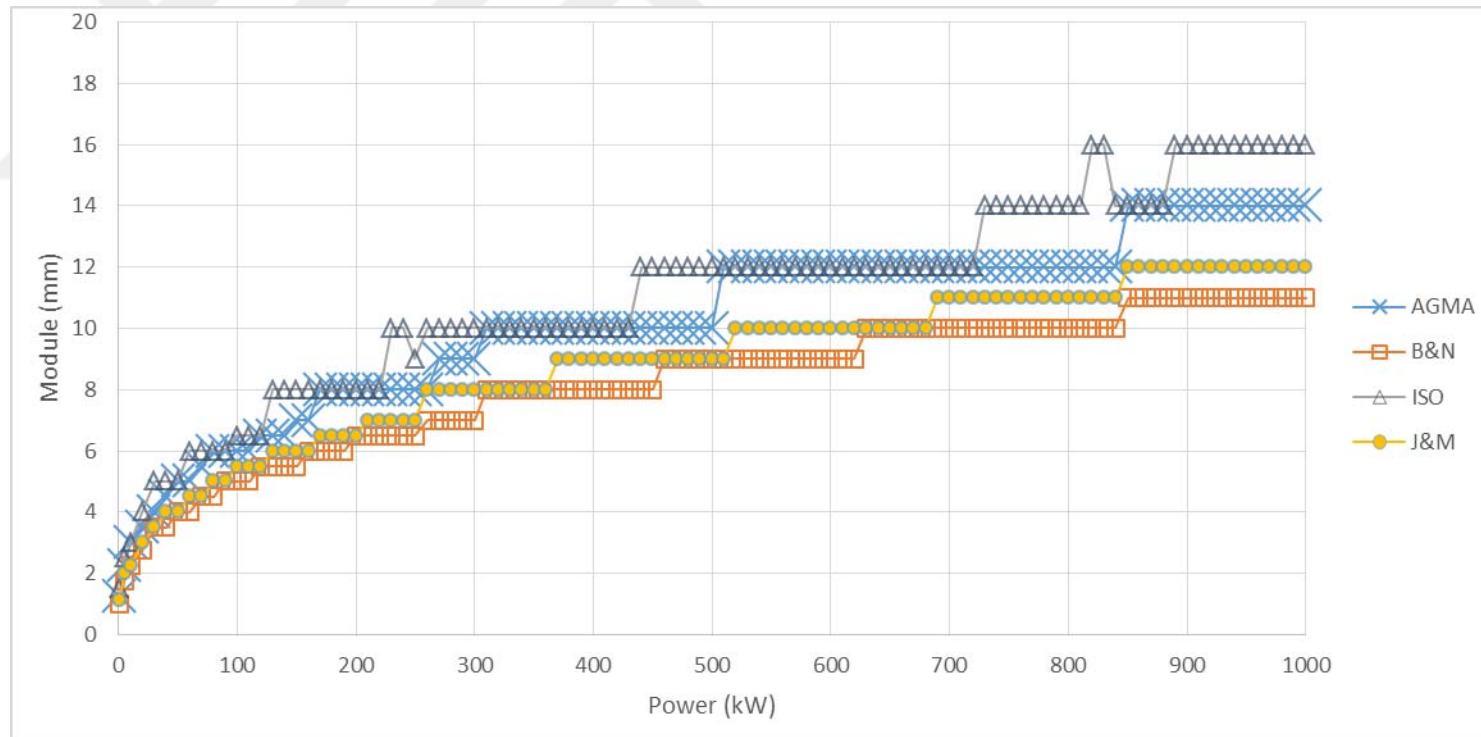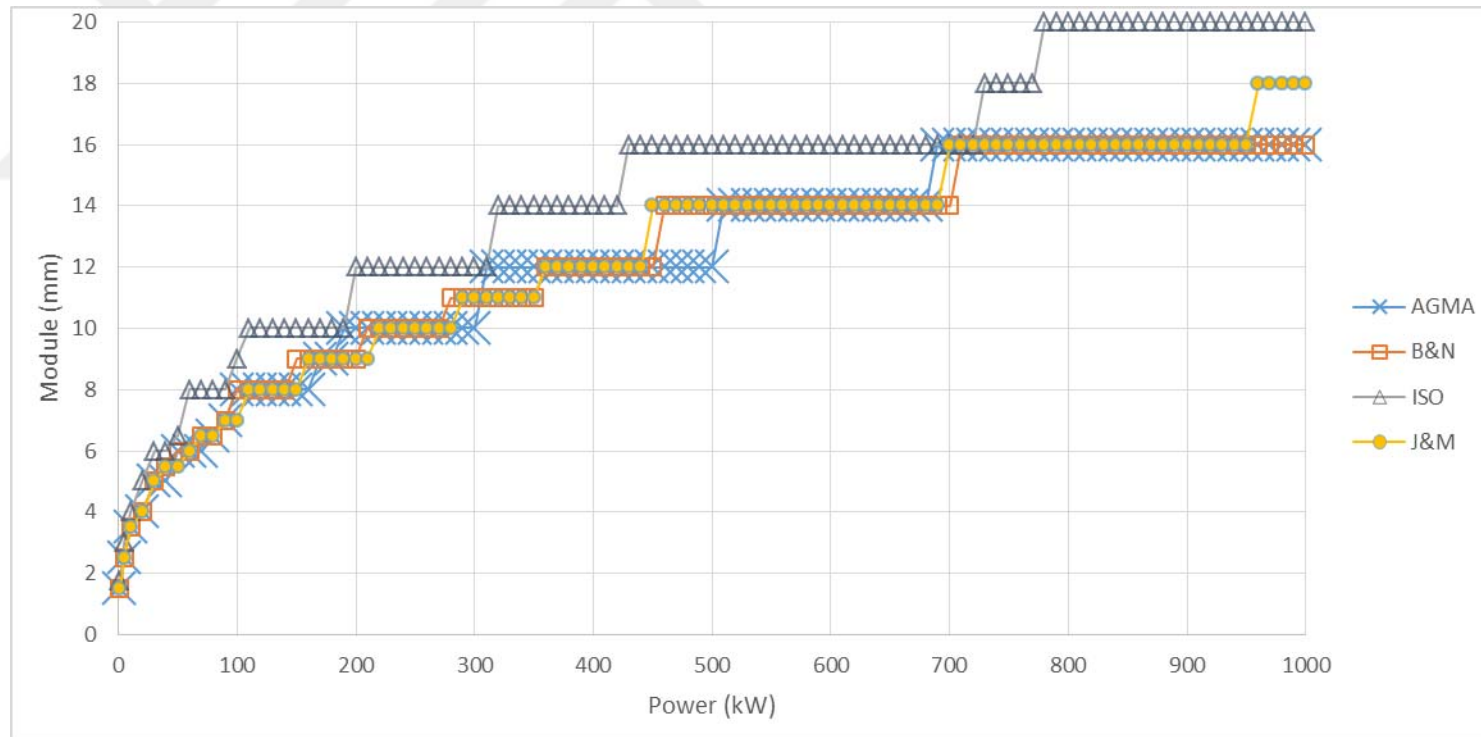
Figure B. 15. Module variation considering bending fatigue failure under increasing power at 8:1 speed ratio (Ø=20°, Type 2)
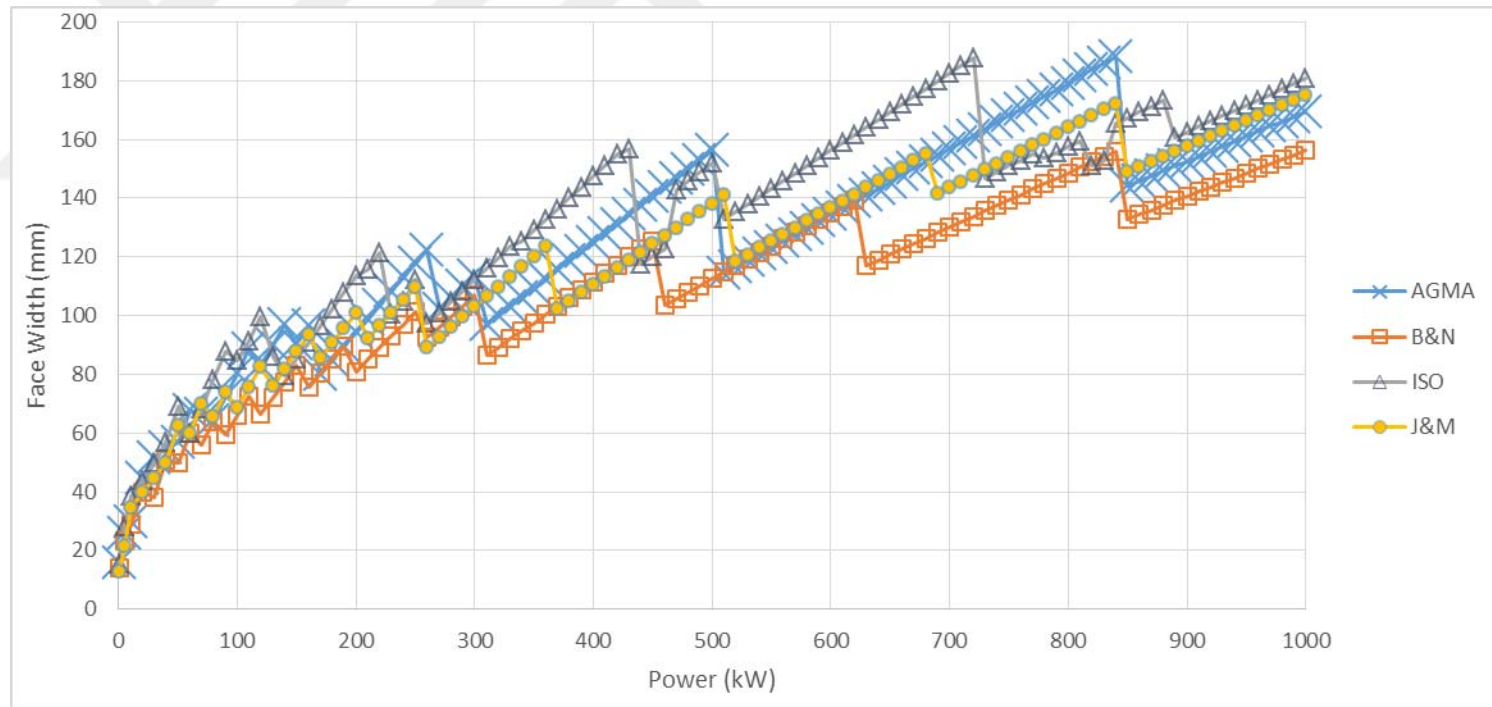
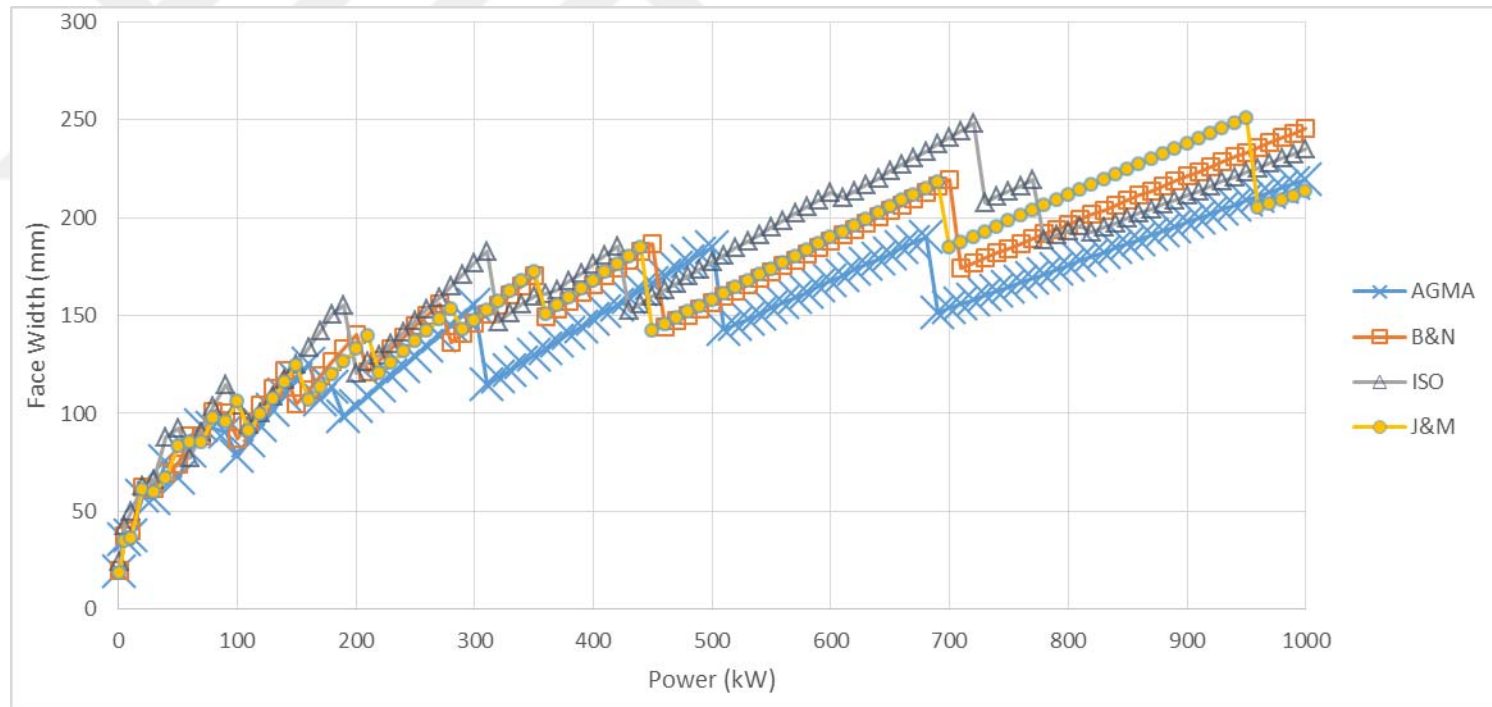Figure B. 16. Face width variation considering bending fatigue failure under increasing power at 8:1 speed ratio (Ø=20°, Type2)

B.2. Comparison of the Results Based on Bending Fatigue Failure Considering Speed Ratio for the Selected Power Transmissions for Ø=20°, Material type 2
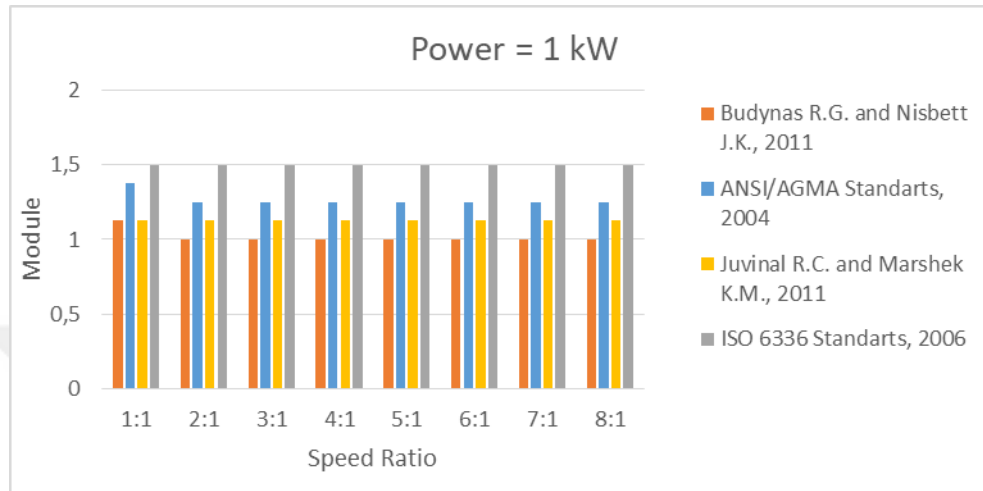
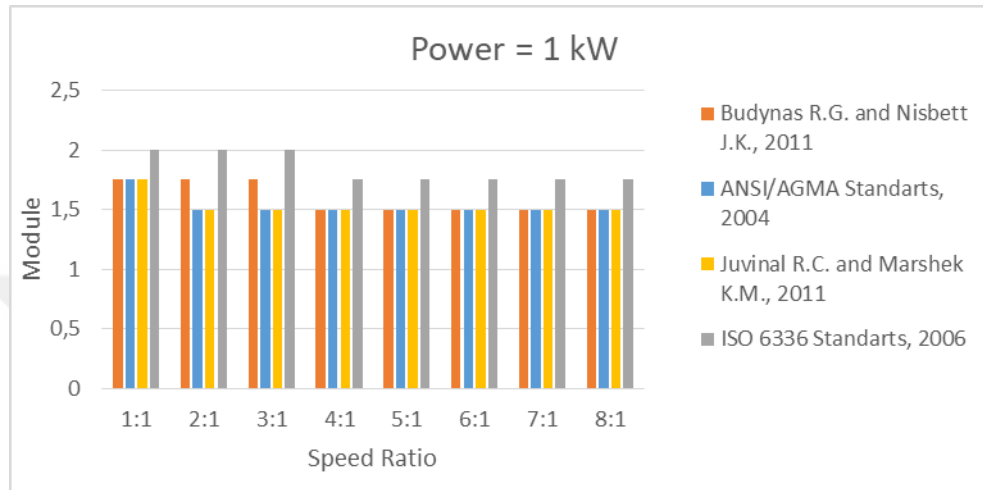Figure B. 17. The effect of speed ratio on module selection based on bending fatigue failure at 1 kW power transmission (Ø=20°, Type 2)
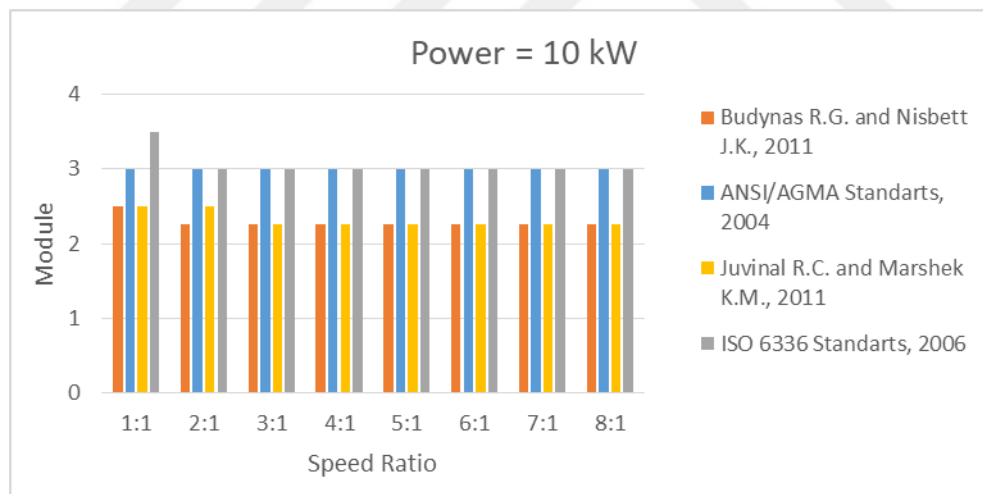
Figure B. 18. The effect of speed ratio on module selection based on bending fatigue failure at 10 kW power transmission (Ø=20°, Type 2)
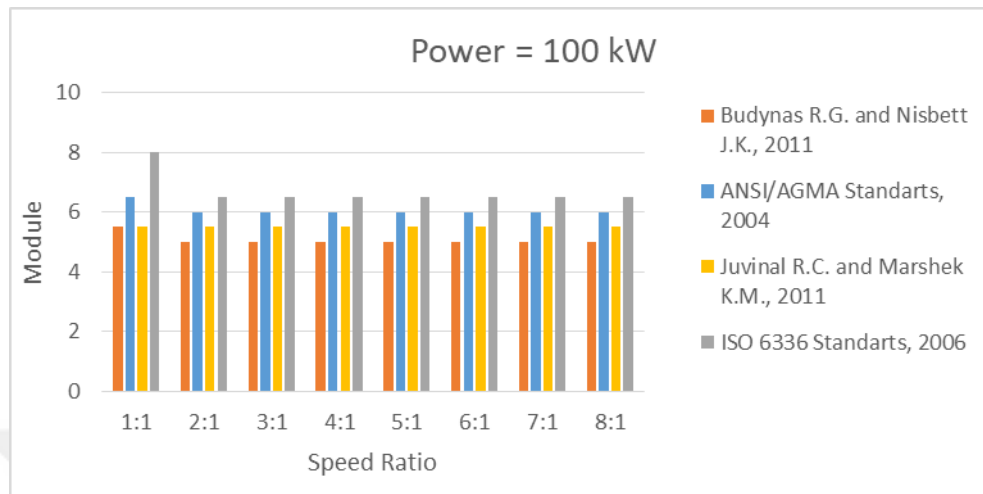
Figure B. 19. The effect of speed ratio on module selection based on bending fatigue failure at 100 kW power transmission (Ø=20°, Type 2)
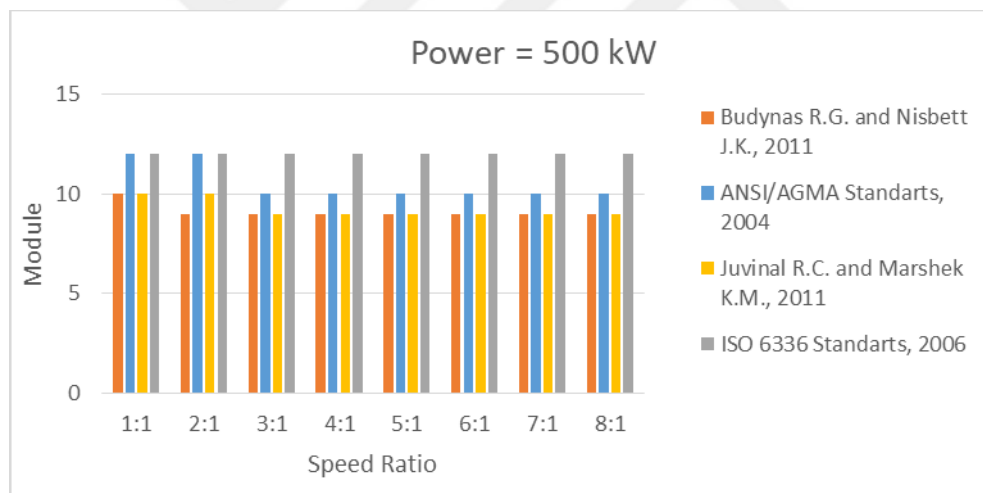
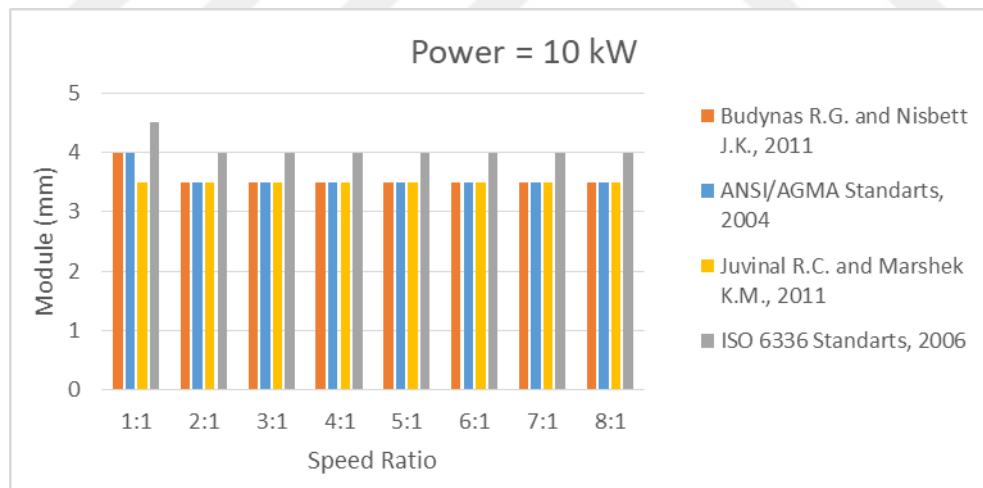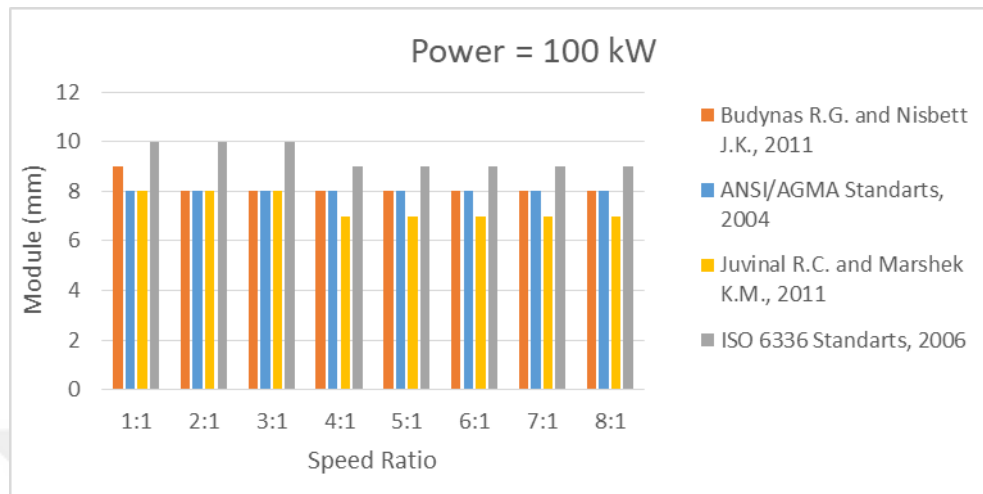Figure B. 20. The effect of speed ratio on module selection based on bending fatigue failure at 500 kW power transmission (Ø=20°, Type 2)
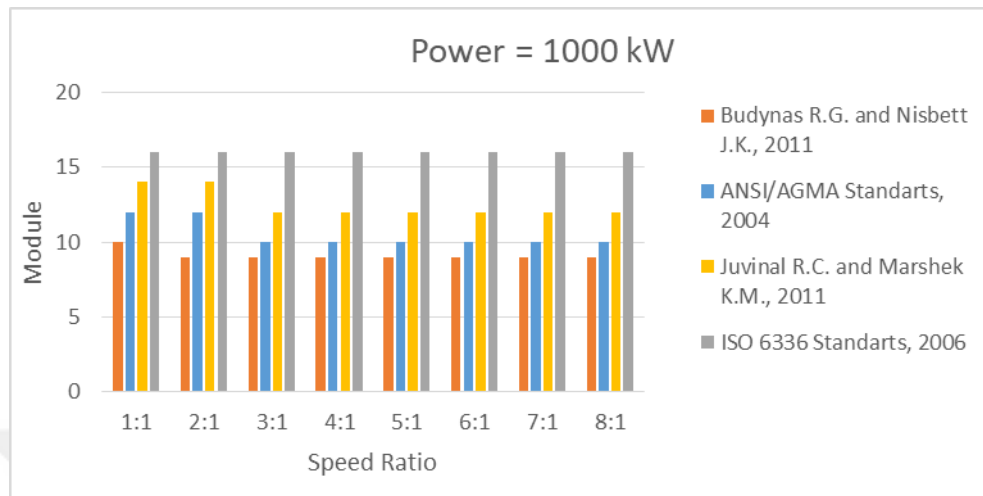
Figure B. 21. The effect of speed ratio on module selection based on bending fatigue failure at 1000 kW power transmission (Ø=20°, Type 2)

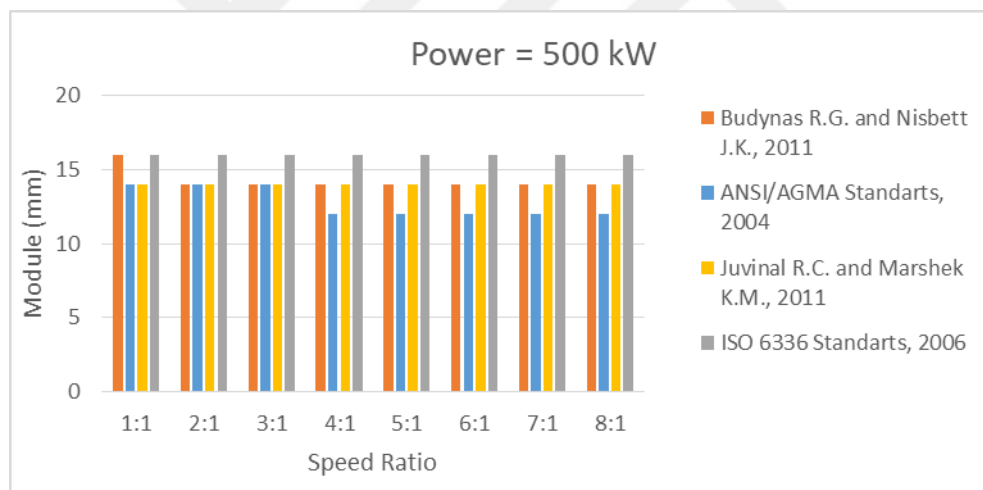**B.3. Obtaining Geometric Rating Number (GRi) for Design Approaches for Ø=20°, Material type 2**
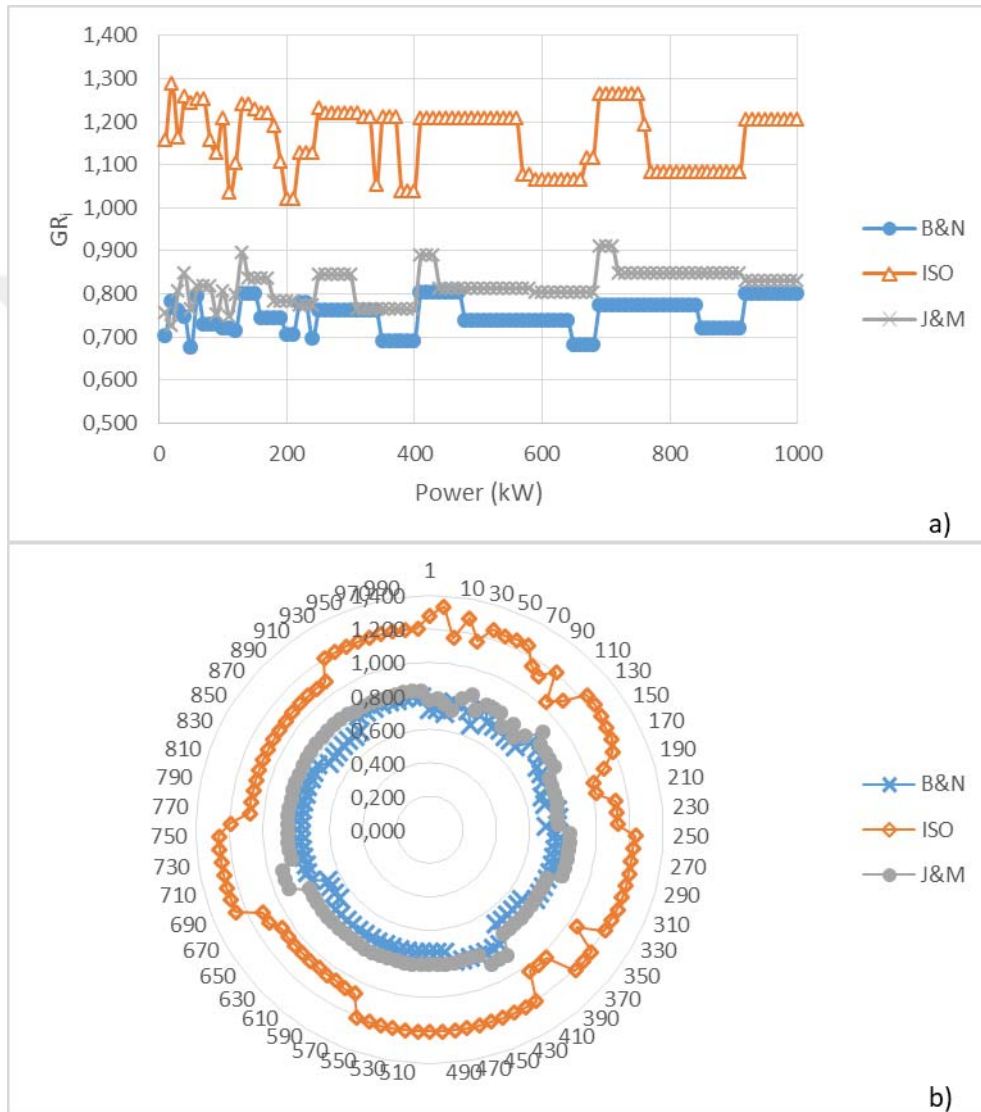
Figure B. 22. Comparison of GR_i results obtained from the design approaches at 1:1 speed ratio (Ø=20°, Type 2), a) scatter chart, b) radar chart

Figure B. 23. Comparison of GR_i results obtained from the design approaches at 2:1 speed ratio (Ø=20°, Type 2), a) scatter chart, b) radar chart

143

Figure B. 24. Comparison of GR_i results obtained from the design approaches at 3:1 speed ratio ($\varnothing=20^o$, Type 2), a) scatter chart, b) radar chart

144

Figure B. 25. Comparison of GR_i results obtained from the design approaches at 4:1 speed ratio ($\varnothing$=20°, Type 2), a) scatter chart, b) radar chart
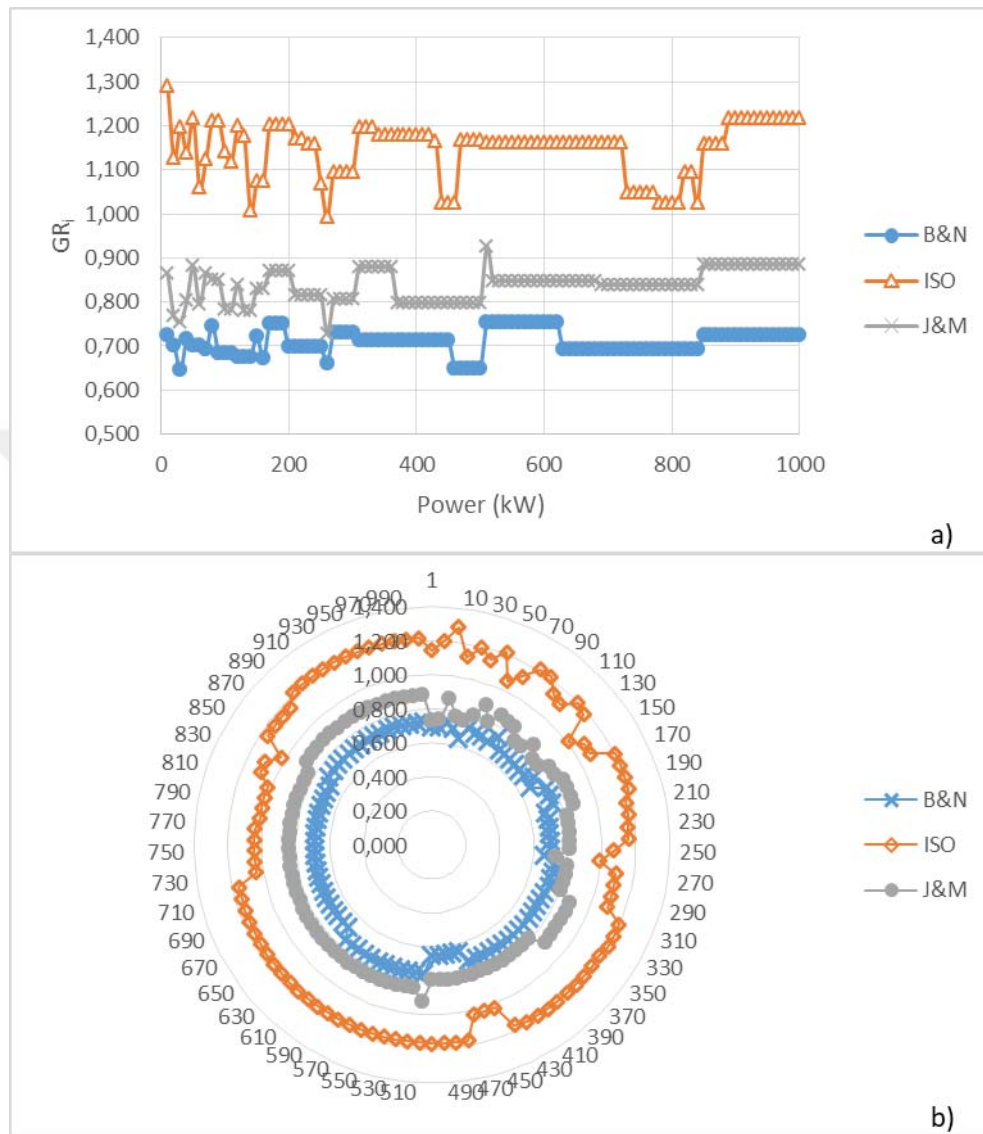
Figure B. 26. Comparison of GR_i results obtained from the design approaches at 5:1 speed ratio ($\varnothing=20^{o}$, Type 2), a) scatter chart, b) radar chart

146
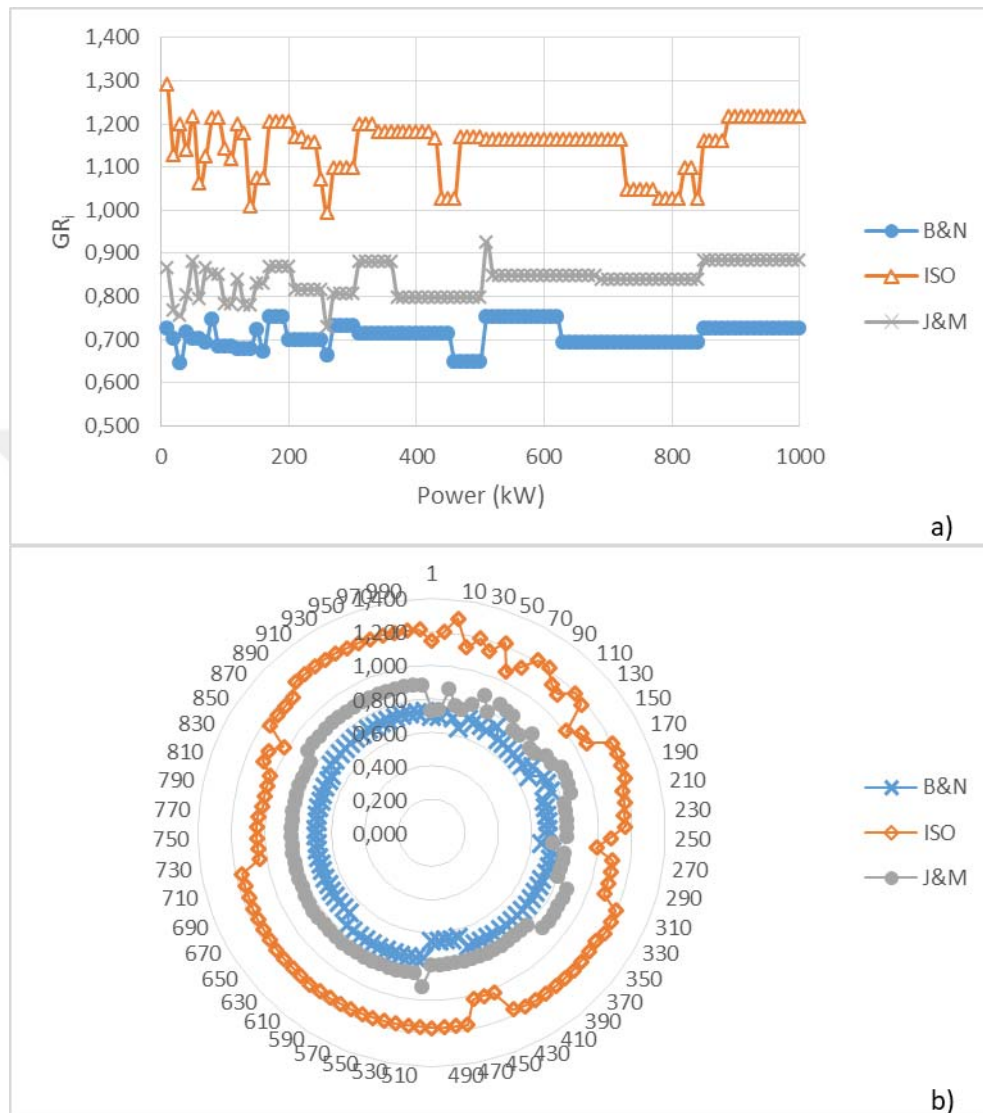
Figure B. 27. Comparison of GR_i results obtained from the design approaches at 6:1 speed ratio (Ø=20°, Type 2), a) scatter chart, b) radar chart
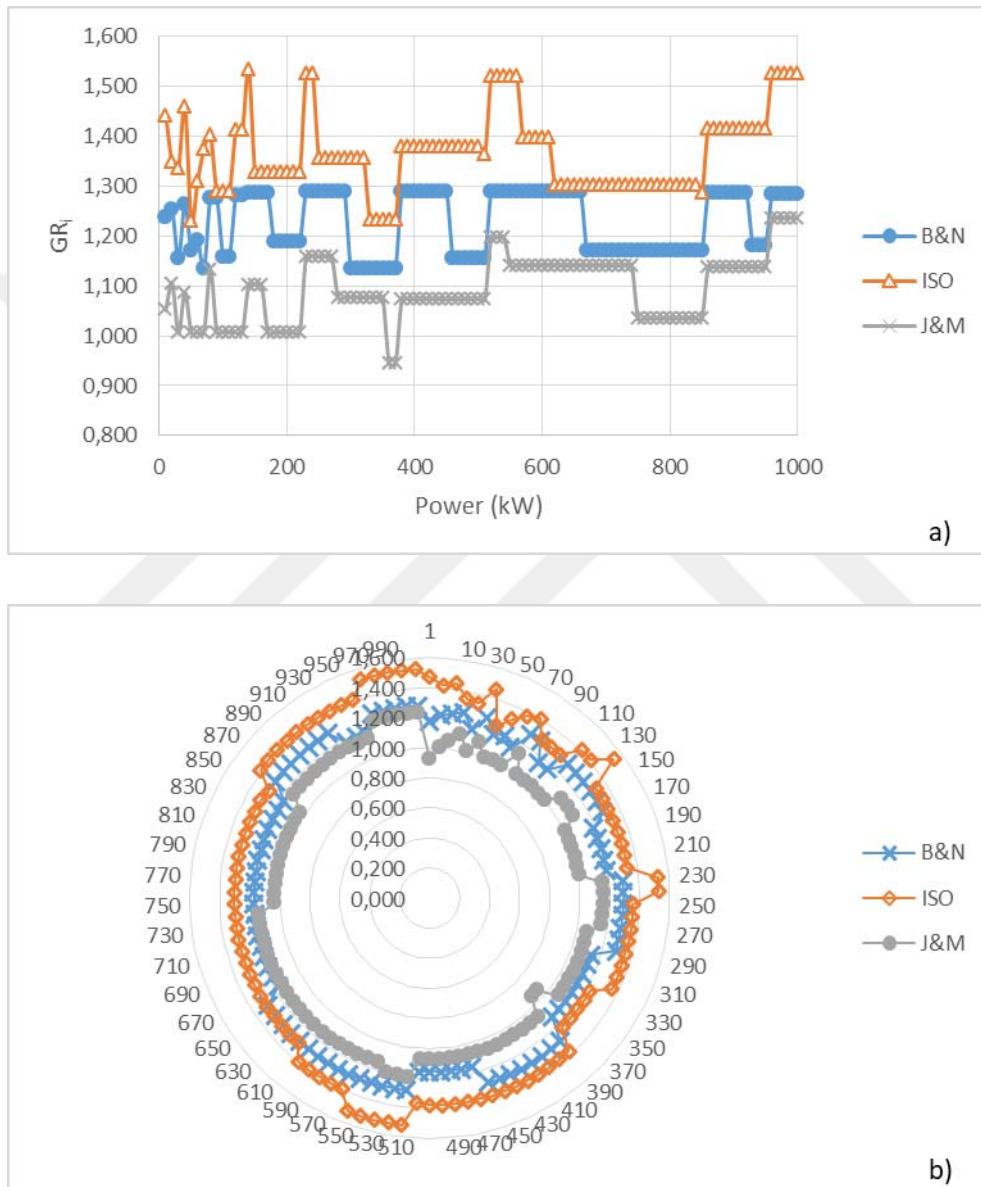
147
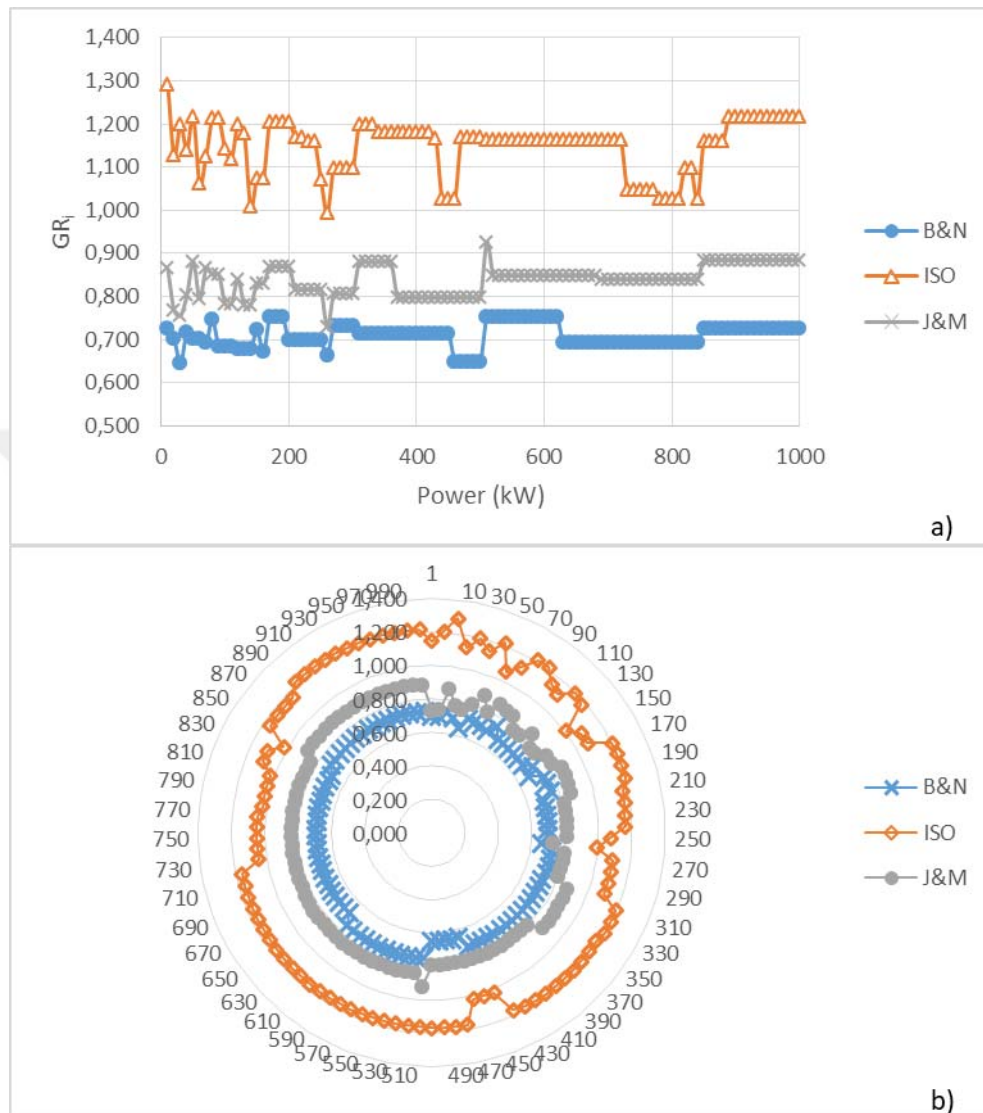
Figure B. 28. Comparison of GR_i results obtained from the design approaches at 7:1 speed ratio ($\emptyset=20^o$, Type 2), a) scatter chart, b) radar chart

Figure B. 29. Comparison of GR_i results obtained from the design approaches at 8:1 speed ratio ($\emptyset=20^o$, Type 2), a) scatter chart, b) radar chart

APPENDIX C

C.1. Comparison of Module Selection and Face Width Results of the Design Approaches for Ø=20°, Material type 3
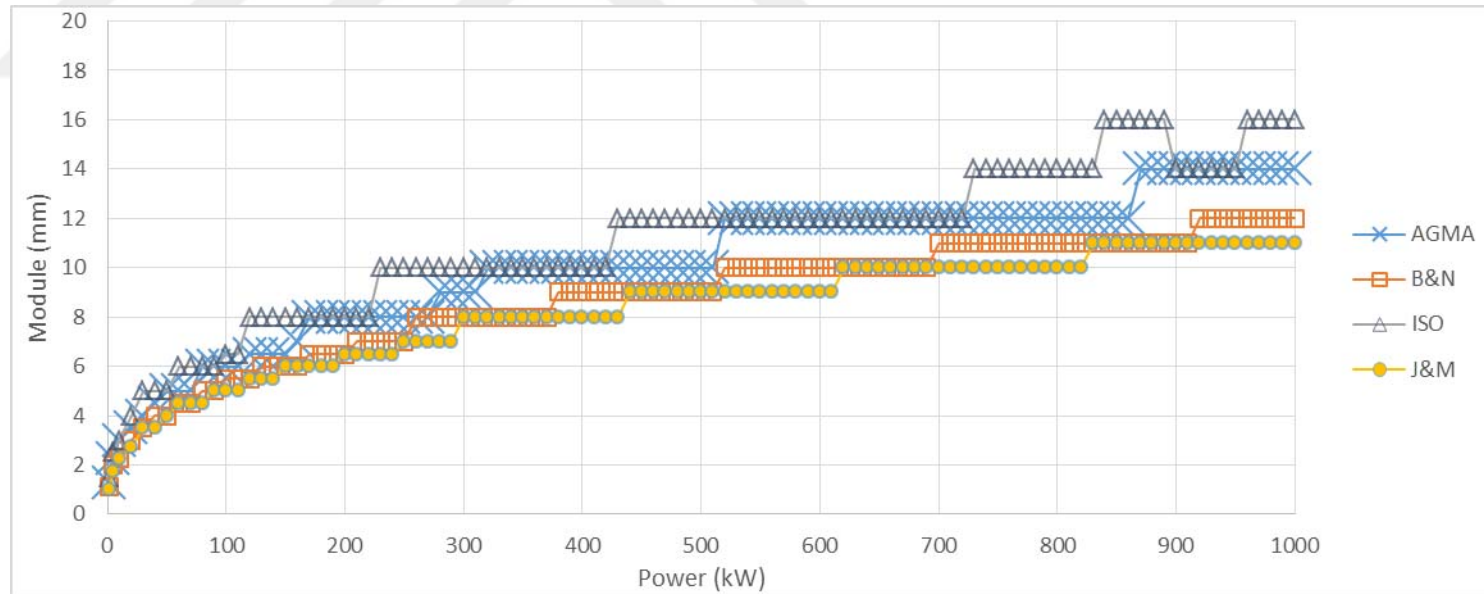
Figure C. 1. Module variation considering bending fatigue failure under increasing power at 1:1 speed ratio (Ø=20°, Type 3)
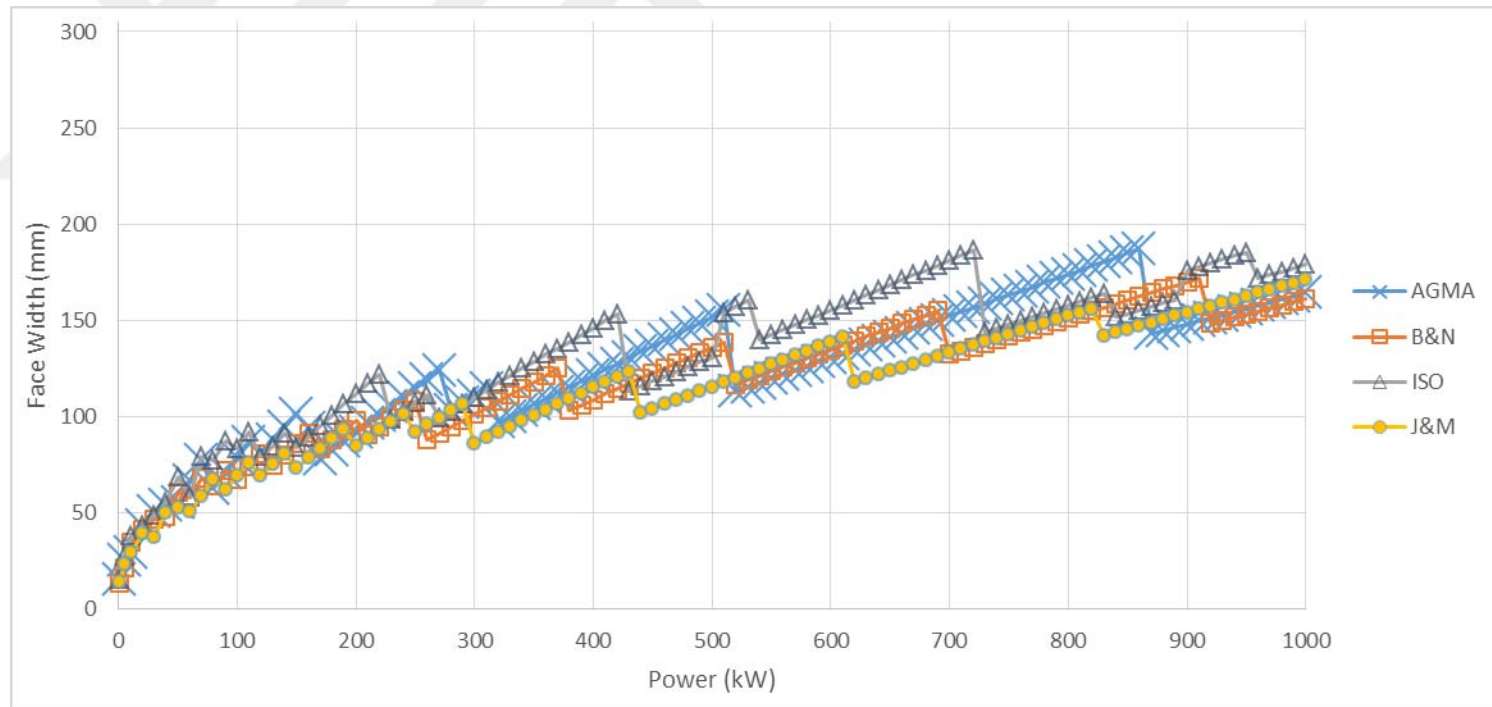
Figure C.2.Face width variation considering bending fatigue failure under increasing power at 1:1 speed ratio (Ø=20°, Type 3)
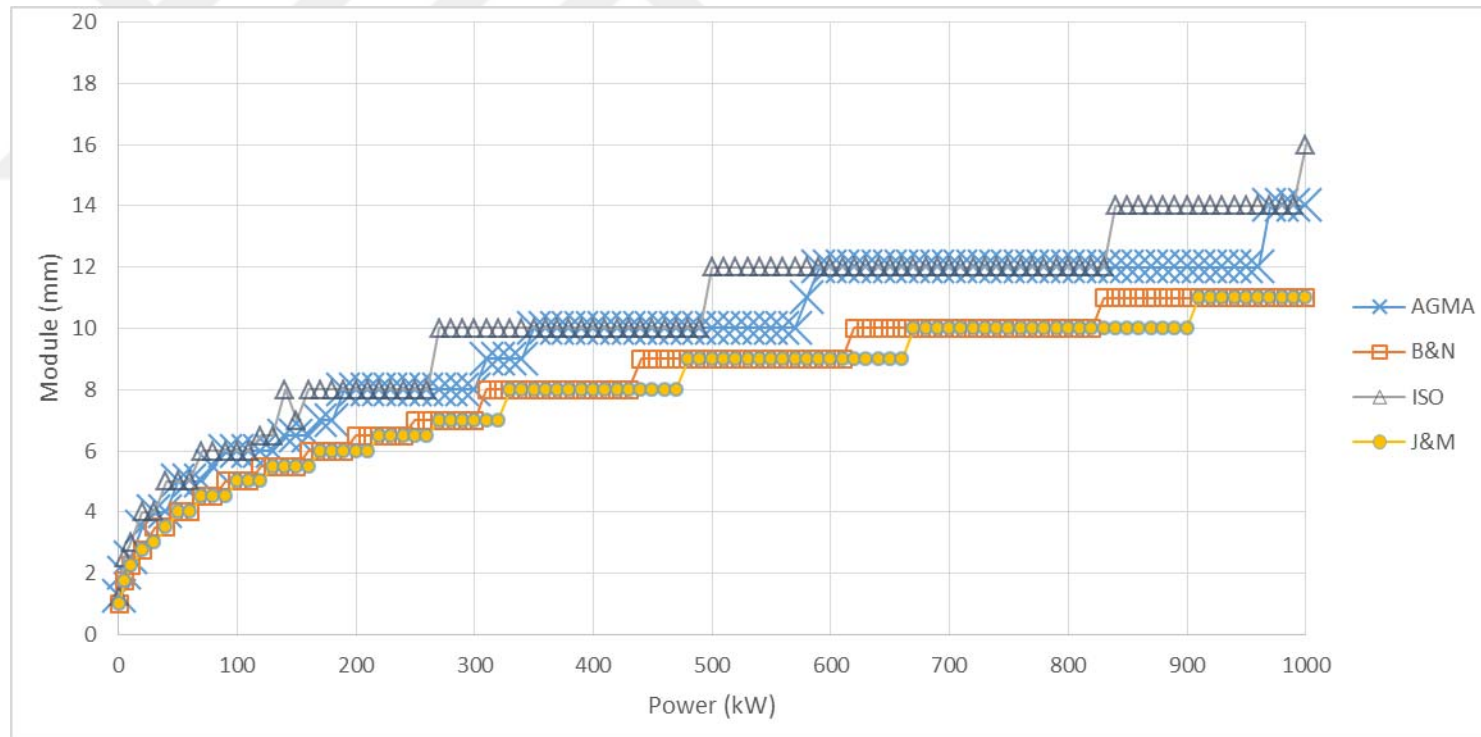
Figure C. 3. Module variation considering bending fatigue failure under increasing power at 2:1 speed ratio (Ø=20°, Type 3)
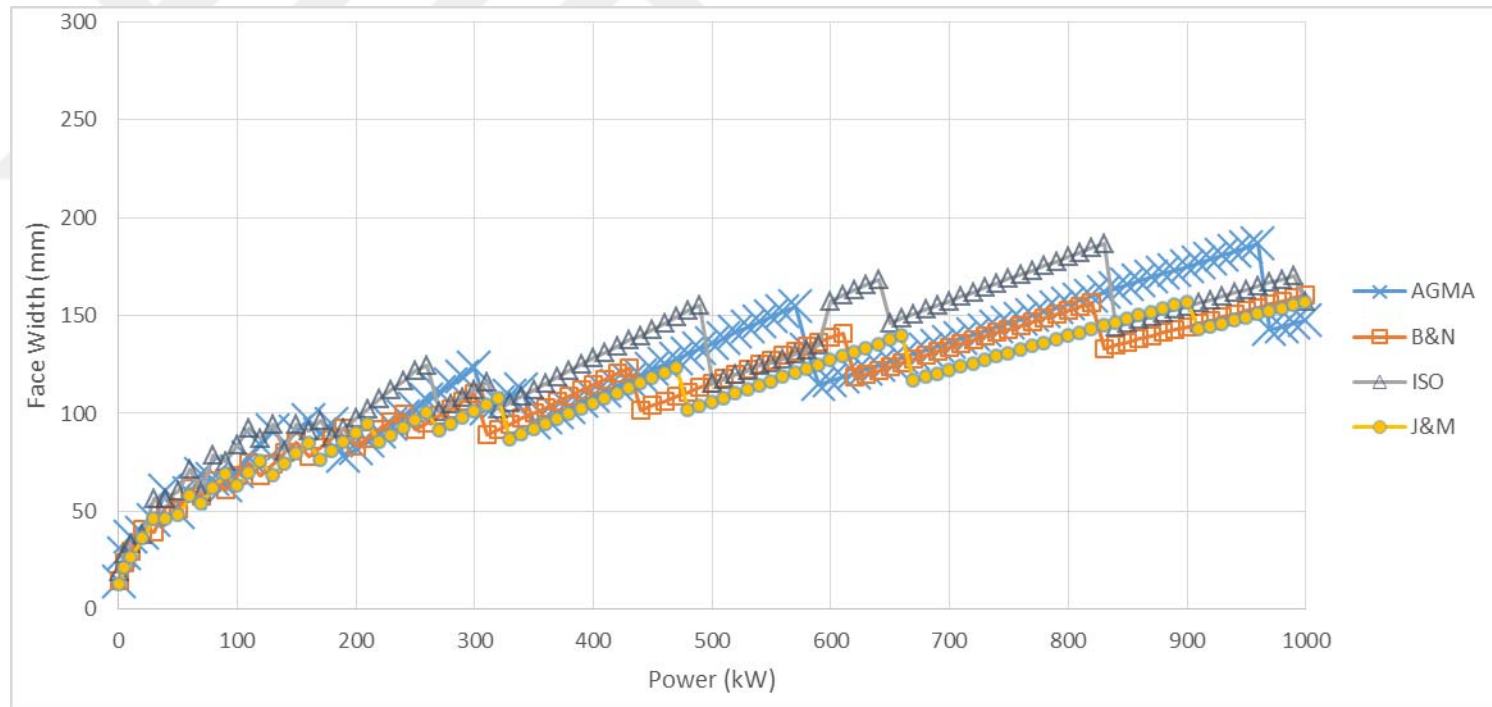
Figure C.4.Face width variation considering bending fatigue failure under increasing power at 2:1 speed ratio (Ø=20°, Type 3)
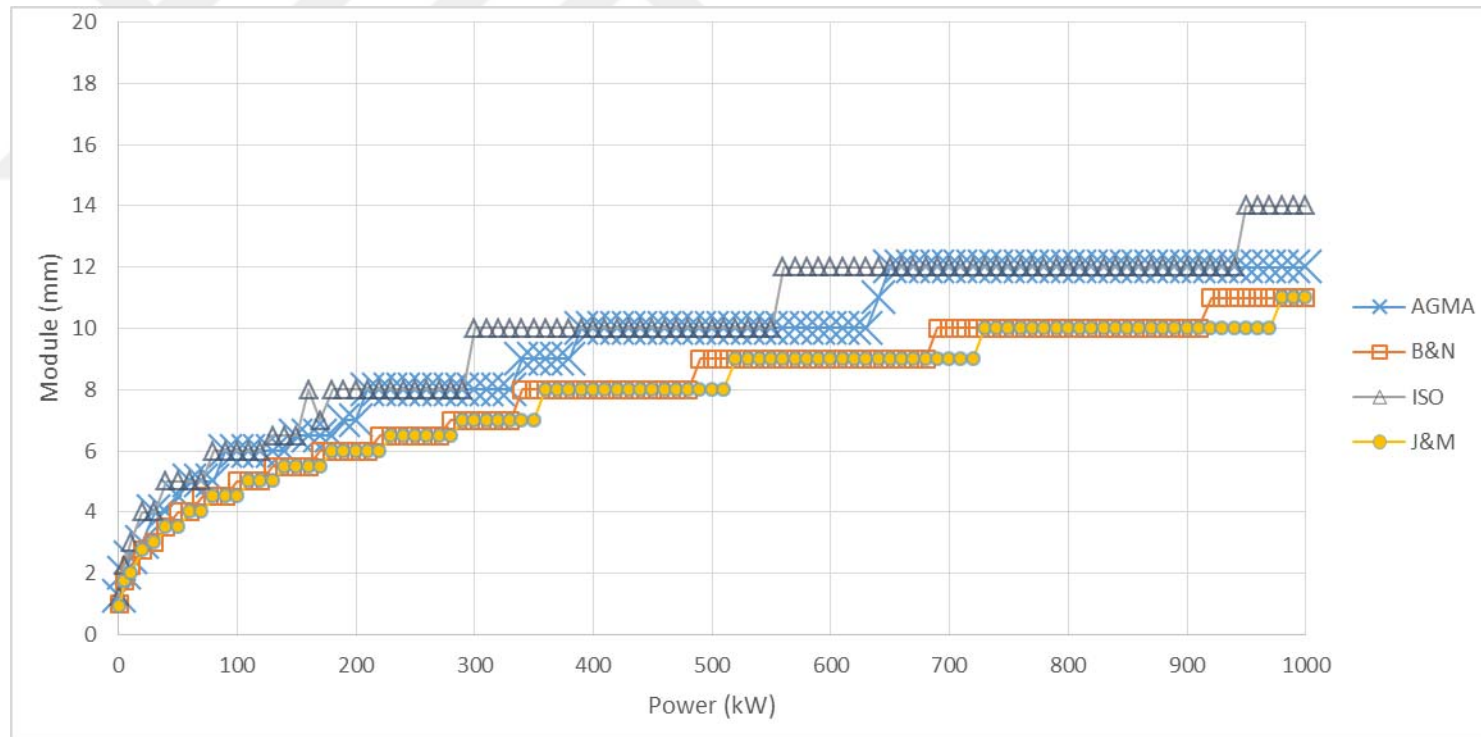
Figure C. 5. Module variation considering bending fatigue failure under increasing power at 3:1 speed ratio (Ø=20°, Type 3)
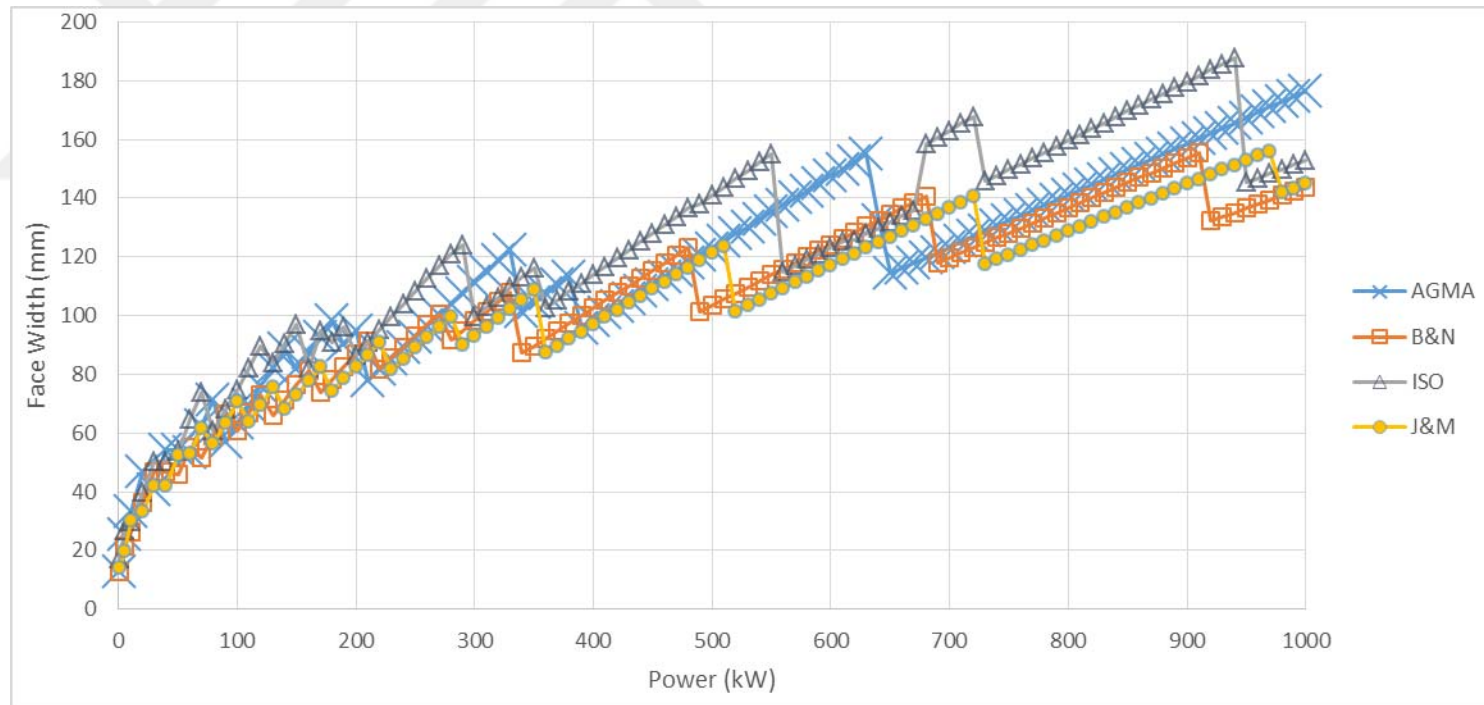
Figure C.6.Face width variation considering bending fatigue failure under increasing power at 3:1 speed ratio (Ø=20°, Type 3)
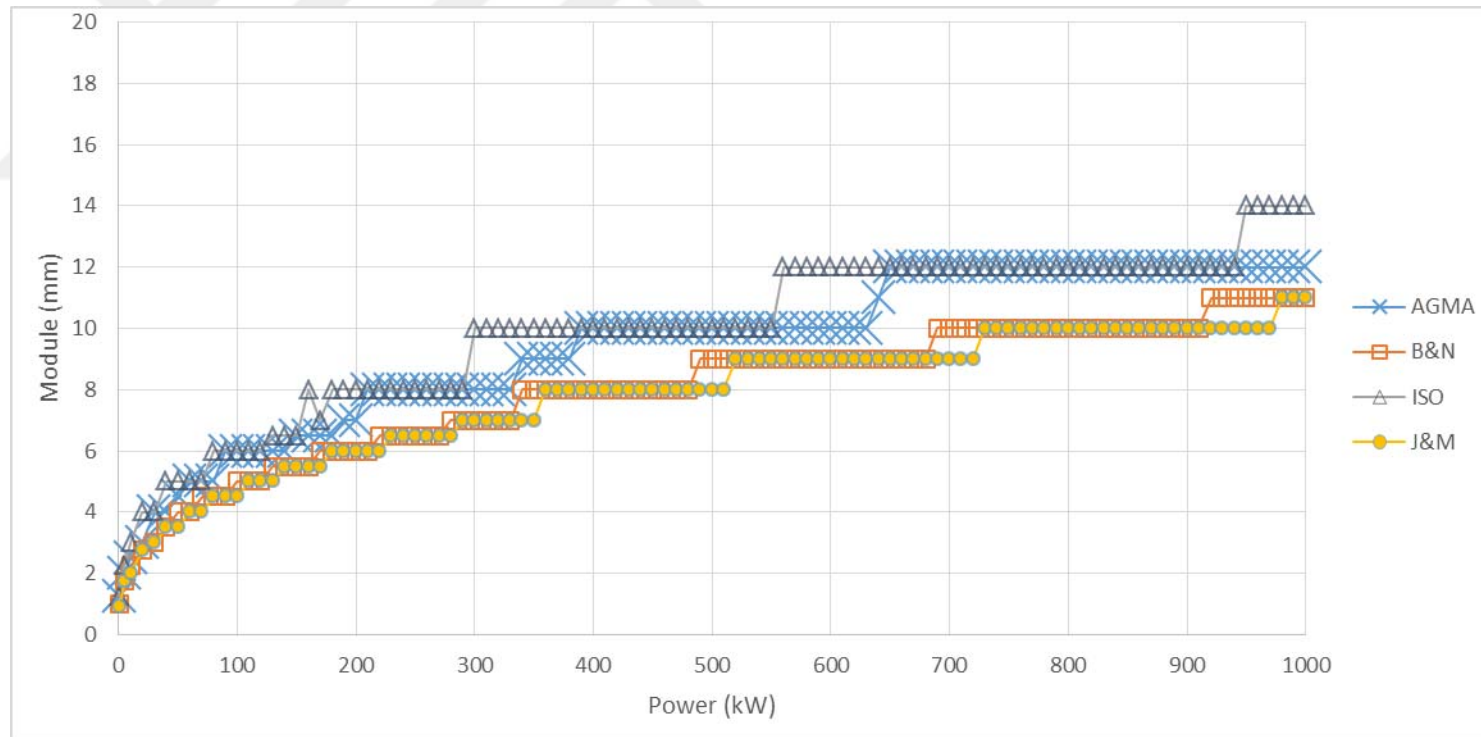
Figure C. 7. Module variation considering bending fatigue failure under increasing power at 4:1 speed ratio (Ø=20°, Type 3)
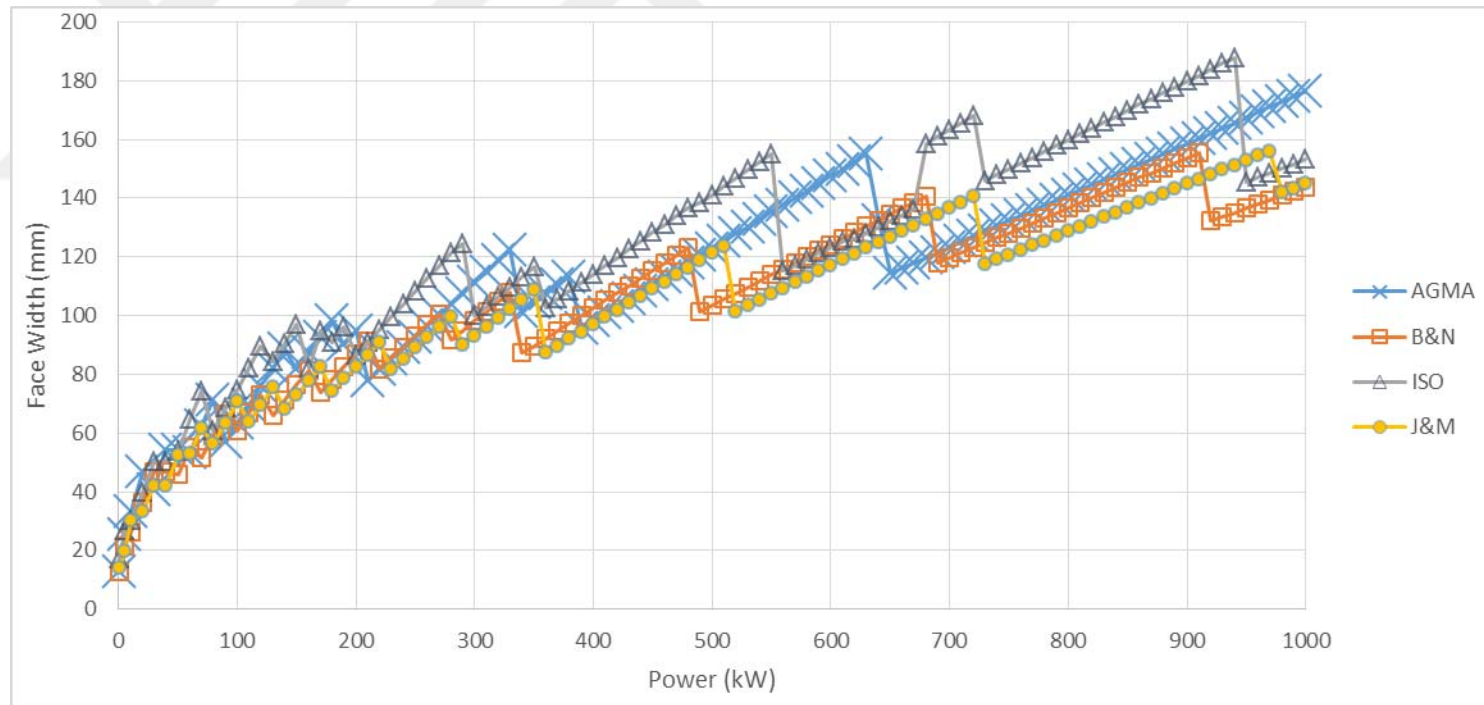
Figure C.8.Face width variation considering bending fatigue failure under increasing power at 4:1 speed ratio (Ø=20°, Type 3)
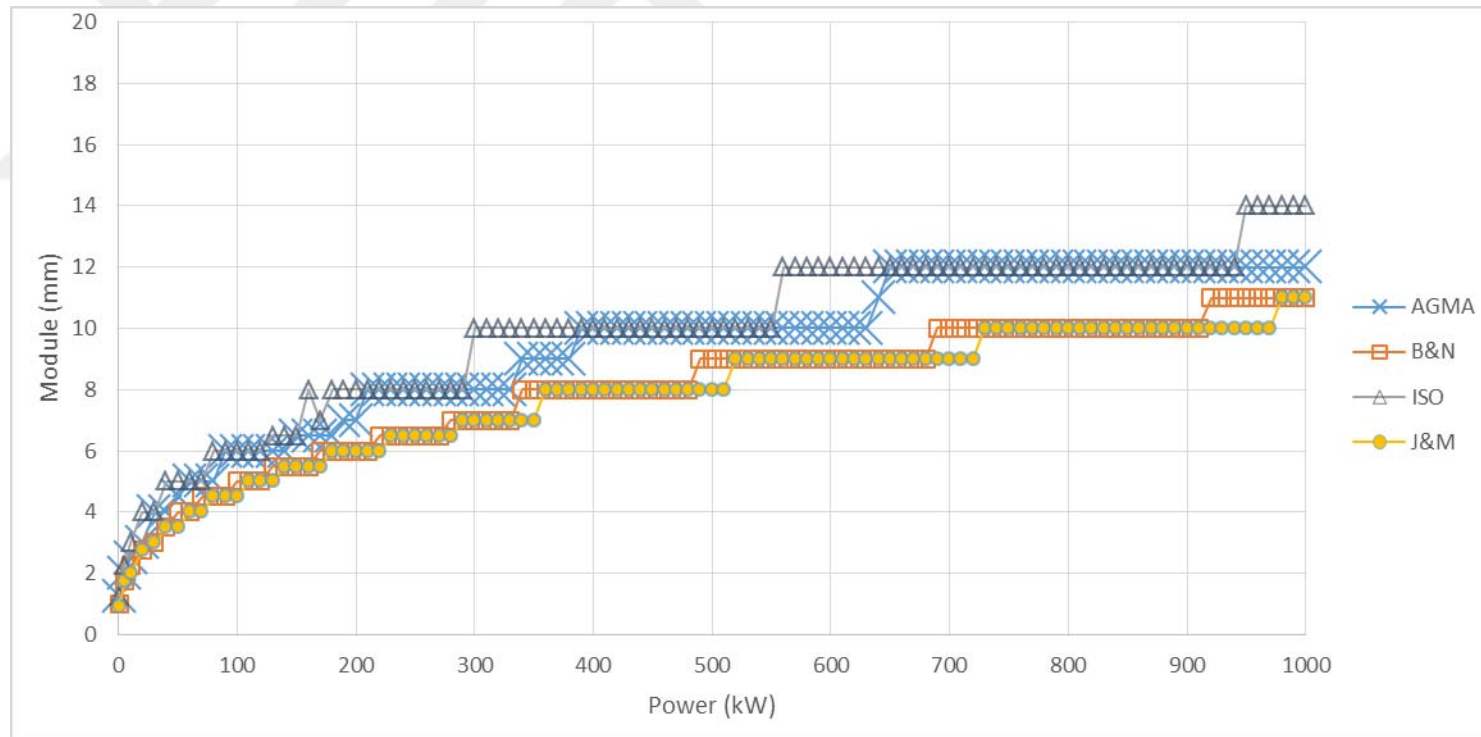
Figure C. 9. Module variation considering bending fatigue failure under increasing power at 5:1 speed ratio ($\varnothing=20^{o}$, Type 3)
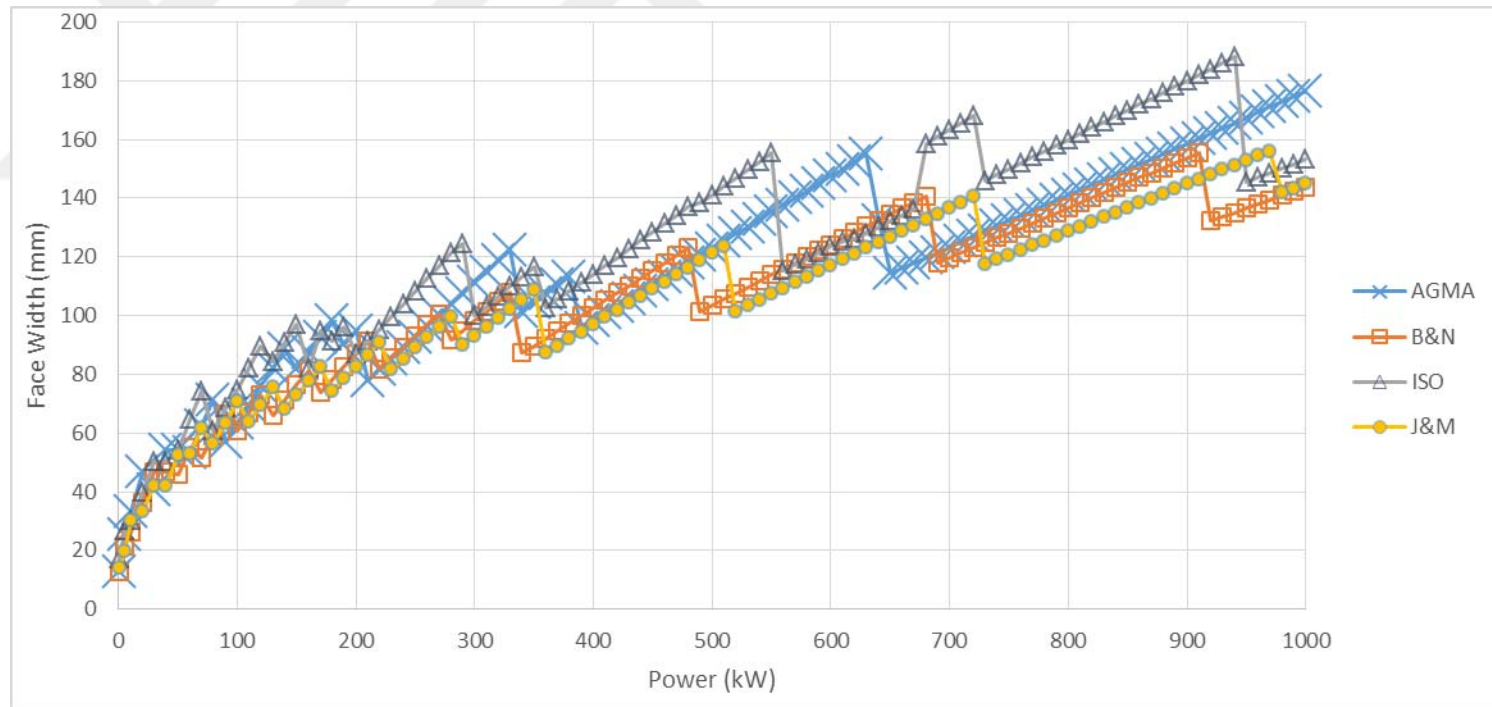
Figure C. 10. Face width variation considering bending fatigue failure under increasing power at 5:1 speed ratio (Ø=20°, Type3)
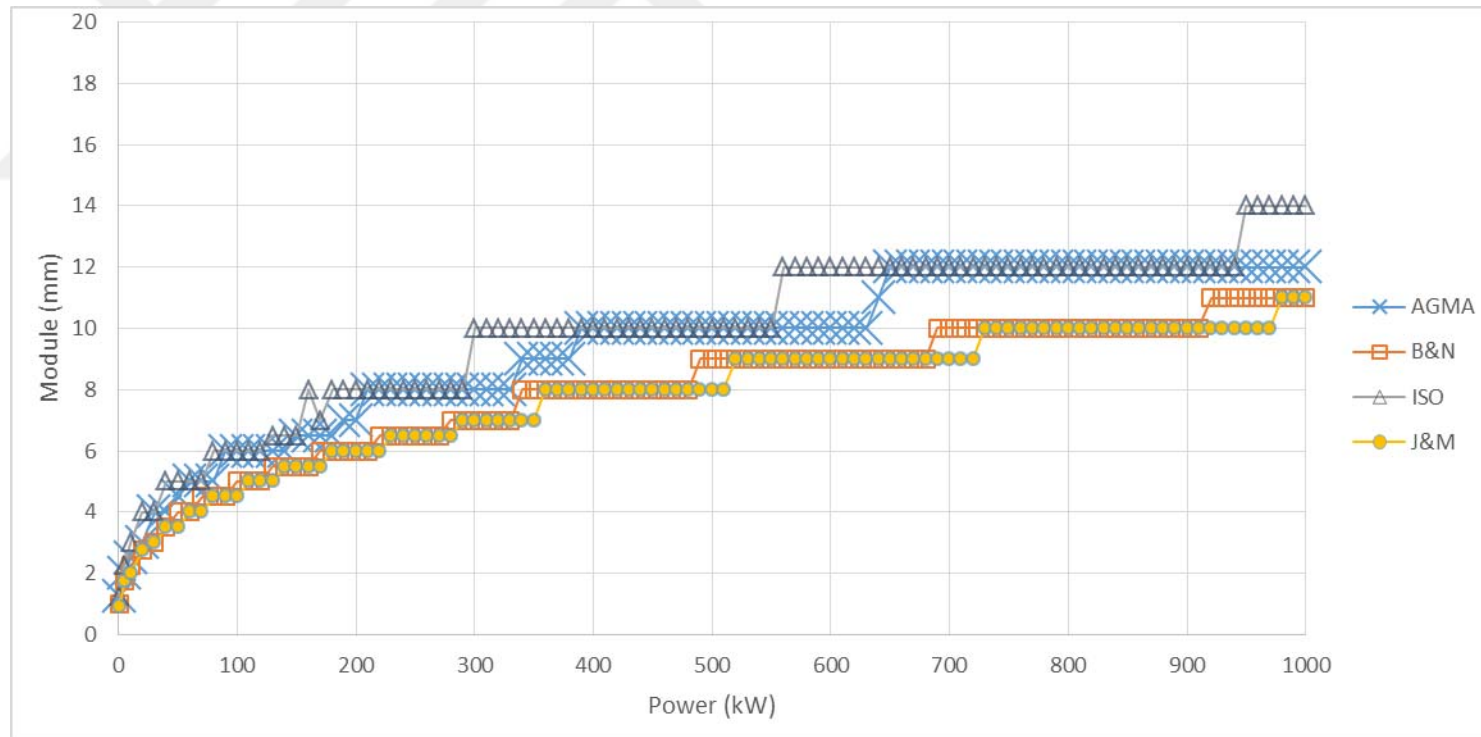
Figure C. 11. Module variation considering bending fatigue failure under increasing power at 6:1 speed ratio (Ø=20°, Type 3)
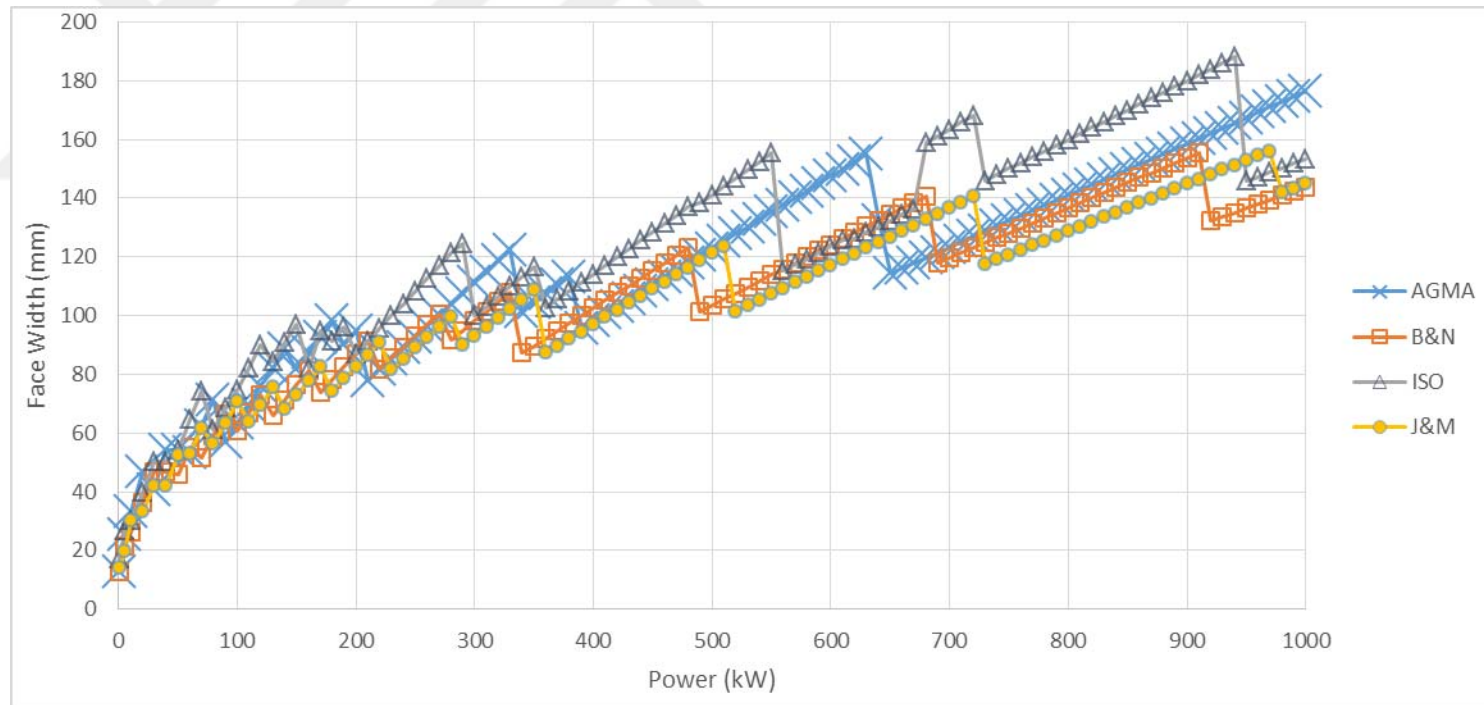
Figure C. 12. Face width variation considering bending fatigue failure under increasing power at 6:1 speed ratio (Ø=20º, Type3)

Figure C. 13. Module variation considering bending fatigue failure under increasing power at 7:1 speed ratio (Ø=20°, Type 3)
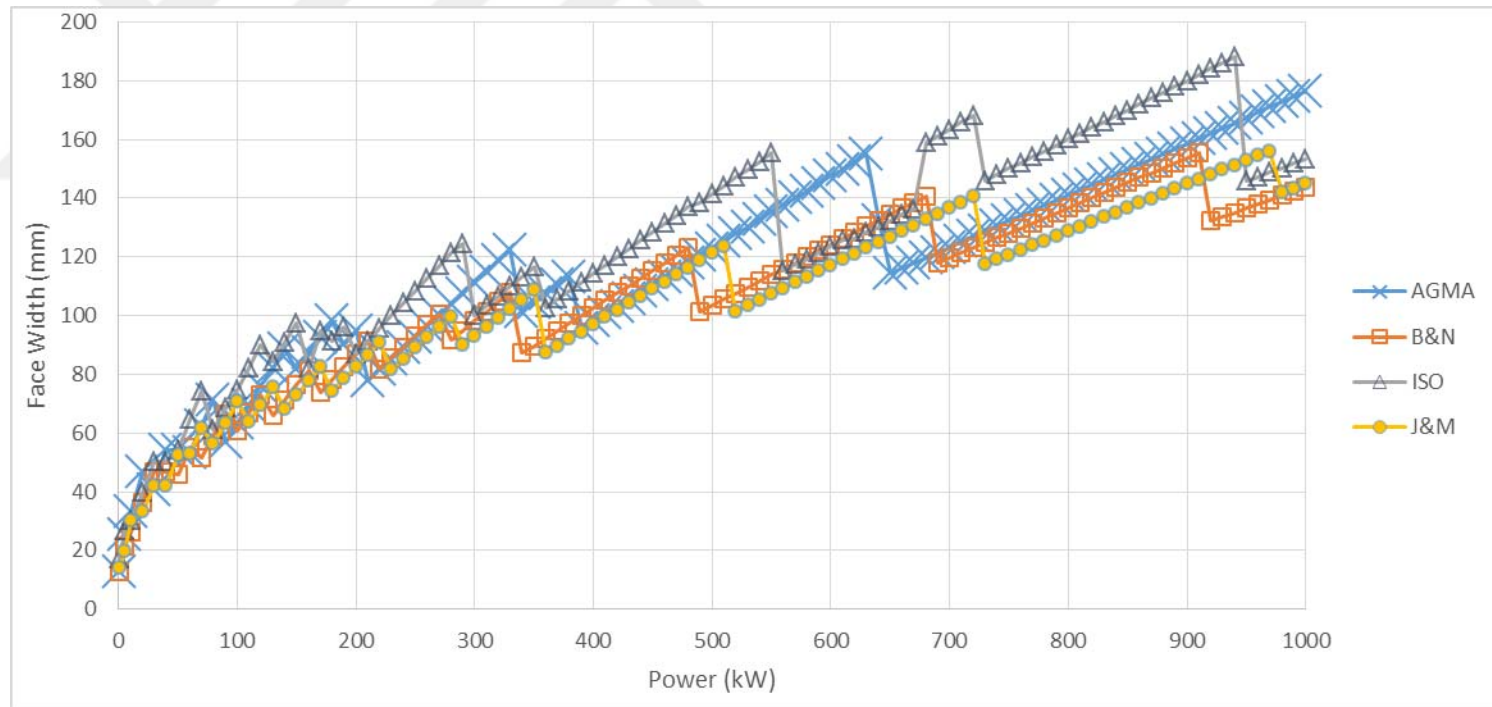
Figure C. 14. Face width variation considering bending fatigue failure under increasing power at 7:1 speed ratio (Ø=20°, Type3)
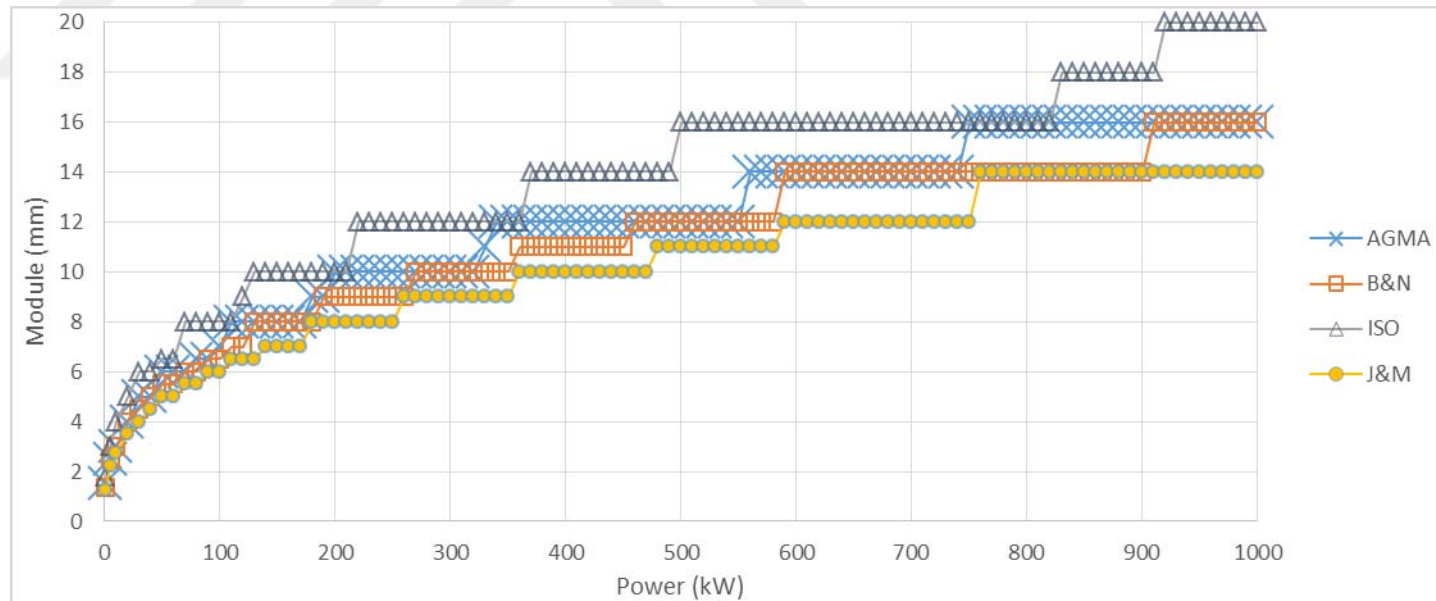
Figure C. 15. Module variation considering bending fatigue failure under increasing power at 8:1 speed ratio (Ø=20$^{\text{o}}$, Type 3)
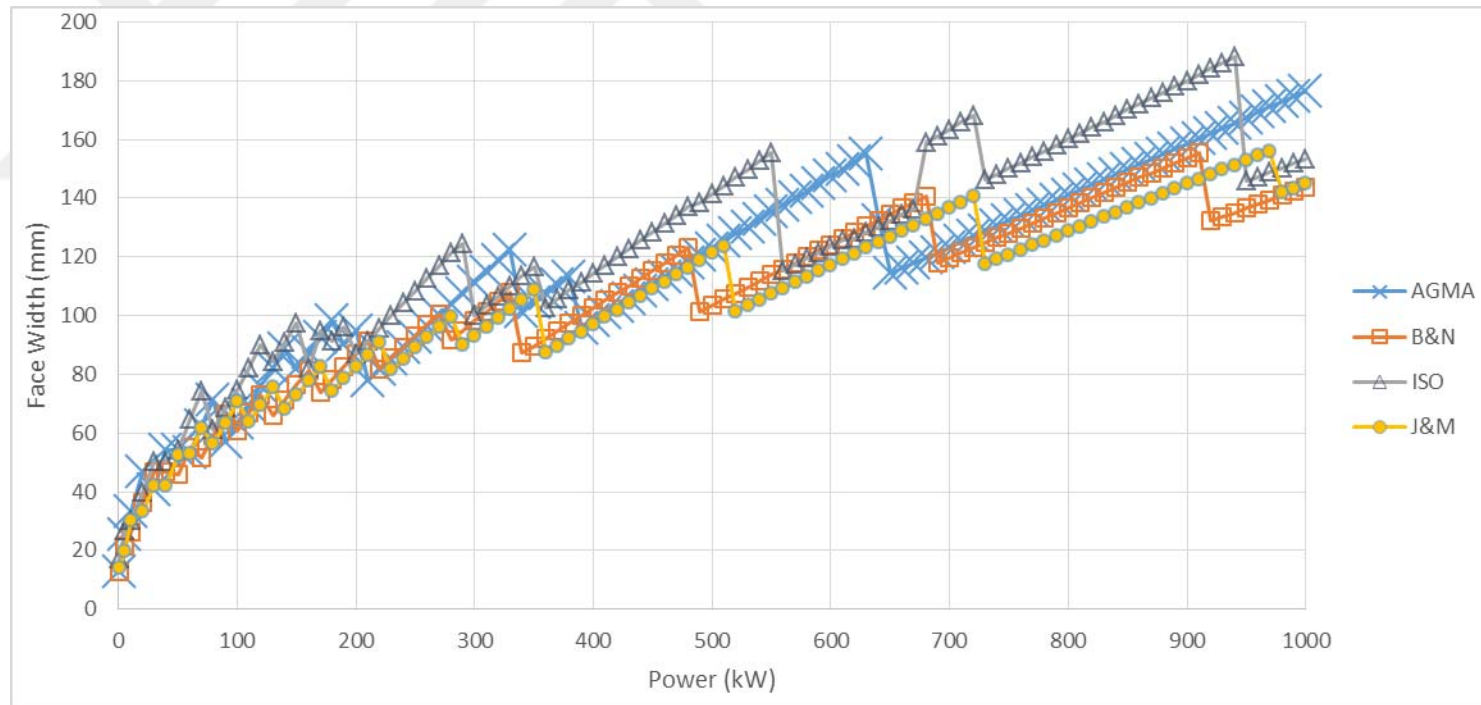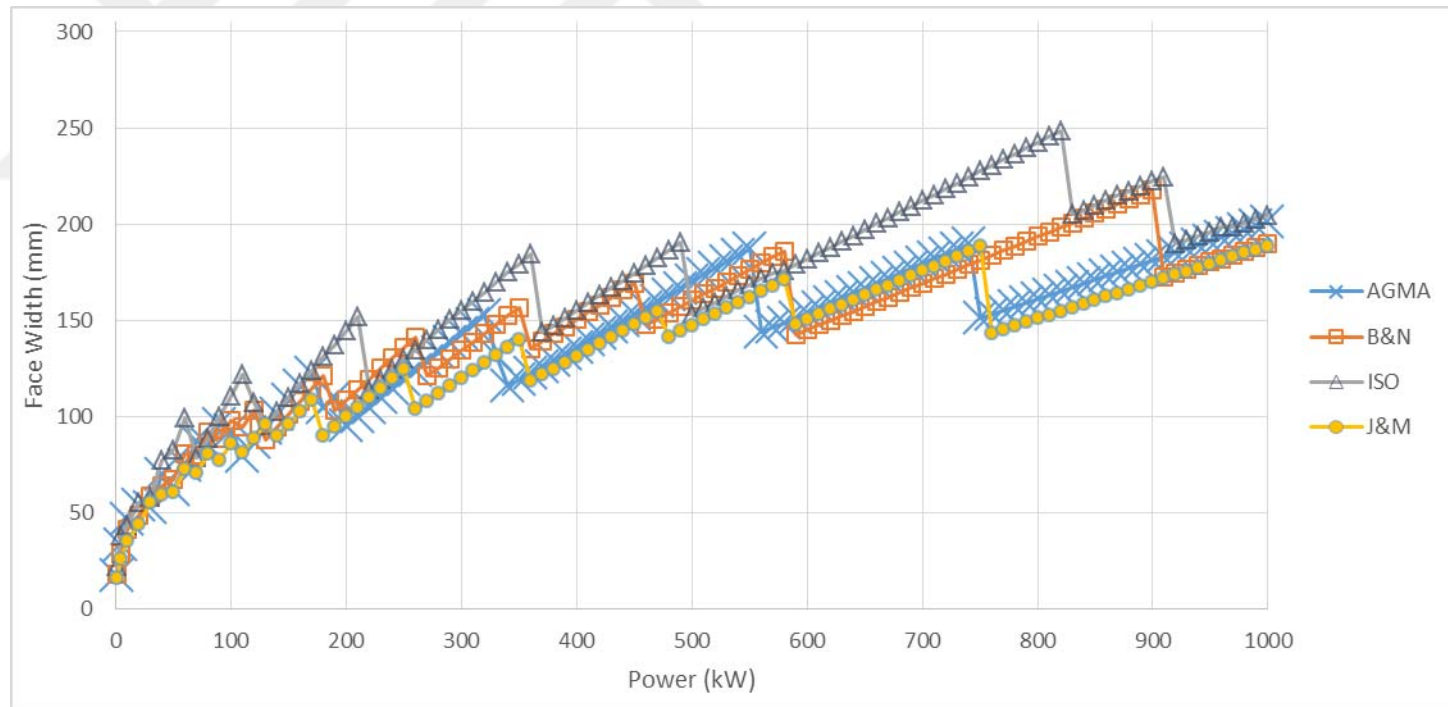
Figure C. 16. Face width variation considering bending fatigue failure under increasing power at 8:1 speed ratio (Ø=20º, Type3)

C.2. Comparison of the Results Based on Bending Fatigue Failure Considering Speed Ratio for the Selected Power Transmissions for Ø=20°, Material type 3
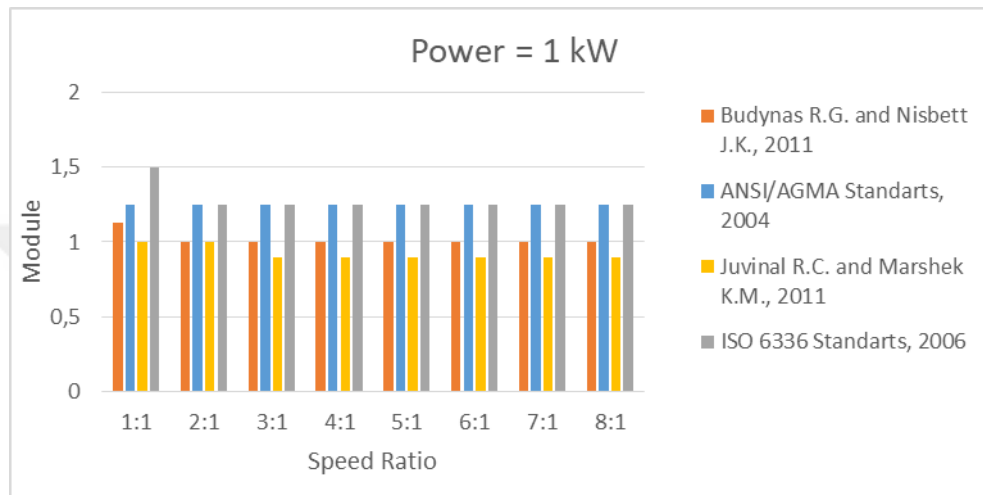
Figure C. 17. The effect of speed ratio on module selection based on bending fatigue failure at 1 kW power transmission (Ø=20°, Type 3)
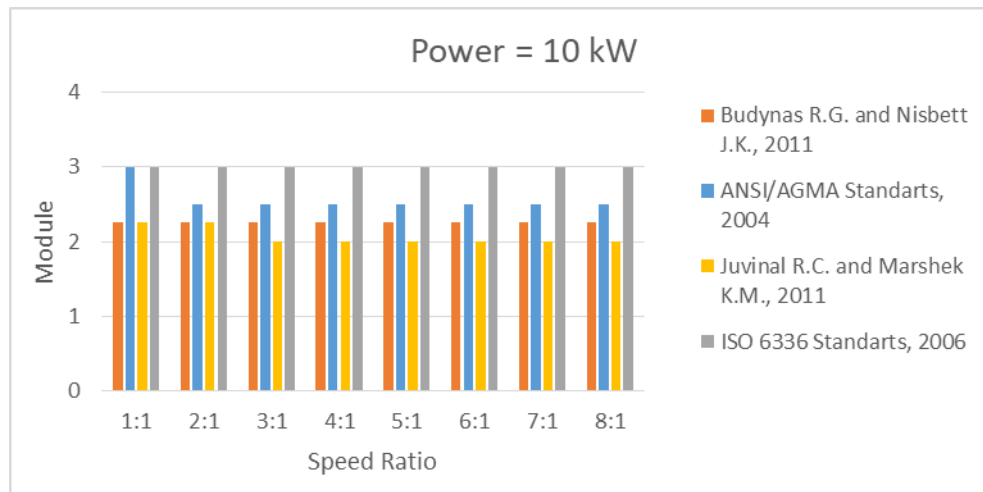
Figure C. 18. The effect of speed ratio on module selection based on bending fatigue failure at 10 kW power transmission (Ø=20°, Type 3)
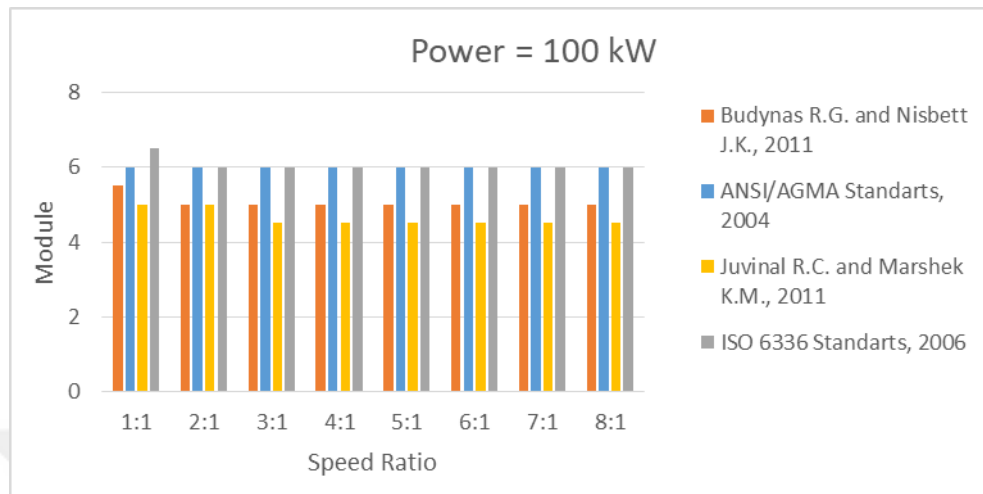
Figure C. 19. The effect of speed ratio on module selection based on bending fatigue failure at 100 kW power transmission ($\emptyset=20^{\circ}$, Type 3)
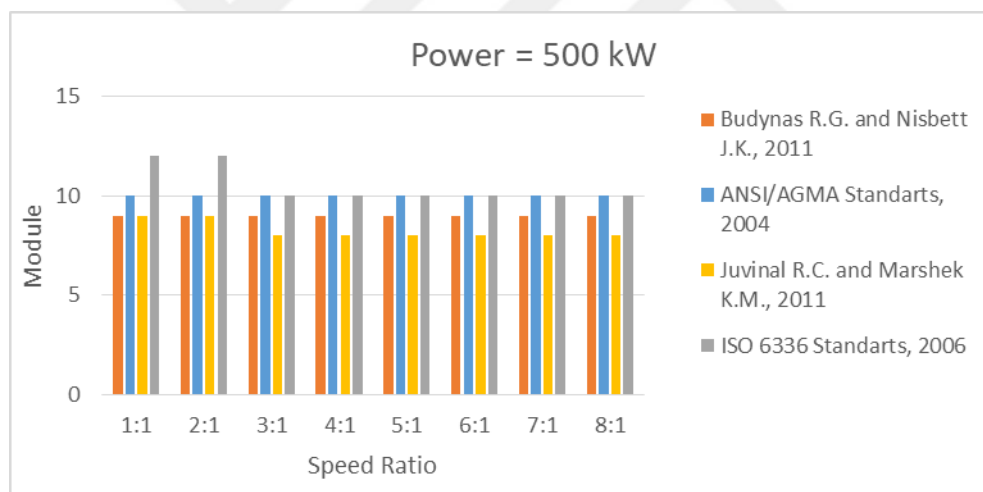
Figure C. 20. The effect of speed ratio on module selection based on bending fatigue failure at 500 kW power transmission ($\emptyset=20^{\circ}$, Type 3)
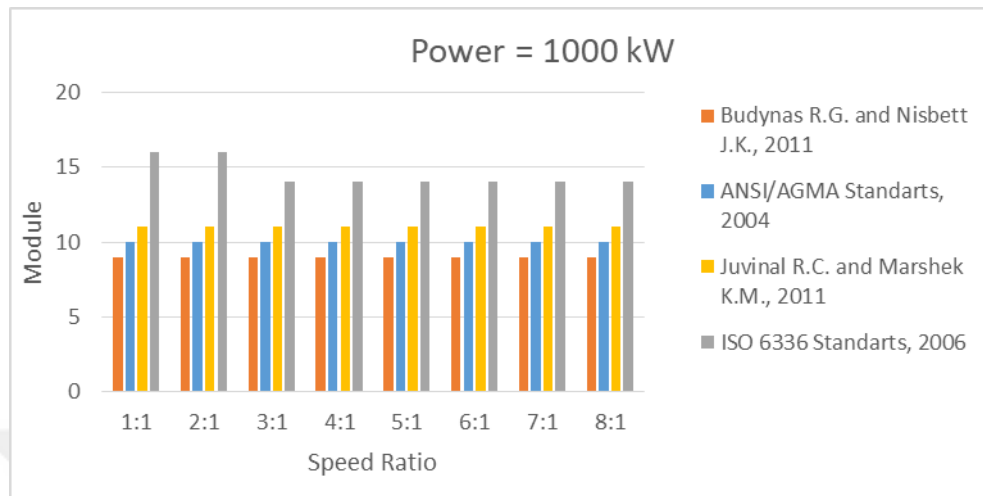
Figure C. 21. The effect of speed ratio on module selection based on bending fatigue failure at 1000 kW power transmission (Ø=20°, Type 3)

C.3. Obtaining Geometric Rating Number (GR$_i$) for Design Approaches for Ø=20°, Material type 3
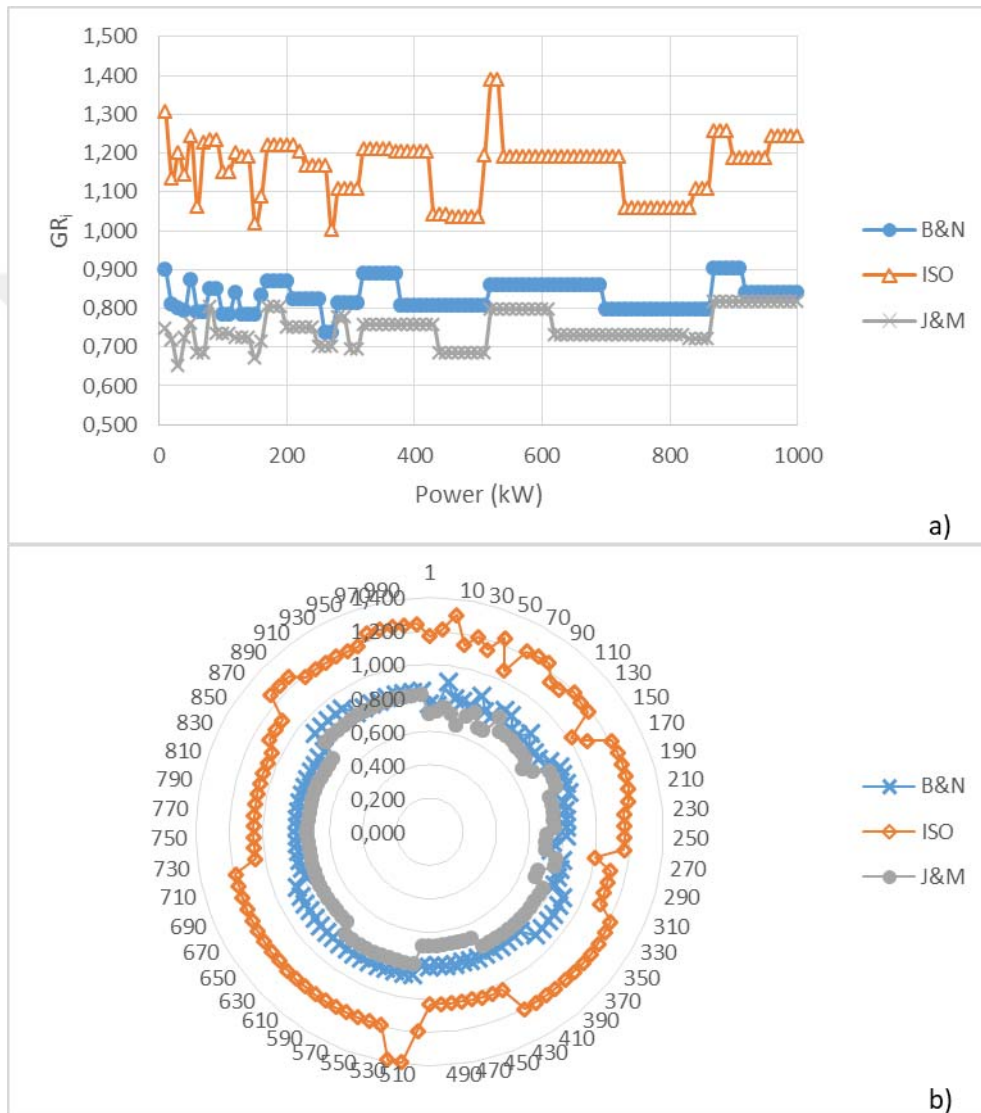
Figure C. 22. Comparison of GR$_i$ results obtained from the design approaches at 1:1 speed ratio (Ø=20°, Type 3), a) scatter chart, b) radar chart
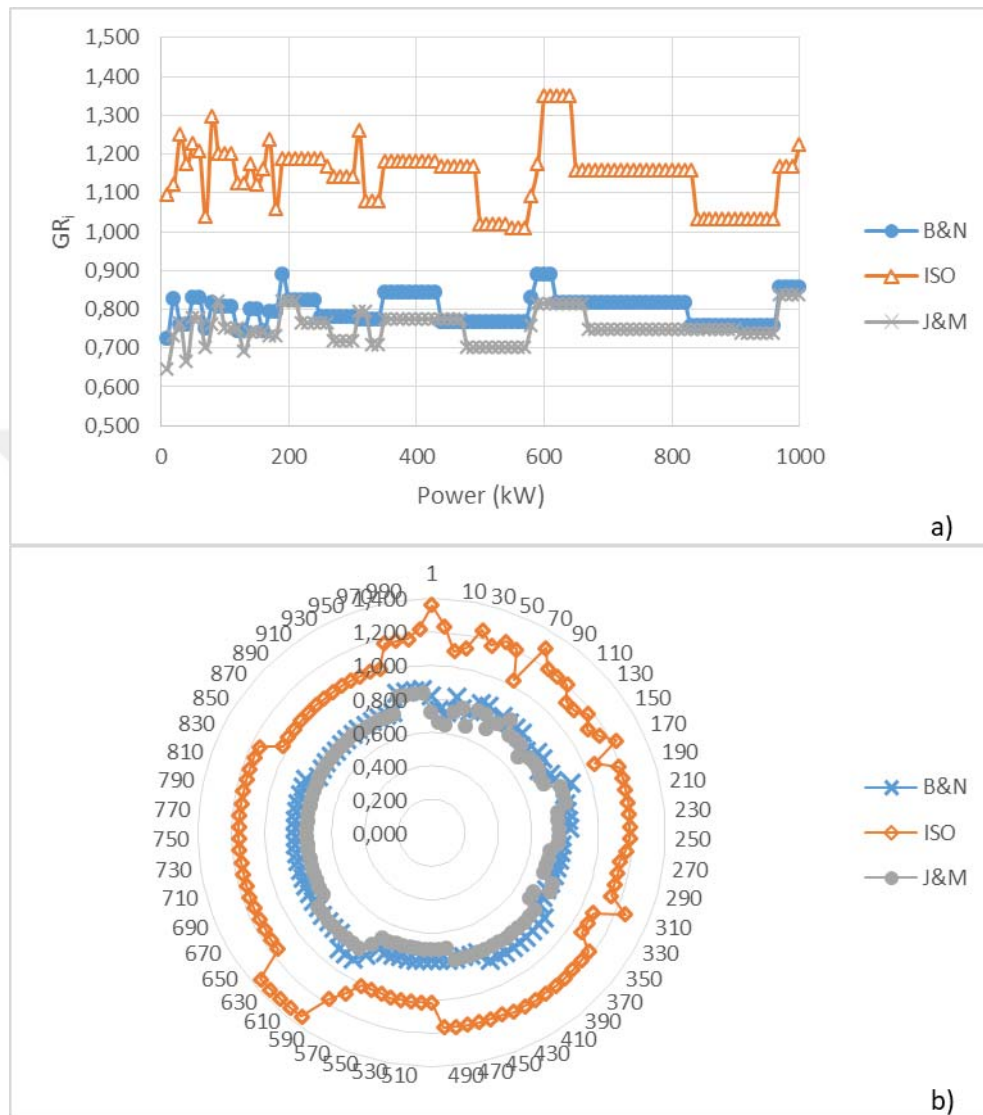
Figure C. 23. Comparison of GR_i results obtained from the design approaches at 2:1 speed ratio (Ø=20°, Type 3), a) scatter chart, b) radar chart

170
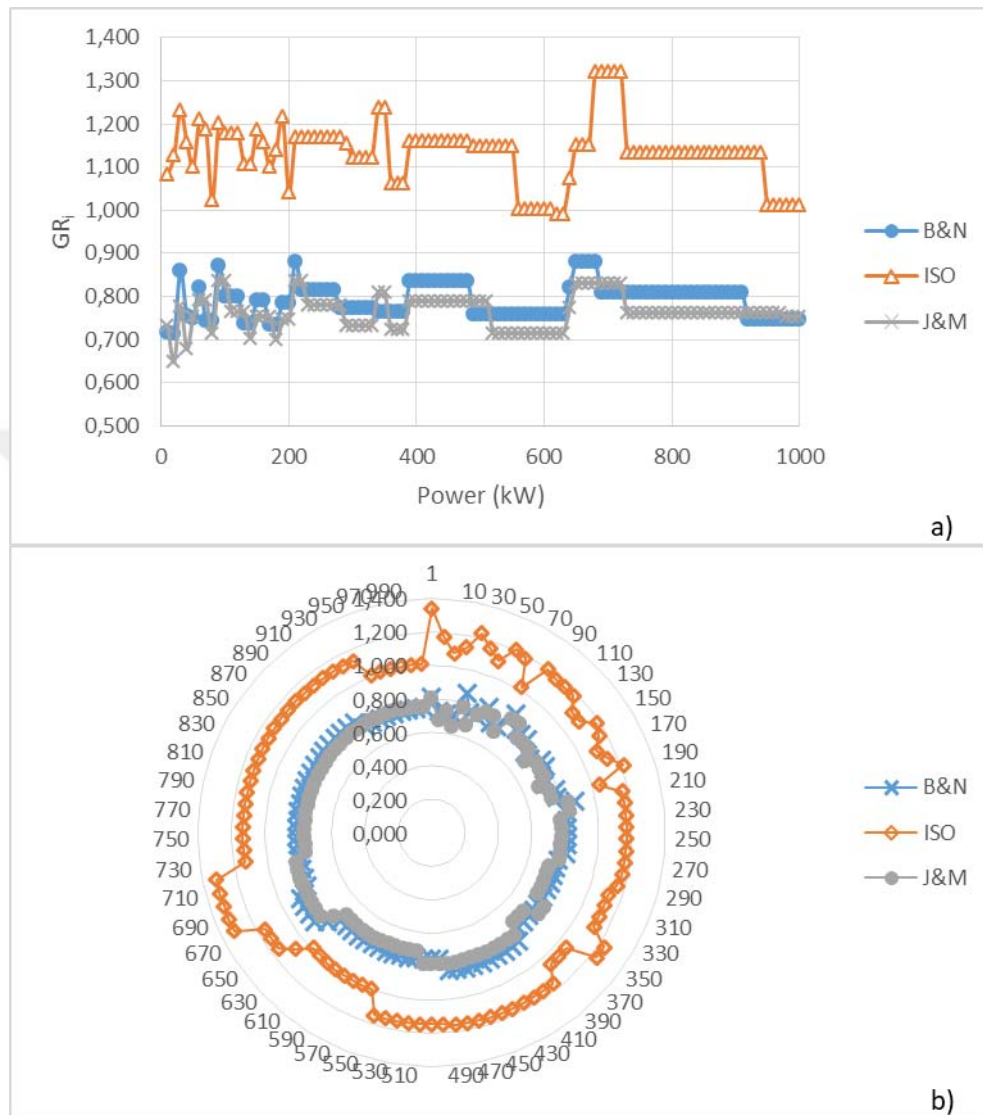
Figure C. 24. Comparison of GR_i results obtained from the design approaches at 3:1 speed ratio ($\emptyset=20^o$, Type 3), a) scatter chart, b) radar chart

171
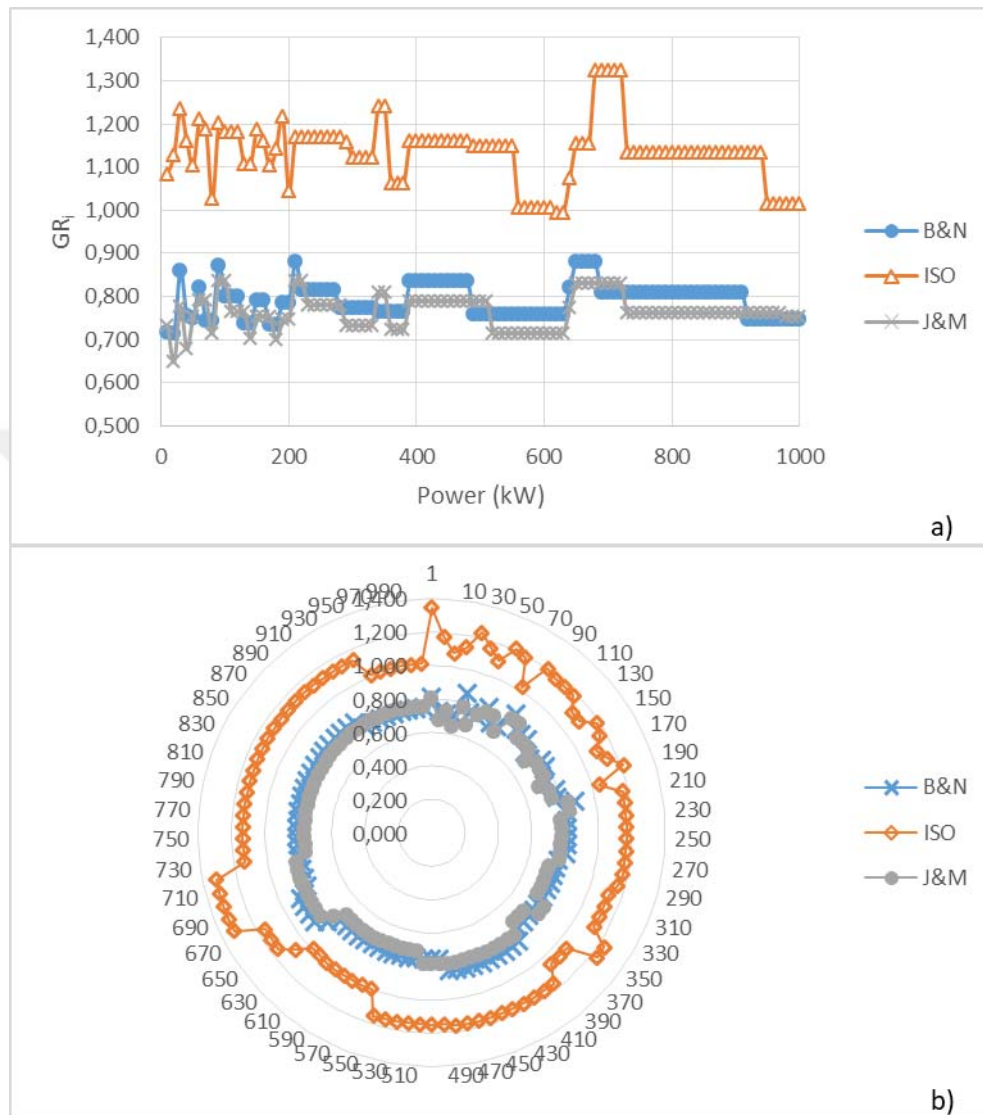
Figure C. 25. Comparison of GR_i results obtained from the design approaches at 4:1 speed ratio ($\varnothing=20^{o}$, Type 3), a) scatter chart, b) radar chart

172
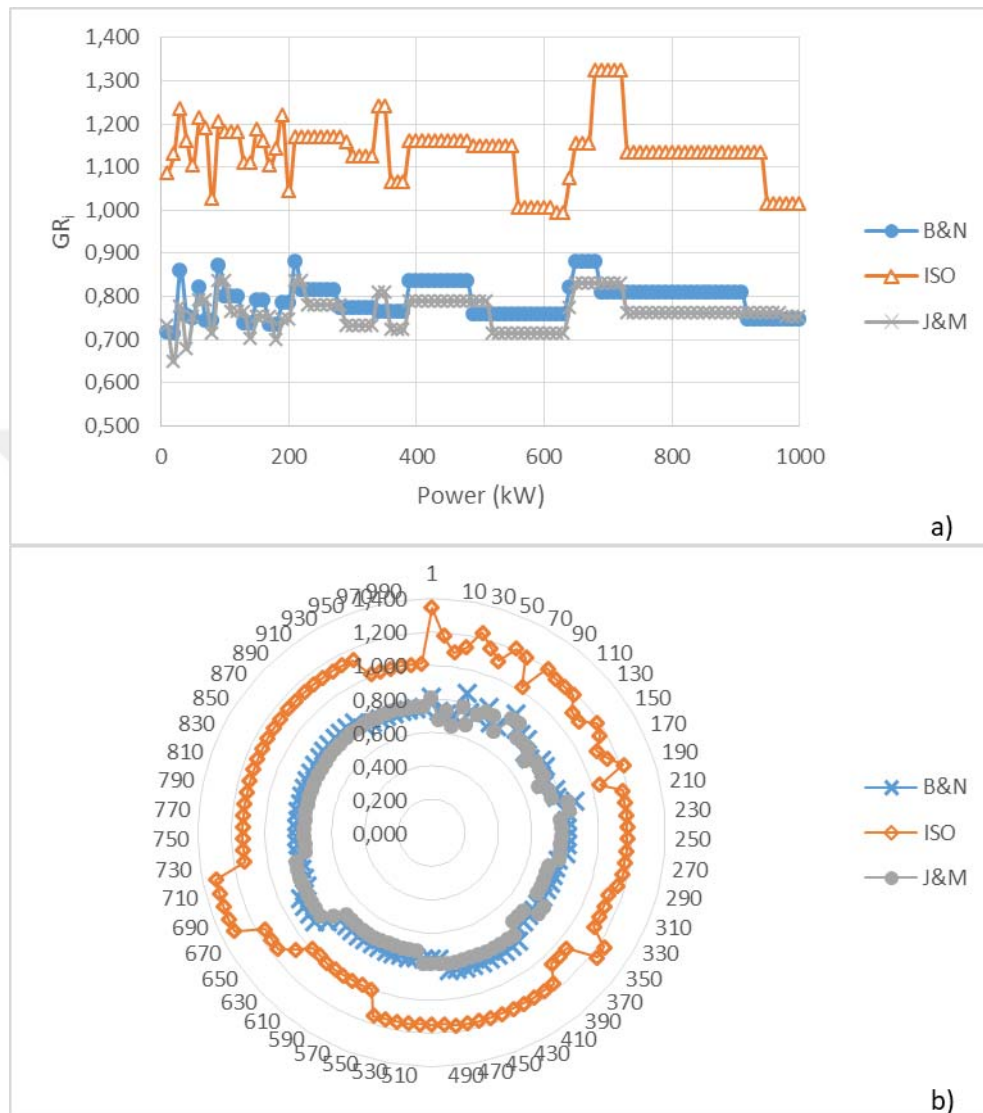
Figure C. 26. Comparison of GR_i results obtained from the design approaches at 5:1 speed ratio ($\varnothing$=20°, Type 3), a) scatter chart, b) radar chart
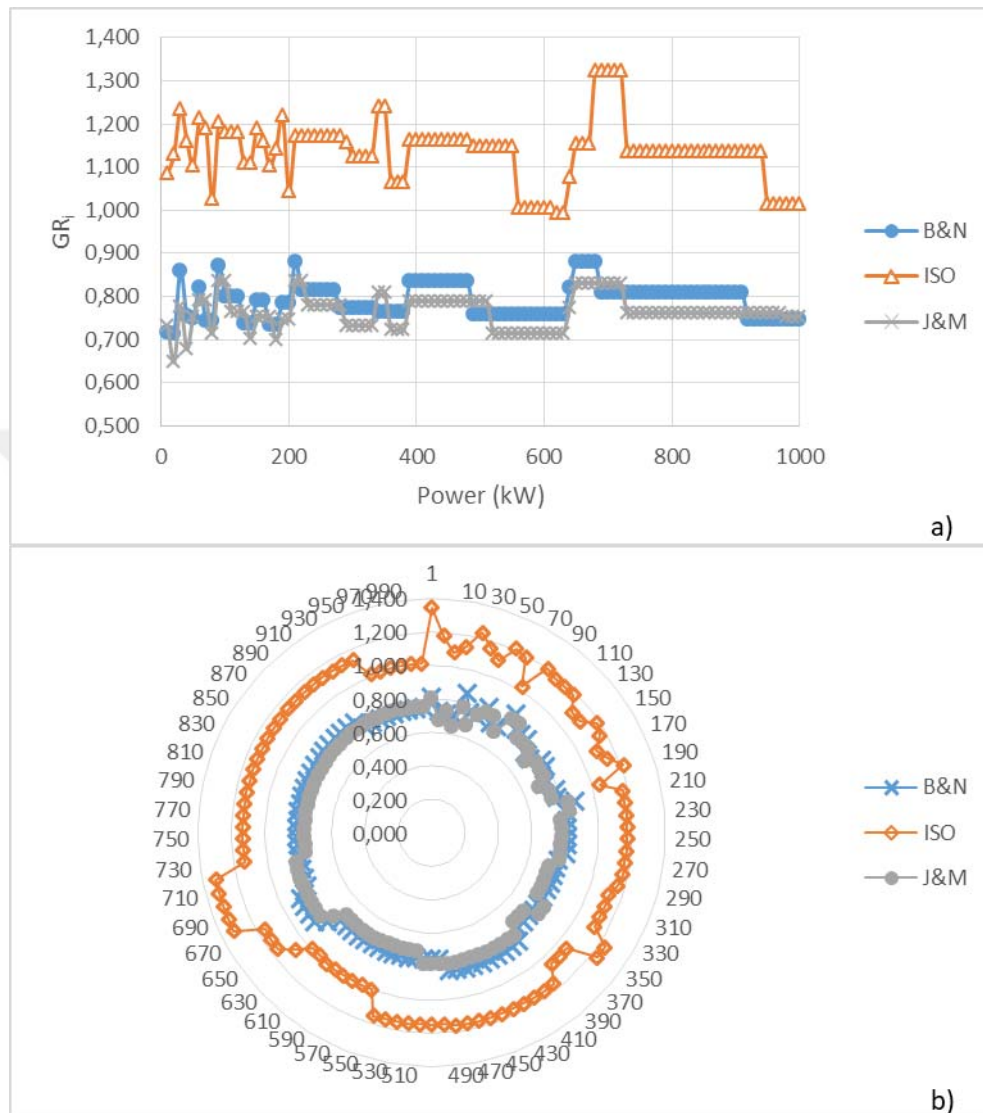
Figure C. 27. Comparison of GR_i results obtained from the design approaches at 6:1 speed ratio (Ø=20°, Type 3), a) scatter chart, b) radar chart
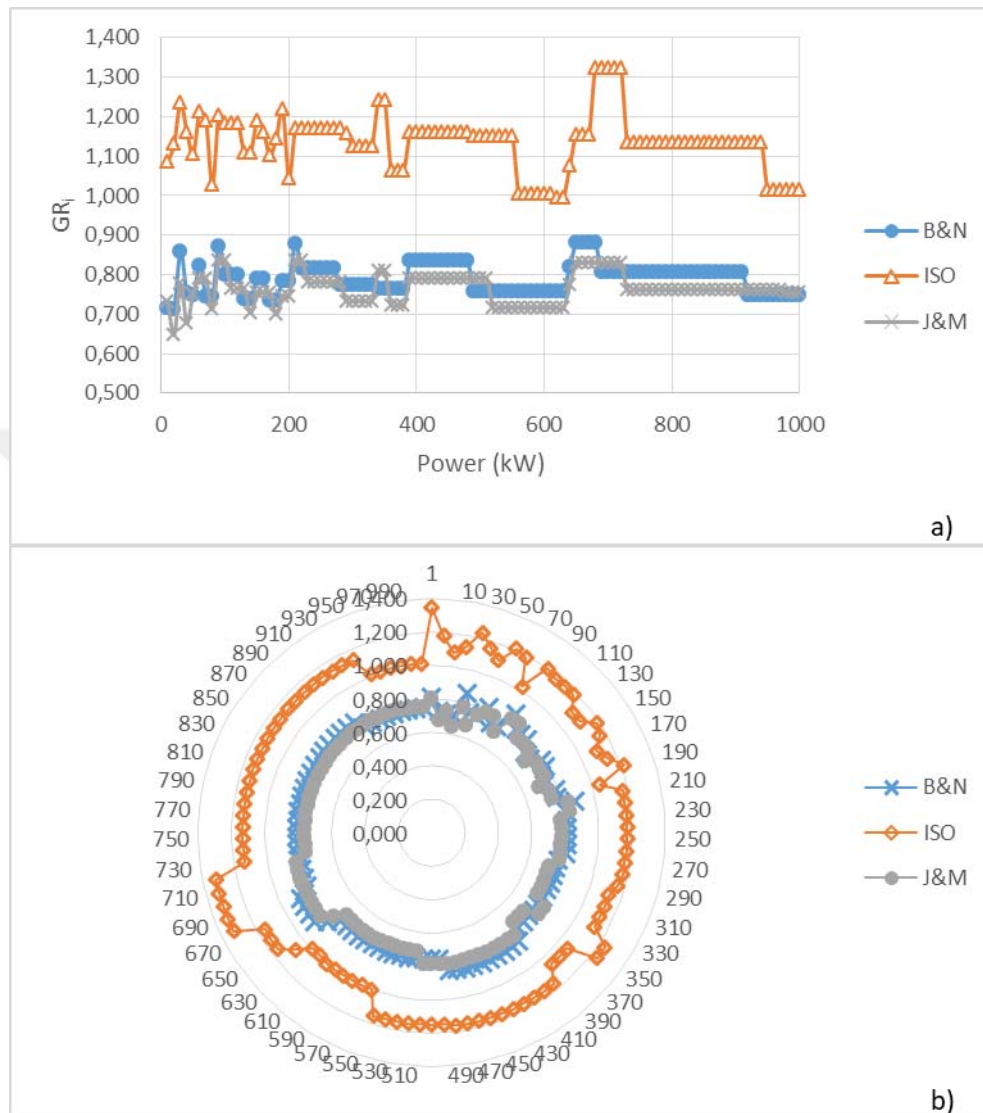
Figure C. 28. Comparison of GR_i results obtained from the design approaches at 7:1 speed ratio ($\varnothing=20^o$, Type 3), a) scatter chart, b) radar chart
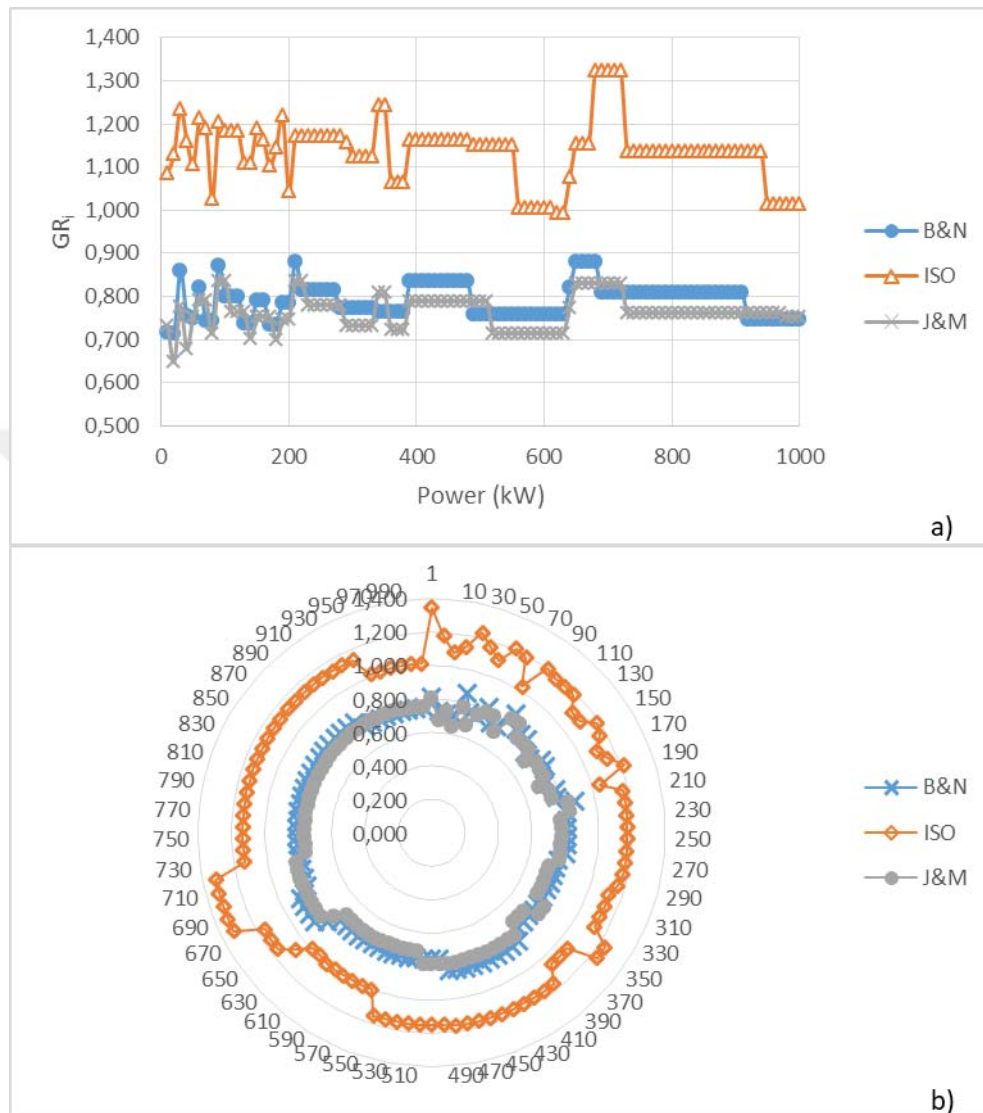
Figure C. 29. Comparison of GR_i results obtained from the design approaches at 8:1 speed ratio ($\emptyset=20^{\circ}$, Type 3), a) scatter chart, b) radar chart

176

APPENDIX D

D.1. Comparison of Module Selection and Face Width Results of the Design Approaches for Ø=25°, Material type 1

Figure D. 1. Module variation considering bending fatigue failure under increasing power at 1:1 speed ratio (Ø=25°, Type 1)
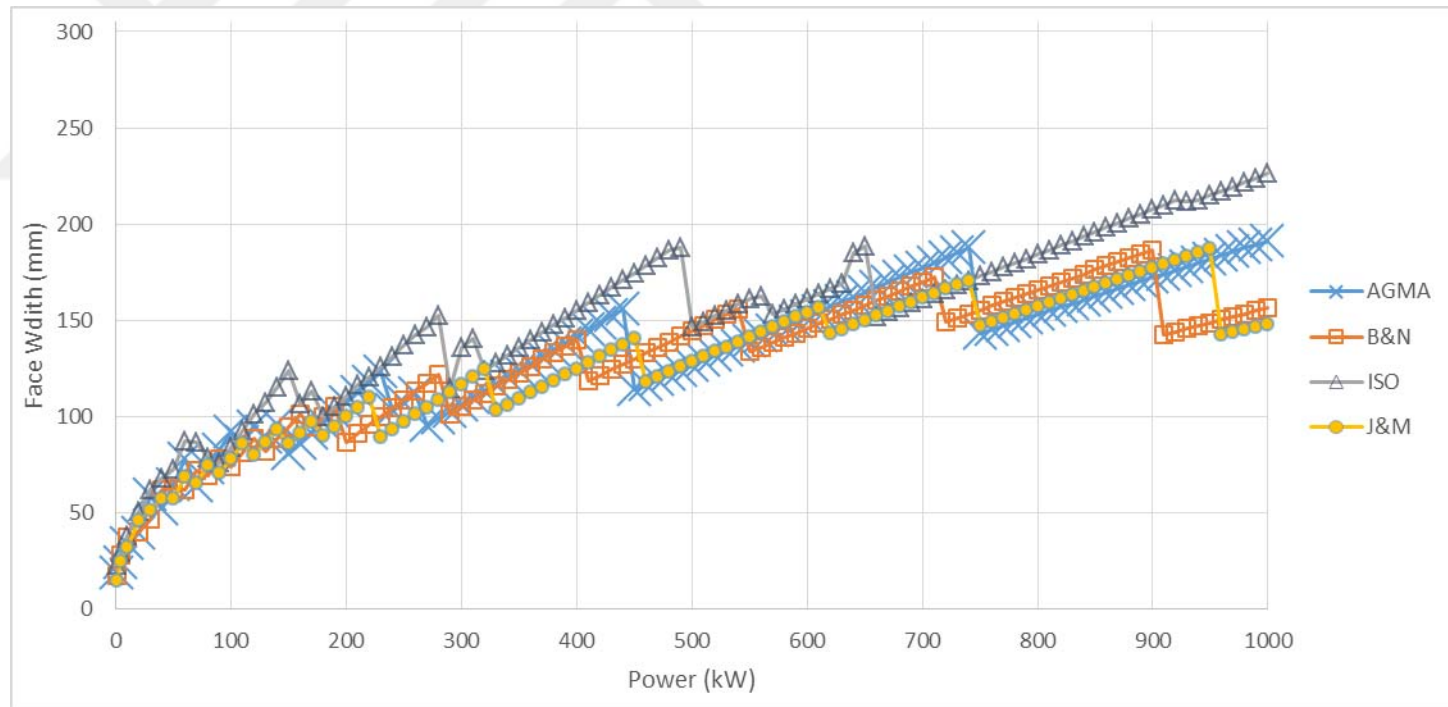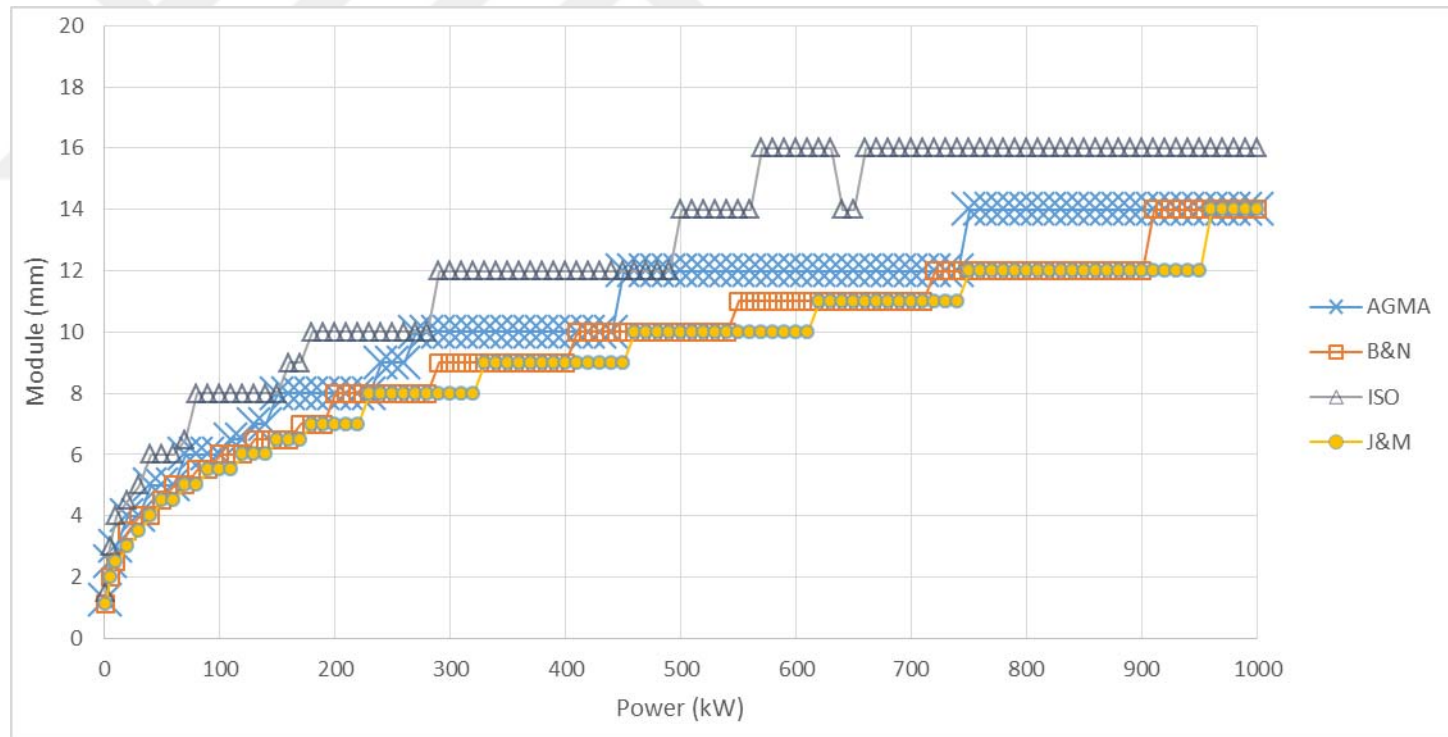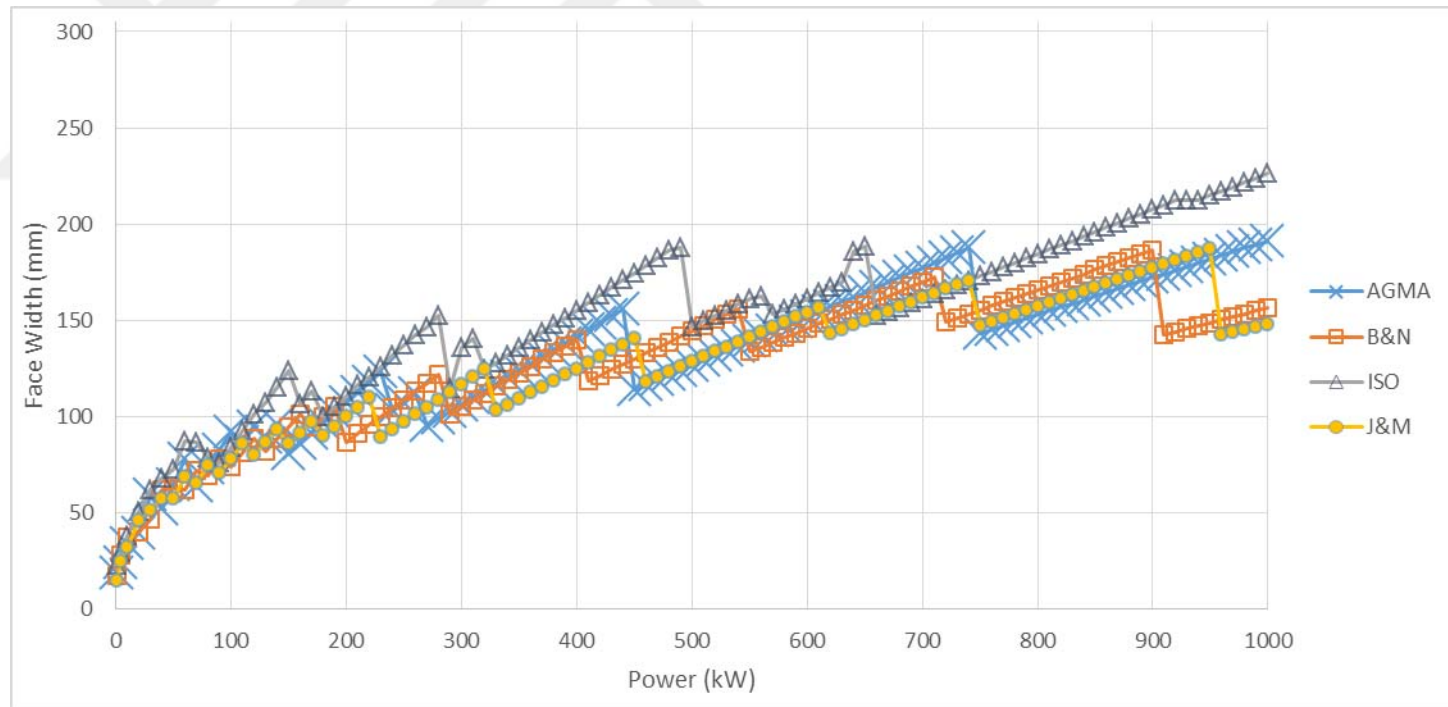
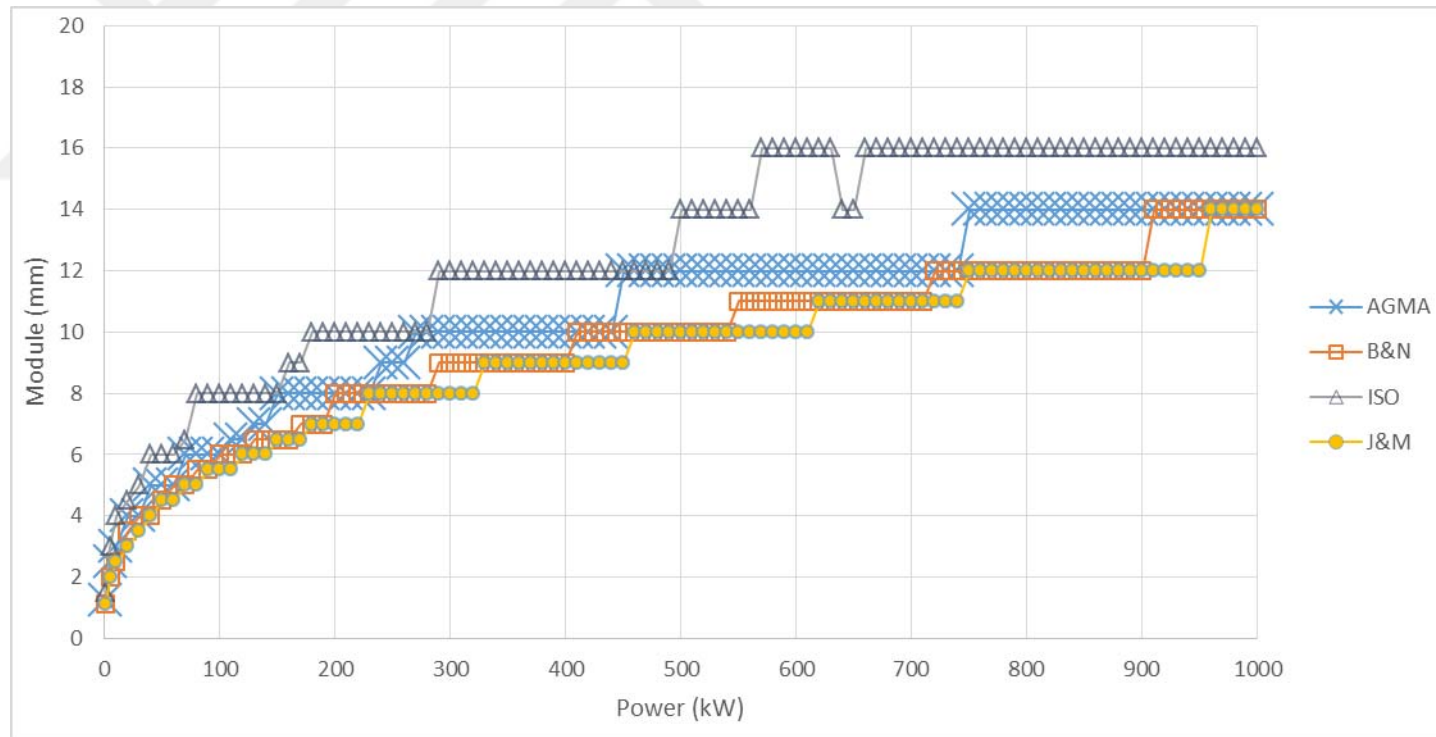Figure D. 2. Face width variation considering bending fatigue failure under increasing power at 1:1 speed ratio (Ø=25°, Type1)
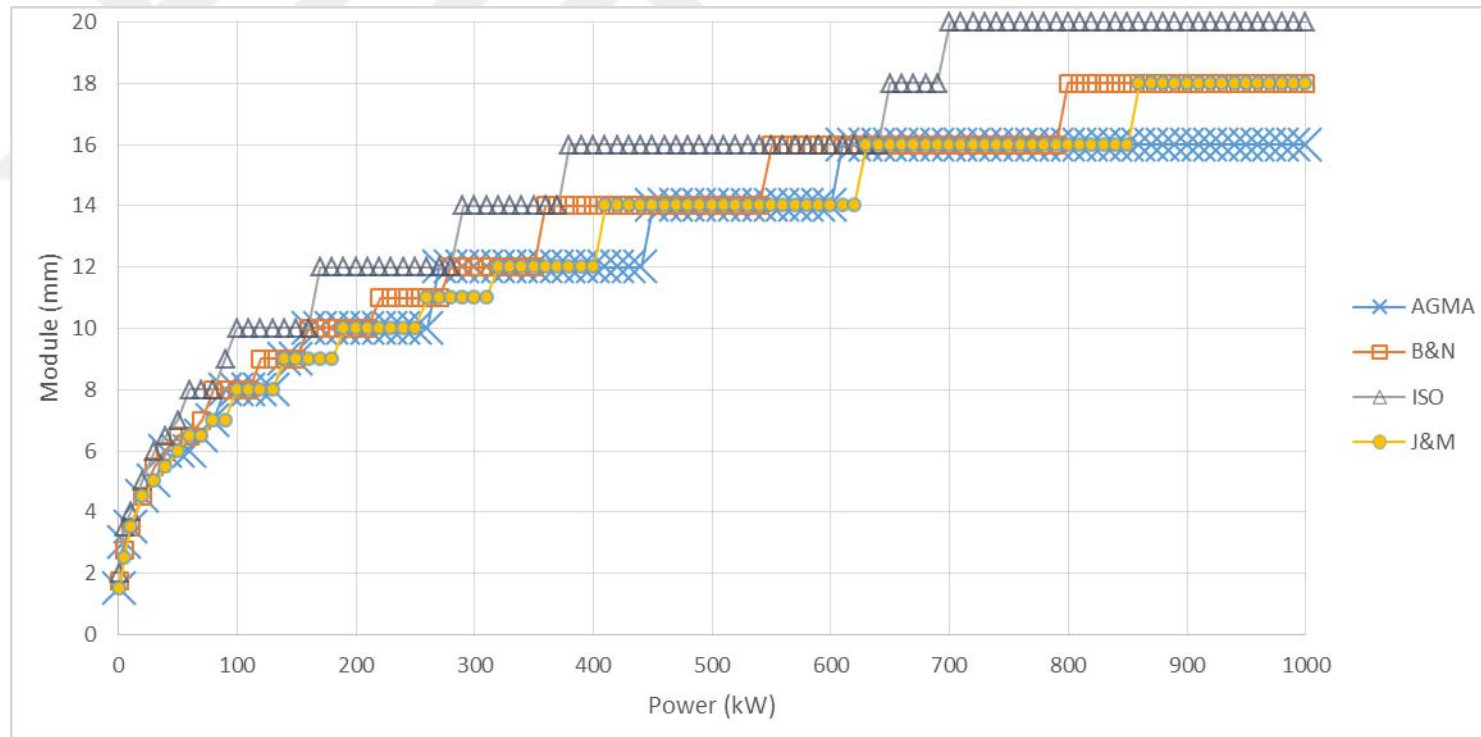
Figure D. 3. Module variation considering bending fatigue failure under increasing power at 2:1 speed ratio (Ø=25°, Type 1)
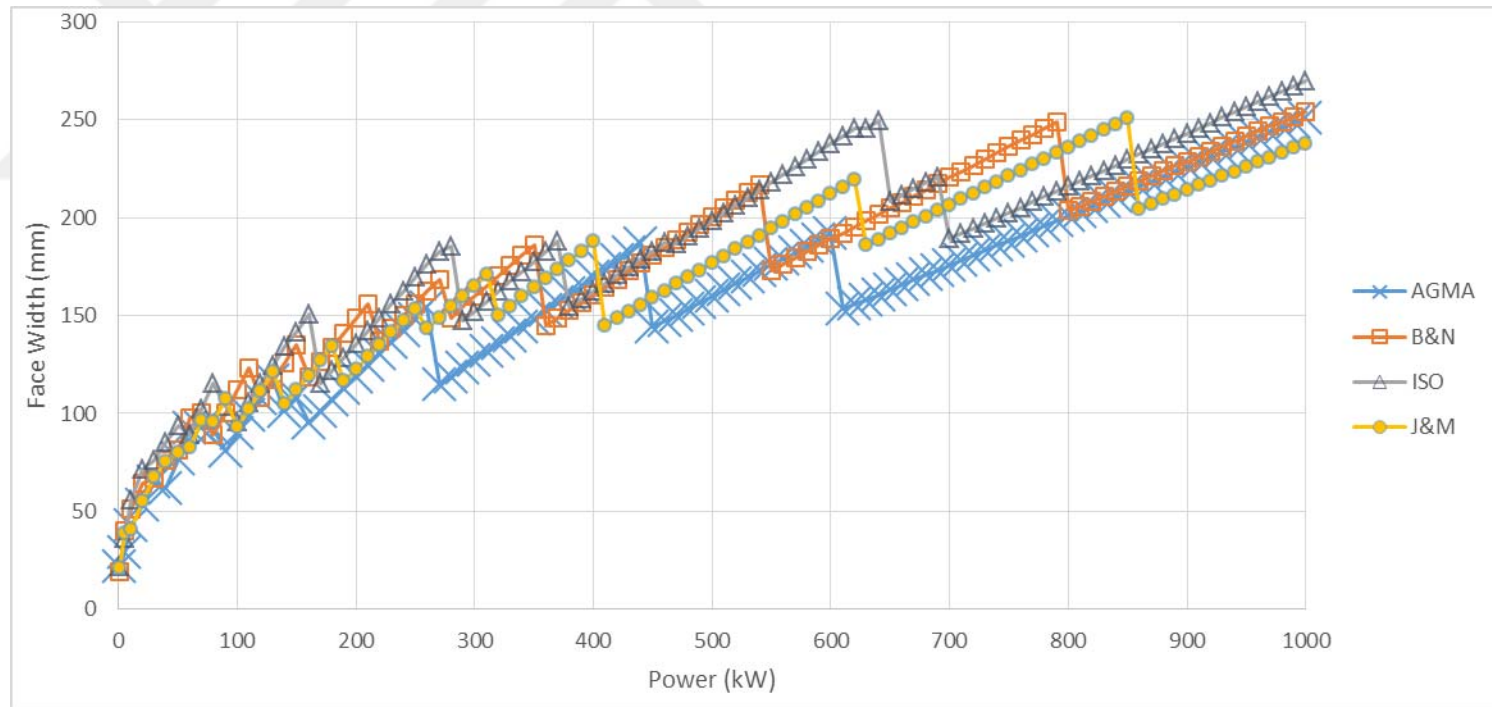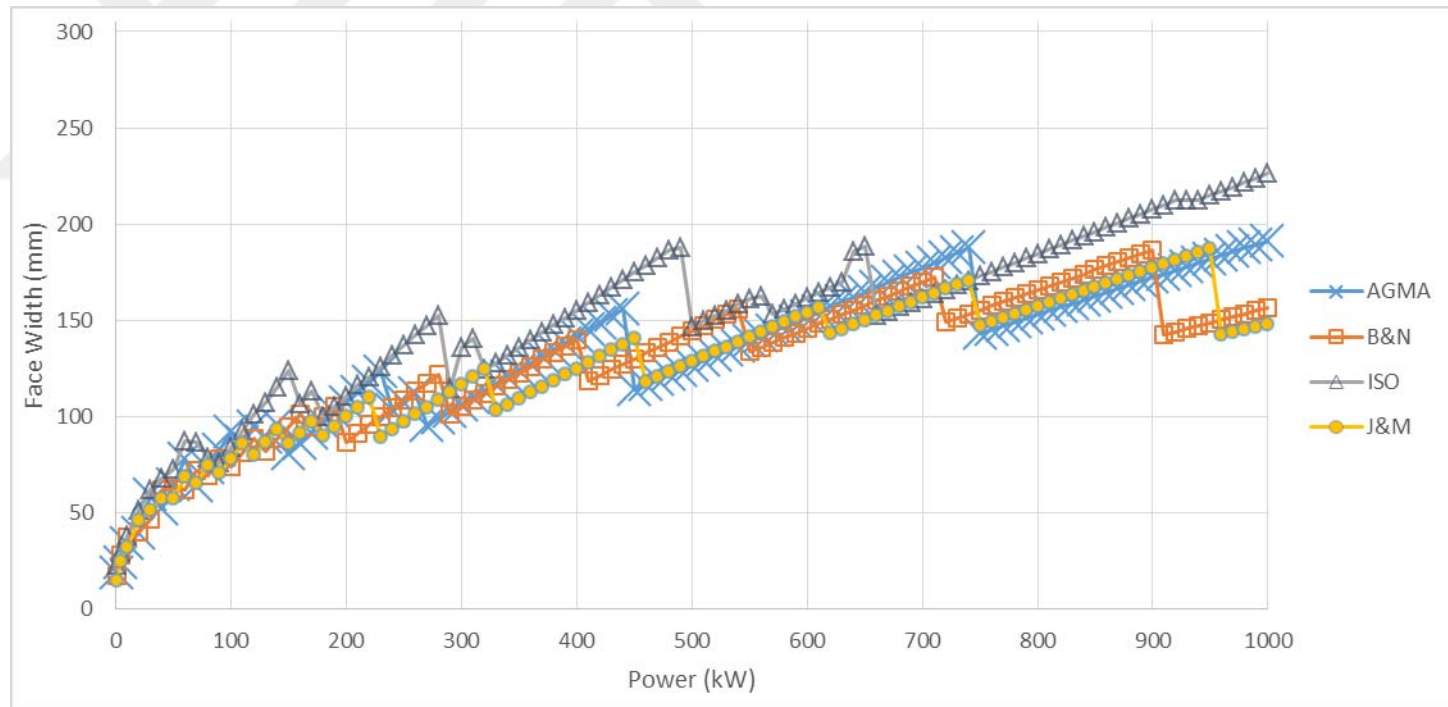
Figure D. 4. Face width variation considering bending fatigue failure under increasing power at 2:1 speed ratio (Ø=25°, Type1)
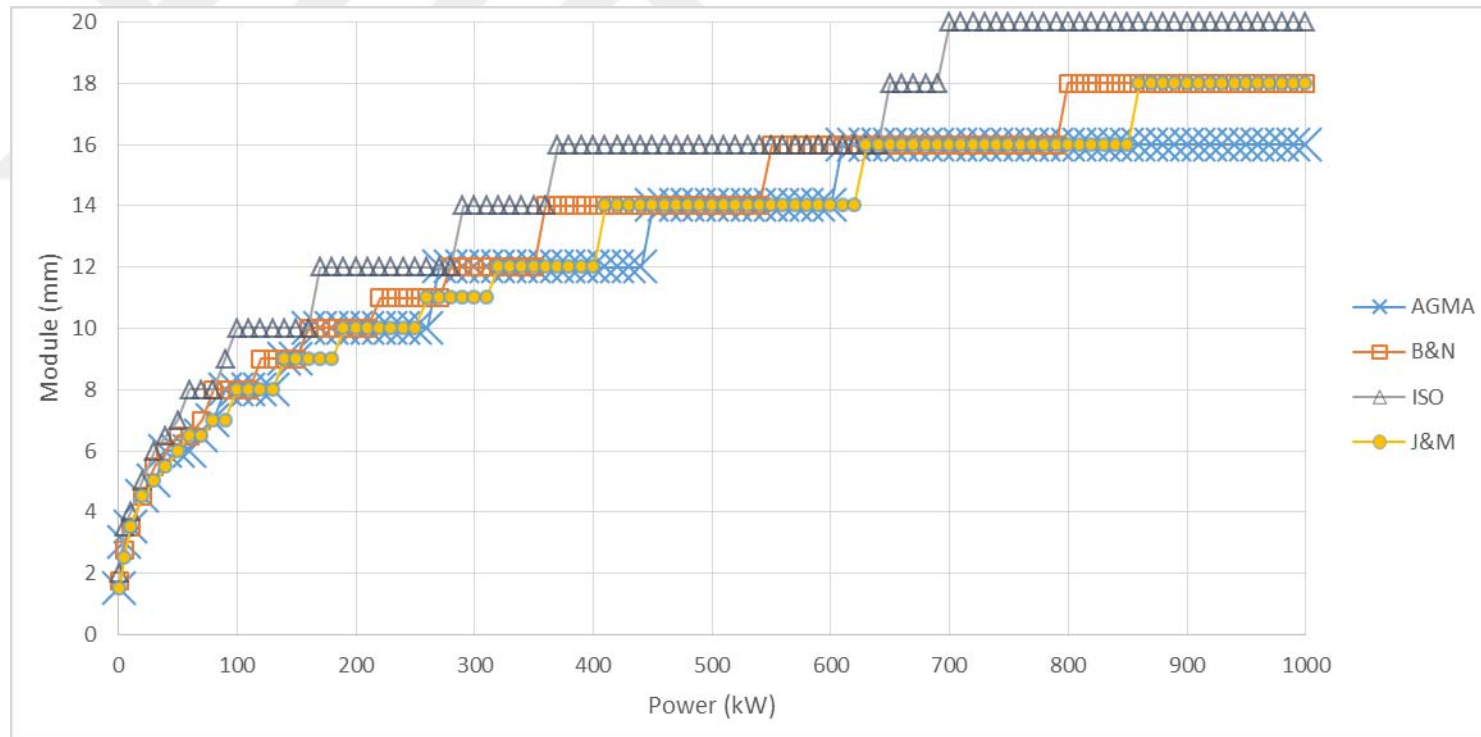
Figure D. 5. Module variation considering bending fatigue failure under increasing power at 3:1 speed ratio (Ø=25°, Type 1)
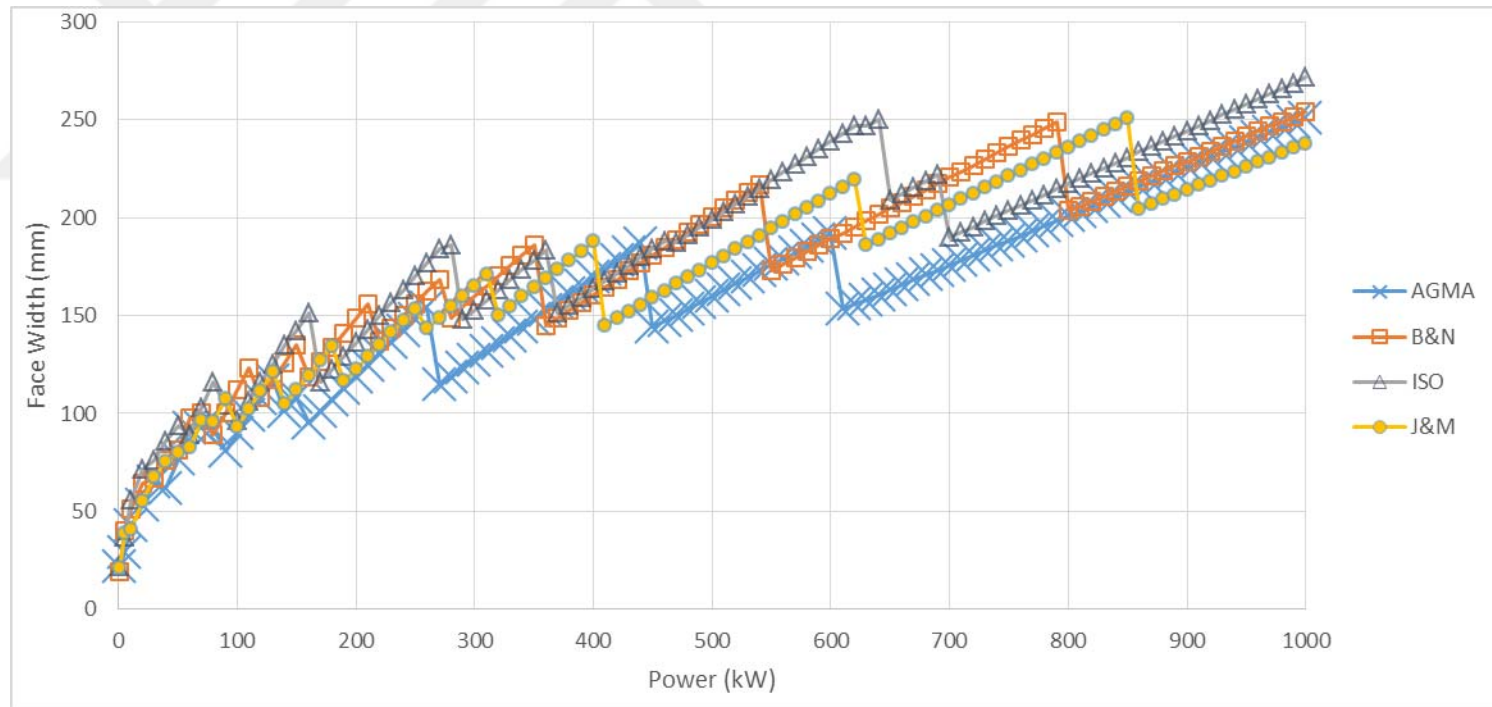
Figure D. 6. Face width variation considering bending fatigue failure under increasing power at 3:1 speed ratio (Ø=25°, Type1)

Figure D. 7. Module variation considering bending fatigue failure under increasing power at 4:1 speed ratio (Ø=25°, Type 1)

Figure D. 8. Face width variation considering bending fatigue failure under increasing power at 4:1 speed ratio (Ø=25°, Type1)

Figure D. 9. Module variation considering bending fatigue failure under increasing power at 5:1 speed ratio (Ø=25°, Type 1)

Figure D. 10. Face width variation considering bending fatigue failure under increasing power at 5:1 speed ratio (Ø=25º, Type1)
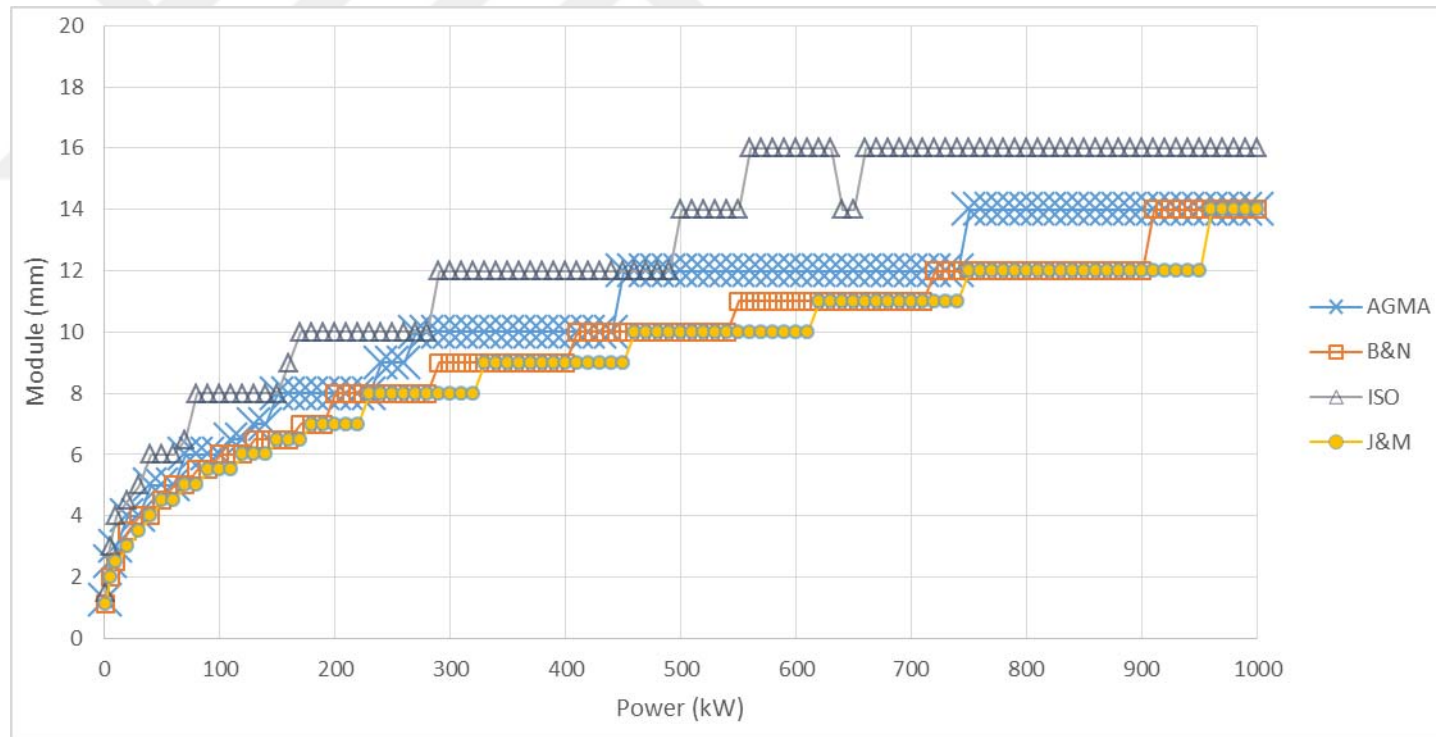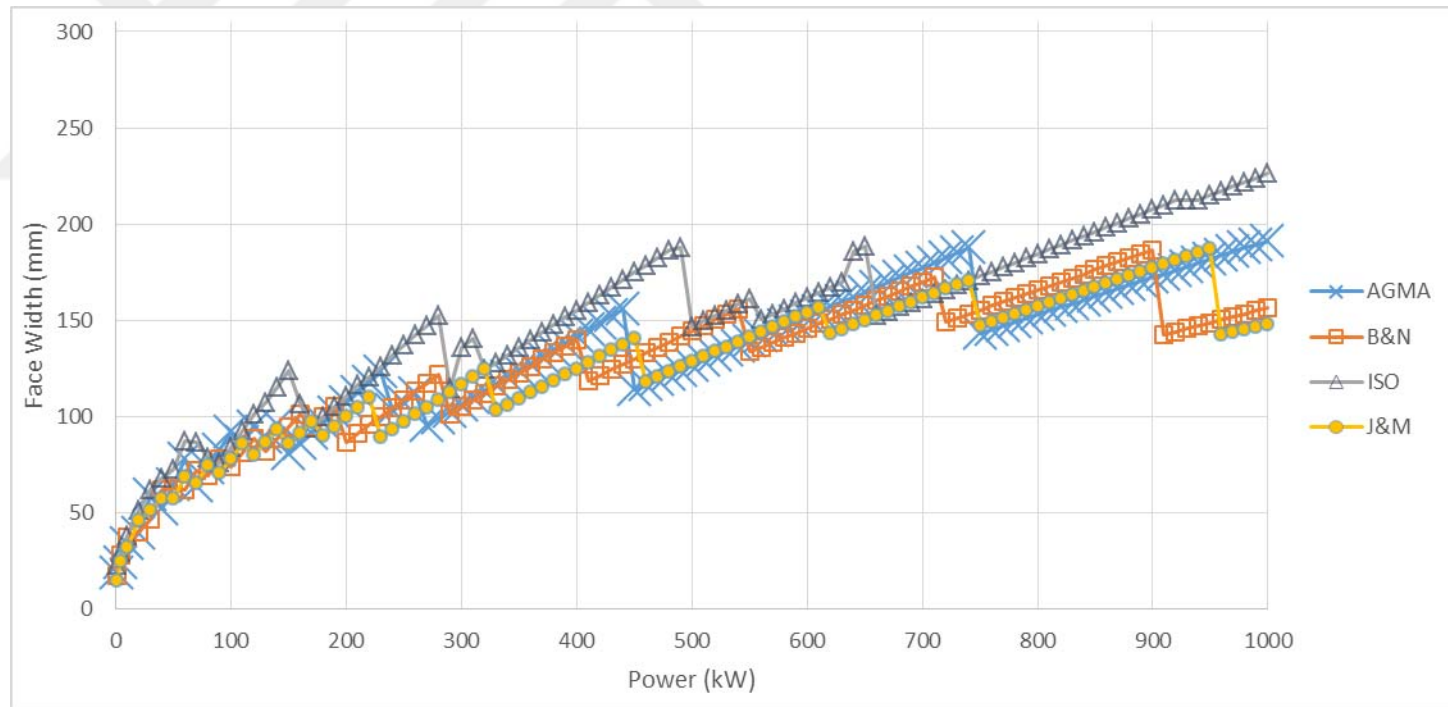
Figure D. 11. Module variation considering bending fatigue failure under increasing power at 6:1 speed ratio (Ø=25°, Type 1)

Figure D. 12. Face width variation considering bending fatigue failure under increasing power at 6:1 speed ratio (Ø=25°, Type1)

Figure D. 13. Module variation considering bending fatigue failure under increasing power at 7:1 speed ratio (Ø=25°, Type 1)

Figure D. 14. Face width variation considering bending fatigue failure under increasing power at 7:1 speed ratio (Ø=25º, Type1)

Figure D. 15. Module variation considering bending fatigue failure under increasing power at 8:1 speed ratio (Ø=25°, Type 1)

Figure D. 16. Face width variation considering bending fatigue failure under increasing power at 8:1 speed ratio (Ø=25º, Type1)

D.2. Comparison of the Results Based on Bending Fatigue Failure Considering Speed Ratio for the Selected Power Transmissions for Ø=25°, Material type 1

Figure D. 17. The effect of speed ratio on module selection based on bending fatigue failure at 1 kW power transmission (Ø=25°, Type 1)

Figure D. 18. The effect of speed ratio on module selection based on bending fatigue failure at 10 kW power transmission (Ø=25°, Type 1)
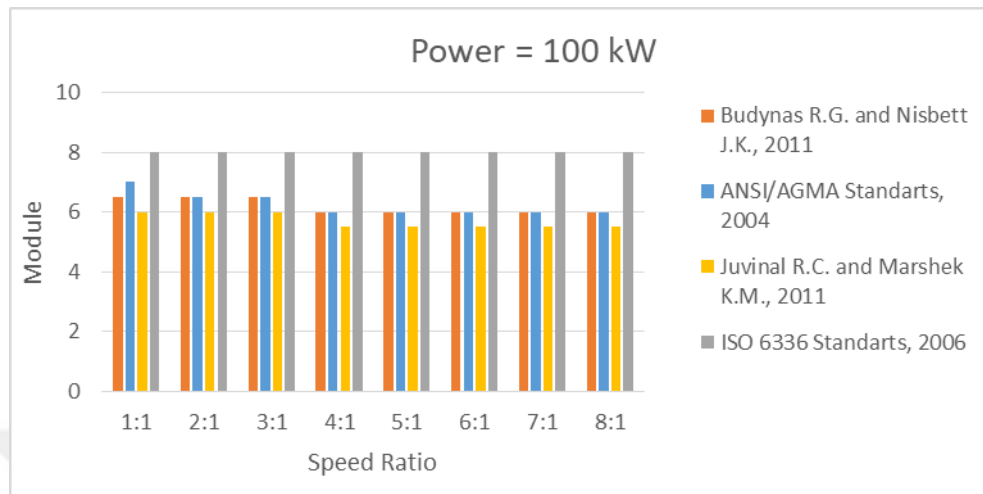
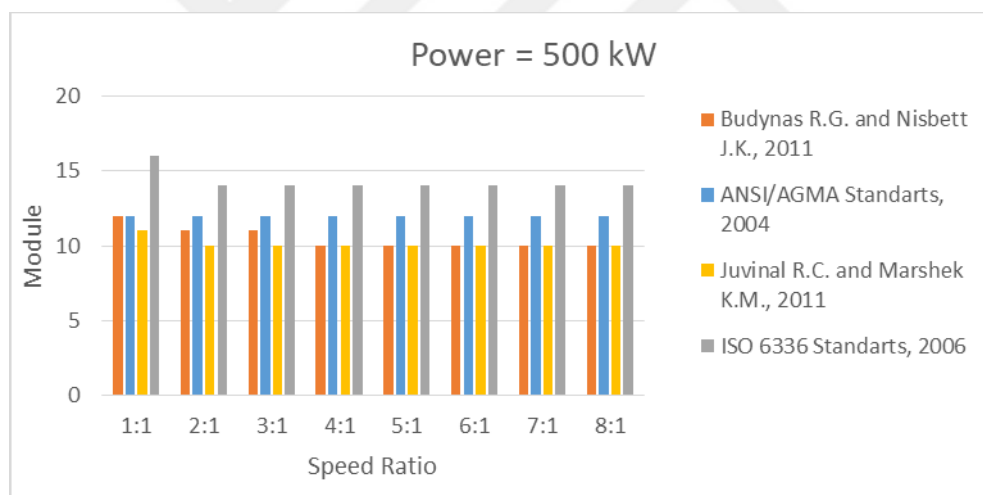Figure D. 19. The effect of speed ratio on module selection based on bending fatigue failure at 100 kW power transmission (Ø=25°, Type 1)

Figure D. 20. The effect of speed ratio on module selection based on bending fatigue failure at 500 kW power transmission (Ø=25°, Type 1)
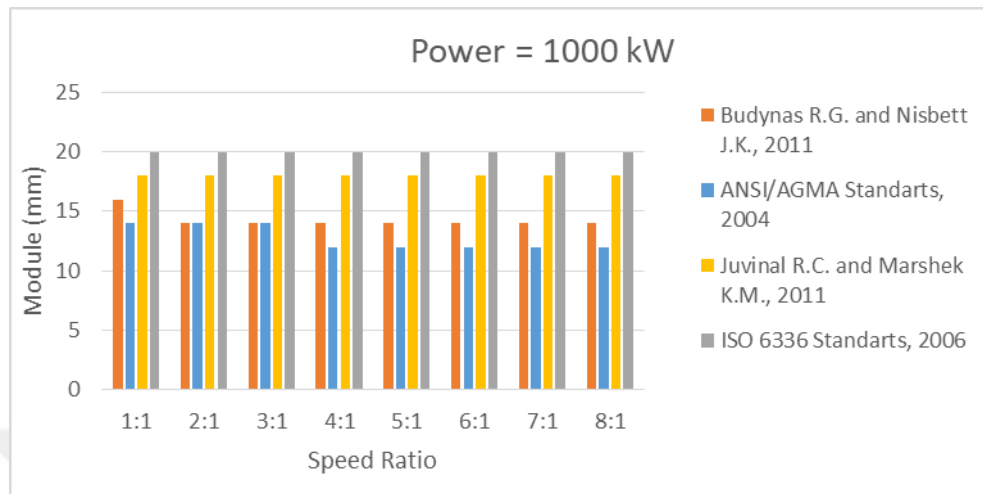
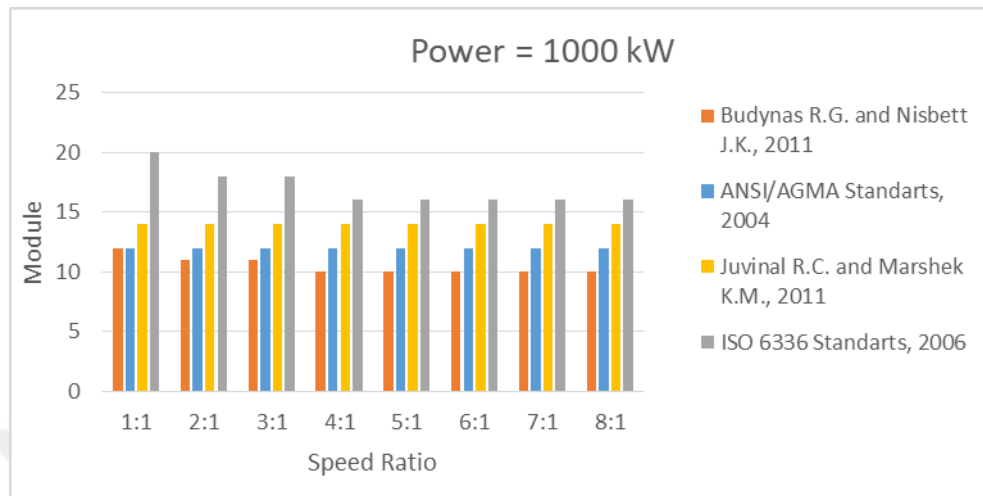Figure D. 21. The effect of speed ratio on module selection based on bending fatigue failure at 1000 kW power transmission (Ø=25°, Type 1)

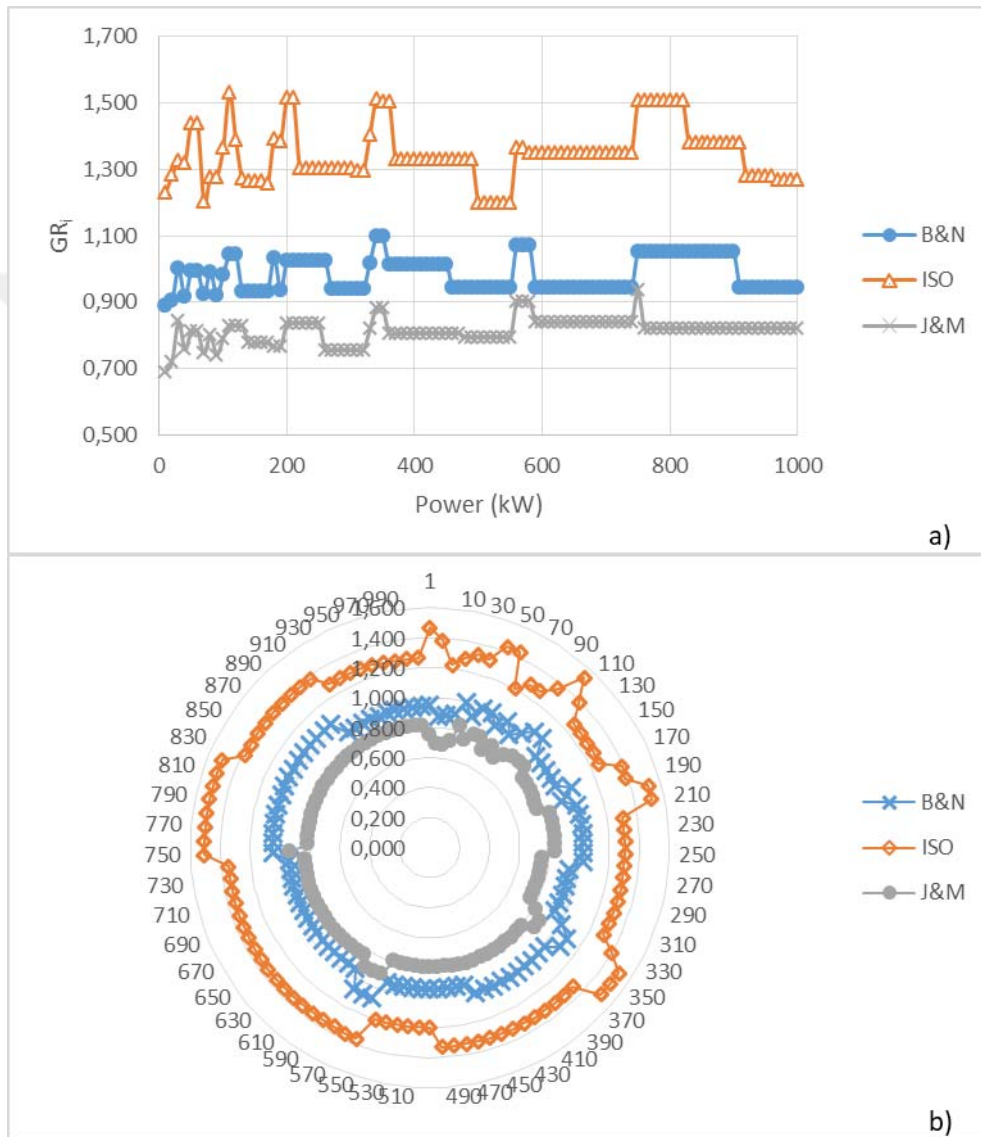## D.3. Obtaining Geometric Rating Number (GR$_i$) for Design Approaches for Ø=25°, Material type 1

Figure D. 22. Comparison of GR$_i$ results obtained from the design approaches at 1:1 speed ratio (Ø=25°, Type 1), a) scatter chart, b) radar chart
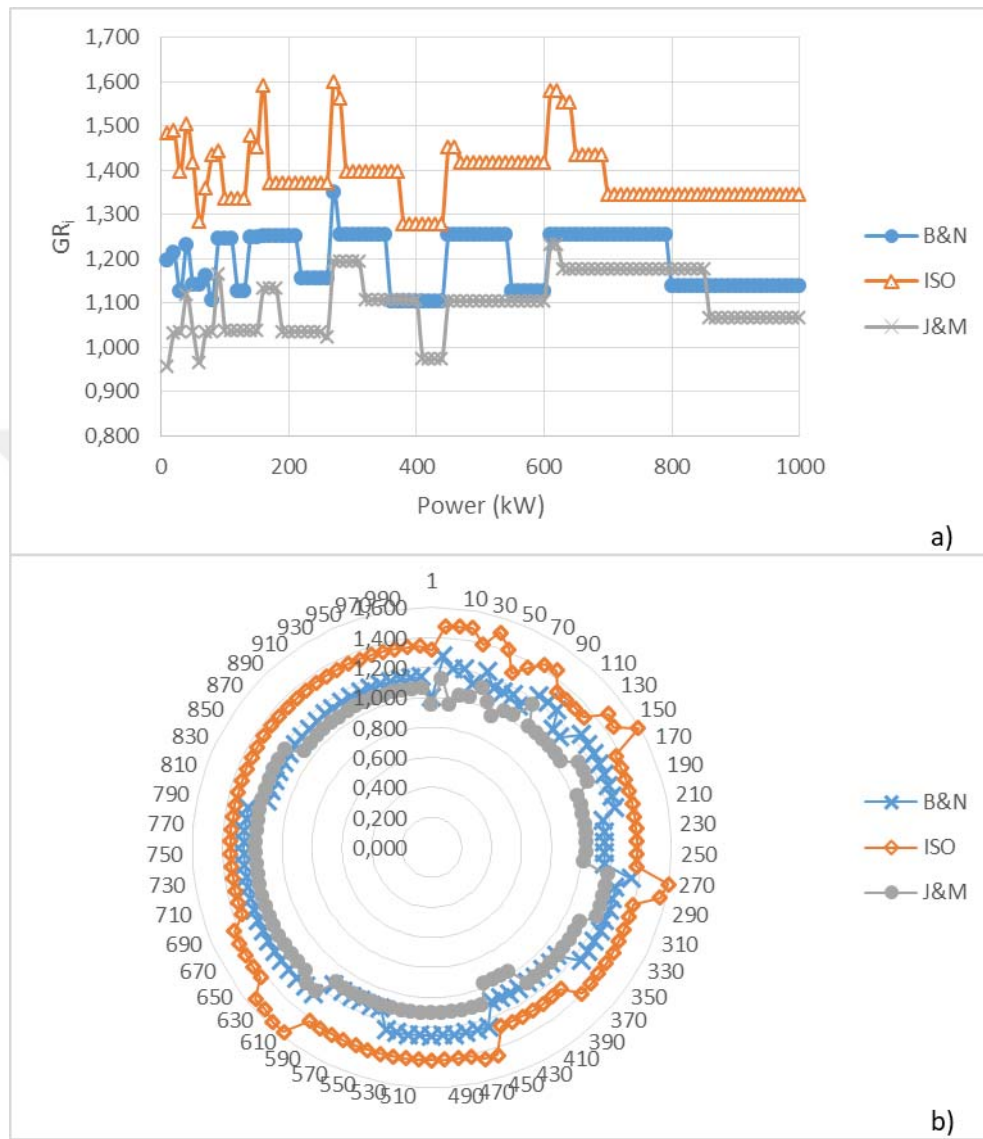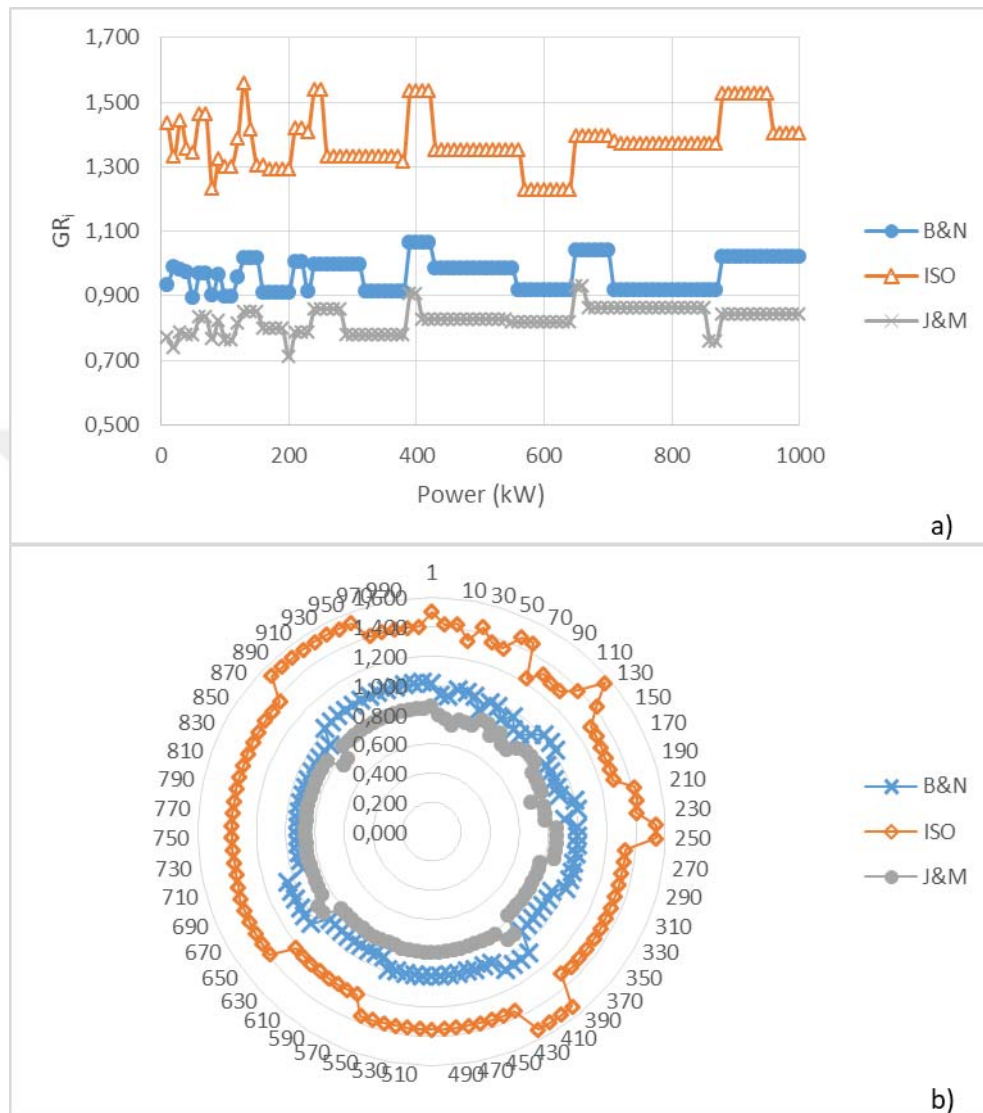
Figure D. 23. Comparison of GR_i results obtained from the design approaches at 2:1 speed ratio (Ø=25°, Type 1), a) scatter chart, b) radar chart
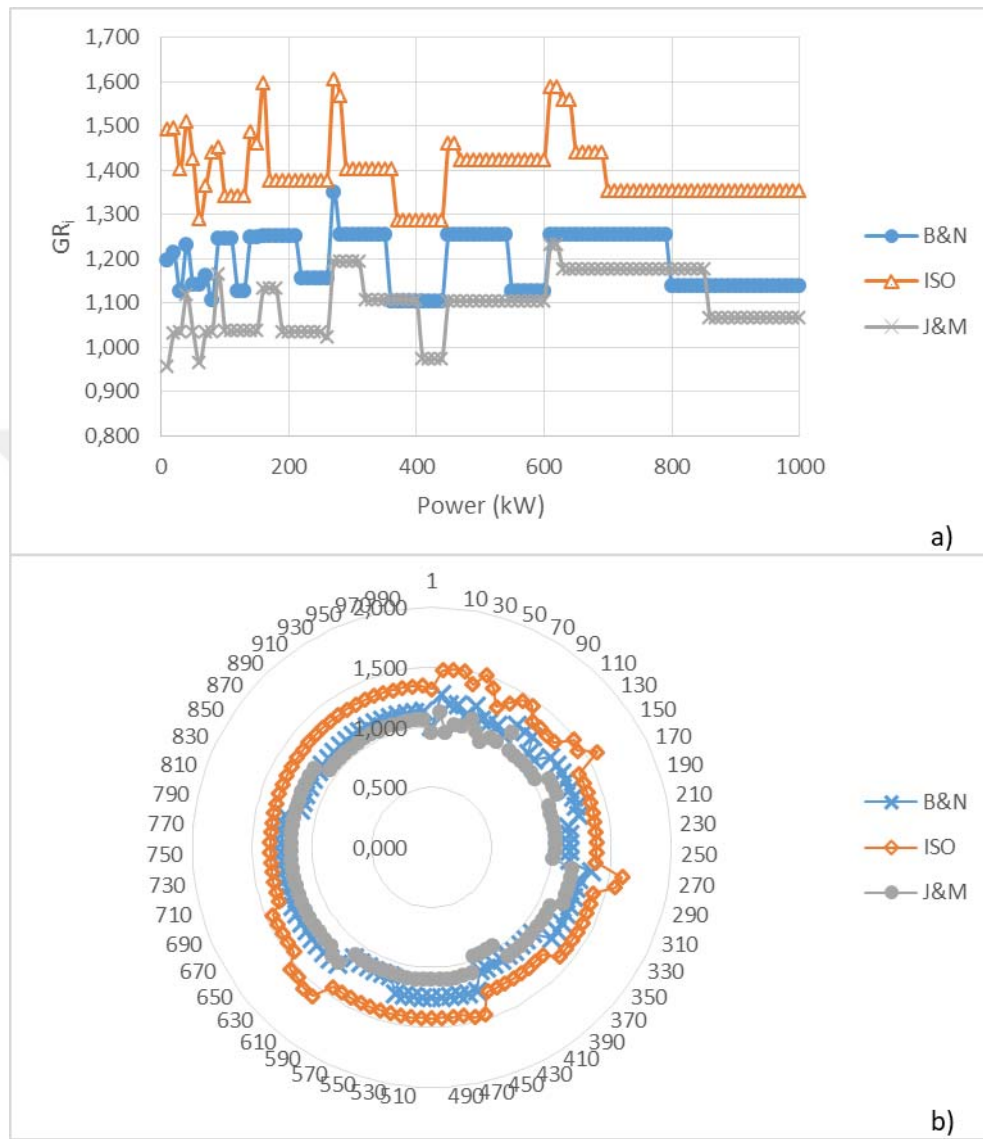
Figure D. 24. Comparison of GR_i results obtained from the design approaches at 3:1 speed ratio ($\varnothing=25^{o}$, Type 1), a) scatter chart, b) radar chart
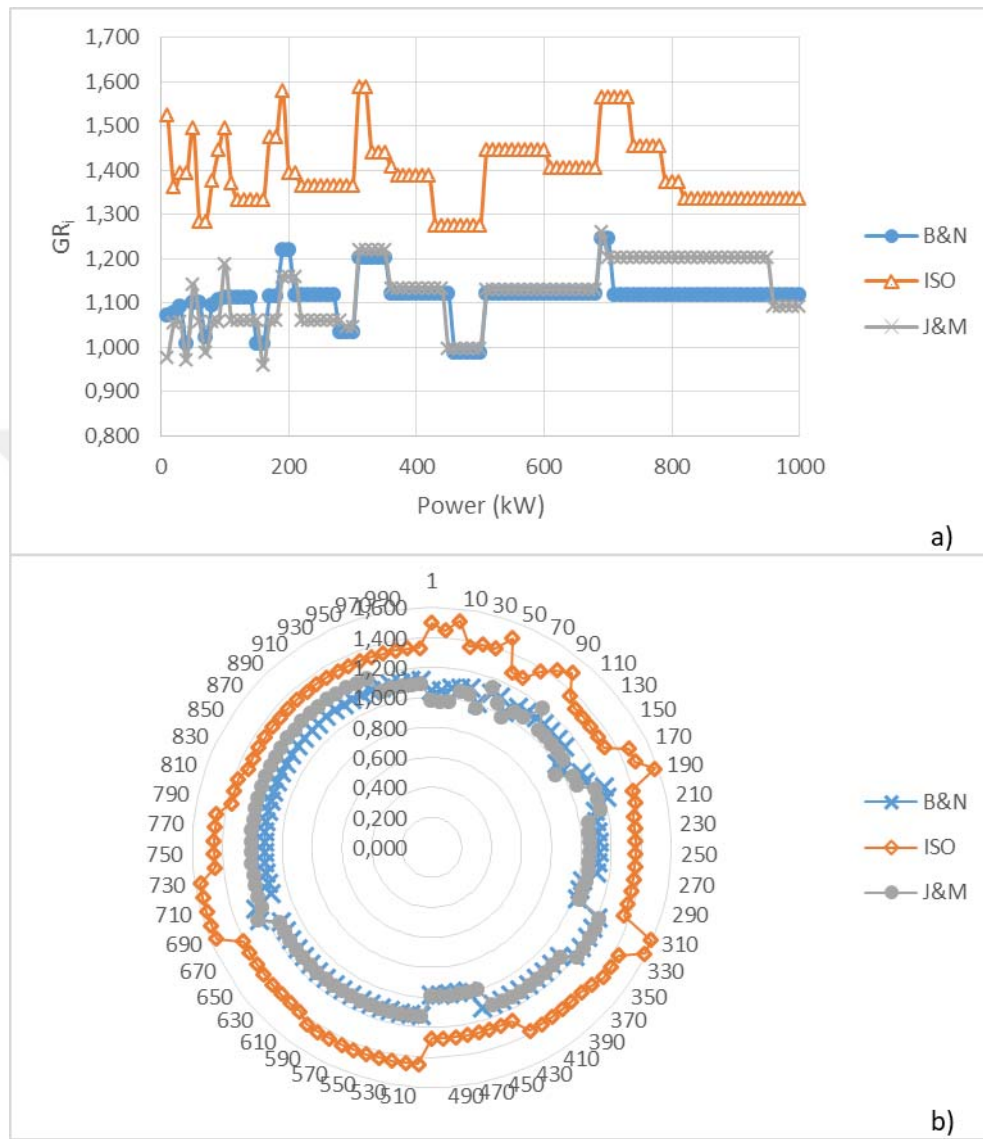
Figure D. 25. Comparison of GR_i results obtained from the design approaches at 4:1 speed ratio ($\varnothing$=25°, Type 1), a) scatter chart, b) radar chart
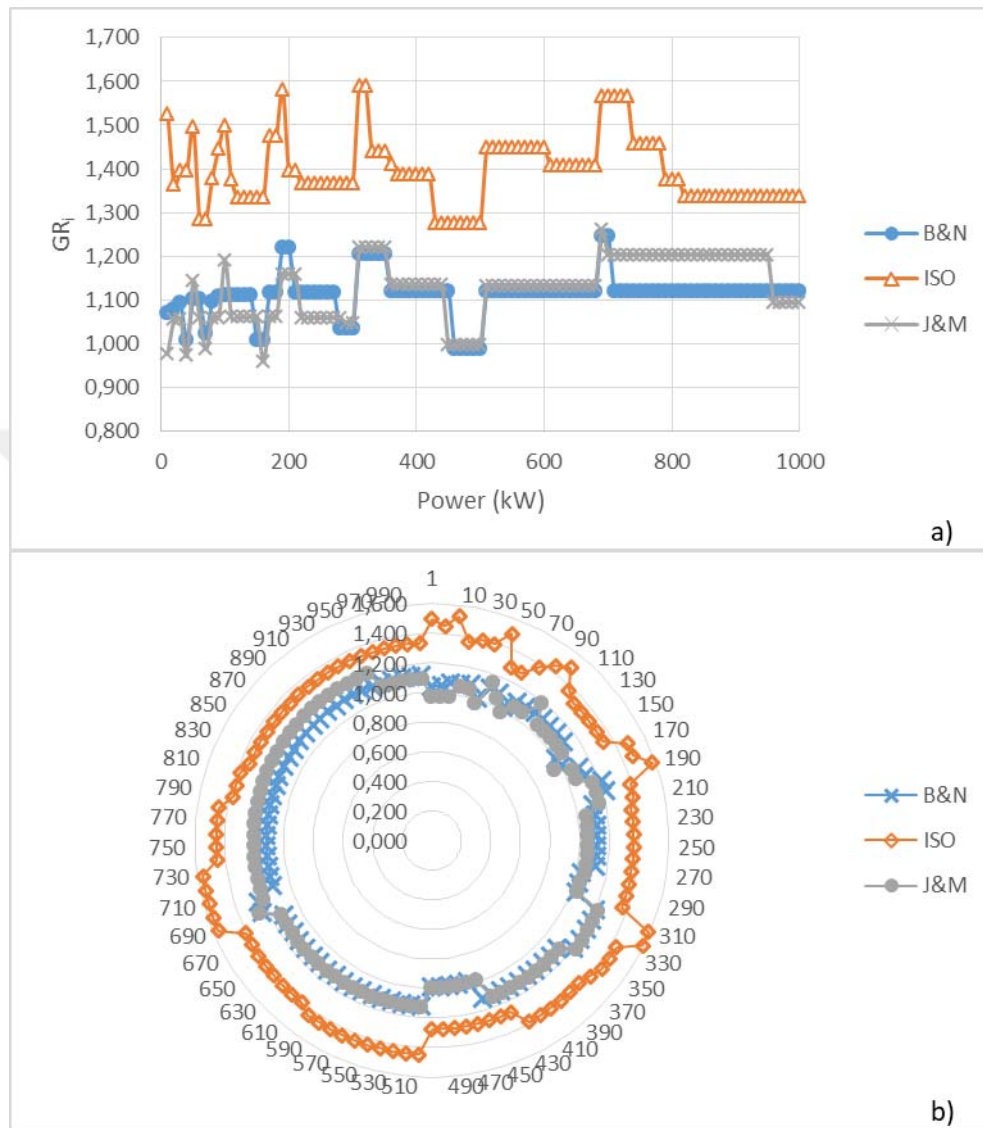
Figure D. 26. Comparison of GR_i results obtained from the design approaches at 5:1 speed ratio ($\varnothing=25^\circ$, Type 1), a) scatter chart, b) radar chart
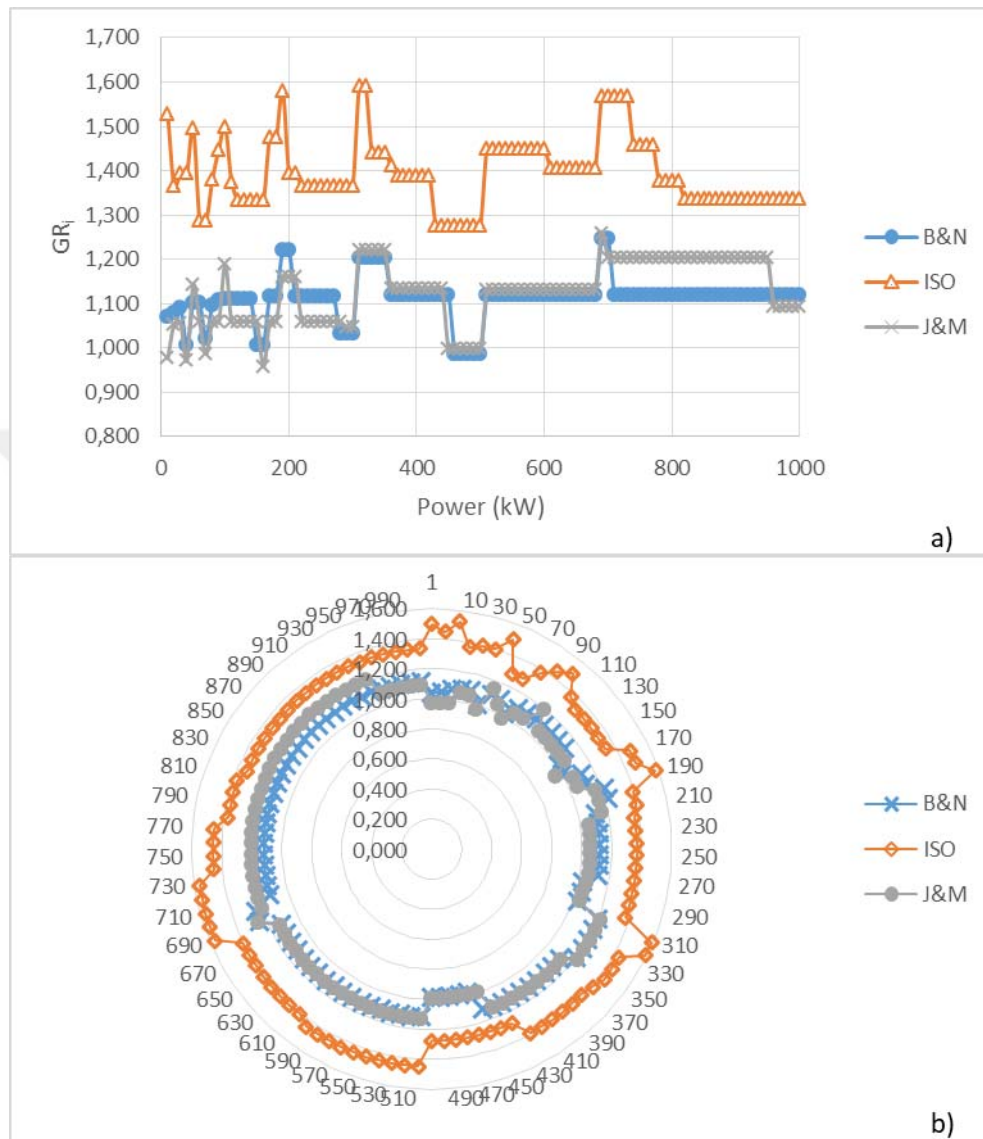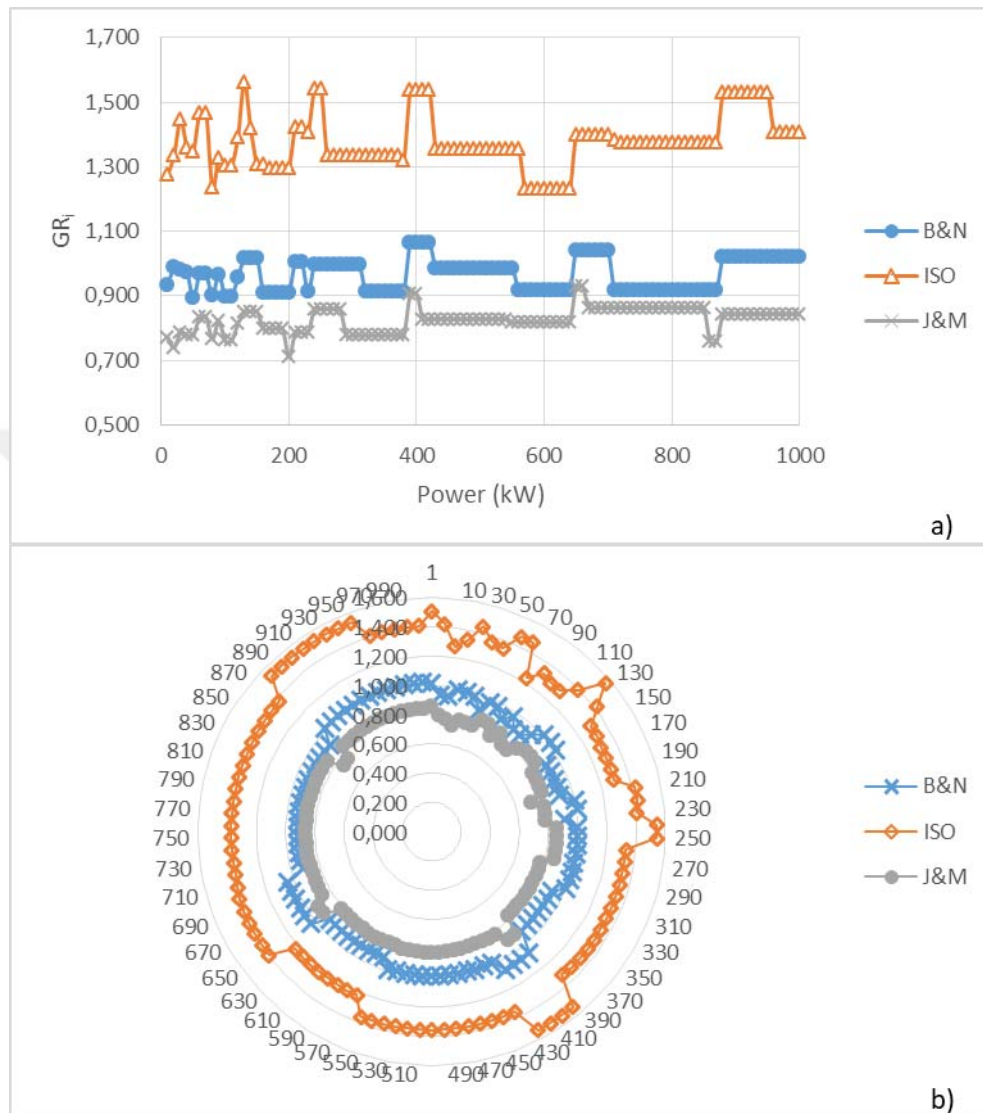
Figure D. 27. Comparison of GR_i results obtained from the design approaches at 6:1 speed ratio ($\varnothing=25^{\circ}$, Type 1), a) scatter chart, b) radar chart
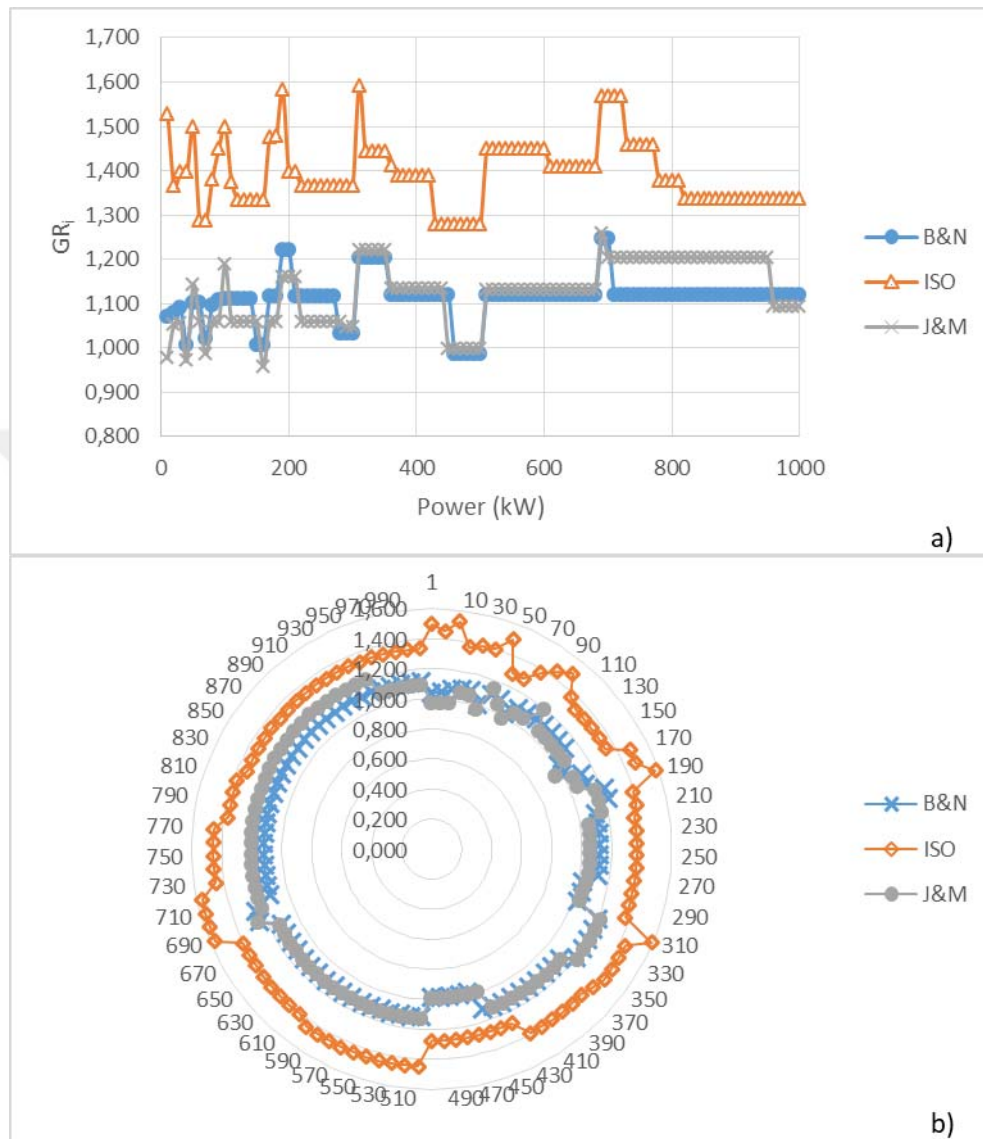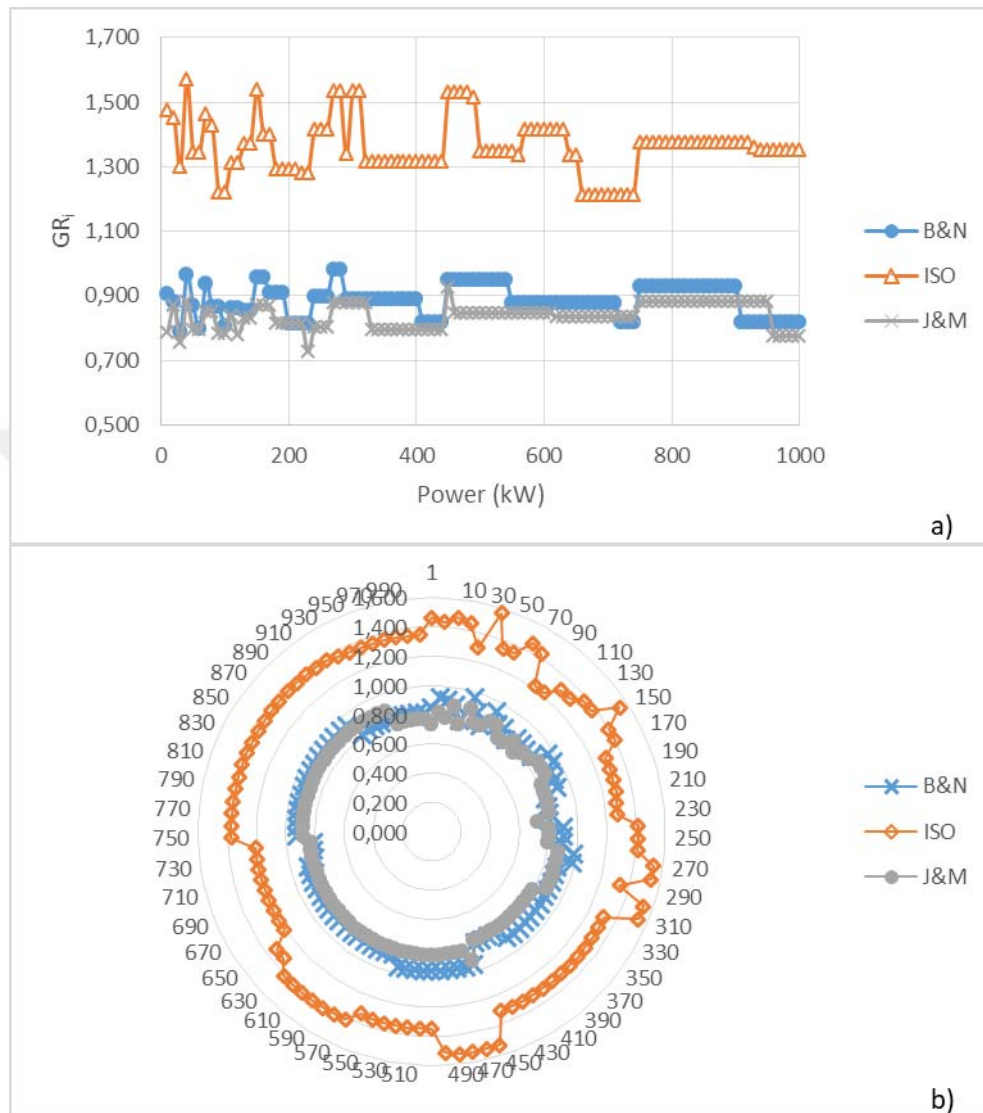
Figure D. 28. Comparison of GR_i results obtained from the design approaches at 7:1 speed ratio ($\varnothing$=25°, Type 1), a) scatter chart, b) radar chart
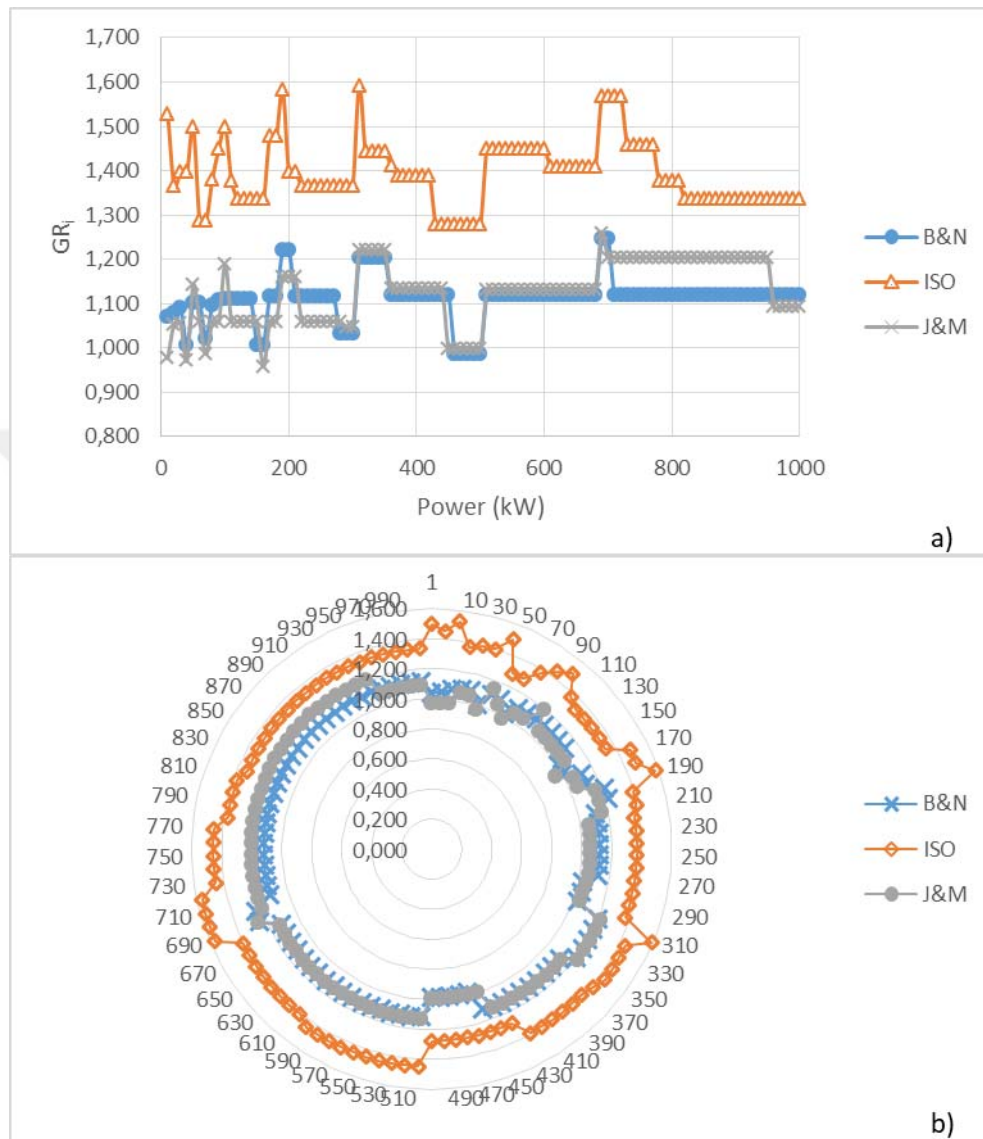
Figure D. 29. Comparison of GR_i results obtained from the design approaches at 8:1 speed ratio (Ø=25°, Type 1), a) scatter chart, b) radar chart

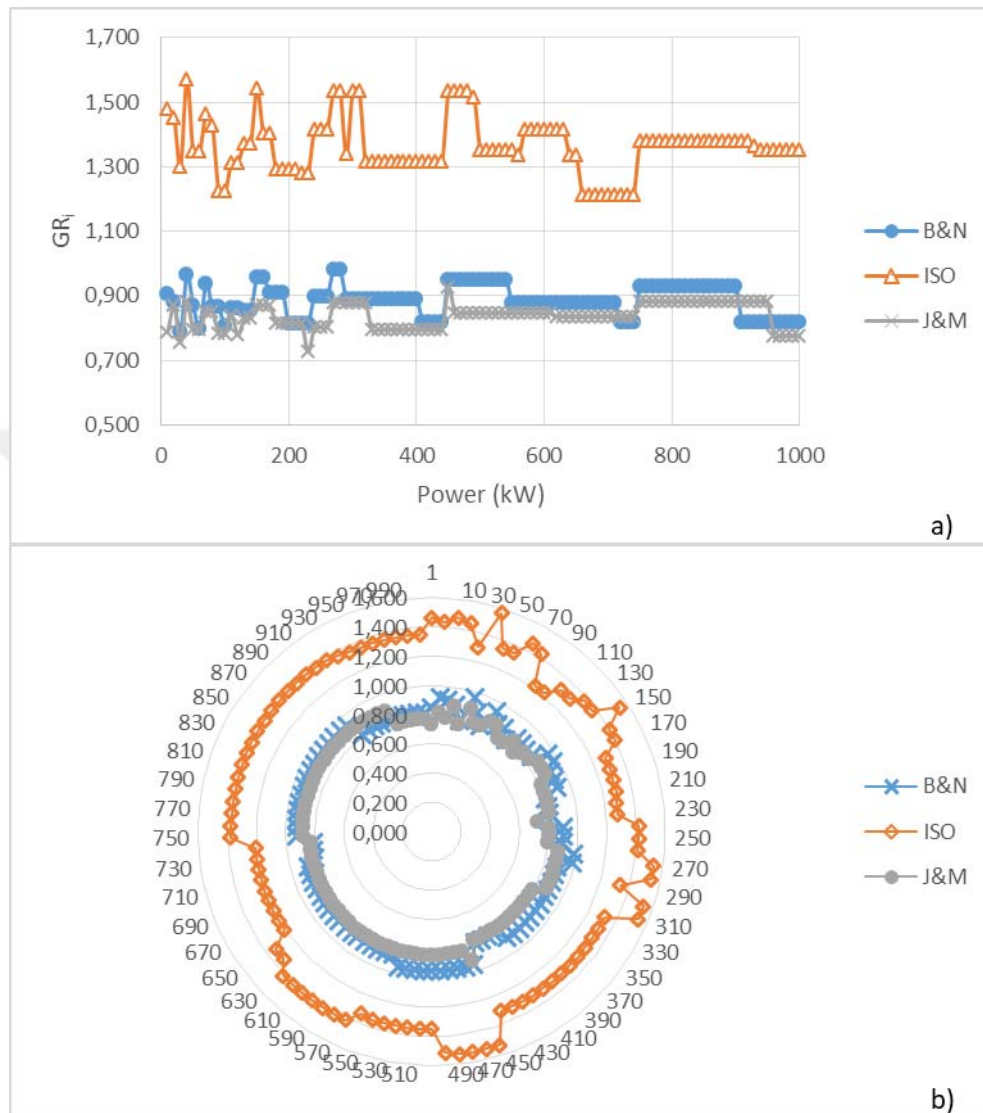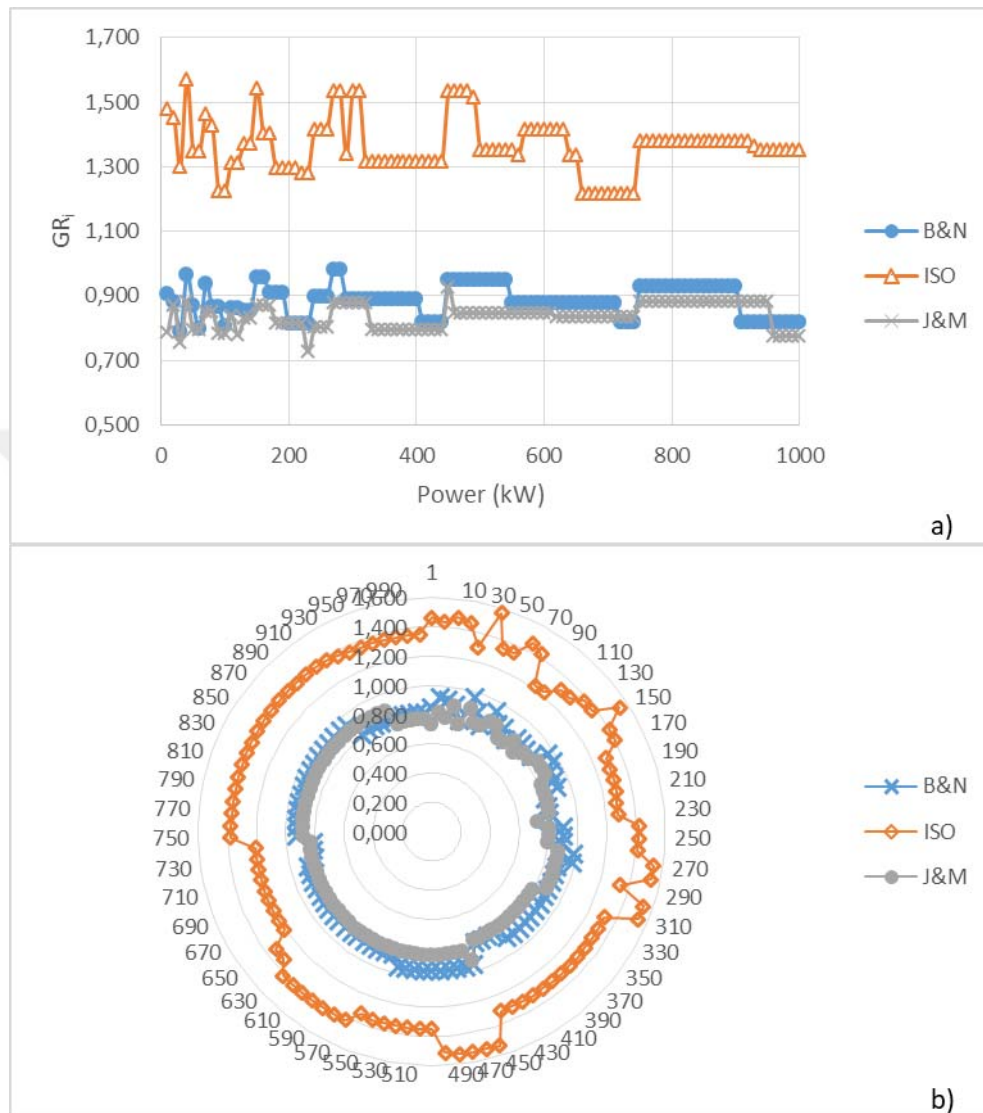## E.1. Comparison of Module Selection and Face Width Results of the Design Approaches for Ø=25°, Material type 2

Figure E. 1. Module variation considering bending fatigue failure under increasing power at 1:1 speed ratio (Ø=25°, Type 2)

Figure E.2.Face width variation considering bending fatigue failure under increasing power at 1:1 speed ratio (Ø=25°, Type 2)
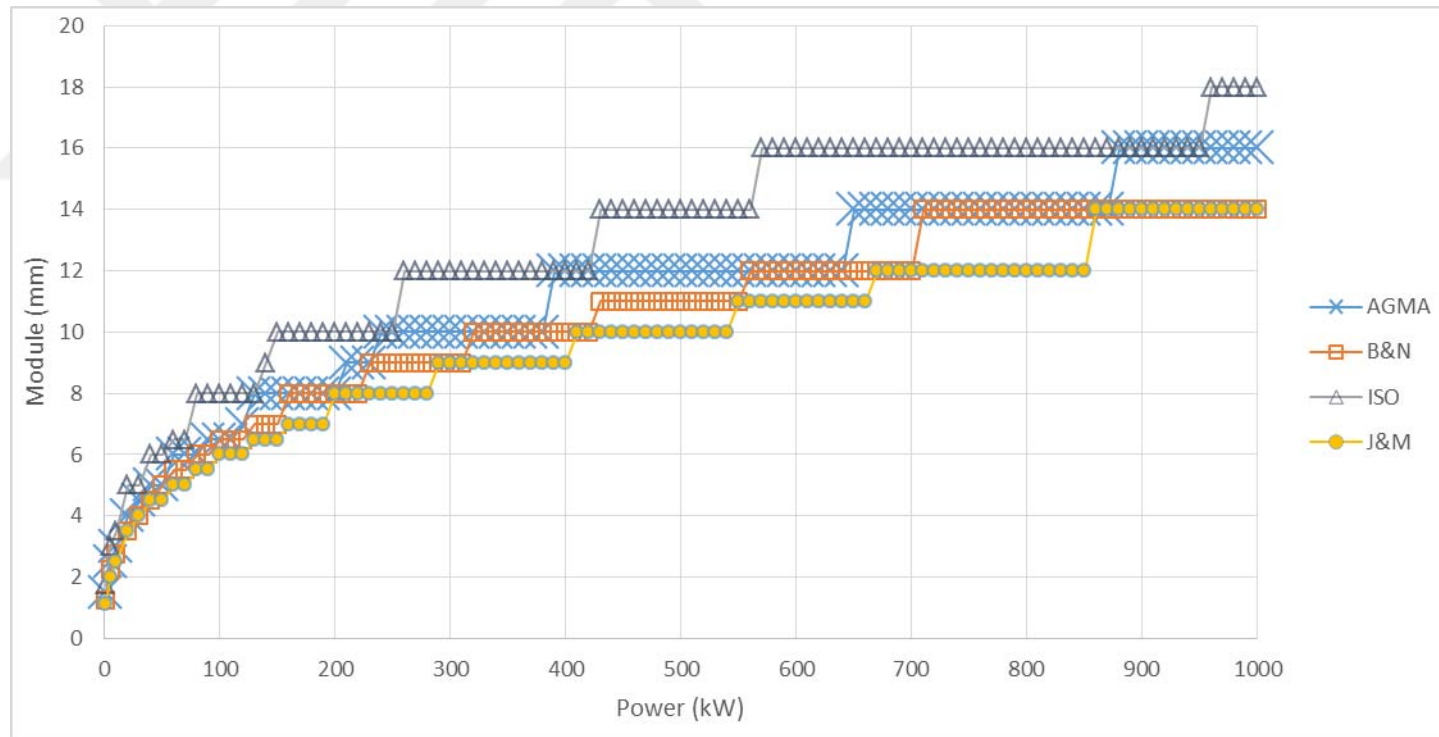
Figure E. 3. Module variation considering bending fatigue failure under increasing power at 2:1 speed ratio (Ø=25°, Type 2)
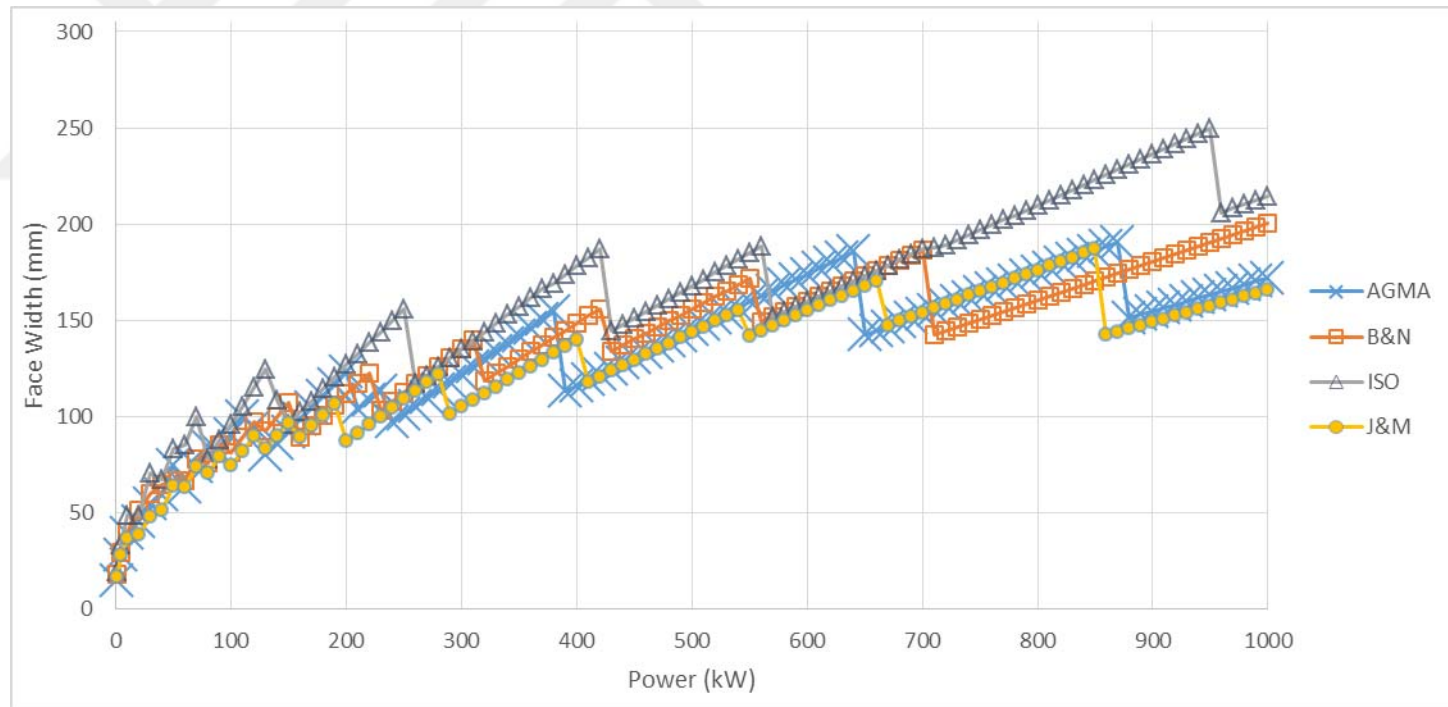
Figure E.4.Face width variation considering bending fatigue failure under increasing power at 2:1 speed ratio (Ø=25º, Type 2)
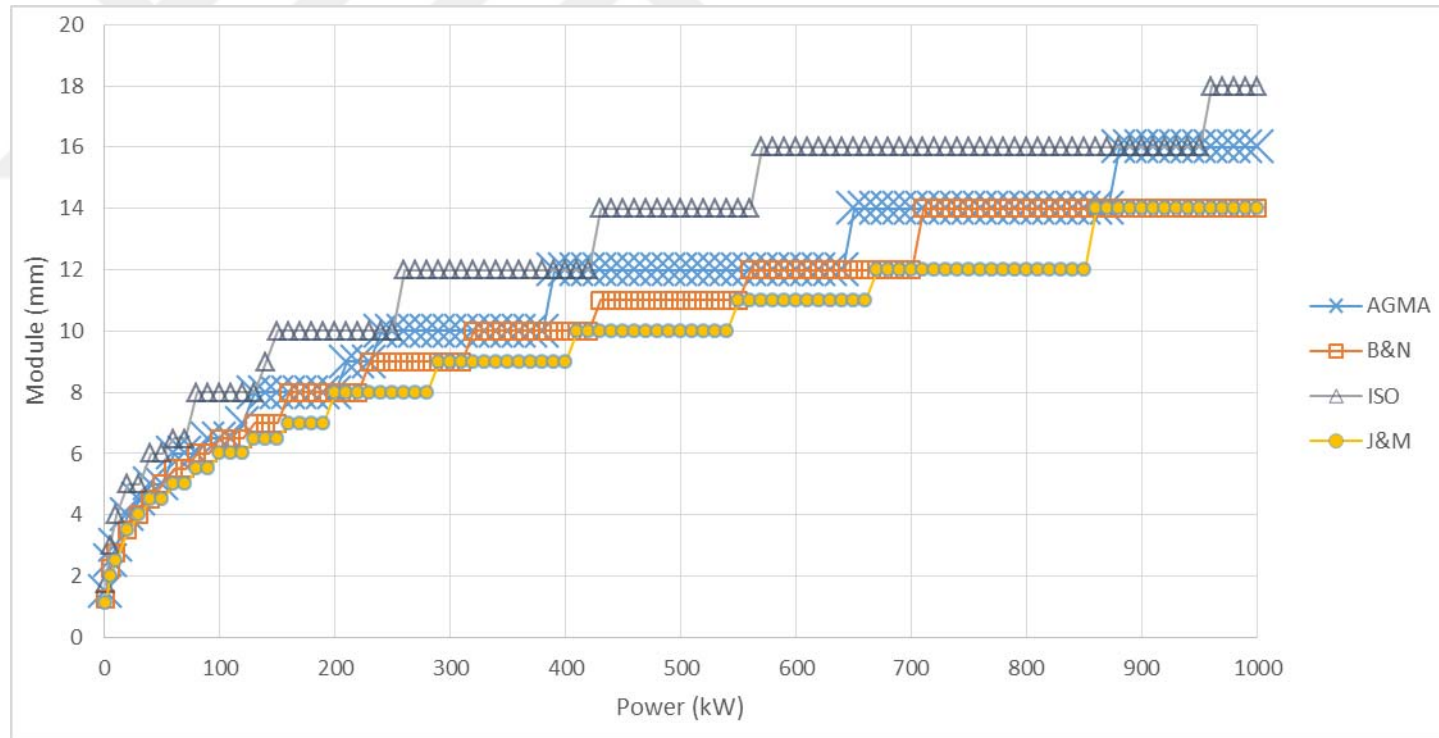
Figure E. 5. Module variation considering bending fatigue failure under increasing power at 3:1 speed ratio (Ø=25°, Type 2)
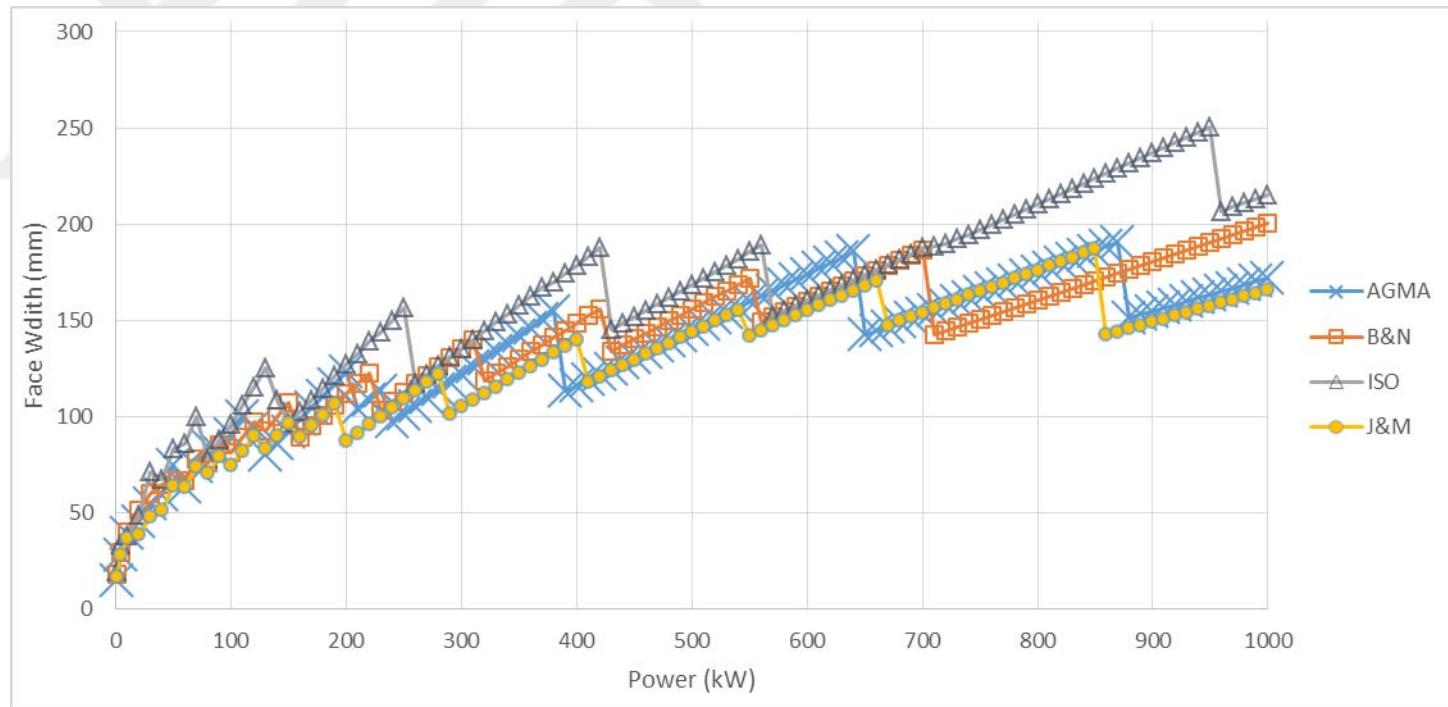
Figure E.6.Face width variation considering bending fatigue failure under increasing power at 3:1 speed ratio (Ø=25°, Type 2)
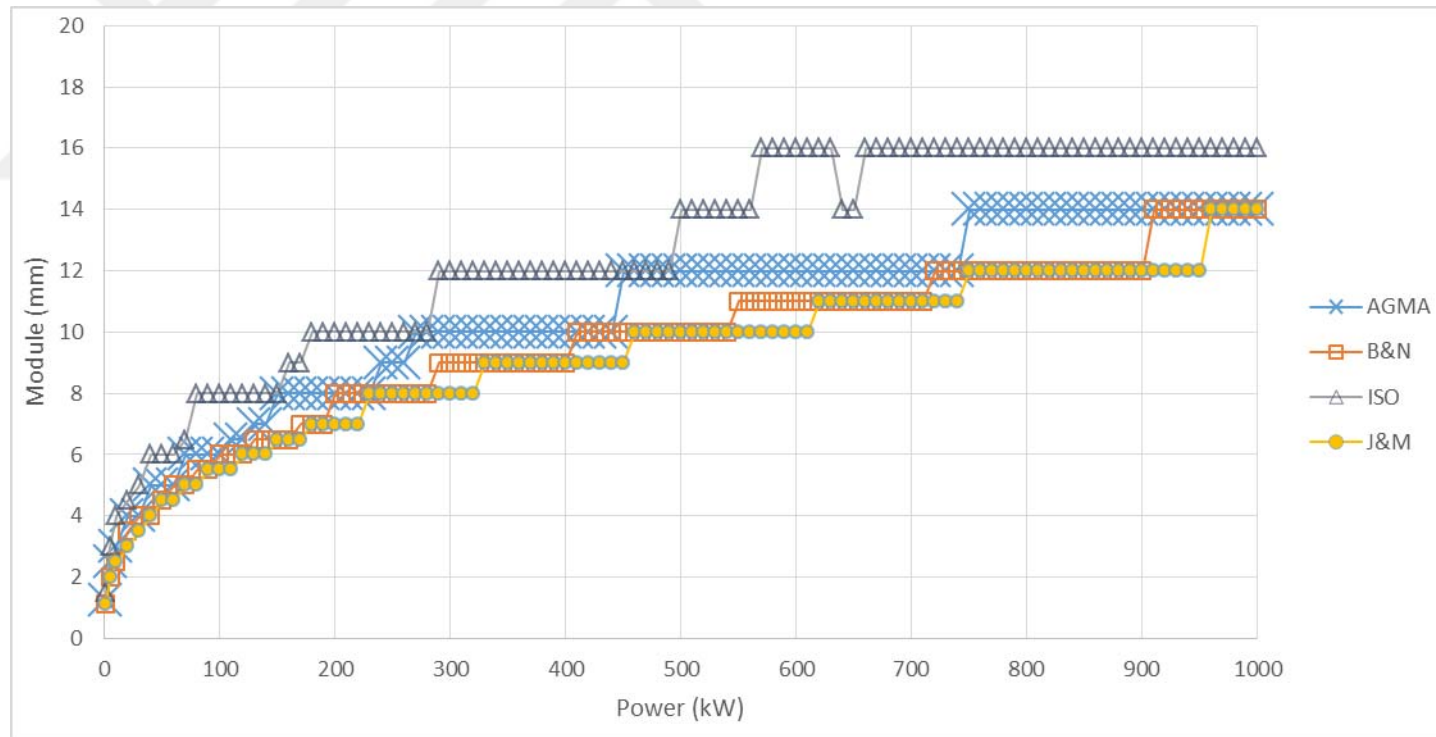
Figure E. 7. Module variation considering bending fatigue failure under increasing power at 4:1 speed ratio (Ø=25°, Type 2)
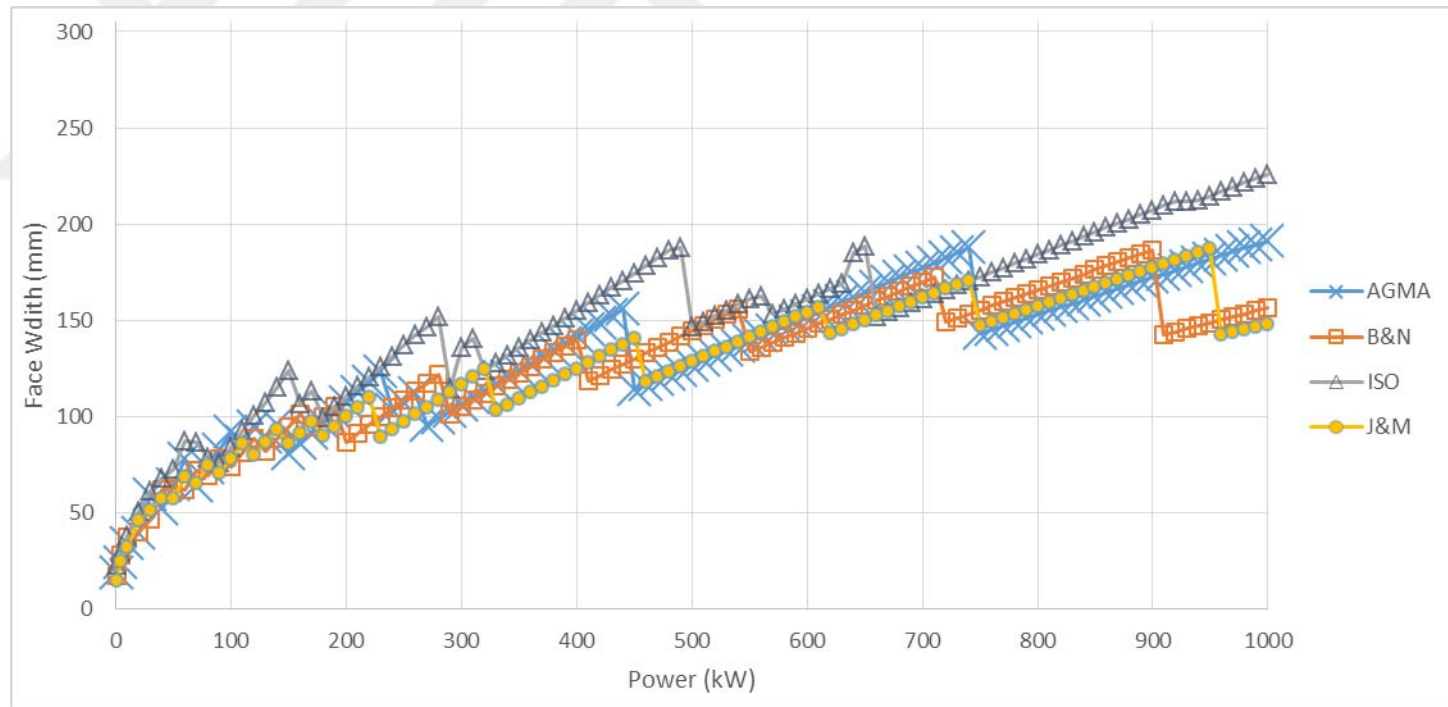
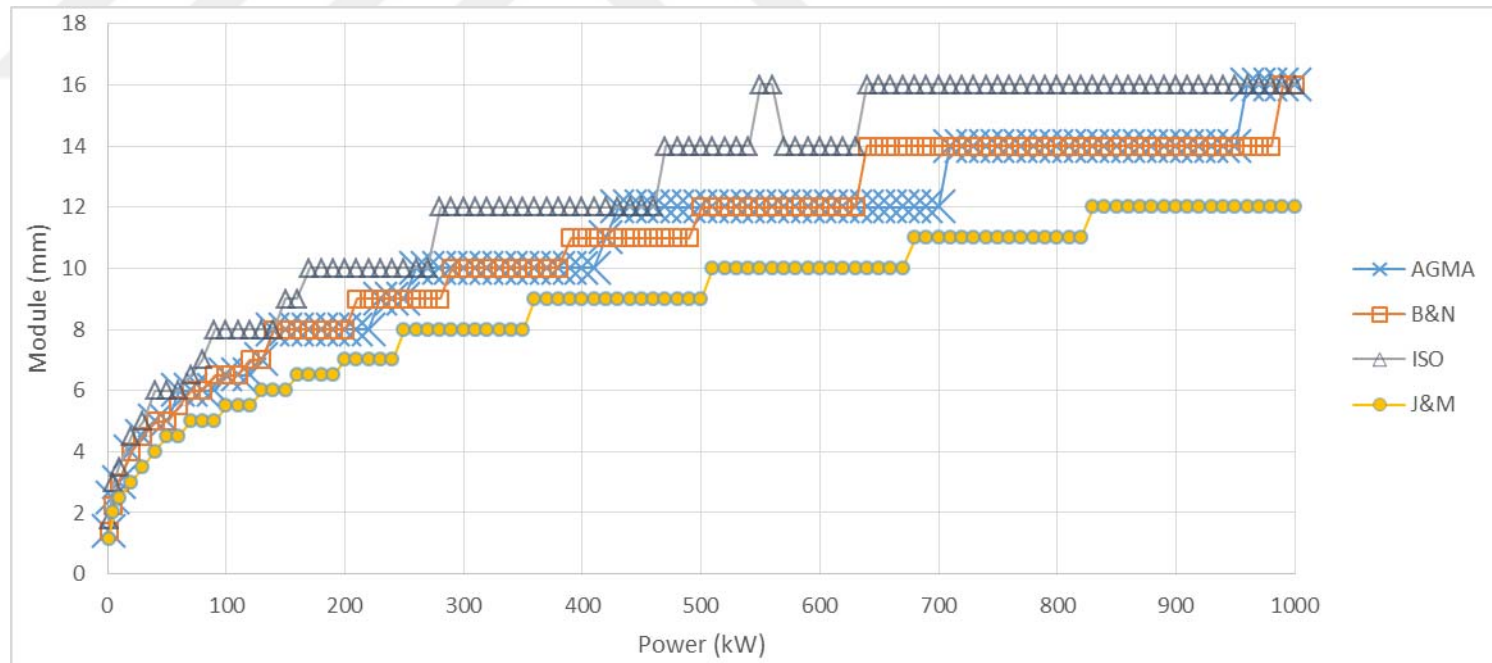Figure E.8.Face width variation considering bending fatigue failure under increasing power at 4:1 speed ratio (Ø=25º, Type 2)
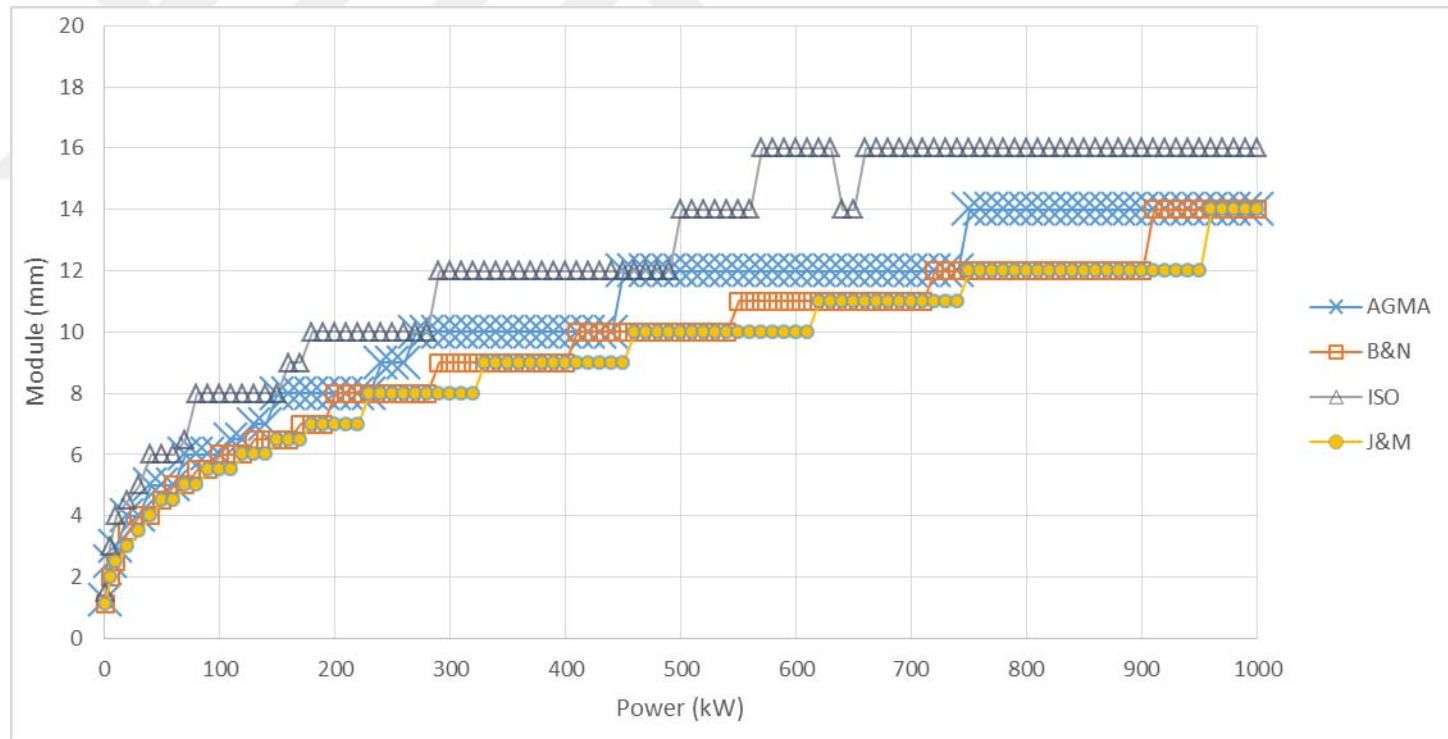
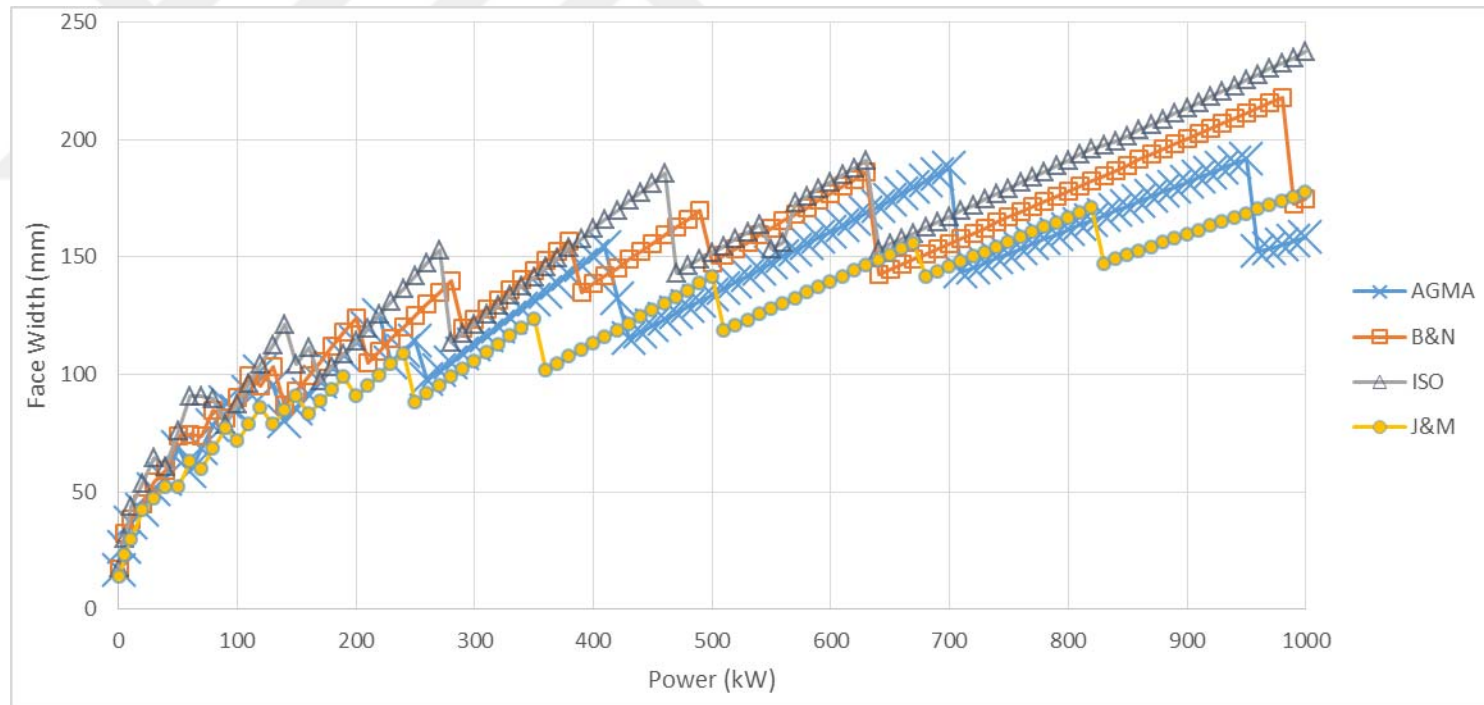Figure E.9. Module variation considering bending fatigue failure under increasing power at 5:1 speed ratio (Ø=25°, Type 2)

Figure E. 10. Face width variation considering bending fatigue failure under increasing power at 5:1 speed ratio (Ø=25°, Type2)
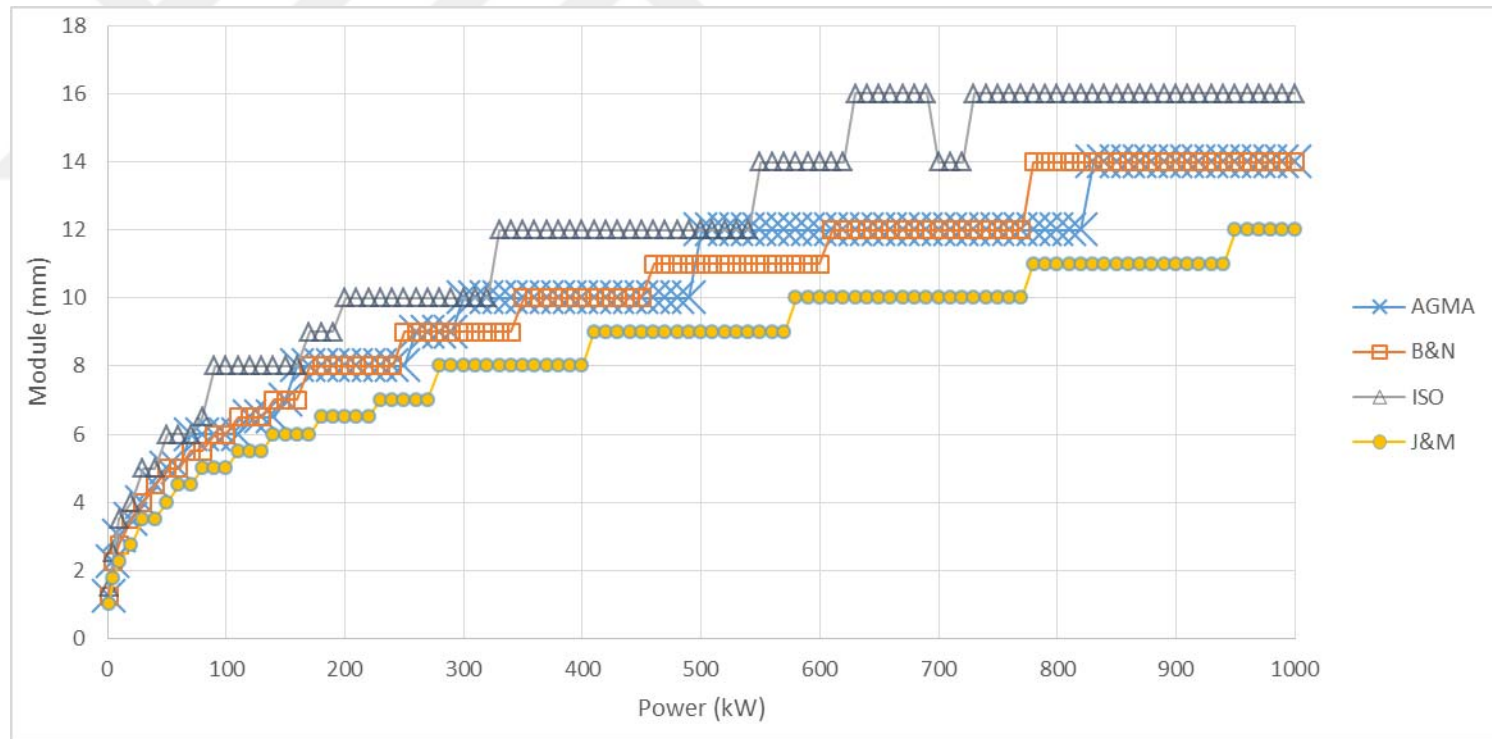
Figure E. 11. Module variation considering bending fatigue failure under increasing power at 6:1 speed ratio (Ø=25°, Type 2)

Figure E. 12. Face width variation considering bending fatigue failure under increasing power at 6:1 speed ratio (Ø=25°, Type2)

Figure E. 13. Module variation considering bending fatigue failure under increasing power at 7:1 speed ratio (Ø=25°, Type 2)
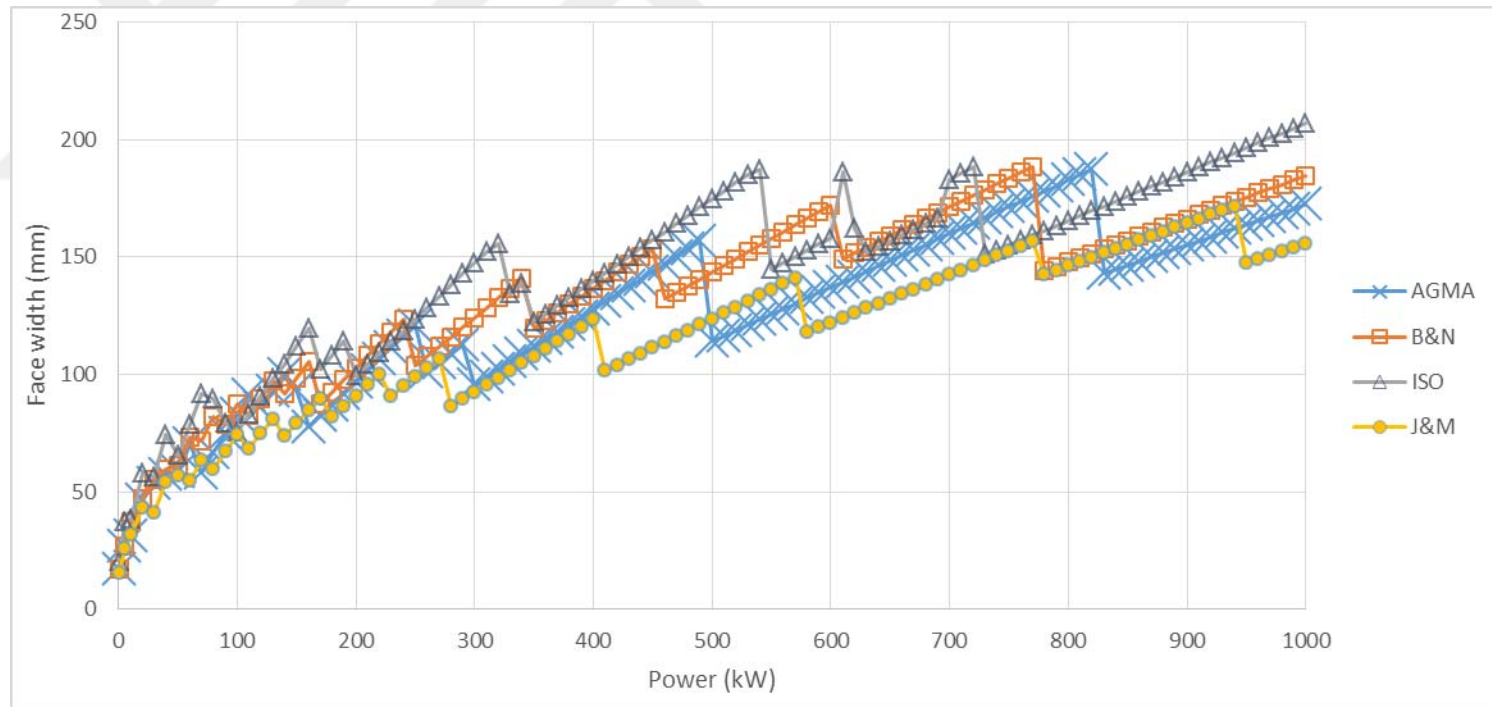
Figure E. 14. Face width variation considering bending fatigue failure under increasing power at 7:1 speed ratio ($\varnothing=25^\circ$, Type2)
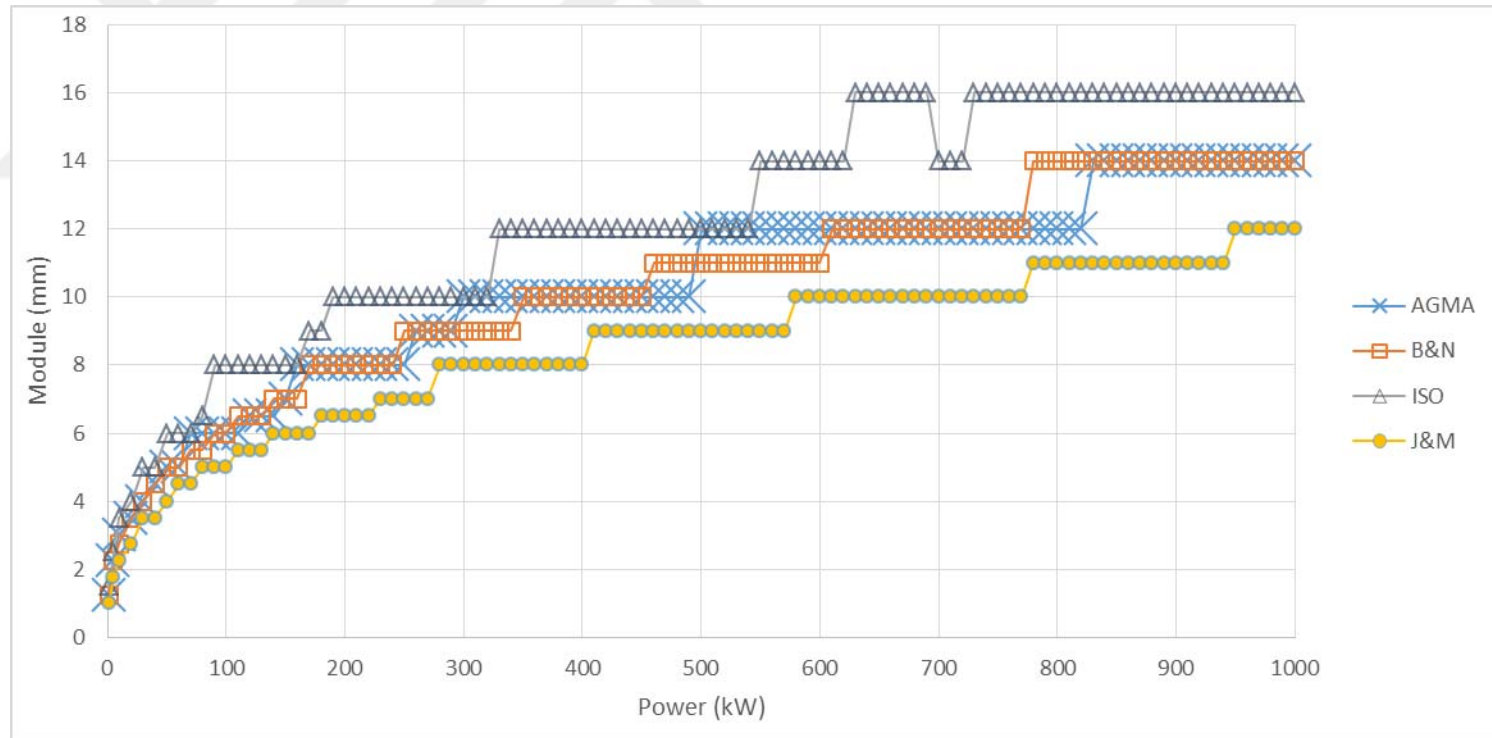
Figure E. 15. Module variation considering bending fatigue failure under increasing power at 8:1 speed ratio (Ø=25°, Type 2)
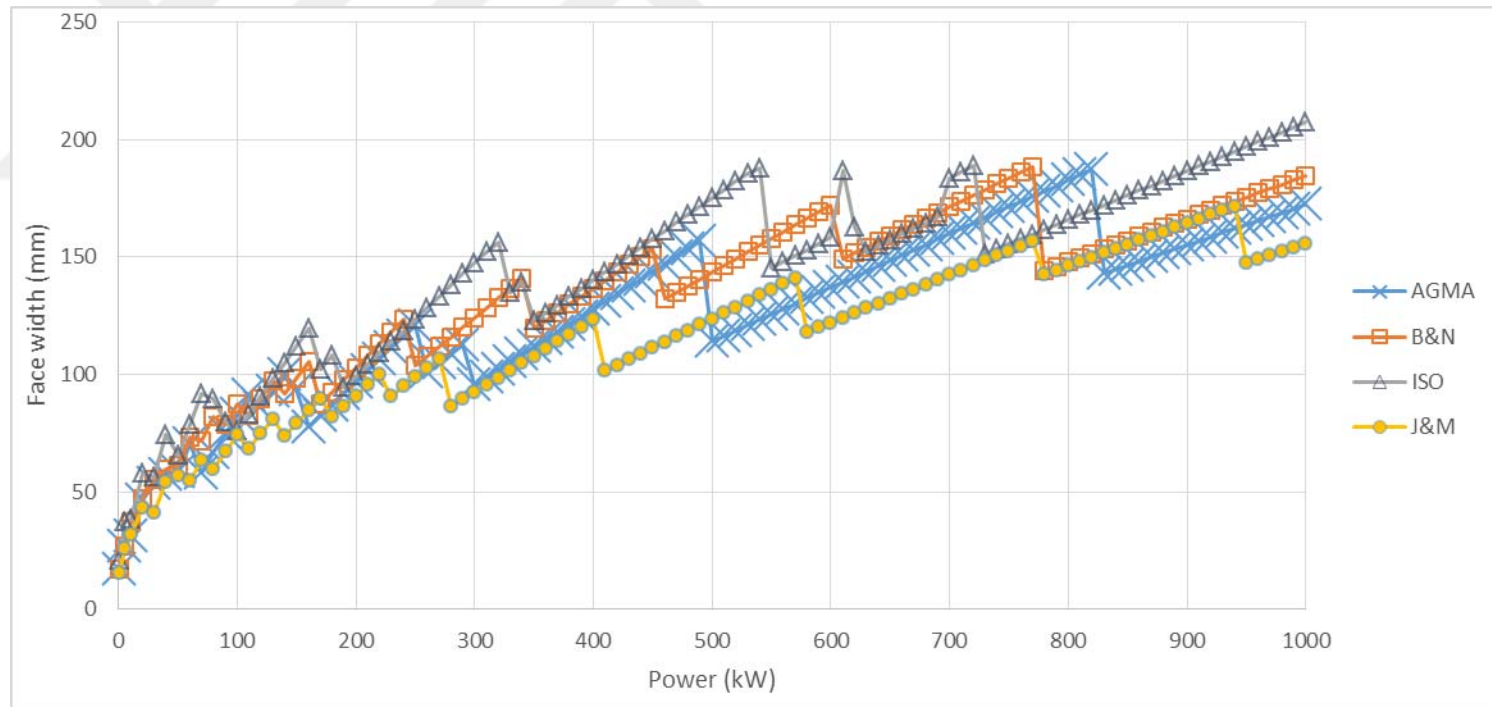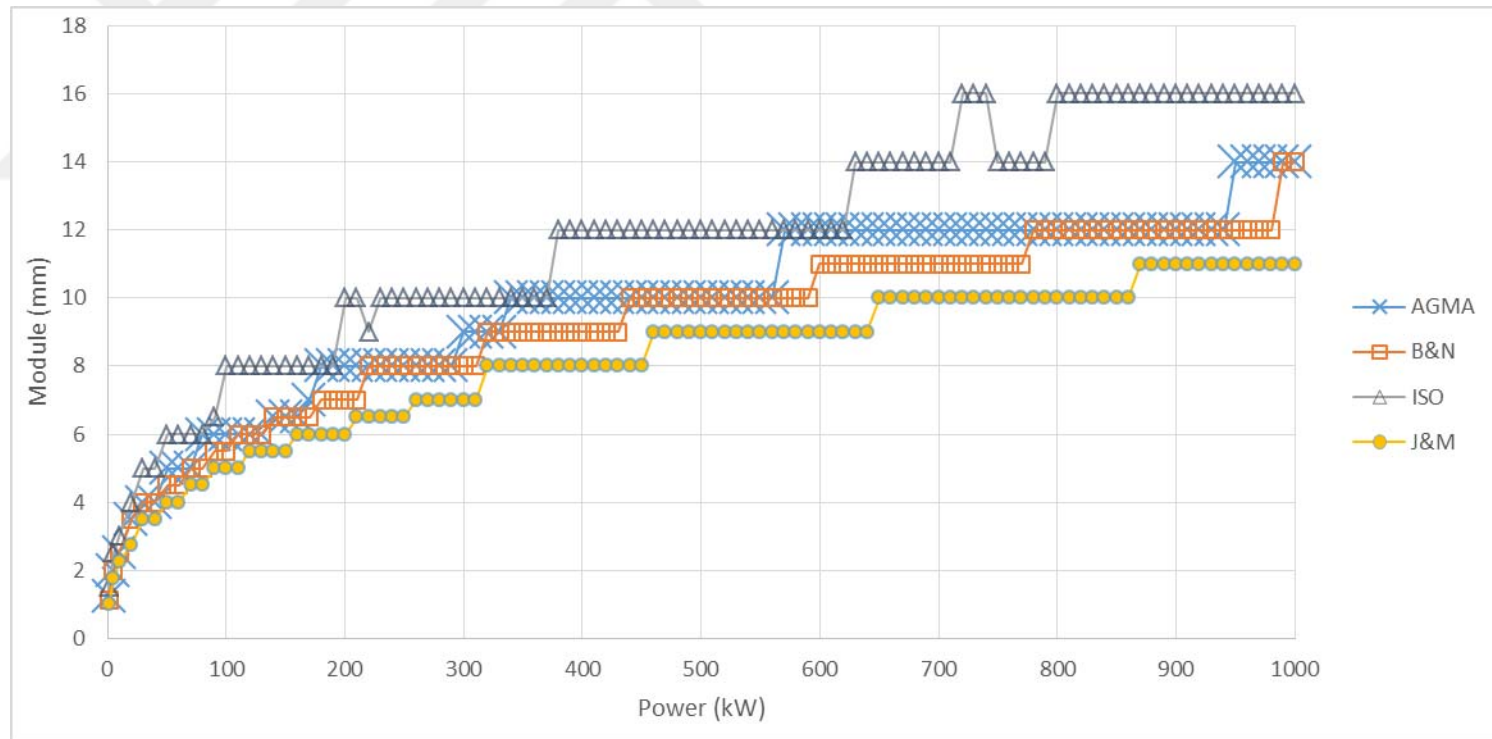
Figure E. 16. Face width variation considering bending fatigue failure under increasing power at 8:1 speed ratio (Ø=25°, Type2)

E.2. Comparison of the Results Based on Bending Fatigue Failure Considering Speed Ratio for the Selected Power Transmissions for Ø=25°, Material type 2
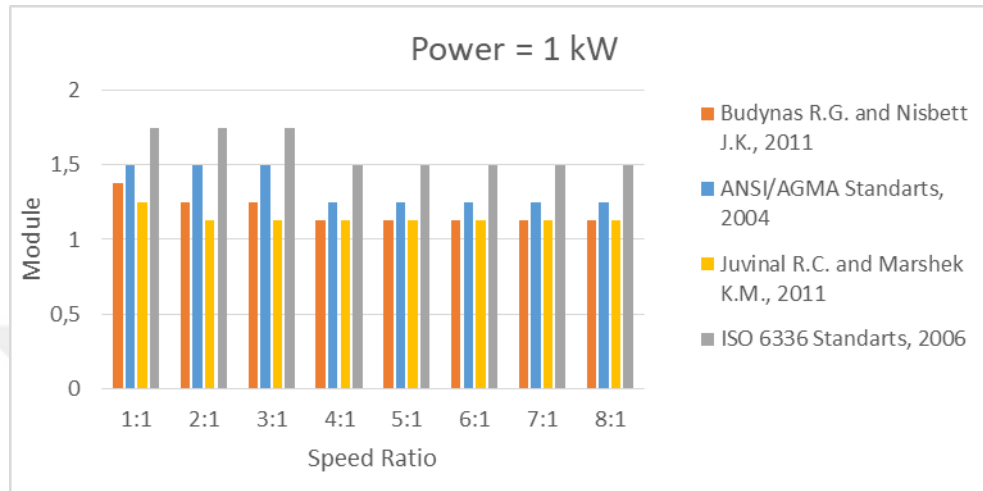
Figure E. 17. The effect of speed ratio on module selection based on bending fatigue failure at 1 kW power transmission (Ø=25°, Type 2)
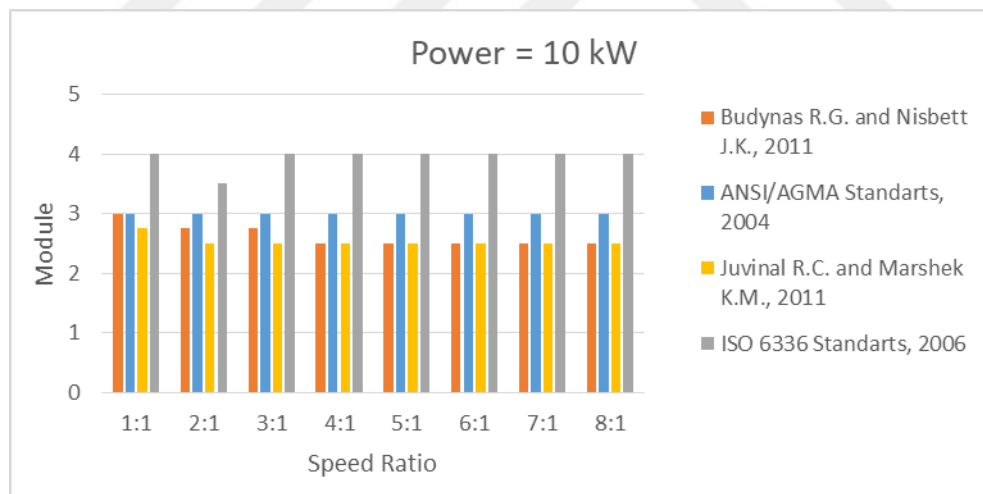
Figure E. 18. The effect of speed ratio on module selection based on bending fatigue failure at 10 kW power transmission (Ø=25°, Type 2)

Figure E. 19. The effect of speed ratio on module selection based on bending fatigue failure at 100 kW power transmission (Ø=25°, Type 2)

Figure E. 20. The effect of speed ratio on module selection based on bending fatigue failure at 500 kW power transmission (Ø=25°, Type 2)

221

Figure E. 21. The effect of speed ratio on module selection based on bending fatigue failure at 1000 kW power transmission (Ø=25°, Type 2)

E.3. Obtaining Geometric Rating Number (GR$_i$) for Design Approaches for Ø=25°, Material type 2

Figure E. 22. Comparison of GR$_i$ results obtained from the design approaches at 1:1 speed ratio (Ø=25°, Type 2), a) scatter chart, b) radar chart

Figure E. 23. Comparison of GR_i results obtained from the design approaches at 2:1 speed ratio (Ø=25°, Type 2), a) scatter chart, b) radar chart

Figure E. 24. Comparison of GR_i results obtained from the design approaches at 3:1 speed ratio ($\emptyset=25^{\circ}$, Type 2), a) scatter chart, b) radar chart

225

Figure E. 25. Comparison of GR_i results obtained from the design approaches at 4:1 speed ratio ($\emptyset=25^o$, Type 2), a) scatter chart, b) radar chart
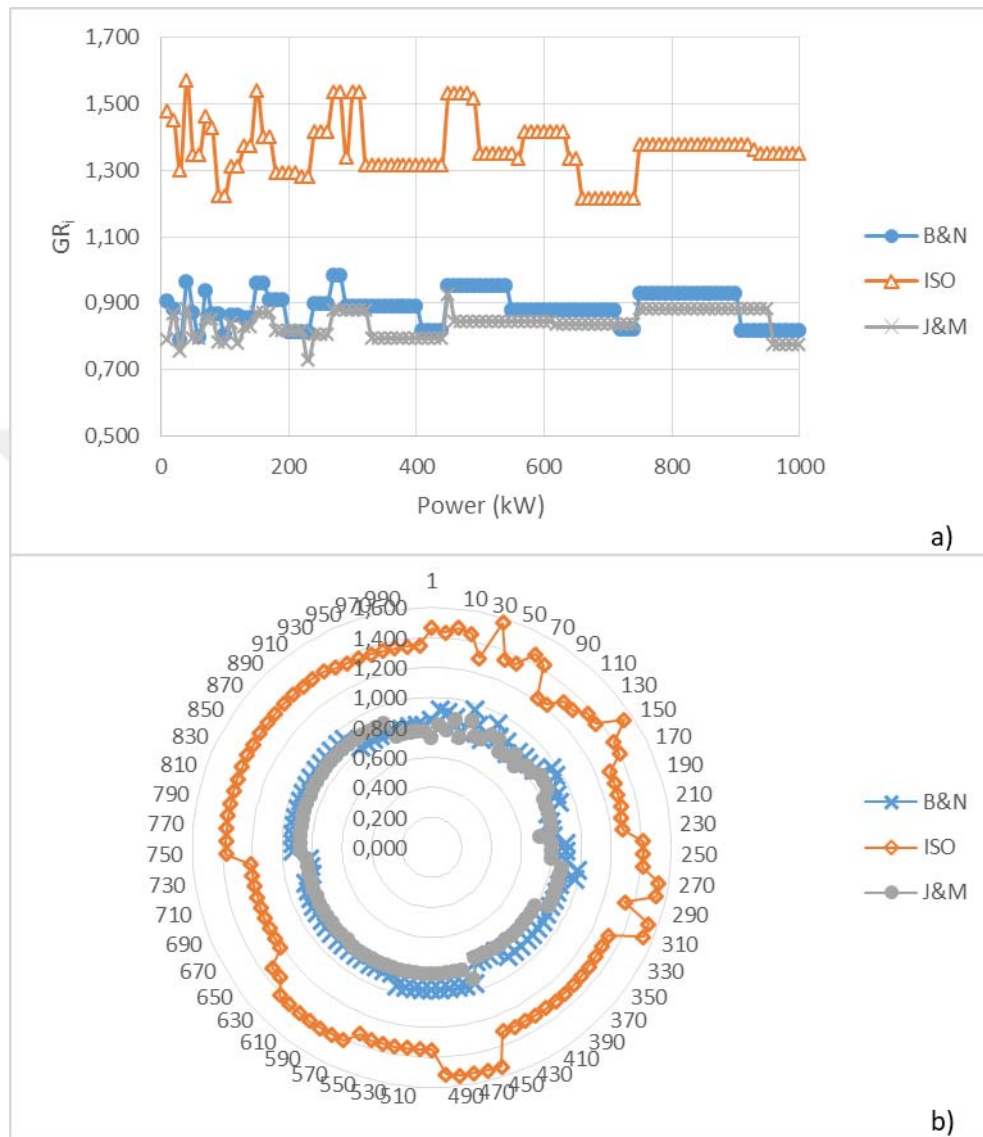
Figure E. 26. Comparison of GR_i results obtained from the design approaches at 5:1 speed ratio (Ø=25°, Type 2), a) scatter chart, b) radar chart

227

Figure E. 27. Comparison of GR_i results obtained from the design approaches at 6:1 speed ratio (Ø=25°, Type 2), a) scatter chart, b) radar chart

Figure E. 28. Comparison of GR_i results obtained from the design approaches at 7:1 speed ratio ($\emptyset = 25^\circ$, Type 2), a) scatter chart, b) radar chart

229
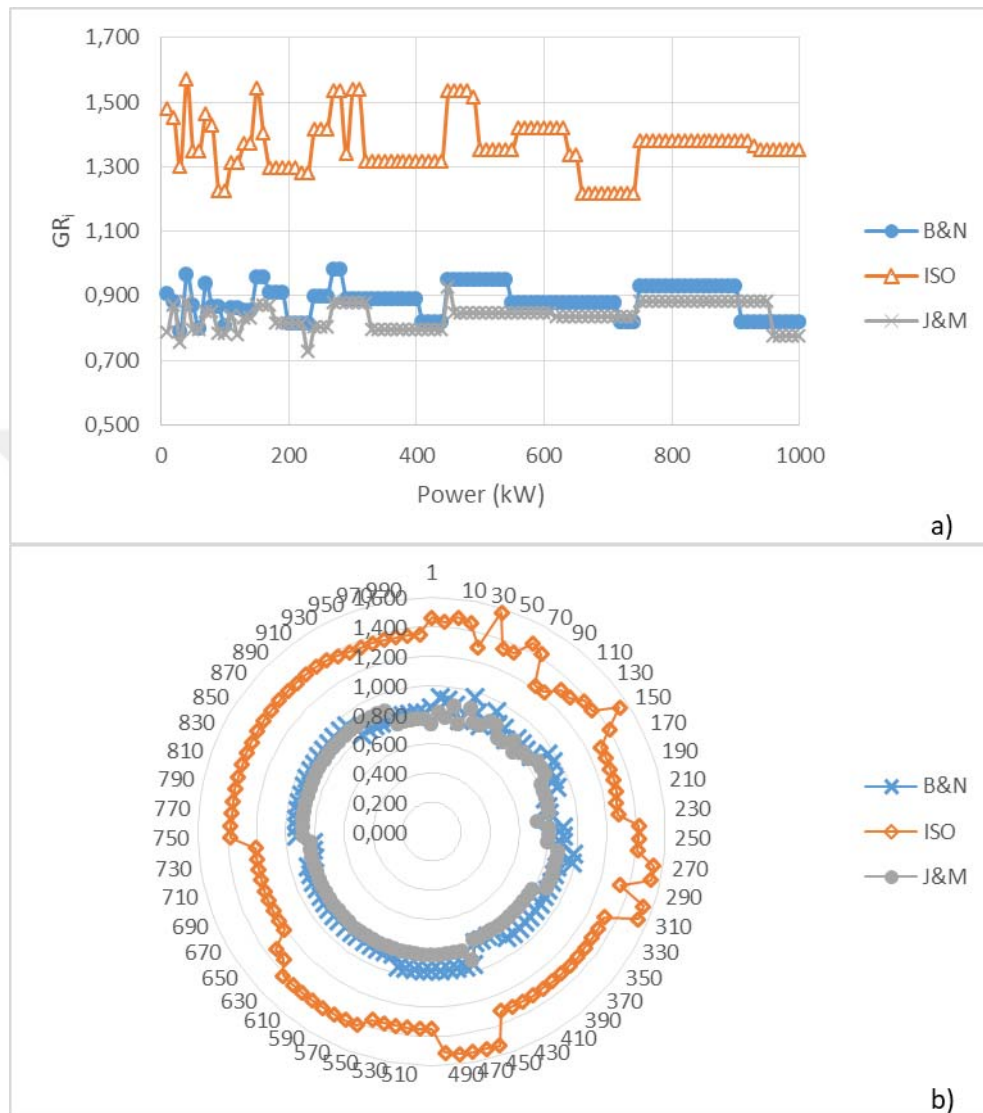
Figure E. 29. Comparison of GR_i results obtained from the design approaches at 8:1 speed ratio (∅=25°, Type 2), a) scatter chart, b) radar chart

F.1 Comparison of Module Selection and Face Width Results of the Design Approaches for Ø=25°, Material type 3

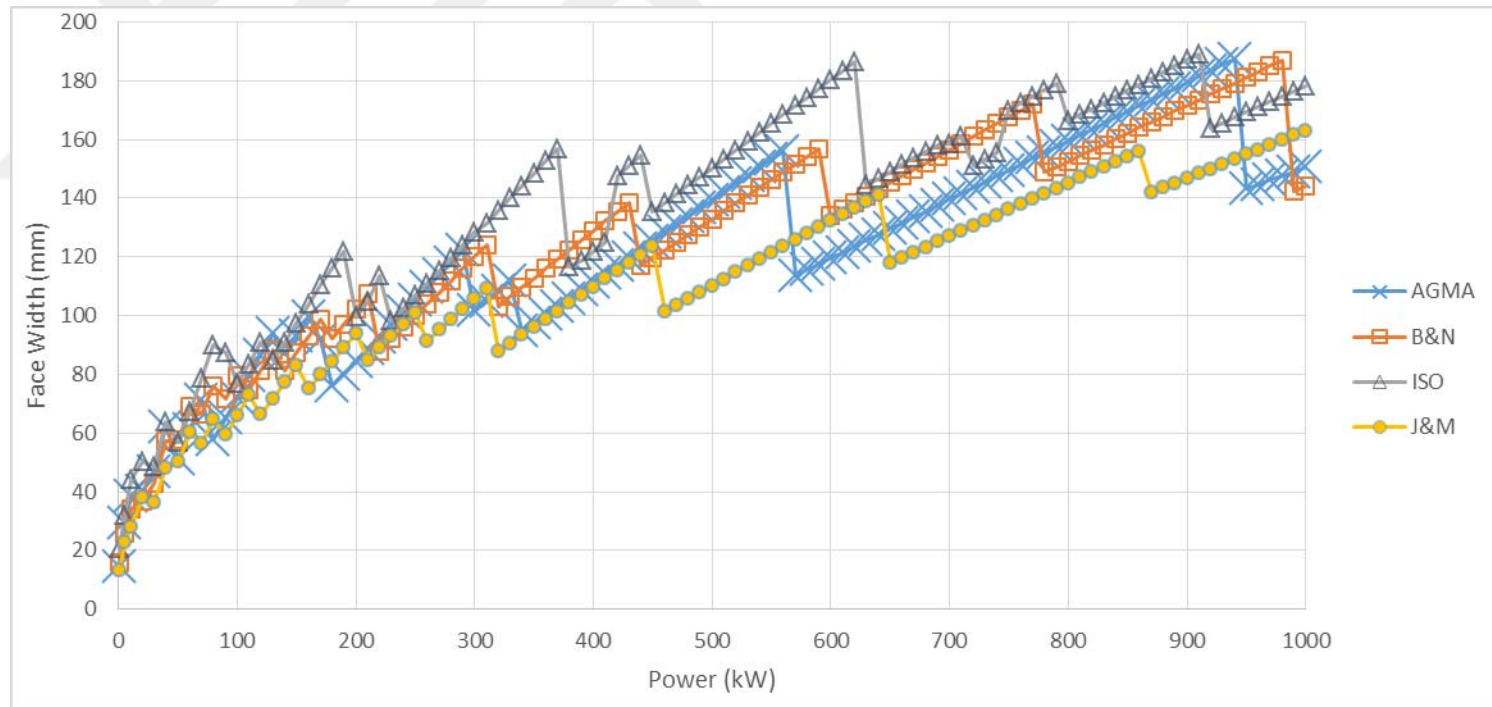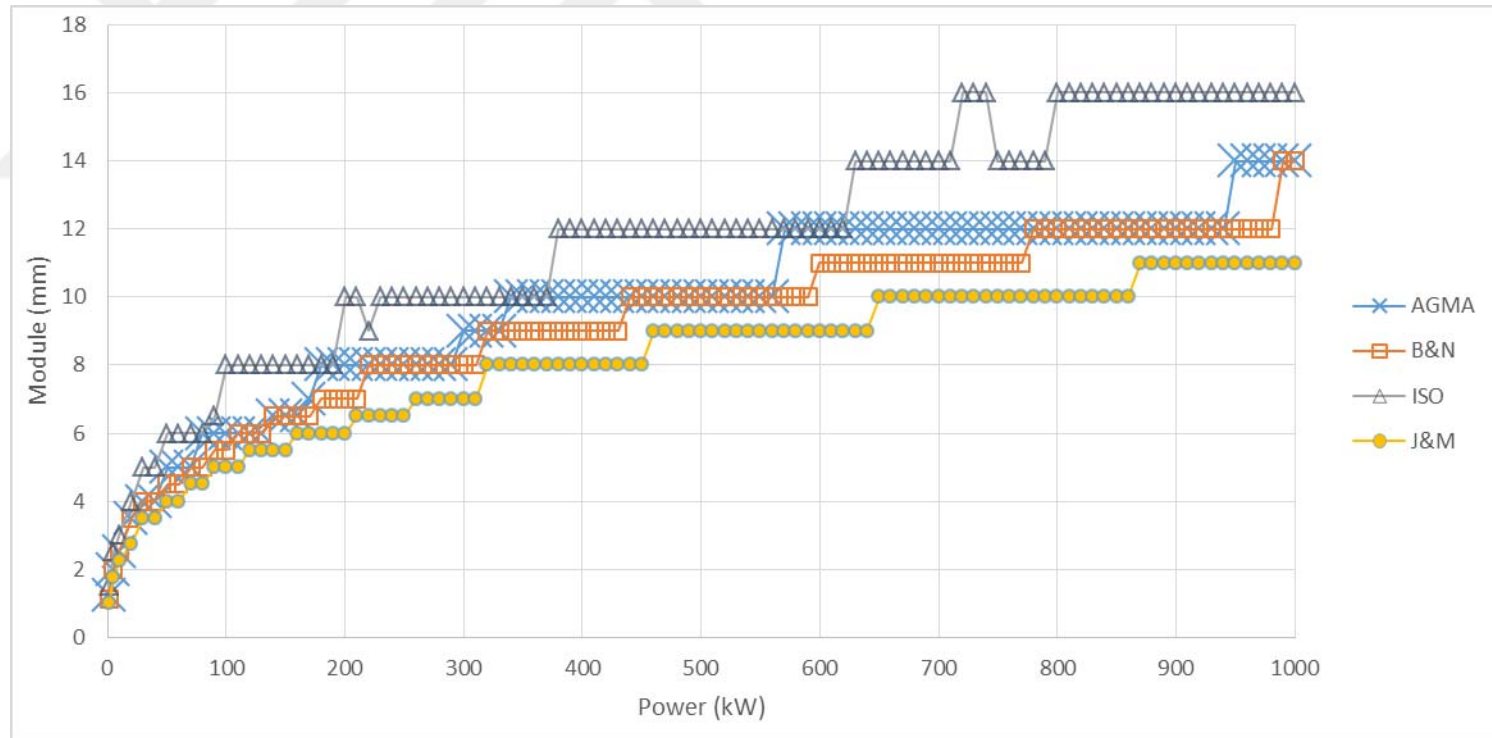Figure F. 1. Module variation considering bending fatigue failure under increasing power at 1:1 speed ratio (Ø=25°, Type 3)

Figure F.2.Face width variation considering bending fatigue failure under increasing power at 1:1 speed ratio (Ø=25°, Type 3)

Figure F. 3. Module variation considering bending fatigue failure under increasing power at 2:1 speed ratio (Ø=25°, Type 3)

Figure F.4. Face width variation considering bending fatigue failure under increasing power at 2:1 speed ratio (Ø=25°, Type 3)

Figure F. 5. Module variation considering bending fatigue failure under increasing power at 3:1 speed ratio (Ø=25°, Type 3)
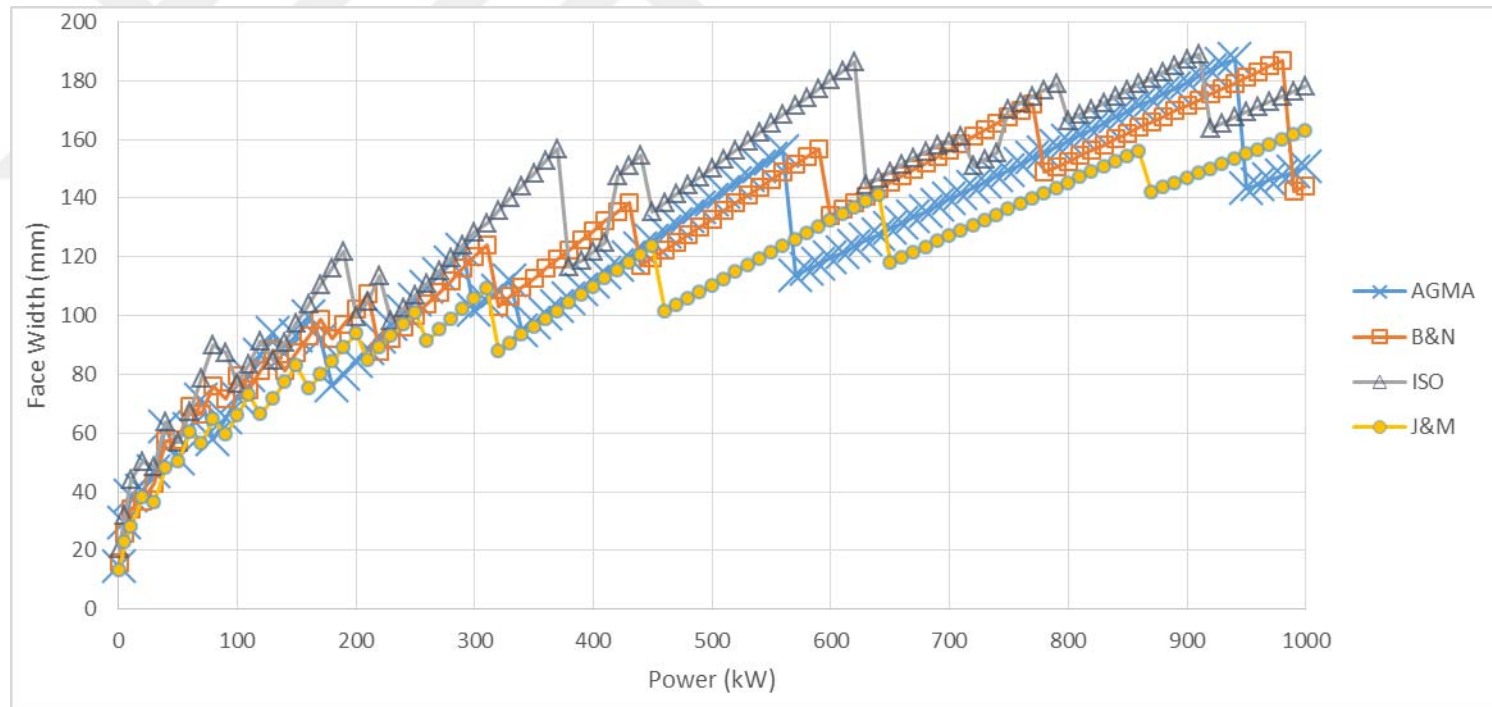
Figure F.6. Face width variation considering bending fatigue failure under increasing power at 3:1 speed ratio (Ø=25°, Type 3)

Figure F. 7. Module variation considering bending fatigue failure under increasing power at 4:1 speed ratio (Ø=25°, Type 3)
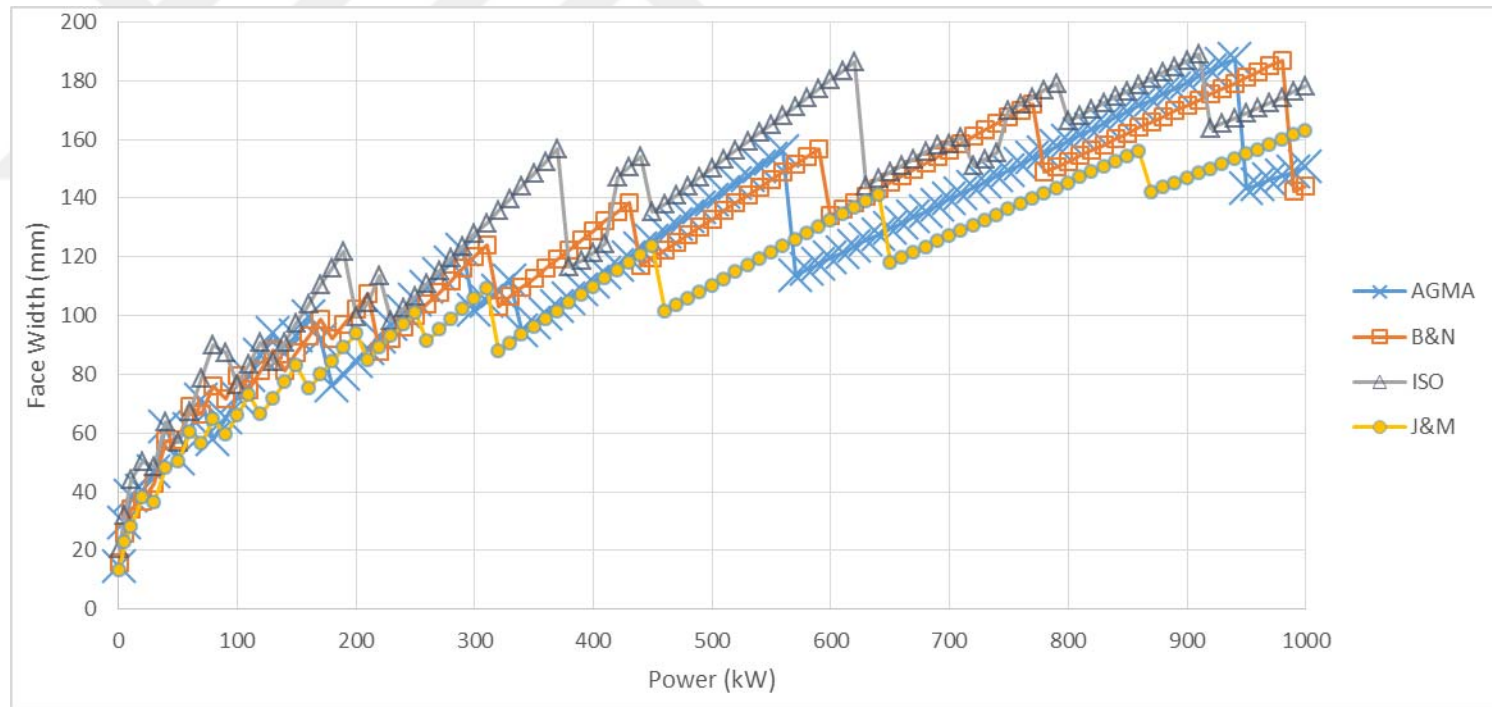
Figure F.8. Face width variation considering bending fatigue failure under increasing power at 4:1 speed ratio (Ø=25º, Type 3)
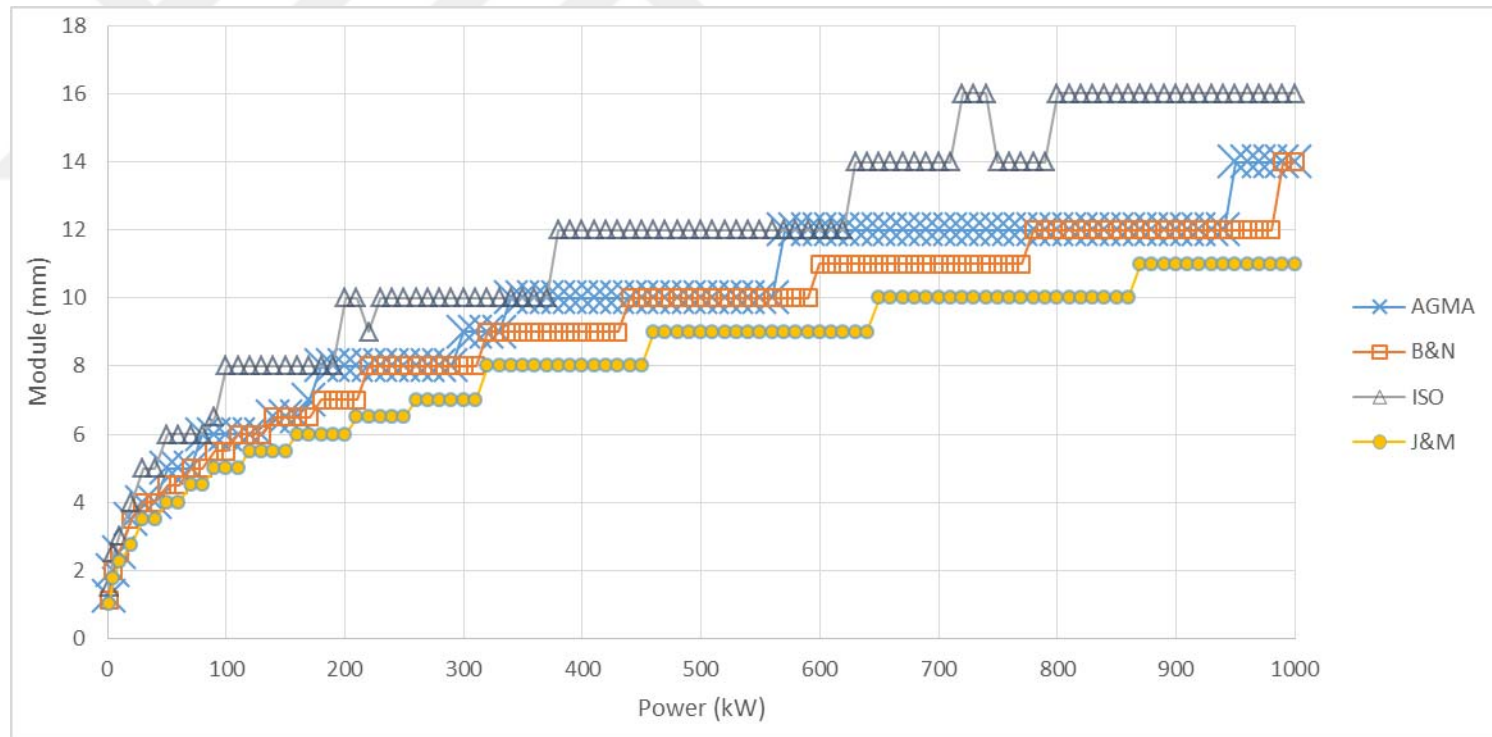
Figure F. 9. Module variation considering bending fatigue failure under increasing power at 5:1 speed ratio (Ø=25°, Type 3)
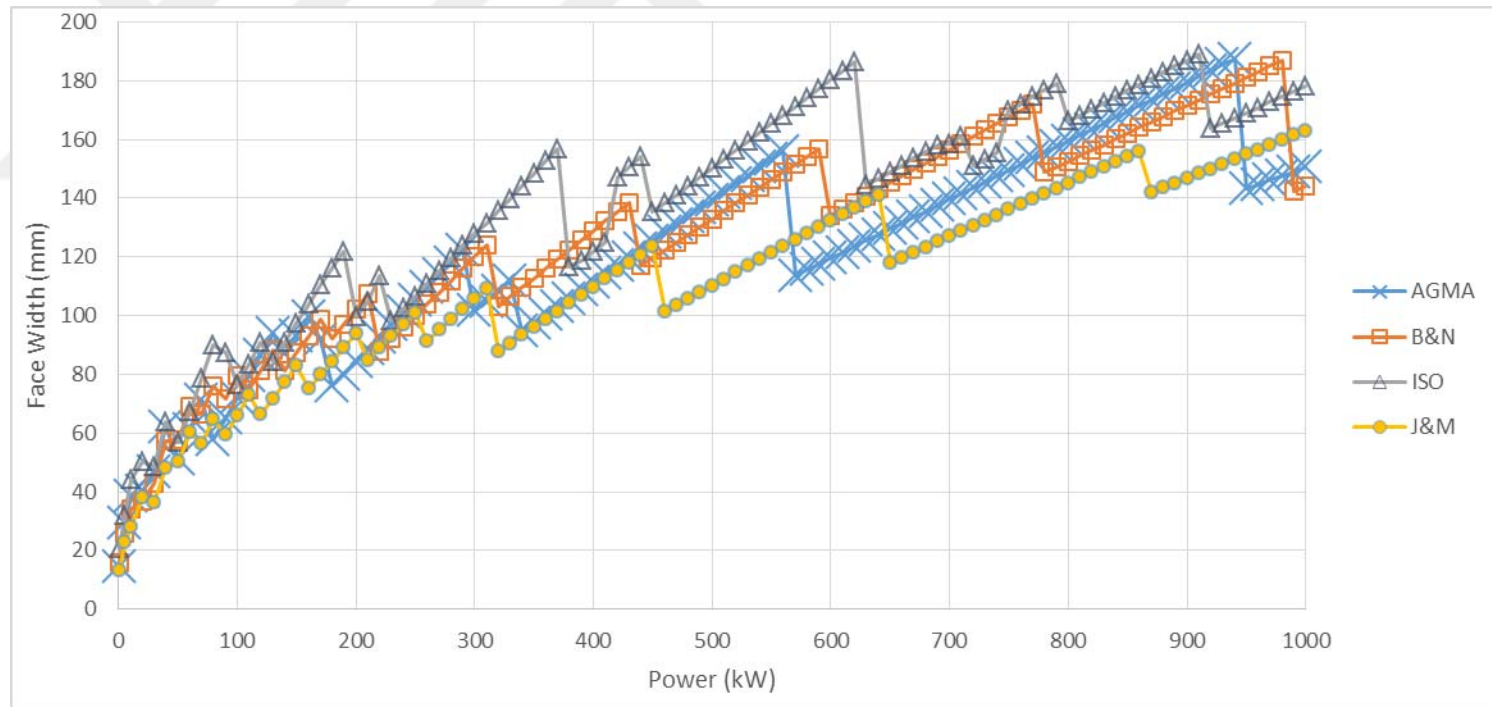
Figure F. 10. Face width variation considering bending fatigue failure under increasing power at 5:1 speed ratio (Ø=25°, Type3)
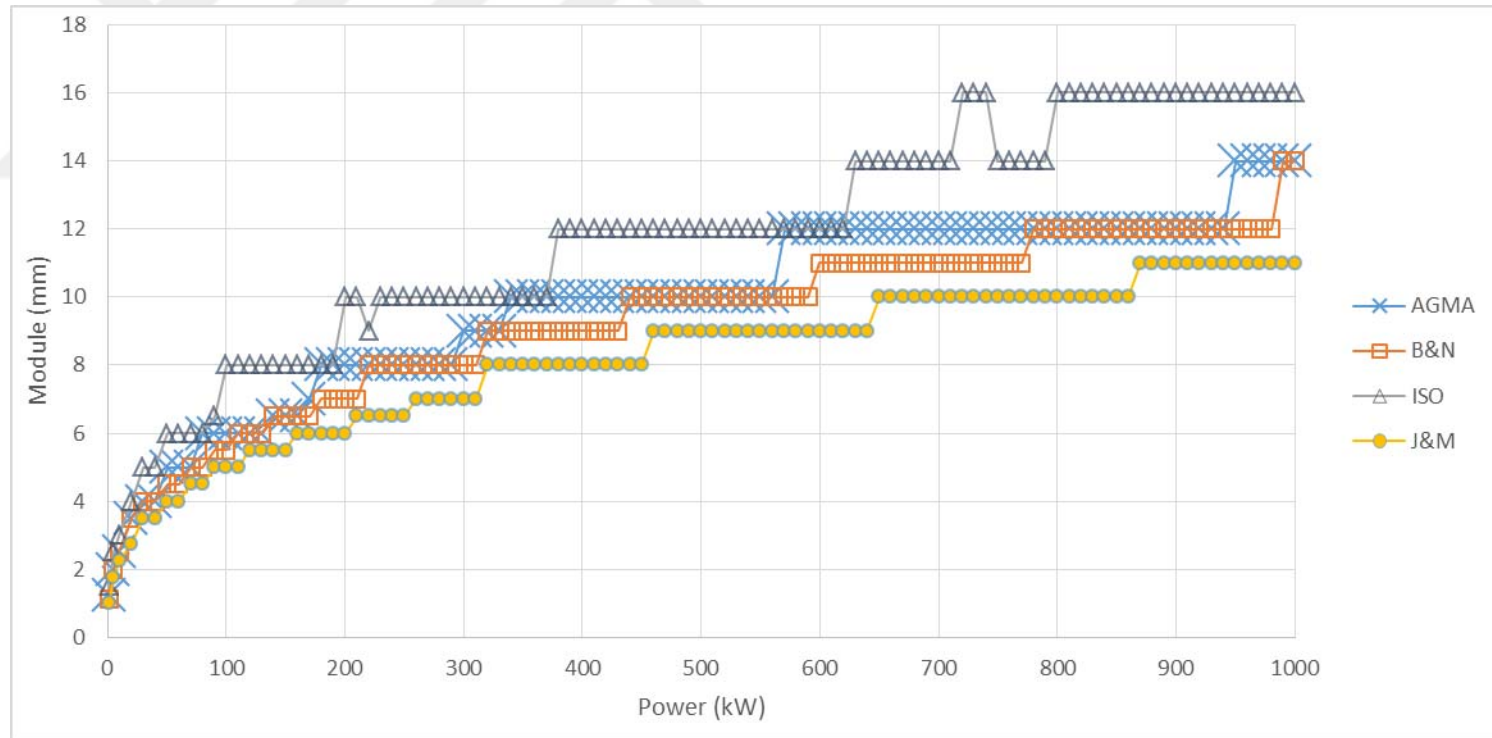
Figure F. 11. Module variation considering bending fatigue failure under increasing power at 6:1 speed ratio (Ø=25°, Type 3)

241
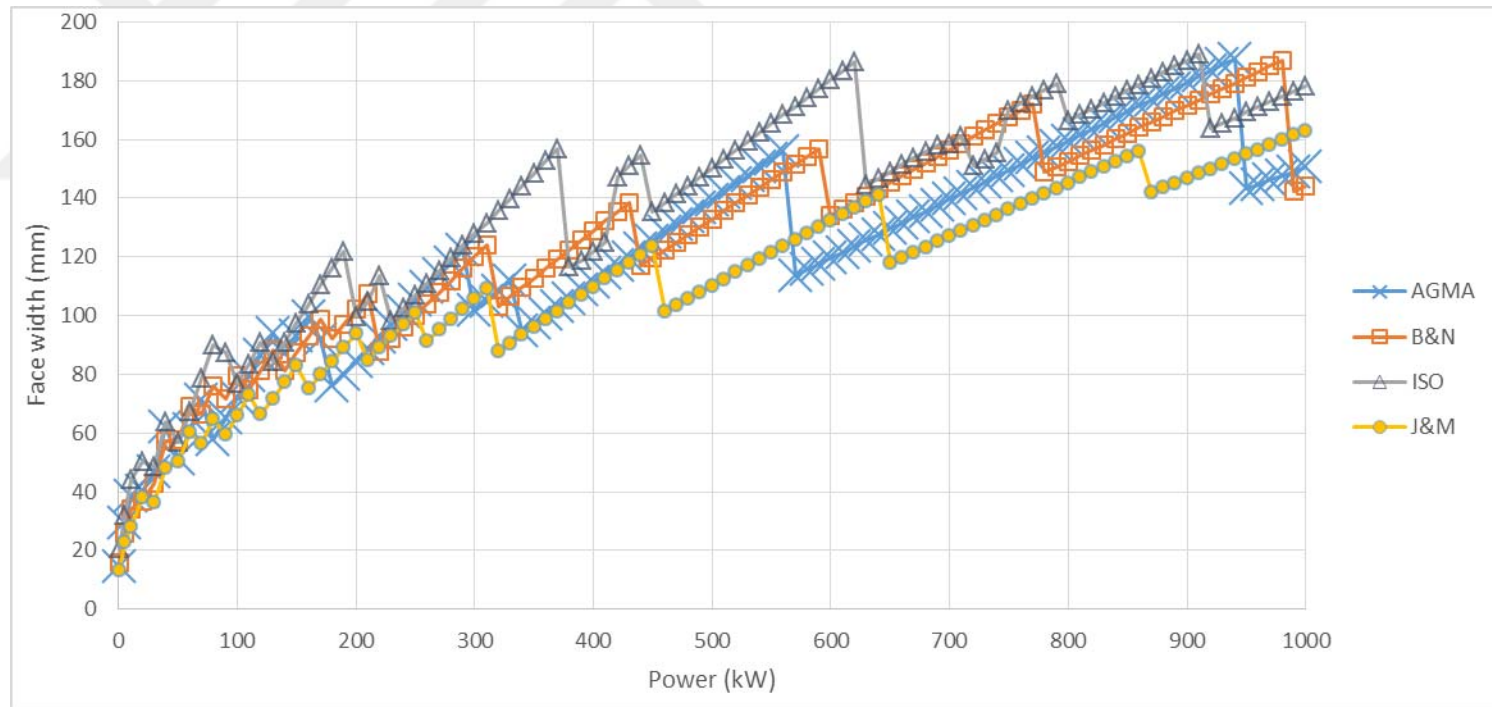
Figure F. 12. Face width variation considering bending fatigue failure under increasing power at 6:1 speed ratio (Ø=25°, Type3)
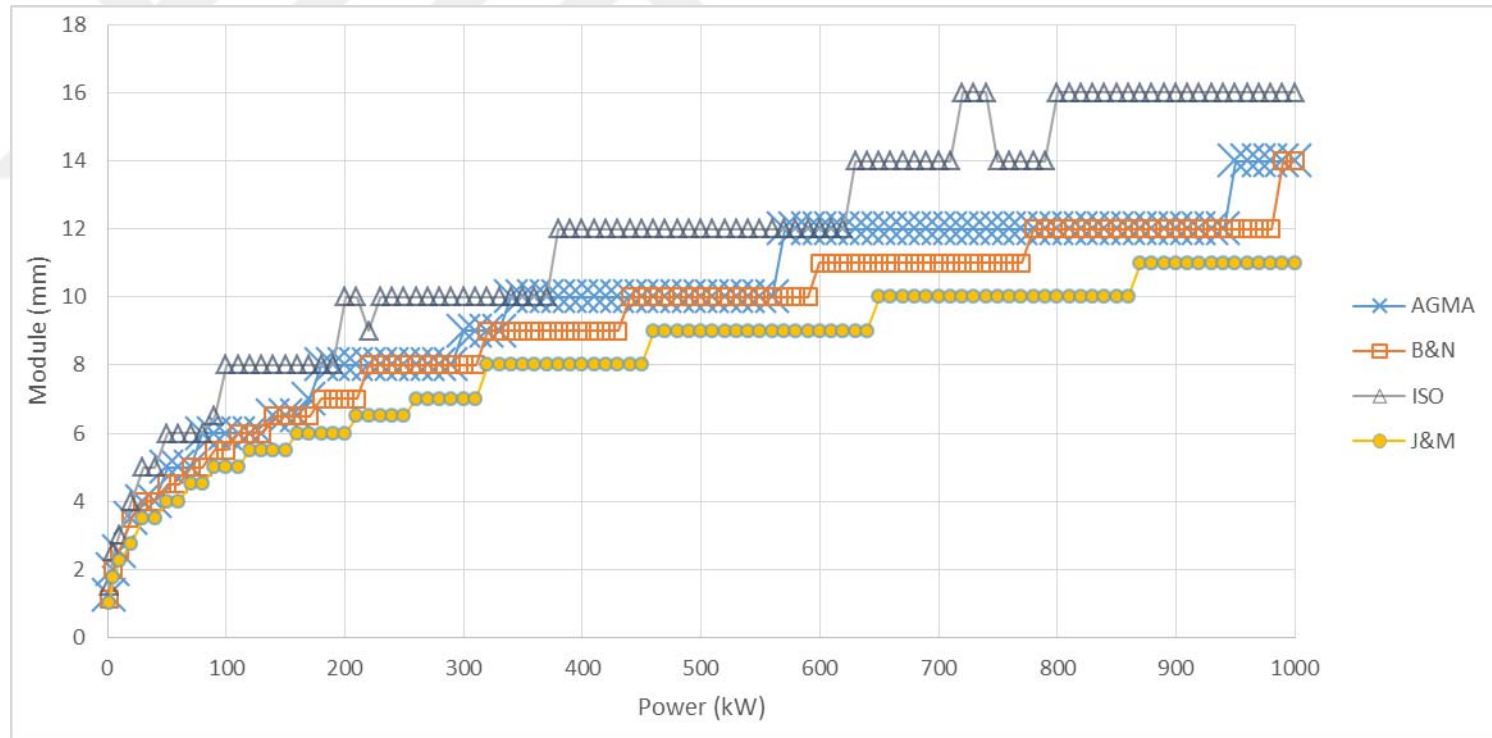
Figure F. 13. Module variation considering bending fatigue failure under increasing power at 7:1 speed ratio (Ø=25°, Type 3)

Figure F. 14. Face width variation considering bending fatigue failure under increasing power at 7:1 speed ratio (Ø=25°, Type3)

Figure F. 15. Module variation considering bending fatigue failure under increasing power at 8:1 speed ratio (Ø=25°, Type 3)

Figure F. 16. Face width variation considering bending fatigue failure under increasing power at 8:1 speed ratio (Ø=25°, Type3)

F.2. Comparison of the Results Based on Bending Fatigue Failure Considering Speed Ratio for the Selected Power Transmissions for Ø=25°, Material type 3
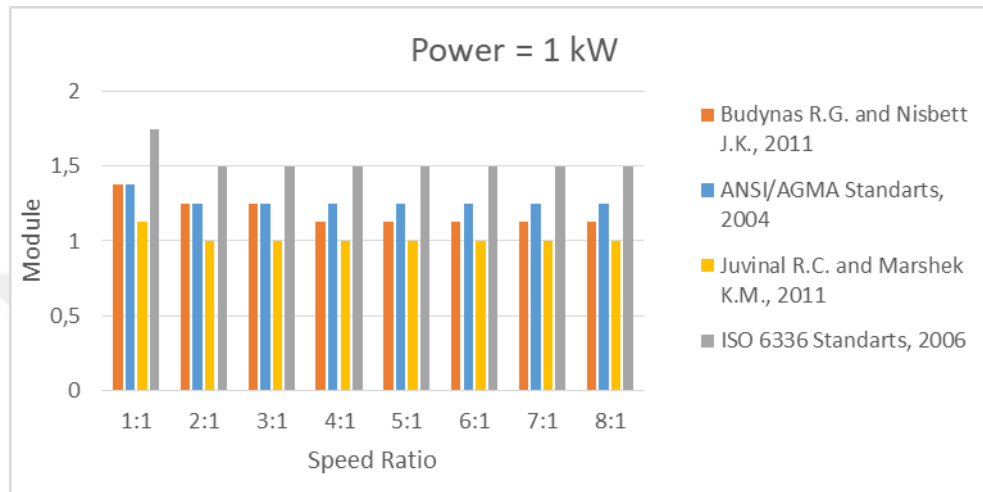
Figure F. 17. The effect of speed ratio on module selection based on bending fatigue failure at 1 kW power transmission (Ø=25°, Type 3)
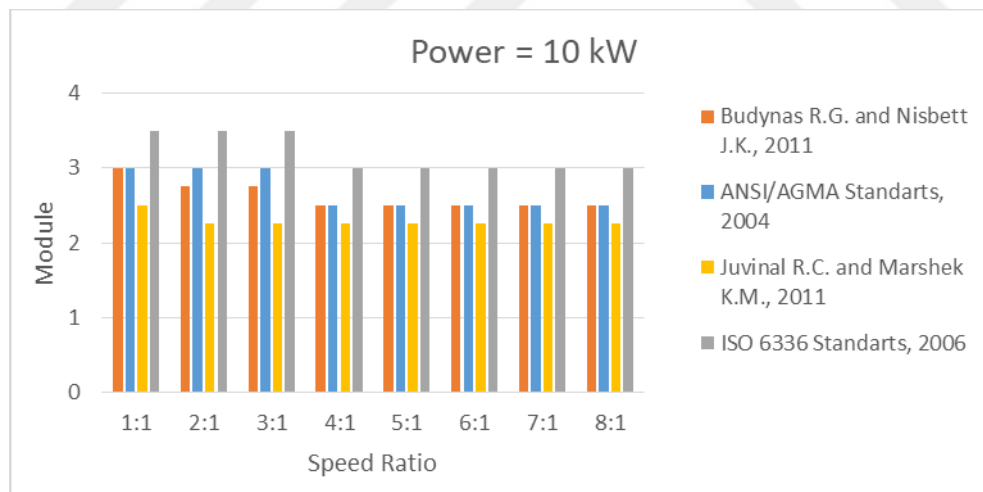
Figure F. 18. The effect of speed ratio on module selection based on bending fatigue failure at 10 kW power transmission (Ø=25°, Type 3)
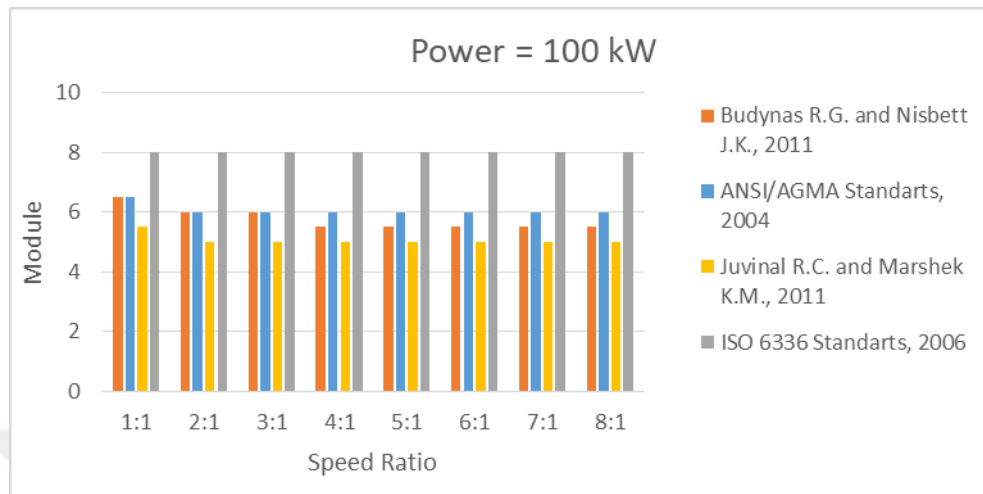
Figure F. 19. The effect of speed ratio on module selection based on bending fatigue failure at 100 kW power transmission (Ø=25°, Type 3)
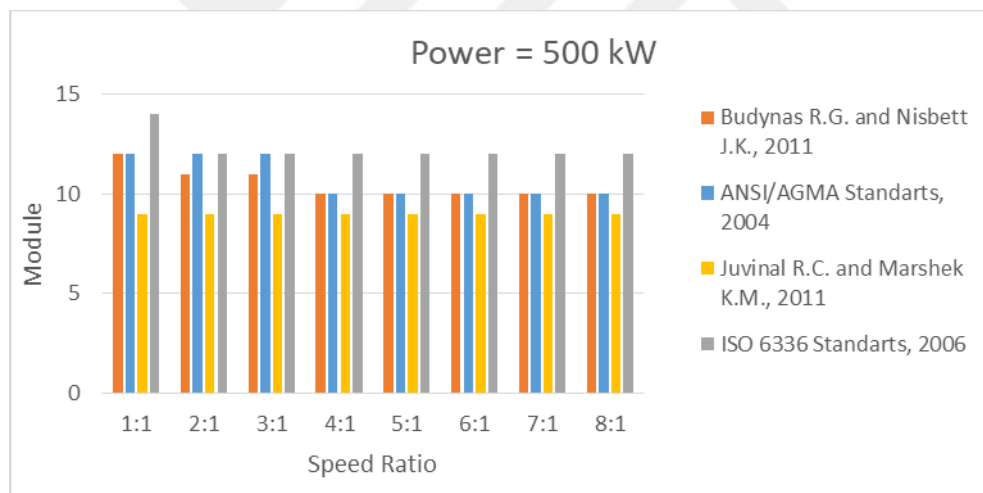
Figure F. 20. The effect of speed ratio on module selection based on bending fatigue failure at 500 kW power transmission (Ø=25°, Type 3)

248
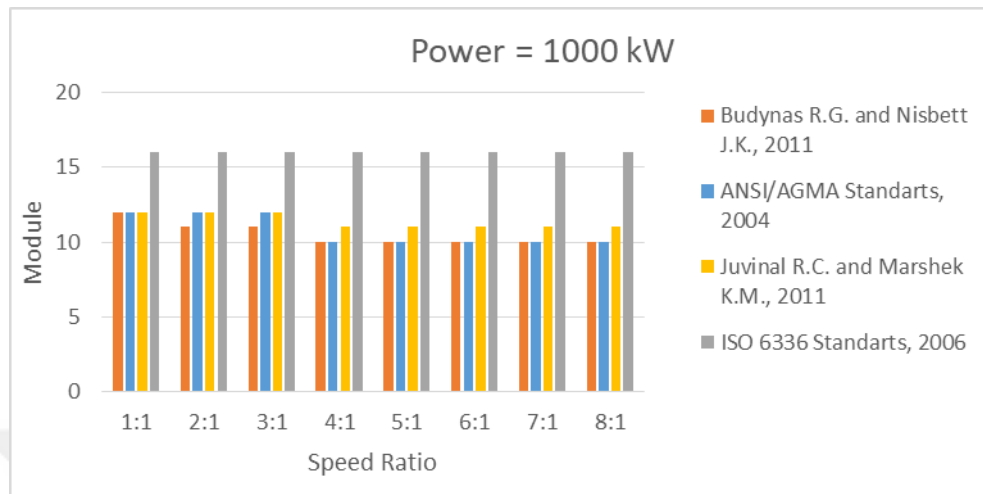
Figure F. 21. The effect of speed ratio on module selection based on bending fatigue failure at 1000 kW power transmission (Ø=25°, Type 3)

F.3. Obtaining Geometric Rating Number (GR$_i$) for Design Approaches for Ø=25°, Material type 3
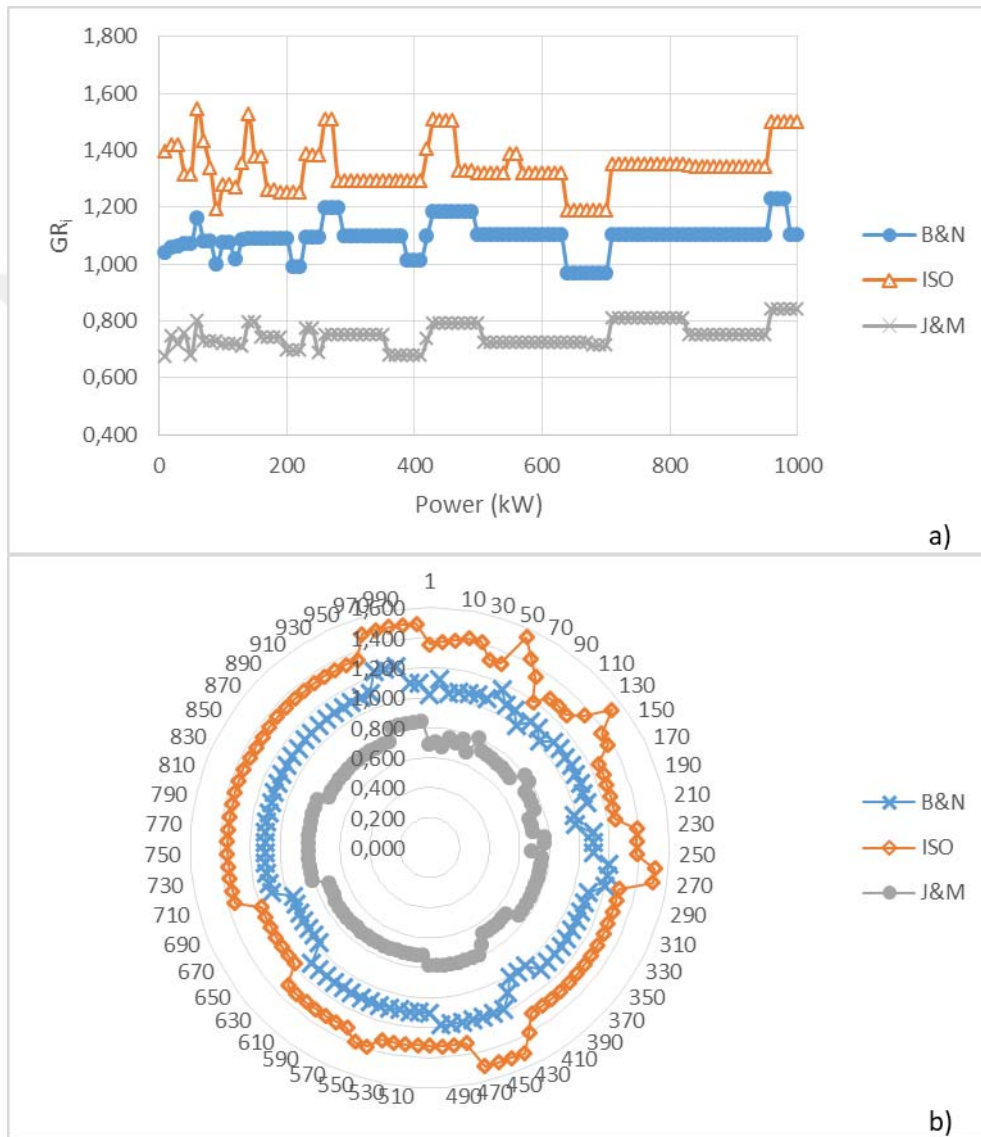
Figure F. 22. Comparison of GR$_i$ results obtained from the design approaches at 1:1 speed ratio (Ø=25°, Type 3), a) scatter chart, b) radar chart
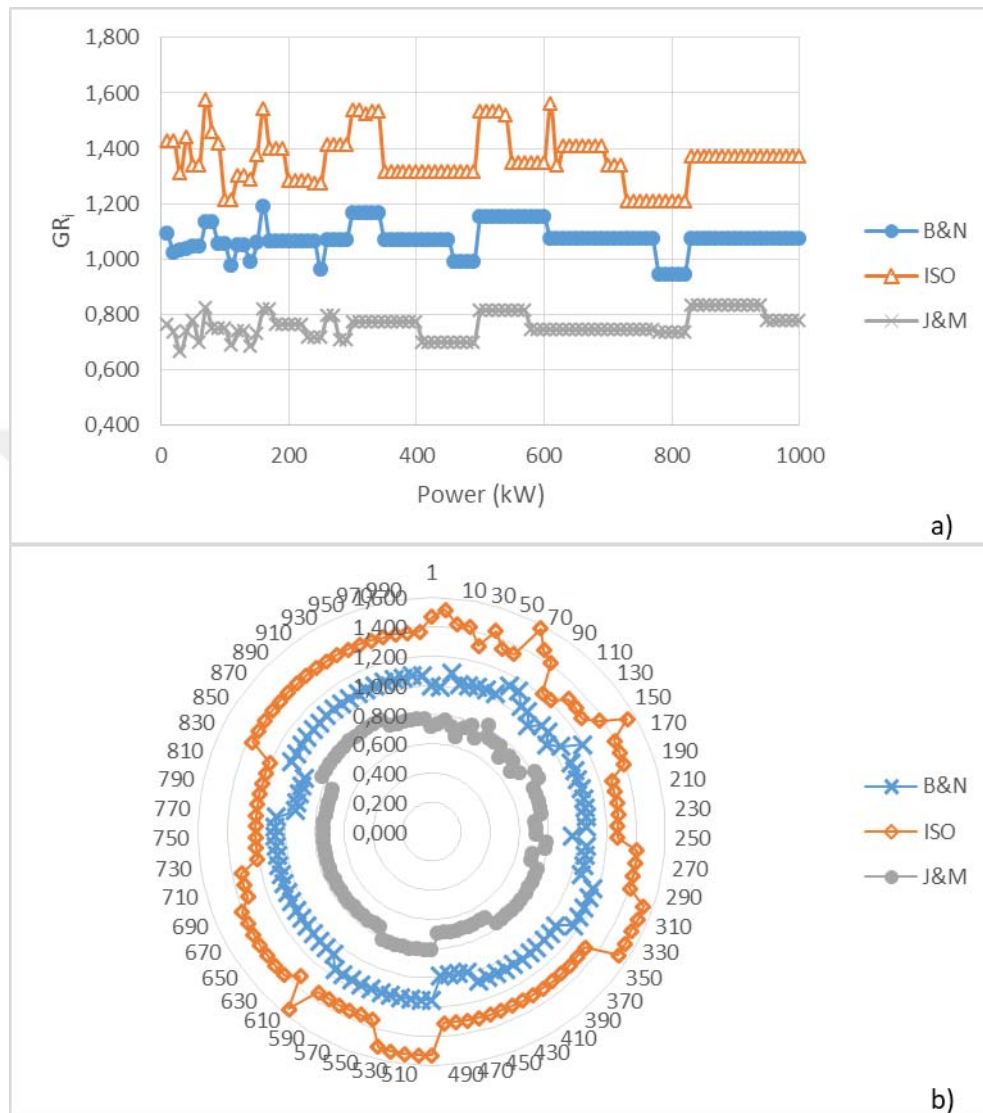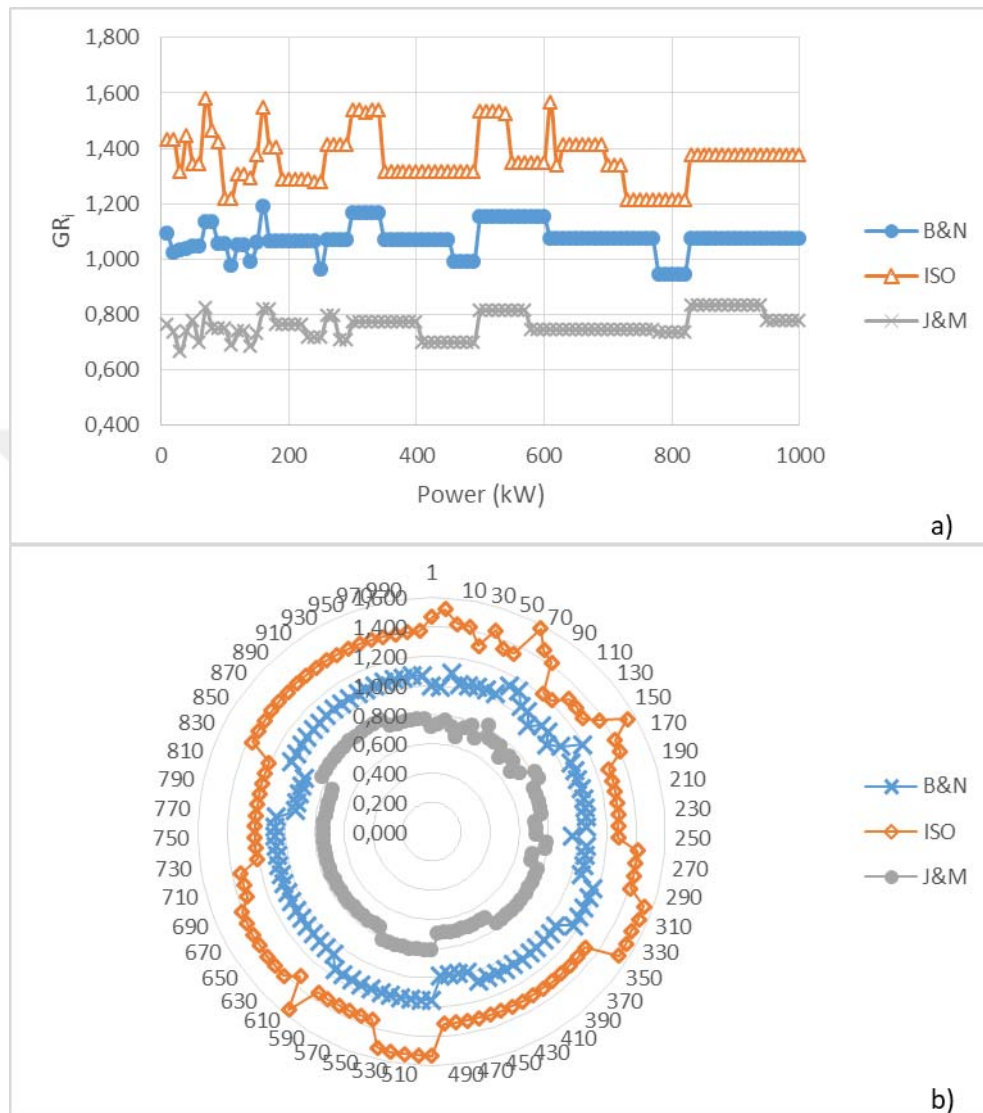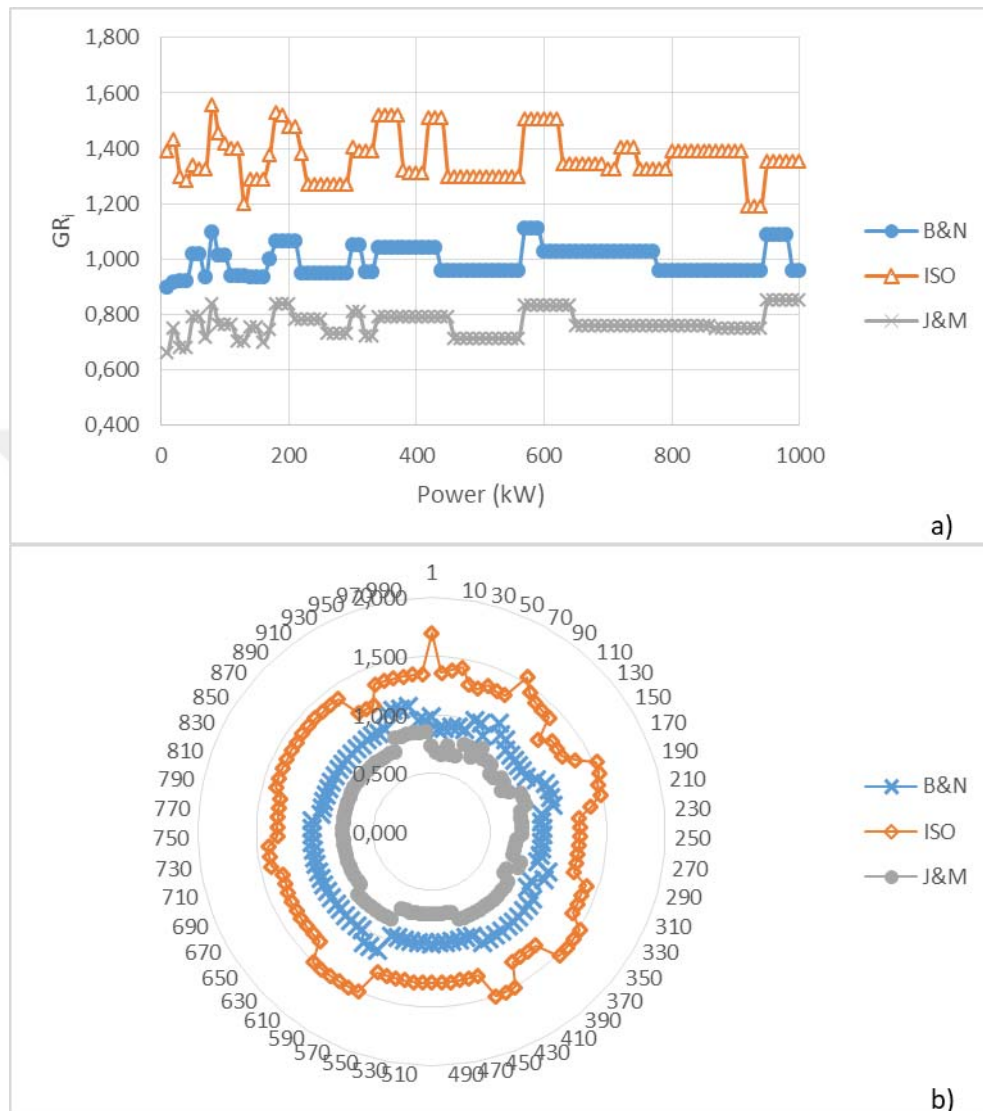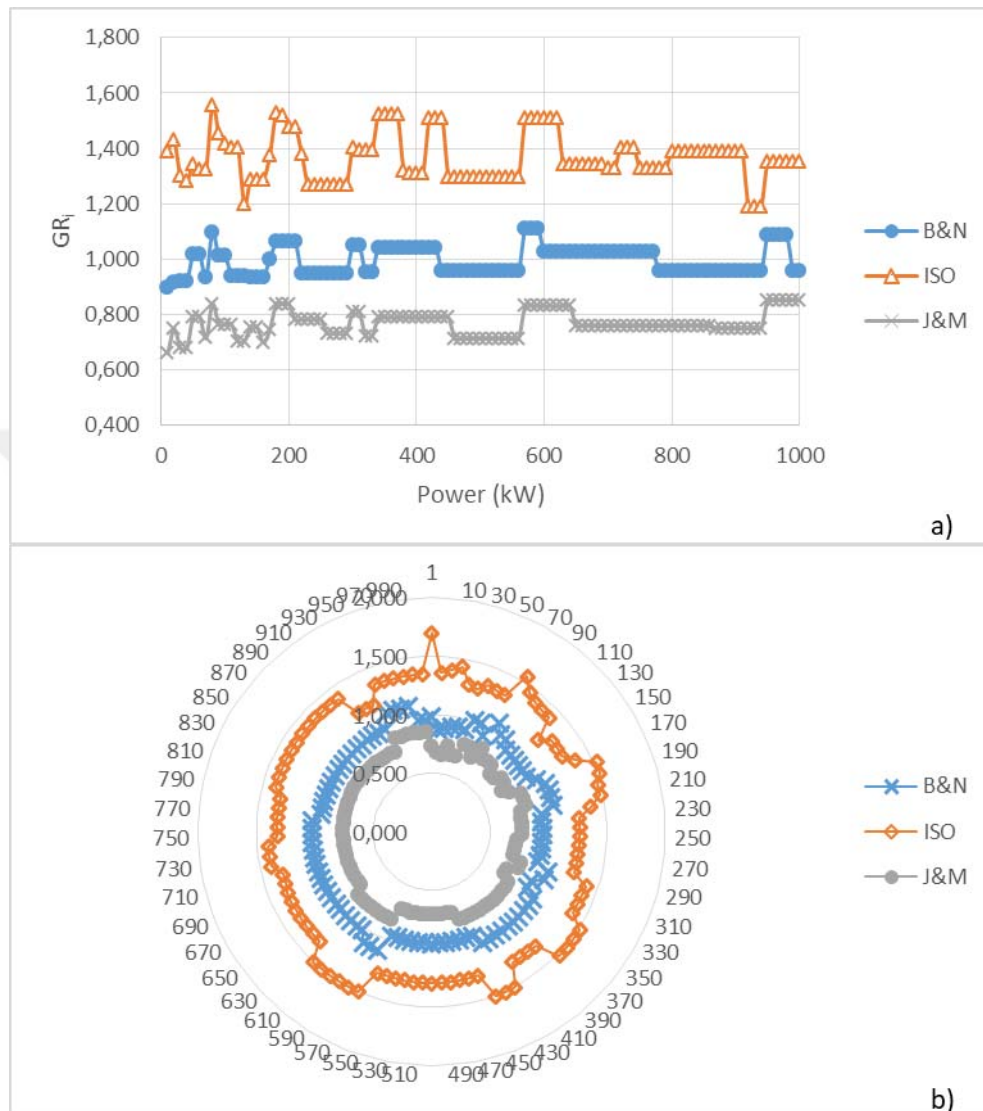
Figure F. 23. Comparison of GR_i results obtained from the design approaches at 2:1 speed ratio ($\emptyset=25^o$, Type 3), a) scatter chart, b) radar chart

Figure F. 24. Comparison of GR_i results obtained from the design approaches at 3:1 speed ratio (Ø=25°, Type 3), a) scatter chart, b) radar chart

Figure F. 25. Comparison of GR_i results obtained from the design approaches at 4:1 speed ratio (Ø=25°, Type 3), a) scatter chart, b) radar chart
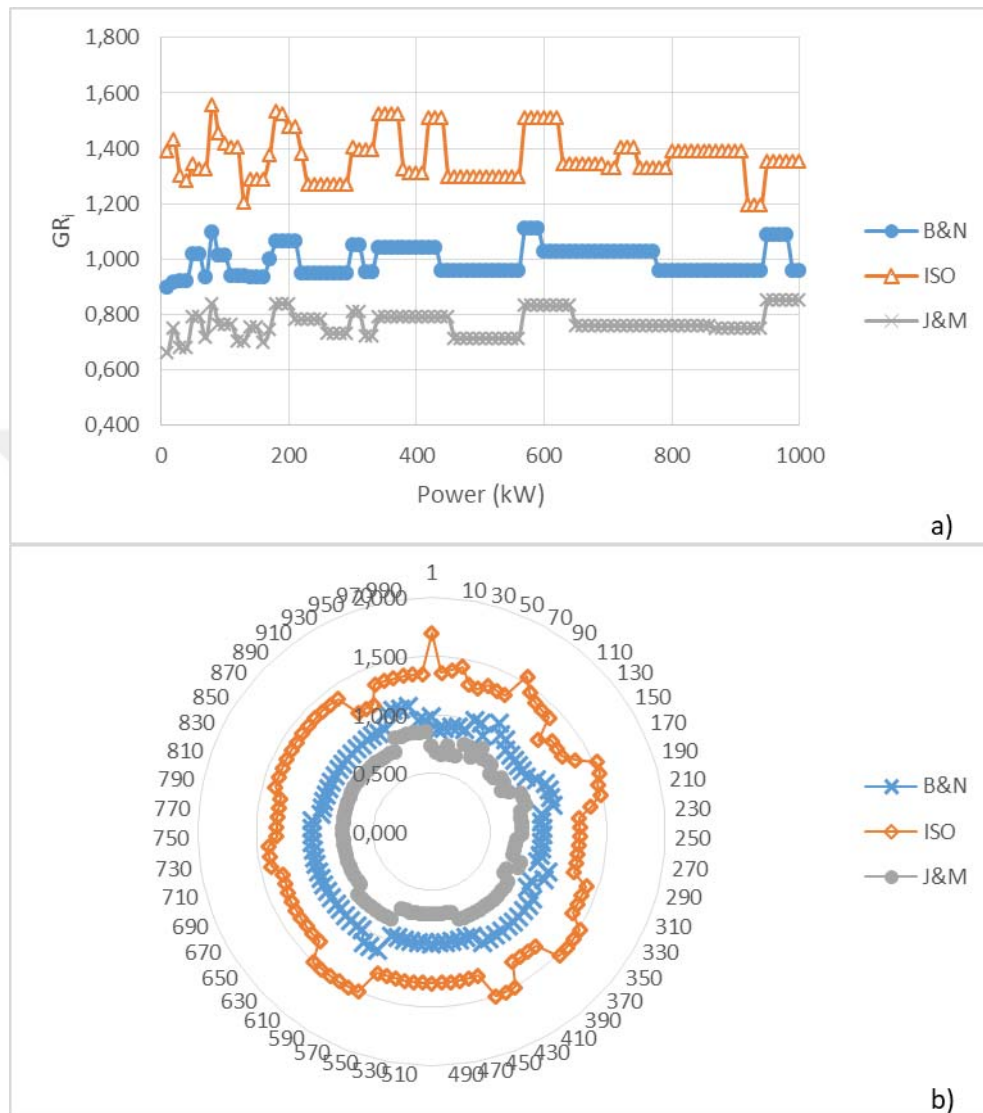
Figure F. 26. Comparison of GR_i results obtained from the design approaches at 5:1 speed ratio ($\varnothing = 25^{\circ}$, Type 3), a) scatter chart, b) radar chart

254

Figure F. 27. Comparison of GR_i results obtained from the design approaches at 6:1 speed ratio ($\varnothing=25^{\circ}$, Type 3), a) scatter chart, b) radar chart
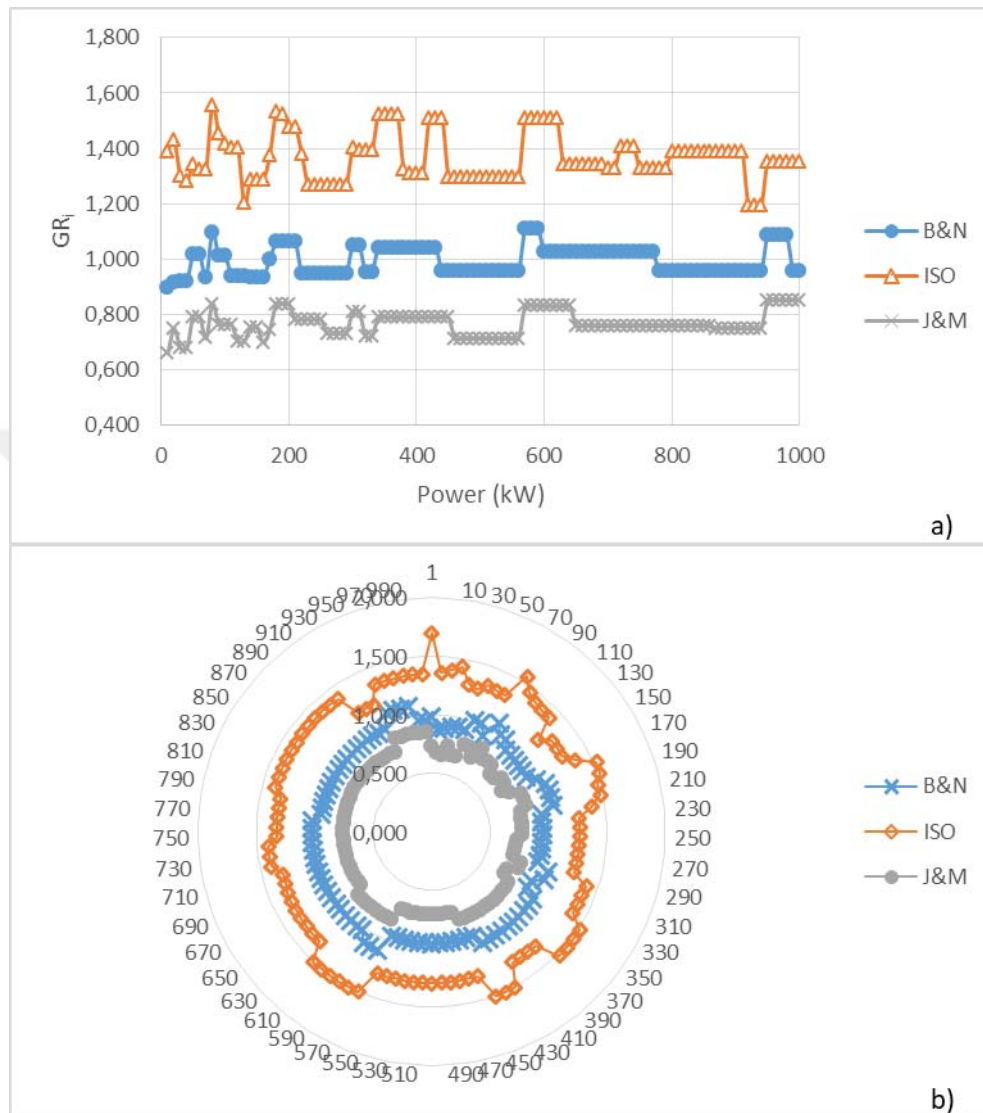
Figure F. 28. Comparison of GR_i results obtained from the design approaches at 7:1 speed ratio ($\varnothing=25^o$, Type 3), a) scatter chart, b) radar chart
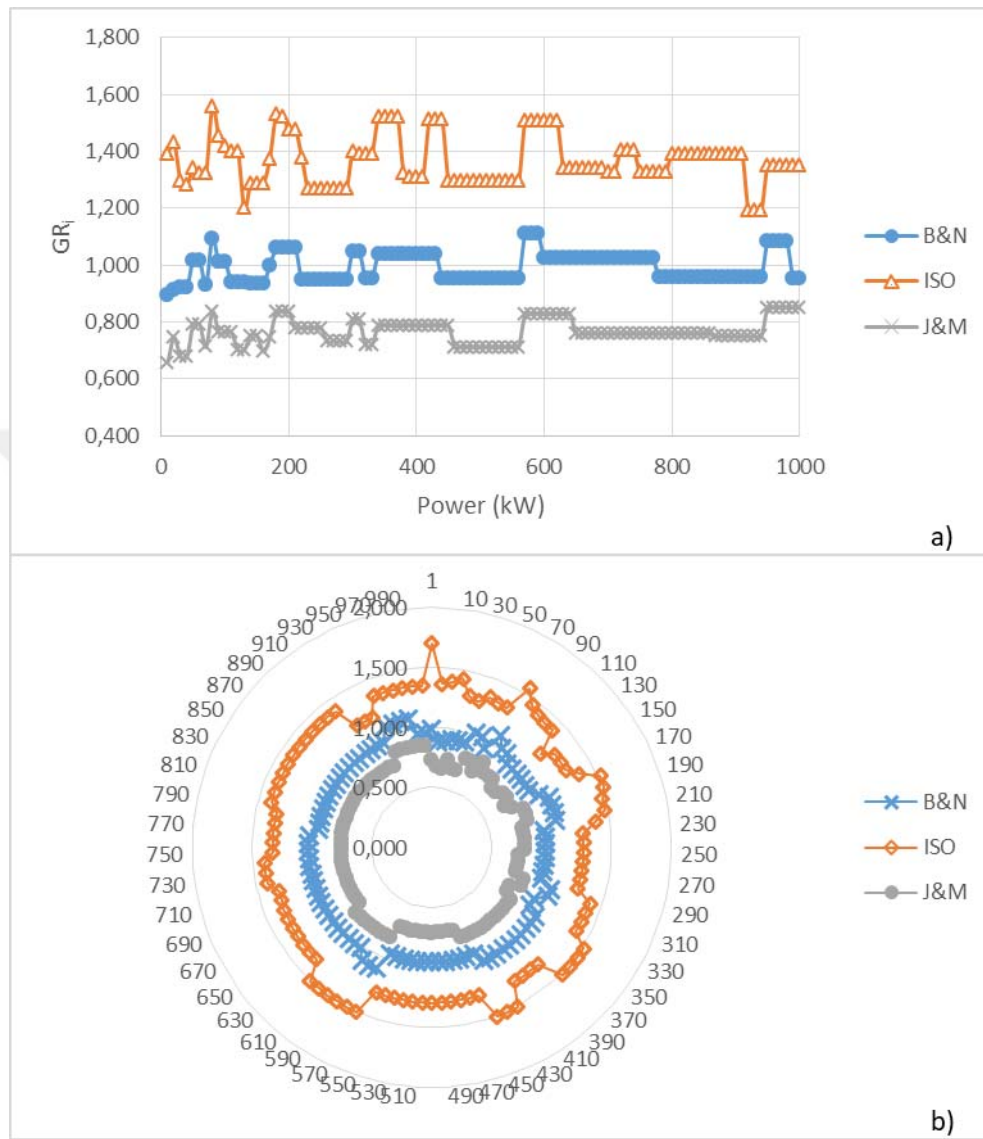
256

Figure F. 29. Comparison of GR_i results obtained from the design approaches at 8:1 speed ratio ($\emptyset=25^o$, Type 3), a) scatter chart, b) radar chart